The UNIVERSITY OF HULL

AN INVESTIGATION INTO THE EFFECT OF PROCESS PARAMETERS ON CARBON FILM PHYSICAL PROPERTIES PRODUCED BY DIFFERENT DEPOSITION TECHNIQUES

being a Thesis submitted for the Degree of

Doctor of Philosophy

at the University of Hull

by

Azzeddine DEHBI - ALAOUI, (DEA, DUES (Hons.)) (Limoges, France)

FEBRUARY 1994

CONTENTS

PART 3 EXPERIMENTAL, RESULTS, DISCUSSIONS AND CONCLUSIONS 63

CHAPTER VI INVESTIGATION INTO FAB SOURCE FILMS 64

ACKNOWLEDGEMENTS

I am particularly grateful to my supervisor, Prof. Allan Matthews, for his guidance, expert advice and for his efforts in finding financial support for my researches.

I would like to thank Prof. M. L. Theye ("Laboratoire d'optique des solides") at the University " P.et Marie Curie" of Paris for her precious collaboration in the optoelectronic measurement .

My sincere thinks also go to Dr Yahya Bounouh who was preparing his doctorate under the direction of Prof M. L. Theye, for his collaboration in the measurement of the optoelectronic properties of the samples he received from Hull. And I thank Dr Trevor Dines (University of Dundee) for Raman spectroscopy.

I am very greatful to Dr R B Moyes, Dr D F Ewing and Mr I. Theaker (Chemistry Department of Hull University) for the help and advice I recieved while I was using the spectrophotometry equipment.

I would also like to express my sincere thanks to Mr Garry Robinson for SEM , photographic and materials preparation work, Mr John Hebden, Mr Tony Pace, Mr Tony Pawson, Mr John Robson, and other members of the mechanical workshop for technical support.

To all my colleagues at the Research Centre in Surface Engineering, particularly Dr Peter Stuart Holiday, Dr. Adrian James., Dr Peter Robinson, Dr Kevin Fancey and Dr Adrian Leyland, I am indebted for their friendly assistance.

The author acknowledges an Overseas Research Studentship award and gratefully thanks Ion Coat Ltd, Howmedica International Inc., and the Science and Engineering Research Council for the provision of equipment and financial support.

A. DEHBI-ALAOUI

SUMMARY

This thesis reports research to investigate the effect of process parameters on the physical properties of carbon films produced using different deposition techniques. The deposition techniques utilised are a FAB source, an r.f./d.c. EBPVD system and a hot filament CVD system.

The findings of this study indicate that the films produced by the FAB source technique are relatively hard (~2000 H_K at 25g). Occasionally some films showed a hardness up to 8000H_K due, in part, to elastic recovery during testing.

FAB source films are transparent in the infrared, however they suffer from a relatively poor transmission in the visible. The optical band gap is about 1eV. The refractive index is around 2.2 and their hydrogen content is low.

When the carbon content in the source gas was reduced by mixing hydrogen with the hydrocarbon used, the transparency, the content of bonded hydrogen in the films and the optical band gap increased slightly but the hardness, adhesion, refractive index and deposition rate decreased.

The impact energy has a dominant influence on the film properties. This has been demonstrated by changing the sample orientation.

FAB source films have good wear and friction properties with only a small sign of localised failure after pin on disc sliding tests for 100 metres

A study on titanium nitride/DLC multilayer films showed that the adhesion at the TiN/DLC interface can be improved (and therefore the wear performance). The best adhesion and wear results were obtained by utilising an over-stoichiometric composition of titanium nitride.

FAB source films have been deposited on PET and were shown to be as good as that of sputtered gold on PET, and much superior to evaporated titanium on PET. The transparency of the coated PET has been improved by optimising the deposition conditions.

The properties of films grown by plasma-assisted evaporation of graphite depends on the carrier gas used, substrate type and bias voltage (under both d.c and r.f. conditions). Films grown on tool steel in a butane r.f. plasma have a hardness around 4000 H_K (25g). The growth rate on glass under similar conditions is very low, but the film is completely transparent with an optical band gap of 2.6 eV. When argon is used as the carrier gas, no film is formed on tool steel, but on glass a completely transparent film is produced.

Nanohardness measurement showed that r.f. EBPVD films are extremely hard (33-44 GPa) and the lowest elastic recovery was obtained for the non-hydrogenated film (11% against 44% for the a-C:H film).

Pin on disc tests of r.f. a-C:H films exhibited a typical film wear of 48×10^{-6}mm^3/Nm against steel, which represents a modest reduction in wear compared to an uncoated steel substrate.

All d.c. EBPVD films showed poor performance in the pin on disc machine due to their poor adhesion. The concentration of bonded hydrogen (α_S) in d.c. films is up to five times more than that of FAB source films. Their relatively low refractive index reflects a polymeric type of film. They were more brittle and usually less well adhered than those produced by other methods. Their optical band gap varied between 1eV to 3.5eV.

The concentration of total hydrogen (bonded or eventually non-bonded) has been found by coworkers to be 33% in dc EBPVD films and 25% in FAB source films. The decrease of the concentration of bonded hydrogen with cathode voltage and the absence of such correlation for the total hydrogen in dc/EBPVD an FAB source films, suggests the presence of nonbonded hydrogen in the films.

One of the achievements of the work is that an empirical relationship is developed, linking the optical band gap with the amount of bonded hydrogen in the film, the relative carbon to hydrogen flow input ratio , and other plasma electrical parameters for carbon coatings produced using a thermionically enhanced plasma-assisted d.c. PVD process. It explains observed properties in terms of process parameters and highlights the difficulties in obtaining consistent coatings on sample surfaces at different locations and orientations in the deposition chamber.

Finally a new system is described for the deposition of hard carbon films. This new system allows the generation of very high ionisation levels and produces films with hardnesses over 8000 H_K (200g) (thickness ~ 2.5μm, substrate; tool steel). The deposition rate is higher than previously reported for such hard films (2-3μm/hr) in a 0.5-1% CH_4 in H_2 plasma. SEM microscopy showed particles having octahedral shapes. Raman spectroscopy indicates a DLC structure with some disordered graphite present. Infrared spectrophotometry showed very little evidence of bonded hydrogen in the films. The optical band gap is 2 eV for a film deposited on silica.

INTRODUCTION

The synthesis of ultra-hard thin films produced from cheap and soft material has been considered as a the major breakthrough in coating technology over the last decade. Their application, however, is limited mainly to the areas of tribology and corrosion. On the other hand when films with excellent optical, chemical or electronic properties are produced, their mechanical properties are generally compromised. Diamond is the exception, it has always been the dream of scientists because of its unusual properties; it combines the best of almost all the physical properties.

Since graphite and diamond are made from the same atoms (carbon), though different in structure, scientists have tried to reorganise the atoms in graphite in order to reach the structure of diamond. It took many years to eventually produce synthetic diamond (1955, H. T. Hall and co-workers, General Electric Company), by applying very high pressures exceeding 500 kb (5×10^{10} Pa) to graphite at high temperature (2760°C). The process is now working industrially but is still very expensive.

Evaporation of graphite in vacuum was also attempted as early as the last century but the process was quickly abandoned because only soft films with poor physical properties were produced.

Hope started to rise, however, when observations of hard carbon based films formed by plasma discharges in hydrocarbon gases were reported. These films were usually considered an incidental feature of the discharge process. The particles created in the plasma discharge and the bombardment of the films during growth are believed to provide the high impact pressure on an atomic scale. It was Aisenberg and Chabot [1] in 1971 who first took this new technique seriously and produced hard carbon films from carbon ions extracted from a carbon arc in argon. Subsequent confirmation by Spencer et al [2] led to an explosive growth of the field. Among the earliest workers were Holland [3,4] and Weissmantel [5,6].

Nowadays, dozens of different techniques are available for producing carbon films with a variety of different properties close to those of diamond [7,8]. The last decade has witnessed the emergence of an extremely massive amount of reviews, publications and conferences.

However, because of the complexity of the techniques and the mechanism of growth of these hard carbon films, intensive research is still needed before industrial applications in this field will appear. Intensive exploration of every technique is still to be effected as, unfortunately, only limited work on the effect of the process parameters (pressure, voltage, type of gas used, energy of particles in the plasma) on the film properties are available. Studies of comparisons between two or three deposition techniques used by the same researcher have not been reported.

For these reasons, an investigation on the effect of deposition conditions on the physical properties of carbon films produced using four different deposition techniques was the aim of this project. These coating processes cover:

i) A FAB source system,

ii) An (r.f./d.c.) EBPVD system,

iii) A hot filament CVD system.

The FAB source rig has been built for this project, the (r.f./d.c.) EBPVD existed previously, and the hot filament CVD (built for this project) is a new configuration of this type of technique. Graphite, and hydrocarbon gases are the carbon sources used.

The optical properties (refractive index, transmittance, absorption and optical band gap.), the structure in terms of C-H bonding type, carbon sites, hydrogen content, the mechanical properties (hardness and adhesion) are the properties studied in every case.

The tribological study of the films produced is not included in this project. The author was however involved with a tribology study of these films since this was done by Dr P. Holiday at Hull in parallel with this present study. Some of his work is presented for information.

The first part (Chap. I, II and III) of this thesis will try to provide a general overview of diamond and diamond-like carbon films.(Although this project is about carbon films in general an overview on diamond is presented since its properties represent the reference).

The second part presents in Chap. IV a brief description of thin film deposition techniques and the principal aspect of the "electric discharge" as fundamental in each technique. This part, also presents in Chap. V a description of the main characterisation technique (spectrophotometry) used by the author to study the films properties. The rest of the standard methods are presented in an Appendix with a brief background of the theory involved in these techniques.

The last part (Chap. VI - IX) will describe the deposition techniques to be used and undertakes to deal with the results obtained by each technique mentioned above. The effect of the process parameters on the film properties is presented. An empirical model correlating the film optical properties with the process parameters is developed. The effect of gas mixtures, sample orientations and plasma parameters on the film properties are studied.

Finally, an account of all the properties obtained for each technique is presented and future recommendations for the remaining problems to investigate are suggested.

PART 1

OVERVIEW OF DIAMOND AND DIAMOND-LIKE PROCESSES AND PROPERTIES

CHAPTER I

NATURAL DIAMOND

1. Introduction

This work deals primarily with diamond-like carbon films, but some information on diamond is vital since it is the ideal to which much of the reported work is aimed. Highly praised reviews have been presented in this field; for example Nicholas Weinstein reported a very elaborate work on diamond. This work is a translated from Russian [9]. Ref.[10] is an excellent book by J. E. Field entirely devoted to the properties of diamond. This chapter briefly summarises some information about natural diamond, more details can be found in the reviews mentioned above.

2. Structure

2.1. Crystal Lattice

The unit cell of diamond is in a cubic space lattice and consists of 18 carbon atoms, of which 8 are located at the vertices of the cubes, 6 at the centres of its faces and 4 at the centres of 4 (of 8) cubes formed by dividing the unit cell by means of three mutually perpendicular bisecting planes (Fig. I.1.). Diamond carbon atoms are arranged in hexagonal rings in the (111) plane (the natural cleavage plane of diamonds). These rings are stacked one above the other in the sequence ...abcabc... The diamond crystal lattice constant equals 3.657Å and the closest distance between atoms is 1.54Å. Each atom in the diamond lattice has four equivalent closest neighbours, located at angles of 109° 28' with respect to one another. In diamond each of the four valence electrons (per atom) has a covalent bond with one of the electrons of a neighbouring atom. These bonds are of sp^3 nature (Fig. I.2.), which are especially strong. The elements of diamond's crystal structure combine into crystals that are usually of octahedral, icosahedral, cubic or sometimes a combination of these shapes.

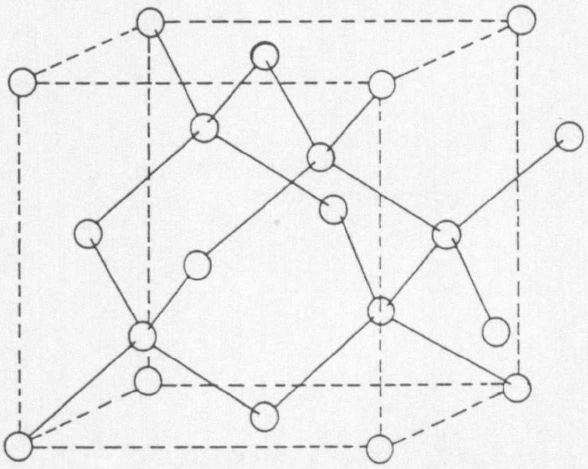

Fig. I.1. The Diamond Cubic Crystal Lattice

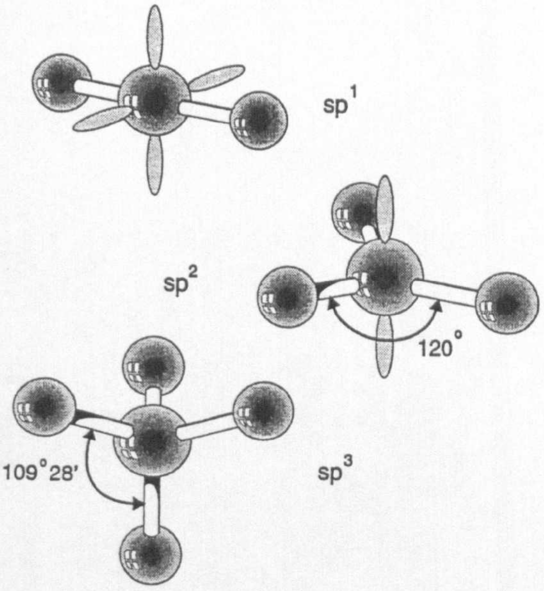

Fig. I.2. The bonding Configurations of Carbon

Carbon atoms can be arranged in another crystal lattice having a different type of atomic bond and forming a substance with properties drastically differing from diamond. Graphite can be taken as an illustration. It is of a complex lamellar (layered) structure with the distance 3.39Å between the layers The atoms in the layers form regular hexagons having sides 1.42Å long. The arrangement of the atoms in graphite consists of a parallel stacking of layers of hexagonal carbon rings (Fig.I.3.). In contrast to the structure of diamond, the stacking sequence of graphite can be either ....abab.... or ....abcabc.... The structure for graphite is trigonal sp^2 (Fig. I.2.). Table I.1 summarises some structural constants of diamond and graphite. As with diamond, the cleavage plane in graphite is parallel to the stacked layers, although graphite is cleaved with extreme ease compared with diamond. Three vertices of three adjacent hexagons coincide at a point that is directly under (and above) the centre of the hexagon in the adjacent layer. Therefore, complete repetition of the structure of graphite occurs at twice the distance that exists between the layers.

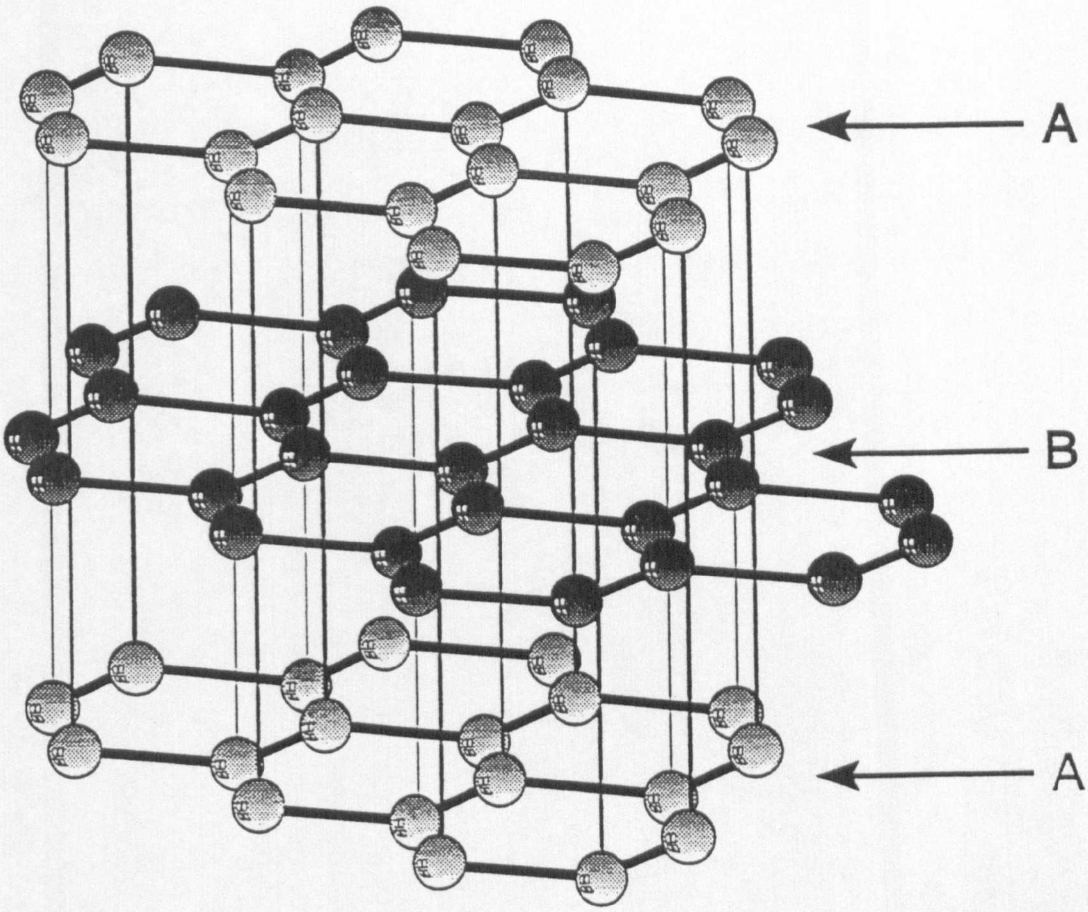

Fig.I.3. The Lattice Network of Graphite

Table I.1. Structural Properties of Cubic and Hexagonal Diamond and Graphite

	Cubic	Hexagonal	Graphite
Unit cell constants (nm)	a = 0.357	a = 0.252	a = 0.246
		c = 0.412	c = 0.671
C-C nearest neighbour distance (nm).	0.154	0.152	0.142
Bonding	sp^3	sp^3	sp^2

3. General properties

3. 1. Graphitisation

When diamonds are heated to a high temperature, the changes that will take place depend notably on the environment around the diamond. True graphitisation involves the transition of diamond to graphite without the aid of external agents. If diamond is heated in an inert atmosphere, the onset of graphitisation can be detected at ~1800K. If oxygen, or other active agents, are present, a black coating can form on the surface of diamond above 900K.

3. 2. Resistance to Chemical Attack

Diamond is chemically extremely inert and is not affected at all by any acids or any other chemicals, except those which at high temperature act as oxidising agents. Substances such as sodium nitrate are known to attack diamond in the molten state at temperatures as low as 700K.

The only other possible form of chemical attack is by two groups of metals. The members of the first group are avid carbide formers and include tungsten, tantalum, titanium and zirconium. At high temperatures these will react chemically with diamond to form their respective carbides. The second group includes iron, cobalt, manganese, nickel and chromium, and also the platinum group of metals. In the molten state, these metals are true solvents for carbon.

3. 3. Hardness

Diamond is considered the hardest material on earth. A method of testing hardness is to measure the deformation of a material under a given load (Appendix). The hardness of Diamond is around 10000 kgmm^{-2} with normal loads of 500g, 1kg and 2kg.

Although diamond has high mechanical durability, it is regarded as a brittle material. It can be easily destroyed by impacts. It is this specific property - brittlenessthat hinders the use of diamond crystals in cutting tools for machining surfaces that are interrupted by holes and grooves. Such a tool is subject to impacts when it cuts across a hole and hits the other side.

3. 4. Transparency

High purity diamond is transparent to photons in a spectral range that is the widest among all the known solid materials [10-13]. Perfect diamond crystals absorb photons strongly at wavelengths below 285nm, corresponding to the diamond minimum indirect band-gap energy. They also have relatively weak vibrational absorption in the two-phonon and three-phonon absorption bands. This sets a limit to the transmittance of thick diamond windows to wavelengths between 2.5μm and 6.7μm. As a result, the whole visible spectral region is free of absorption or luminescence bands [14]. High-purity diamonds therefore transmit photons with wavelengths from well beyond far-infrared through the visible spectrum up to far ultraviolet. Any coloration is due to absorption bands. Although every material absorbs X-rays to some extent [15] ultra thin diamond films of micrometer [16] or submicrometer [17] thickness are very efficient in transmitting X-rays, including low energy ones emitted from light elements [17].

3. 5. Optical Band Gap

The band gap Eopt of natural diamond is 5.45 eV. It is a large band gap as compared to 1.1 eV for silicon. This large value of the band gap makes diamond comparatively insensitive to temperature changes and radiation, and yields good insulation characteristics.

CHAPTER II

SYNTHETIC DIAMOND

1. History

Almost as soon as it became obvious that diamond consists of carbon attempts to synthesise it began. In 1880, experiments were conducted on diamond synthesis by the English scientist James Bannantyne Hannay. Many years have passed since that time and dozens of other ideas were advanced for the production of synthetic diamond. In 1955, scientists finally succeeded in synthesising diamond by applying high pressures to graphite (by high pressures we mean pressures corresponding to the region of diamond stability (Fig.I.1)). Synthetic diamond is in regular production at the present time in many countries (eg England, Japan, France, Ireland and the USA). Methods for synthesising diamond are continuously being improved.

2. Diamond synthesis at high pressure

2. 1. Source material for diamond synthesis

The container is charged with a mixture of graphite and metal: nickel, iron, manganese, etc. The synthesis of diamond begins after melting the metal. Mainly, metals of the iron group are used with various admixtures.

The role of metal in the synthesis process is not fully understood. Some scientists regard the metal simply as solvent for the carbon, whereas others emphasise the catalytic properties of the metal.

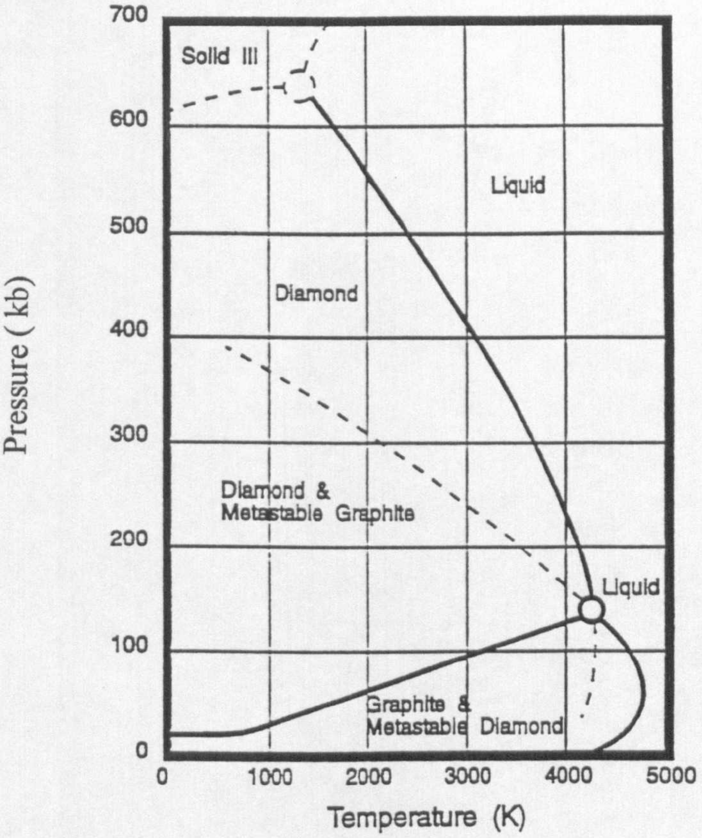

Fig. II.1. The Leipunsky carbon Phase Diagram [8]

3. Production of diamond films at low pressure

3.1. Essence of the process

Diamond growth is possible in the region of pressures and temperatures in which it becomes the less stable form of carbon, and graphite is the stable form. This is said to be diamond production at low pressures. A low pressure may be hundreds of atmospheres or a fraction of an atmosphere. The probability of diamond growth is substantially increased if a diamond seed crystal is available. In a proper hydrocarbon medium, for example in methane, the following decomposition reaction proceeds on the surface of the seed diamond:

$$CH_4 \xrightarrow{\hspace{3em}} C + 2H_2$$

where C can grow as diamond or graphite.

It turned out (from experimental investigations) that the addition of hydrogen to the initial methane considerably reduced the rate of graphite growth, but did not retard the growth rate for diamond.

The primary difficulty of diamond growth at low pressures is to avoid the deposit of this stable phase of carbon (graphite) or to get rid of its overgrowth.

3. 1. Deposition Processes

All the early attempts to make diamond films were slow and impractical; they relied on a two-step process - alternately producing diamond layers and removing the graphite. It wasn't until the late 1970s that substantial progress was made - groups of scientists in the former Soviet Union and Japan began experimenting with deposition of film from vapour activated by a plasma. As a result they learned how to change the traditional two-step process into a single step.

Russian investigators were first to report a single-step process for crystalline diamond. Five years later Matsumoto and co-workers (Japan) discovered that the proportion of methane in hydrogen has to be very low (~ 1%) in order to obtain films with low hydrogen content and an enhanced tendency toward diamond crystallisation.

What most diamond film processes have in common is the use of ionised gases and deposition of metastable diamond from the vapour phase. The gas can be ionised by different means, eg: a glow discharge (d.c. or r.f.), emitted electrons from a hot filament, microwave power, a flame, etc. Each new way of ionising the gas leads to a new process. The carbon source can be gas or solid. The most important parameters to be controlled are the substrate temperature and the carbon content in the plasma.

Substrate temperature has to be between 600 °C to 1000 °C and often 1% methane or less is used in H_2.

3. 2. Deposition rate.

Diamond films have been grown on different kinds of substrates, Si, Mo, W, etc. All the reported techniques suffer from a very low deposition rate 0. 1- 5 µm/h. However over the last few years several plasma-assisted chemical vapour deposition (PACVD) techniques have been developed for high-rate synthesis of diamond from the vapour phase. These techniques, including d.c. plasma CVD [18], dc plasma jet CVD [19] and arc discharge PACVD [20], normally operate at pressures of 100-400 Torr in an atmosphere of hydrogen / hydrocarbon mixture and use an arc (or glow) discharge to generate the active species taking part in the growth process. Growth rates of 100-250 µm/h, and even 930 µm/h [21] have been reported. Recently it has been shown that in the case of microwave PACVD, the addition of water vapour [22] or oxygen [23] to the reactant gas can considerably increase the growth rates and improve the crystallinity of the deposited diamond film. Similar results have been reported for other oxygen-containing systems[24-26].

Although these high deposition rate techniques are very promising, still they suffer from a poor surface adherence and high substrate temperature (> 800°C) [27].

For more information about diamond processes at low pressure, a good description of a dozen techniques including their typical deposition conditions can be found in [9].

4. Synthetic diamond films properties and applications

4. 1. Mechanical properties and applications

Several authors have reported test results for CVD diamond thick-film inserts. Nakamura at al. [28] prepared 0.1 mm thick CVD diamond tips which were brazed to carbide substrates and tested on Al-12% Si and Al-17 % Si alloys. In their tests, the CVD diamond exhibited 25-50 % less flank wear than sintered diamond in turning tests and performed comparably in milling tests.

P. M. Stephan [29] found that in general CVD thick film (100-500 μm thick) diamond exhibits better wear resistance and comparable impact resistance to sintered diamond as cutting tool inserts and far better wear resistance than tungsten carbide in end mill applications. Thin-film diamond tools also showed considerable improvement in wear life over tungsten carbide inserts and end mills in machining abrasive materials [29].

The most important characteristic for such applications is the quality of the adhesion between the films and the substrate. The numerous attempts to grow diamond films on steels have yielded only highly undesirable non diamond carbons [30-37]. Mo and Ni as well as a single layer of TiN on steel were explored [33] and were proved to be good interlayers for adhesion.

The friction coefficient is high because of the high roughness of the films. Laser beams and argon bombardment have been used to polish the film surface, in order to minimise the friction coefficient [34].

4. 2. Optical properties and applications

The reported band gap of the diamond films is as high as natural diamond (5 eV). In addition, diamond is transparent to photons having energies less than its large band gap; thus, it has potential application as an ultraviolet detector.

These advantages make diamond films applicable as optical windows or other analytical devices for the food industry [12]. Diamond's high resistance to chemical attack has also allowed it to serve as an optical window for examining highly corrosive molten fluoride salts.

Complication comes from the fact that inhomogeneous residual stress in the diamond films tends to bend them. A considerable amount of diamond must be removed from the non flat diamond film before further smoothing and the finishing can be done.

Polycrystalline CVD diamond films have various structural defects and impurities that can lead to loss of crystal symmetry. This allows one-phonon absorption, and an absorption band above 7.5 μm as well as a strong absorption band around 3.5 μm caused by the vibration of hydrogen-carbon bonds. Shown in Fig II.2 is an IR absorption spectrum from a polycrystalline CVD diamond film that was deposited by a hot filament CVD method using a methane-hydrogen mixture [35].

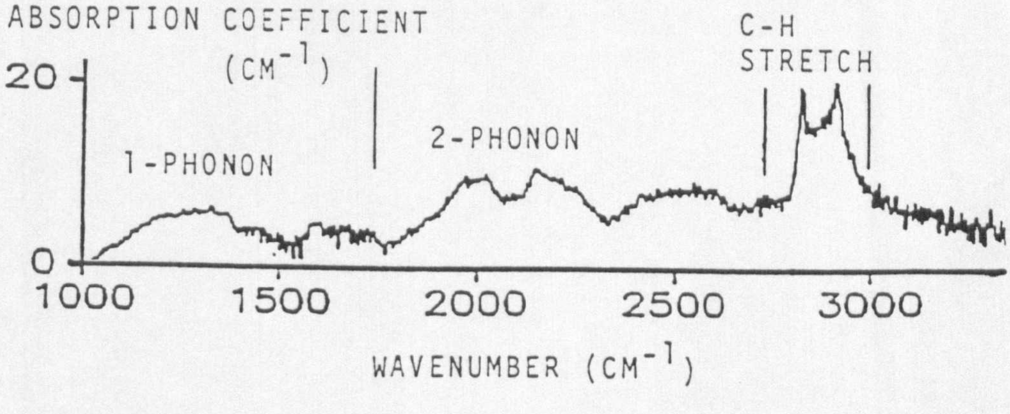

Fig. II.2. IR absorption spectrum from a polycrystalline CVD diamond film deposited by a hot filament CVD method using a methane-hydrogen mixture [35]

CHAPTER III

CARBON FILMS

1. Introduction

Hard carbon-based films formed by plasma discharges in hydrocarbon gases were originally produced accidentally [36]. Aisenberg and Chabot [1] were the first to report a serious study of hard carbon films. Their films were produced from carbon ions extracted from a carbon arc in argon. Big interest in this field started when Spencer et al [2] confirmed the possibility of production of such a hard carbon film. Holland [3,4,37,38] and Weissmantel [39,43] were among the most active of the early workers in this field. An interesting review on diamond-like films written by John C. Angus et al. was published in 1986 [7], when interest in this field was just growing.

Diamond like films are often produced from a plasma of ionised hydrogen and carbon species. Depending on the process, they may contain a substantial amount (up to 50 at %) of hydrogen. Thus the films are in fact amorphous hydrogenated carbon. Some workers prefer the designation a-C: H for diamond like films as a-Si:H is for amorphous hydrogenated silicon films. When hydrogen is not involved in the process, i-carbon or i-C is used instead.

2. Categorisation and Nomenclature

The term "diamond-like carbon" (DLC) has been widely used by many authors because of the obvious similarities in properties between the films and diamond. J. Angus [7] has shown that if the term is applied, it clearly should be restricted to films with $\rho_N > 0.2$ g-atom/cm^3 where ρ_N is the gram atom number density, ie the total number of gram atoms per unit volume.

$$\rho_N = \frac{\rho_M}{\sum x_i A_i}$$

where ρ_M is the mass density, x_i the atom fraction, and A_i the atomic mass of element i. This idea has not, however, been used by workers in this field mainly because ρ_M and x_i are not easily obtainable accurately.

Categorisation of the carbon films produced in this work is based on the measure of many properties such as hardness, hydrogen content, optical band gap, transparency, refractive index and the sp^3/sp^2 ratio of the C-sites.

The ratio sp^3/sp^2, has been measured by many authors and used as another important parameter in the categorisation of carbon films; for low hydrogen content films the higher the value of sp^3/sp^2 ratio the closer the films properties to true diamond. This ratio can be measured with good accuracy using the nuclear magnetic resonance (NMR) technique. The film needs, however, to be removed from the substrate in large quantity and contain a high concentration of bonded hydrogen. This is not always the case. An alternative characterisation giving acceptable sp^3/sp^2 value is the infrared technique. The latter is most often used by workers because of its simplicity.

3. Carbon film deposition processes

Diamond-like films have been prepared by a wide range of different techniques. The main difference between DLC and diamond techniques is in the deposition conditions:

-The substrate temperature does not have to be around 900°C as it does for diamond and can even be room temperature.

-The concentration of carbon in the plasma is not necessarily as low as 1%.

-Hydrogen is not always present in the process.

-Different gases can be used to support the discharge or to bombard the substrate during growth.

DLC processes can be divided into two groups: those using hydrocarbon gas and those using solid carbon. However, as it will be shown in this work, the carbon source is not crucially important in the growth of DLC films. It is the plasma and substrate surface properties that are more important and play a critical role in the growth of DLC films.

3. 1. Processes using hydrocarbon gases

Diamond like film has been deposited from hydrocarbon gases using a variety of glow-discharges and ion-beam processes. The glow-discharge techniques employ either rf or dc discharges. The ion-beam processes are of two types: those using beams derived from ionised hydrocarbon gases (see chapter VI) and those using carbon arc sources. Several schemes for growing diamond-like films from hydrocarbon gases are shown in Fig III.1.

3. 2. Processes using solid carbon

Processes for growing diamond like films from solid carbon are shown in Fig III.2. Graphite can be evaporated or sputtered. The advantage in using solid carbon is the possibility of producing non-hydrogenated films by using argon for example instead of a hydrogen plasma. In another category of processes called "hybrid" the carbon source is simultaneously solid carbon and a hydrocarbon gas. This process is among the techniques studied in this work (see chapters VII and VIII).

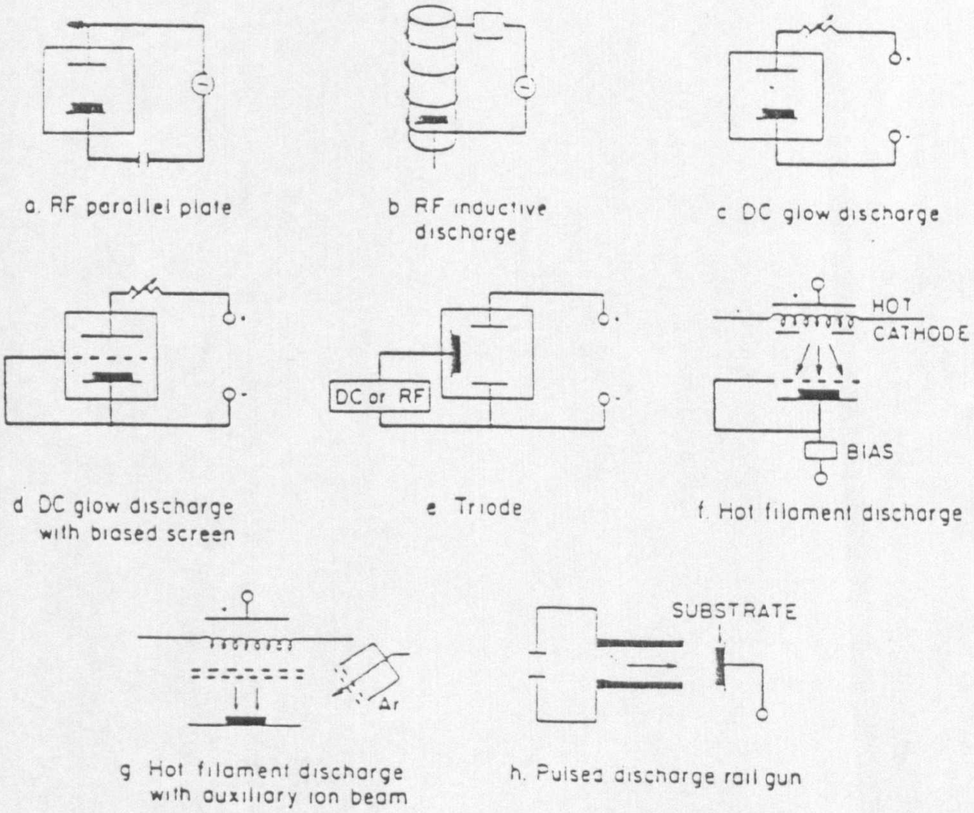
a. RF parallel plate

b RF inductive discharge

c DC glow discharge

d DC glow discharge with biased screen

e Triode

f. Hot filament discharge

g Hot filament discharge with auxiliary ion beam

h. Pulsed discharge rail gun

Fig.III.1 Processes of growing carbon films from hydrocarbon gases [7]

a. Dual beam sputtering

b Single beam sputtering

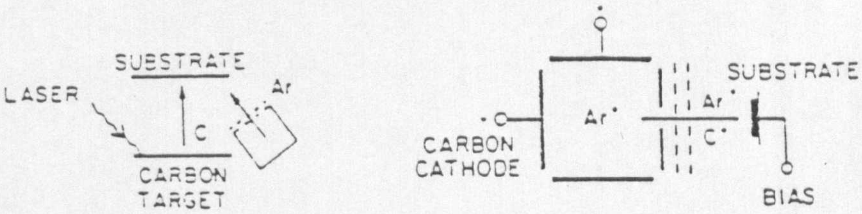

c. Laser evaporation with auxiliary ion beam

d DC glow discharge with accelerating grids

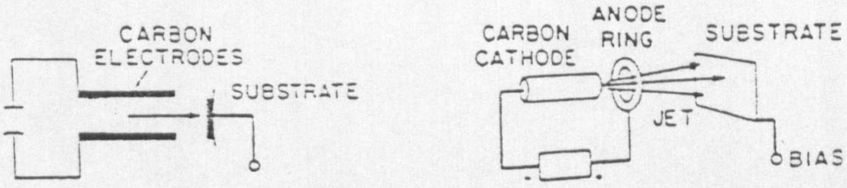

e. Pulsed discharge rail gun

f. Vacuum arc-discharge runs off cathode material

Fig.III.2 Processes of growing carbon films using solid carbon [7]

4. Chemical and physical properties

The elemental composition of carbon films depends upon the details of the method of preparation. When hydrogen is involved in the process the films are usually hydrogenated. Numerous studies has confirmed that carbon films can contain large amount of hydrogen; up to 50% [44-45].

Hydrogen can either be bonded to carbon or chemisorbed in the film [46-47]. Many characterisation techniques such as Nuclear Reaction Analysis, Micro Combustion Analysis [48], NMR and I.R. Spectroscopy, have been used for qualitative or quantitative studies of the carbon film's hydrogen content.

The role of hydrogen is still an unsolved problem, one possibility is that hydrogen exists in several forms: bonded and in clusters [47] intercalated between graphitic bonds [49].

Other elements in the films such as oxygen, argon, krypton and aluminium may be incorporated into the films during the coating process. These impurities come from the inert gas used in the plasma or from the sputtered metallic species from the substrate. Their incorporation in the film will be more significant at low growth rates and high background pressures [48,50]. Their concentration remains, however, very small in comparison to the hydrogen concentration in the film.

5. Mass density

Mass density can be an important parameter in the classification of the different kind of carbon films produced by different techniques. The so-called amorphous carbon, which are basically graphitic in local structure, usually have densities in the range 1.5 to 2.0 g/cm^3. Hydrocarbon polymers typically have densities around 0.9 g/cm^3. The mass density for single-crystal graphite and diamond are respectively 2.26 and 3.515 g/cm^3.

The techniques used for density measurement (direct volume and mass measurement or sink-float technique) are not very accurate. This is because the substrate mass does not remain constant during coating especially when the substrate is subject to heavy particles bombardment during coating. For these reasons many groups of researchers, including ours, do not take the reported density values as very accurate. Correlating mass density with other parameters, such as hydrogen content or particles energy is therefore practically very difficult. Errors in measurement can sometimes exceed the difference between the density of diamond and that of graphite. Although scientists disagree as to how easy or difficult it is to measure the density of these films, they agree on the usefulness of the measurement for purposes of identification. These problems did not stop, however, some work being performed: It has been reported [51] that the density increases linearly with the ratio of bias voltage to the square root of pressure, $V_B/P^{1/2}$. Significantly higher mass densities, in the range of 2.0 to 3.4 g/cm^3 have been reported for films with low hydrogen content [52-54].

6. Electrical Properties

6. 1. Conductivity

The conductivity of carbon films has been studied extensively. A very wide range of conduction of these films has been observed [7]. The electrical conduction of some DLC films can be up to 12 orders of magnitude lower than that of evaporated carbon.

7. Mechanical properties

7. 1 Hardness

Diamond-like carbon films, were discovered as a result of their unusual hardness. Qualitatively, one finds the films difficult to scratch with a steel point. The reported values [Table III.1] for microhardness measurements of hard carbon films vary from 1500 H_K to 10000 H_K. Measurement of the hardness of the thin films is usually done at extremely light loads, e.g. 5 to 50g. Comparison between different workers or correlation between hardness and other parameters must be done with great caution because of the difficulty of obtaining accurate measurement on thin films. The measured hardness of the films depends upon the film thickness, the load used and the nature of the deformation (elastic recovery of the indentation can give anomalously high hardness readings in conventional microhardness testing in which the indent area is measured after removing the load). In some cases total indent recovery can occur. Nevertheless, some qualitative observations may be made. First the hardness is a strong function of the process used and the deposition conditions. It has been reported [55] that the hardness of a film grown by hydrocarbon ion beams increases with beam energy. Weissmantel [56] reported that the hardness in fact goes through a maximum with increasing energy.

7. 2 Friction and wear

DLC films are also known for their relatively low friction coefficient. Values from 0.01 to 0.28 have been reported [57, 58]. The coefficient of friction was found to increase with the humidity [31] and decrease with the number of test cycles [56].

Wear of surfaces can arise from several mechanisms such as adhesion, abrasion and tribochemical reactions. Abrasive wear has been observed in a-C: H [58] while abrasive and tribochemical wear has been studied in sputtered a-C [59].

TableIII.1 Some representative Microhardness data.[7]

Material	Process	Vickers (H_V)	Knoop (H_K)	reference
Diamond (111)		7500-9000	5600-11000	10
Diamond (100)		6900-9600	8300-10300	10
SiC (001)		2355	2150	10
Quartz (001)		1096	700	10
a-C:H	rf	3300		83
a-C:H	Ion beam	3000-5000		57
Dense carbon or a-C:H	dc	3000-5000		84
a-C:H	rf		1250-1650	70

7. 3. Internal Stress and Adhesion

Substantial internal compressive stress (up to 10^{10} N/m^2) is a major problem with DLC films [31,60]. Internal stress can cause delamination of the films from the substrate when the film thickness is of the order of several microns [61]. Best adhesion is obtained on substrates that form carbides e.g.: Si, Fe and Ti. It is believed that this stress is caused by the presence of dissolved hydrogen in the films. Correlation between deposition conditions and internal stress has been reported. It was found [62] that the intrinsic stress for plasma deposited a-C:H films is compressive at low bias and becomes lower and tensile at higher bias. Grill [63] reported that the intrinsic stress declines at higher deposition temperature for his a-C:H films prepared by the rf plasma decomposition of acetylene. These correlations are however not true for all kinds of carbon film. Each deposition process has its own deposition parameters on which the film properties are strongly dependent. The tribological properties of the carbon films produced in this work has been studied in Hull by Dr P.Holiday [64]. A summary of his results is presented in chapter VII.

8. Optical properties

DLC films are known for their relatively good transparency in the infrared regime; more than 90% of the I.R. light can pass through a 1μm thick film. However this transmission can decrease dramatically in the regions of CH_2 and CH_3 absorption band vibrations.

Conversely transparency in the visible regime is relatively poor. The transparency is a parabolic function of the wavenumber and decreases rapidly from 80% in the near infrared to less than 10% in the near ultraviolet for a 1 μm thick film. A film thicker than 2μm is almost opaque in the visible. Attempts to improve the transparency of DLC films have not been very successful. It was reported that films with higher bonded hydrogen concentrations have slightly better transmission in the visible [65], and hydrogen-rich polymer-like films may even be transparent. However increasing the hydrogen in the film decreases its hardness.

The optical band gap, E_{opt}, of carbon films varies from 0.5 to 3.5 eV [5,66]. Higher E_{opt} values were obtained for transparent films with high hydrogen content. Lower values were obtained for hydrogen free evaporated carbon films [66]. Dense hydrocarbons cover the range $0.8 < E_{opt} < 2.5$ eV. Dischler et al [63] reported a linear increase of the optical band gap of plasma-deposited a-C:H films with bonded hydrogen content. Increasing the sample bias decreases the optical band gap [63]. It is believed that the strong variations of E_{opt} reflect differences in the sp^2 and sp^3 bonding ratio [7].

Post-deposition annealing lowers the optical band gap [67,68]. This is consistent with the decrease of hydrogen content in the film (desorption evolution) due to the temperature increase. At T= 600°C most of the hydrogen had been removed [67,68], the sp^3/sp^2 ratio had fallen to zero and the E_{opt} became lower than 0.4 eV [67,69]

The refractive index, n, can be tuned by deposition parameters. Values well above those of typical hydrocarbon ($n > 1.6$) up to the index of diamond ($n = 2.4$) have been reported. Hydrogen appears to lower the refractive index. Typical a-C: H films cover the range $1.8 < n < 2.3$ [51,70]. Polymer-like hydrocarbon films, deposited at low impact energy have refractive indexes <1.8 [71].

9. Bonding and structure

The structure of DLC films is amorphous. The presence of a semiconducting band gap is a crucial difference between DLC films and glassy carbon for example. The properties of carbon films depend strongly on the proportion of sp^2 and sp^3 sites, their local arrangement and, in a-C: H, the proportion and arrangement of the hydrogen atoms. These parameters are used in the classification of carbon films. It is generally believed that glassy carbon contains approximately 100% sp^2 sites, evaporated a-C 1-10 % sp^3 sites, while a-C:H may comprise 30-60% hydrogen with 30% of the carbon sites having an sp^2 configuration, but this is strongly dependent on heat-treatment [72]. Infrared and Nuclear Magnetic Resonance (NMR) characterisation techniques are often used to determine the ratio sp^3: sp^2 in the films. These techniques only work however, for hydrogenated films. There is as yet no technique that gives direct evidence of sp^3 sites in a-C or in films with a very low bonded hydrogen concentration. Direct measurement of the sp^2 and sp^3 site fractions in a-C: H using NMR was reported by Kaplan et al. [73]. They verified the presence of sp^2 sites in a-C: H and showed that their concentration varied with deposition conditions and tended to decrease with hydrogen content. 50% sp^2 sites and 50% sp^3 sites was found in their typical sample with an optical gap of 1.7 eV.

Strong evidence in favour of graphite bonding is confirmed by Raman spectroscopy[7].

The I.R spectrum around 3000 cm^{-1} provides detailed information on the C-H bonding configurations. Dischler et al [63] reported the important C-H bands observed around 3000 cm^{-1} [Table III.2]. Their analysis of the C-H stretch vibrational band around 3000 cm^{-1} indicated that 60% of bonded hydrogen was present as monohydride and 40% as dihydride.

Knowledge of the concentration of sp^3 and sp^2 bonded carbon alone does not provide a full understanding of film microstructure . Sometimes crystalline inclusions in an amorphous matrix have been observed [74,75]. With respect to the amorphous material, different structural models have been proposed. McKenzie et al [76] suggested a non crystalline two-phase structure consisting of polycyclic aromatic hydrocarbon regions interconnected by tetrahedral (sp^3) carbon. A multiphase structure consisting of amorphous graphitic, diamond-like, and polymeric regions in which hydrogen is distributed homogeneously over different carbon fractions is also an acceptable structural model.

Table III.2

Infrared absorption bands observed around 3000cm^{-1}[97,98]

Observed frequencies (cm^{-1})	**Predicted frequency (cm^{-1})**	**Assignment**
3300	3305	sp^1 CH
3045	3050	sp^2 CH (aromatic)
....	3020	sp^2 CH$_2$ (olefinic)
3000	3000	sp^2 CH (olefinic)
....	2960	sp^3 CH$_3$
....	2950	sp^2 CH$_2$ (olefinic)
2920	2925	sp^3 CH$_2$
2920	2915	sp^3 CH
2850	2855	sp^3 CH

PART 2

BACKGROUND ON THIN FILM DEPOSITION TECHNIQUES AND CHARACTERISATION TECHNIQUES

CHAPTER IV

THIN FILM DEPOSITION TECHNIQUES

Introduction

As already discussed in the previous chapters, a deposition technique and its associated process parameters have a characteristic effect on the nucleation and growth-dominated microstructure of a thin film and thereby on its physical properties. This chapter presents a brief description of deposition techniques directly or indirectly related to this project.

A deposition technique is often developed to deposit different kinds of thin films, the source material being changed to switch from one coating to another. For DLC films, graphite or hydrocarbon gases are usually the carbon sources and gases such as Ar or H_2 are used to support the discharge and participate in film nucleation.

A thin film deposition process involves three steps:

(i) creation of atomic/molecular/ionic species,

(ii) transport of these species through a medium,

(iii) condensation of the species on a substrate.

Depending on whether the vapour species has been created by a physical process (such as thermal evaporation and sputtering), by a chemical, electroless, or electrochemical process, the deposition techniques can be broadly classified under the following headings:

(1) Physical Vapour Deposition (PVD)

(2) Chemical Vapour Deposition (CVD)

(3) Electroless or solution growth

(4) Electro-Chemical Deposition (ECD)

By combining PVD with CVD, hybrid techniques such as reactive evaporation/sputtering and plasma deposition have been established. The principles and characteristics of some of the relevant techniques are described in this chapter.

A Vacuum Evaporation

A. 1 Evaporation sources

The temperature of a material for evaporation may be raised by direct or indirect heating. The simplest method is to support the material in a crucible which is directly electrically heated. Evaporated or sublimed crucible particles can, however, be a source of contamination. A better way of evaporating the material is the use of an electron beam gun or a laser beam. In this case only a localised area of the material is evaporated. The crucible temperature remains less than its fusion or sublimation temperature.

A. 2 Reactive Evaporation

By allowing a chemical reaction between vapour species of different elements either during their transport from source to substrate, or on substrate surface itself, it is possible to condense films of a great variety of alloys and compounds.

The effectiveness of the reactive deposition process is considerably enhanced by making the vapour species more reactive. One way to achieve this is to ionise the vapour species by bombardment with energetic electrons from a thermally emitting source. In another version, the ions of one of the reacting species are created by a glow discharge through which the other species traverse. This technique, called "Activated Reactive Evaporation" (ARE), has been used very successfully to get excellent optical and electrical quality films. Another method of making reactions effective is to provide the atomic forms of stable diatomic molecules, e.g.; those of O_2 (for oxidation), H_2 (for hydrides), and N_2 (for nitride). For example, alloy films of hydrogenated amorphous silicon have been obtained by evaporating silicon in the presence of atomic H obtained by the pyrolysis of H_2 on a hot tungsten filament [77].

B. Sputtering Techniques

Vapour species may be created by kinetic ejection from the surface of a material (called the target or cathode) by bombardment with energetic and non reactive ions. The ejection process, known as sputtering, takes place as a result of momentum transfer between the impinging ions and the atoms of the target surface. The sputtered atoms are condensed on a substrate to form a film.

If the surface of a multicomponent (alloy, compound, or mixture) target does not change metallurgically by thermal diffusion or chemical reaction, the sputtering process ensures atom by atom ejection and hence produces an homogeneous film of composition corresponding to that of the target. This is generally true but different sputtering rates will lead to some variation. As the sputtering yield is low and the ion currents are limited, sputter deposition rates are lower by one to two orders of magnitude compared to thermal evaporation under normal conditions. High ion current densities (~100 mA cm^{-2}) and hence high deposition rates (~ 36μm h^{-1}) are achieved only in special sputtering geometries such as magnetron sputtering (discussed later). In the case of multiple targets, the deposition rate will be determined by the respective areas and yields of the target materials.

B. 1 Magnetron Sputtering

Permanent magnets are placed behind the cathode in various geometries in such a way that the cathode surface has at least one region where the magnetic field lines are parallel to the cathode surface in a closed path. The discharge plasma is constrained near the cathode surface by endless toroidal trapping regions bounded by a tunnel shaped magnetic field. The tunnel shape and thus the ejection paths depend on the magnet geometry and arrangement.

Magnetron sputtering makes it possible to utilise the cathode discharge power very efficiently (up to 60%) to generate high (up to 50 mA cm^{-2}) current densities at relatively low voltages (500-1000V) to yield deposition rates that are at least one order of magnitude higher than those obtained in non magnetron systems. The high deposition rates coupled with the fact that the film is not subjected to plasma and electron bombardment makes magnetron sputtering a very attractive large-area, low-deposition temperature process.

B. 2 Glow Discharge Sputtering

The simplest arrangement to produce ions is provided by a normal glow discharge created at a residual pressure of about 10^{-2} Torr of the required gas (generally argon) by applying 1 to 3 kV dc between a cathode (target) and an anode (on which the substrate is placed). Owing to the competing process of the ejected atoms colliding with the gas atoms (backsputtering), the optimum pressure range for efficient sputter deposition of films is between 25 and 75 mTorr.

Besides the more popular parallel plate diode configuration, wire, cylindrical, and concave cathodes may be used for particular applications. Also, multiple cathodes may be used for simultaneous or sequential sputtering for multicomponent or multilayer coatings.

Lowering the working pressure of a glow discharge is very helpful in reducing the trapped gas content in the film. This is achieved in a triode sputtering configuration in which a heated filament provides electrons that are accelerated in the plasma to sustain the glow discharge at low pressures. The third electrode can also be a cold electrode positively biased up to 300 V. In this case the plasma potential initially at 1 or 2V, becomes equal to the positive electrode-voltage. The ion energy is increased and the voltage needed to start the discharge can be decreased down to 1 kV and the pressure down to 0.5 mTorr. More details about the triode system by a positive electrode can be found in [78]. Film properties (adhesion, mass density, hardness) can be improved by negatively biasing the substrate relative to the anode (usually the chamber) so that the film is bombarded with ions throughout its growth.

B. 3 R.F. Sputtering

Sputtering at low pressures (~ 10^{-3} Torr) is also possible by enhancing gas ionisation with the help of a capacitively coupled external r.f. field. If the cathode is an insulator material, dc sputtering is not possible owing to the building up of positive (Ar^+) surface charges. However, a high-frequency alternating potential may be used to neutralise the insulator surface periodically with plasma electrons, which have a much higher mobility than the positive ions. Whether or not the cathode surface develops a negative bias, which is responsible for sputtering depends on the amplitude and frequency of r.f. and the geometry of the cathode. Typically, an r.f. power supply of 13.56 MHz (allowed by the Federal Communications Commission for commercial applications in US,UK and Europe) and 1-2 kW power with about 2 kV peak-to-peak voltage is used to couple the cathode through a matching network. The r.f. technique can be used with any sputtering geometry in glow discharge or magnetron modes. It is an indispensable technique for deposition of films for semiconductors and various insulators.

B. 4 Reactive sputtering

The high chemical reactivity of ionic species and the atomic form of stable molecules, which are readily formed in a dc or r.f. glow discharge plasma, can be used very effectively to form thin film carbides, nitrides, oxides, hydrides, arsenides, and phosphides. Whether the chemical reaction takes place on the cathode, in the plasma, or at the anode depends on the pressure and chemical activity of the reacting species under given surface and temperature conditions.

C. Ion Beam techniques

C. 1 Ion Beam sputtering

Sputter deposition under controlled high-vacuum can be achieved using an ion beam source. The ions or neutrals (generally Ar) from a beam source are used to sputter a target in vacuum and condense the sputtered species on a substrate.

C. 2 Ion beam direct deposition

In this case a compound gas (eg hydrocarbon or silane) containing the species to be deposited is introduced in the source instead of an inert gas. A beam of monoenergetic ions or neutrals in the energy range from ten to several hundred electron volts impinges directly upon the substrate. Another category of sources uses an arc inside the source between two electrodes made of the material to be deposited. A graphite-arc has been used in a source to create a beam of carbon particles. Ion sources should be distinguished from high-energy ion implantation techniques [79].

The two ion sources commonly employed for deposition are the duoplasmatron and the one developed by Kaufman. In the duoplasmatron source, the ions are created in glow/arc discharge chamber and are then extracted through a second chamber at a much lower pressure (~ 10^{-4} - 10^{-5} Torr). The Kaufman source employs the chamber geometry and applied magnetic field in such a way that the thermionically emitted electrons must travel long spiral paths to an anode cylinder located in the outer diameter of the discharge region. This results in high ionisation efficiency. Applying a potential difference between a pair of grids with precisely aligned holes causes the ions to be extracted from the sheath around the grid holes and then accelerated by this potential difference. The grid optics focus the ions into a well-collimated beam, which can be neutralised by injecting low-energy elections from a hot filament on the target side of the grids. Fully neutralised Ar beams up to 25 cm in diameter with current densities up to 50 mA cm^{-2} at 500-1000 eV have been obtained from the Kaufman source. This source is well suited for both etching and sputter deposition of conducting and non conducting materials. The sputter etch (and hence deposition) rates depend on the material and the angle of incidence of the ions.

Another slightly different kind of source for deposition is the Fast Atom Beam (FAB source). This technique is described in detail in chapter VI because it is among the techniques utilised in this project.

D. Chemical Vapour Deposition (CVD)

Chemical vapour deposition involves, essentially, exposure of the substrate to one or several vaporised compounds or reagent gases, some or all of which contain constituents of the desired deposited substance. A chemical reaction is then initiated, at or near the substrate surface, producing the desired material as a solid-phase reaction product which condenses on the substrate. The chemical reaction may be activated by such different means as: heat, r.f. field, UV light or X rays, electrical arc, a glow discharge or electron bombardment.

The film growth in the CVD process takes place by an atom/molecule condensation process. The growth process is in many ways similar to that of physical vapour deposition processes such as evaporation and sputtering, since in each case the deposit is formed from a vapour phase.

E. Ion plating

Ion plating basically derives from the conventional evaporation and sputtering techniques. Reported in the literature by Mattox in 1963 [80], it is far newer than vacuum evaporation and sputtering. In ion plating, the part to be coated is made the negative electrode of a dc or r.f. glow discharge, the coating material is then evaporated into the gaseous discharge, where it is ionised.

Before reviewing ion plating mechanisms, a brief description of the glow discharge is necessary since it plays a fundamental role in this technique.

E. 1 Glow discharge in Ion plating.

Because of the pressures used (0.1 - 6 Pa) and the voltages applied (1-3 kV) the discharge used is an abnormal glow discharge. This means that the discharge current increases linearly when the voltage applied between cathode and anode increases (Fig.IV.1).

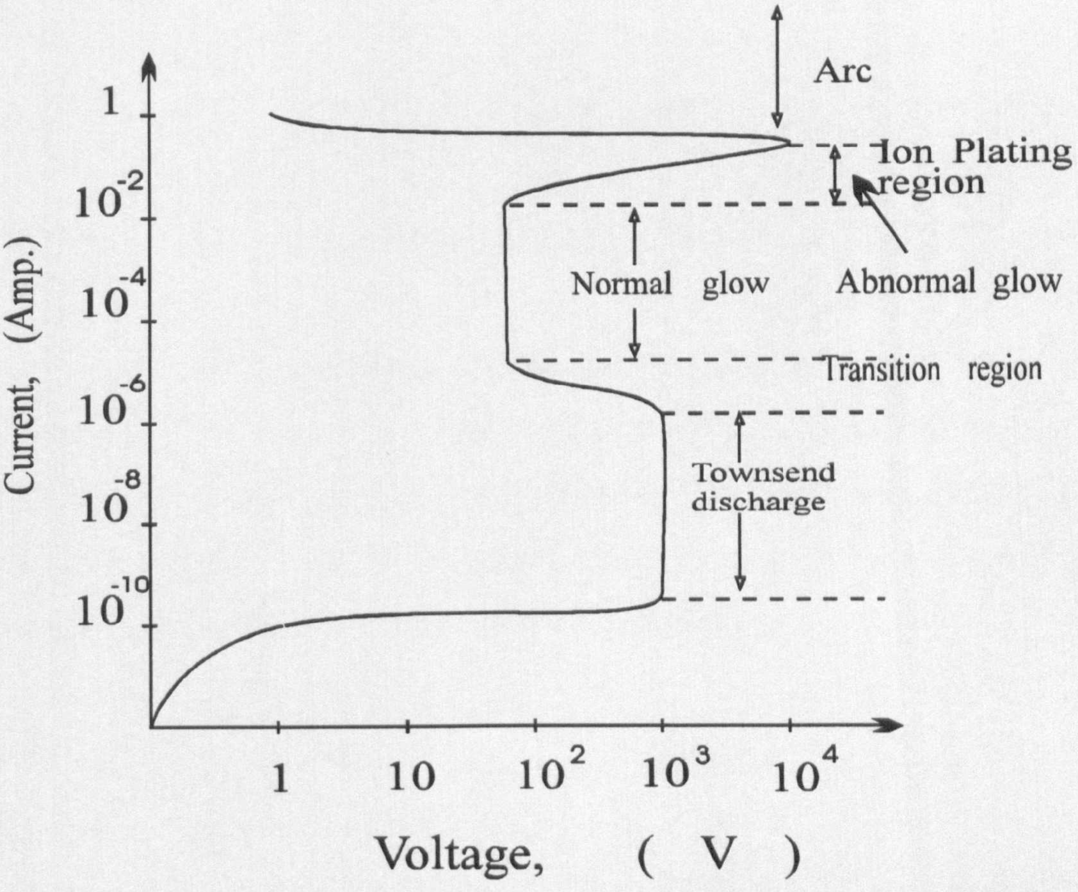

Fig. IV.1 Volt-Ampere characteristics of gas discharge.

This type of discharge is obtained for cathode-anode distance from 10 to 20 cm and pressures between 1 and 6 Pa [81]. Within an abnormal glow discharge a number of dark and bright zones can be distinguished, the most prominent ones are shown in (Fig. IV.2)

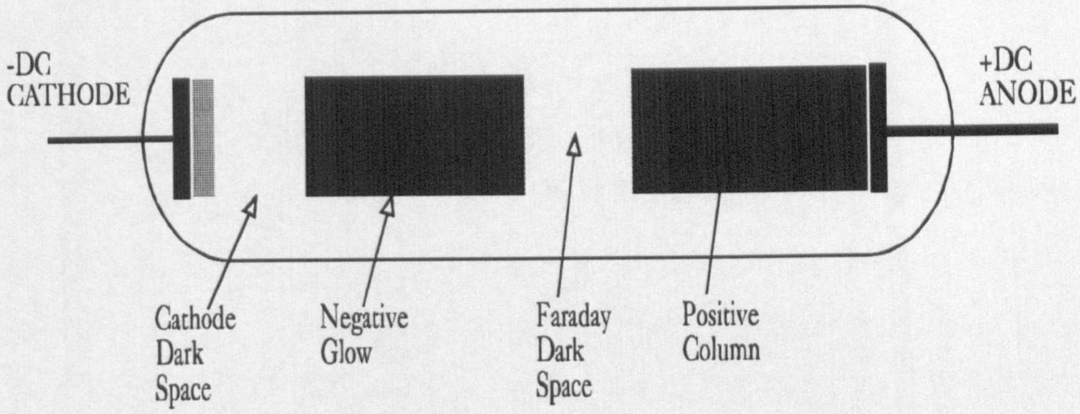

Fig. IV.2 Most prominent light and dark zones of abnormal glow discharge.

In the negative glow region, the voltage is practically constant and hence the electric field is very weak. This voltage is around 1 or 2 V in diode ion plating and is equal to the positive bias applied to the third electrode in a triode system [78]. In the cathodic region there is total break down of the voltage. Typically in ion plating only the cathode sheath and negative glow regions are observed.

E. 2 Mechanisms in Ion Plating

During ion plating the ions are produced in the negative glow region and are accelerated across the cathode dark space to the cathode.

Two types of particles are created in the discharge:

- energetic particles (neutrals)
- ionised particles

The role of the ionised particles is particularly important if the introduced gas is reactive, but the energetic particles play always an important role. When the gas is inert, their participation is mainly physical; they sputter the substrate or the coating during growth.

E. 3 Physical Aspect of the coating process

Three important steps can be considered during coating deposition by ion plating:

- Substrate cleaning before coating
- Interface substrate-film formation
- The coating itself.

E. 3. 1 Substrate cleaning

Before deposition of a coating a discharge is produced in an inert gas (generally argon), so that the substrate is subjected to intense ionic bombardment. The ions, coming essentially from the gas supporting the discharge, sputter-clean the substrate from oxides, water vapour, etc. a relatively clean substrate surface is thus obtained. To avoid recontamination of the substrate, evaporation is started while the cleaning process is continuing.

E. 3. 2 Interface substrate-film formation

The ions of the gas supporting the discharge continue sputtering of the substrate and the film during growth. Therefore, in the substrate vicinity there are:

- ions and atoms of the gas supporting the discharge.
- ions and atoms of the material to deposit.
- ions and atoms of the substrate.

As the pressure is of the order of 2 Pa and the mean free path of the substrate atoms is of the order of 5mm a significant number of the substrate atoms return to the substrate during growth and get mixed with the atoms of the material deposited. Some of the evaporated material atoms are ionised in the negative glow region after collision with electrons. The ions created by these collisions are accelerated through the dark space and reach the substrate with energies high enough to penetrate a few nanometers. An important part of the energy transported by the ions is transformed into heat. The temperature of the substrate or the growing film will be relatively high and help diffusion between coating and substrate. The consequence of these three phenomena is the formation of a substrate-coating interface where the substrate and coating atoms are mixed - a pseudo diffusion interface.

E. 3. 3 Ionic bombardment during coating

Two competitive phenomena are simultaneously occurring at the surface of the part: one, the deposition of the coating-material particles, the other, the sputtering of the coating by the energetic ions and neutrals. The effective rate of deposition is determined by the relative rates of these two phenomena. The deposition rate must exceed the sputtering rate to obtain a coating. The bombardment results in compactness and strong adherence of the film.

The technique suffers, however, from the disadvantage of film sputter-etching during growth and at high energies damage can also result. A better and more meaningful ion plating technique involves ionisation of the vapour by bombardment with accelerated electrons from a thermal source and depositing the ions onto a substrate, with or without post-ionisation acceleration. This technique is a process used in this project (Chapt. VII). It is called filament enhanced r.f. or d.c., PAPVD (Plasma Assisted Vapour Deposition).

E. 4 Ion energy distribution in ion plating

It is now known [79] that the ions arriving at the cathode are not monoenergetic and that the plating flux energy distribution ranges from thermal energies up to the voltage applied to create the discharge. In a dc discharge the voltage across the sheath is the target voltage V_t minus the plasma potential V_p; this is the voltage accelerating the ions towards the cathode. The energy of the ions reaching the cathode is, however, less than $(V_t-V_p) = V_c$ because of charge exchange collisions of the type.

$$Ar + Ar^+ \longrightarrow Ar^+ + Ar$$

The energy distribution for Ar ions striking the target is shown in (Fig IV.3) which shows excellent agreement between experiment and theory [78,82].

The impact energy is physically one of the most important parameters in the deposition of dense films. Since the ion energy is difficult to measure directly in dc and r.f. systems, most workers use the discharge power and gas pressure to study the effect of impact energy on film properties. The ion energy loss by inelastic collisions occurs in the dark space, this region should therefore be as small as possible. This can be achieved in a triode-system (positively biased electrode [83] or negatively biased electron-emitter [84]).

In the case of ion beam techniques, since the substrate is located outside the plasma and in higher vacuum, the ion energy loss by inelastic collisions is therefore minimised and the species energy is accurately controlled. This is a significant advantage over other deposition methods. However low energy ion beams (V ≤ 1000 V) do not exist because of the relatively high voltage needed to extract the beam from the ion source.

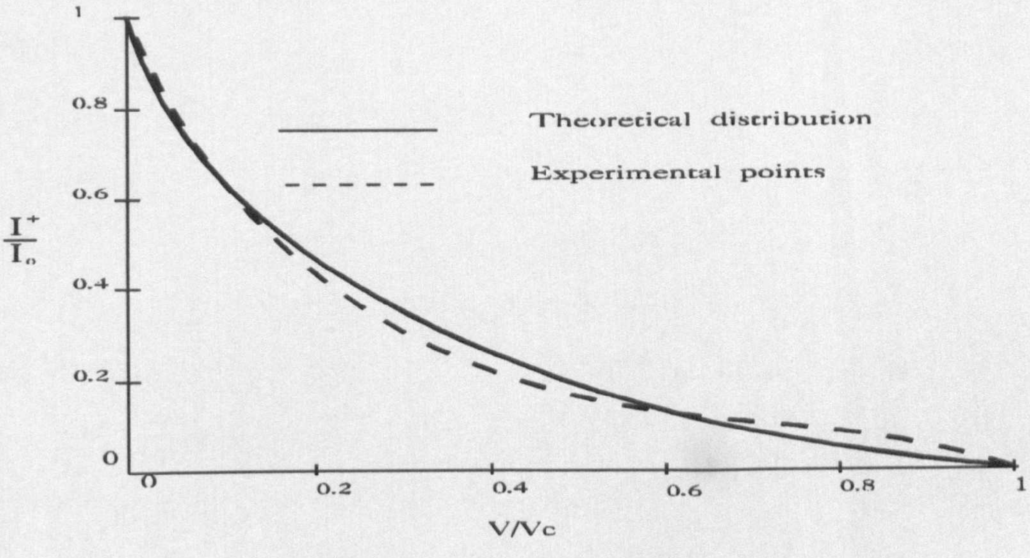

Fig.IV.3 Energy distribution for Ar^+ from an argon discharge [82]

CHAPTER V

SPECTROPHOTOMETRY

1. Infrared absorption

1. 1 Introduction

Infrared spectroscopy is a characterisation technique that gives accurate information on the covalent bonds between atoms. The molecular structure of an organic material, for example, can be determined by comparison of the obtained spectrum and other spectra used as references.

In this study, we are interested mainly in the type of C-H and C-C bonding in the films. This information is obtained from the absorption or transmission spectra obtained by different procedures: Transmission or Reflection.

Quantitative measurement such as relative concentration of bonded hydrogen to carbon, the proportion CH_3 / CH_2/ CH and the ratio sp^3 / sp^2 can be obtained when good spectrum resolution is obtained. This technique is often used by workers in the DLC field [85,86]

A relatively small paragraph on theory is included in this section since this is adequately dealt with elsewhere [87,88]]. This is followed by a brief description of the procedures used for thin films and powder absorption characterisation. Description of the spectrophotometer (double and single beam instruments) is presented at the end of this section.

1. 2 Elementary theory.

In order to understand the origin of infrared absorption spectra it is necessary first to see where the infrared "range" fits into the overall spectroscopic picture. At the same time, the units of measurement should be considered, the two systems in use are based on wavelength, λ, (expressed in μm) and wave number ν ($\nu = 1/\lambda$) (expressed in cm^{-1}). The wave number is actually the number of waves per centimetre and is also directly related to the true frequency $f = c/\lambda$ and the quantum energy $E = hf$ where h is the plank constant ($h = 6.626 \times 10^{-34}$ Js). The ranges and relative unit values are shown in Fig.V. 4:

The energy acquired by a molecule can be utilised in several ways:

a- Electronic excitation

b- Vibration change

c- Rotational change.

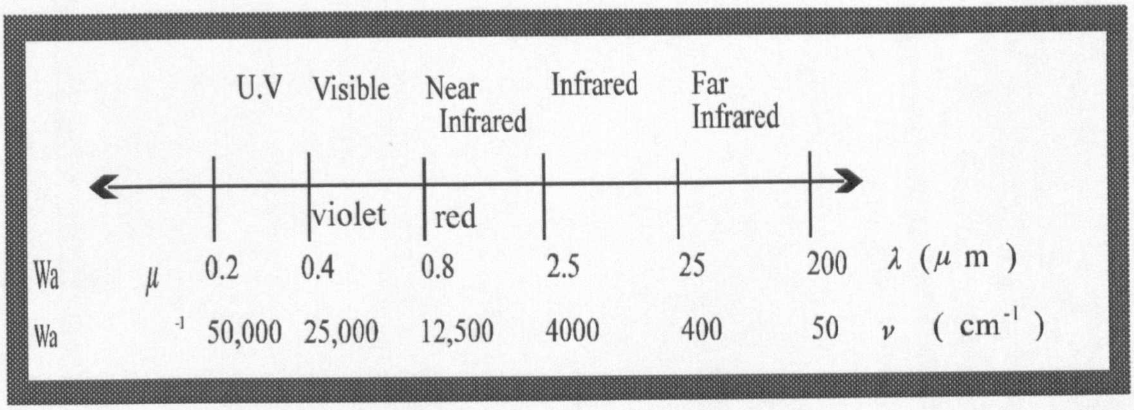

Fig. V. 4 Ranges and relative units for λ and ν from UV to far infrared.

For a molecule, the average energy involved in electronic excitation (E_1-----►E_2) is 5eV. For molecules in a particular electronic state, the average energy involved in a vibrational excitation (V1 ----► V2) is 0.1eV and a rotational excitation (R_1 ----► R_2) involves about 0.005 eV.

Since 1 eV = 1.602 x 10^{-19}J, and E = hf, 5eV corresponds to f = 1.2 x 10^{15} Hz so:

5 eV corresponds to ν = 40000 cm^{-1}

0.1 eV corresponds to ν = 833 cm^{-1}

and 0.005 eV corresponds to ν = 40 cm^{-1}

So that:

Light absorption at 40.000 cm^{-1} (ultraviolet) produces electronic change.

Light absorption at 800 cm^{-1} (infrared) produces vibrational change.

Light absorption at 40 cm^{-1} (far infrared) produces rotational change.

Whilst it is possible to cause a molecule to undergo a rotational change alone, a vibrational change is always accompanied by rotational changes and an electronic change has vibrational and rotational changes superimposed upon it. Thus in infrared spectroscopy we are interested mainly in the vibrations and rotations induced in a molecule by absorption of radiation.

A molecule has to be electrically asymmetrical to react with electromagnetic radiation (and hence absorb it). This is why homopolar molecules (H_2, N_2, O_2,...) have no absorption in the infrared whereas molecules like HCl, CO, CH_n,... do show strong infrared absorption.

1. 2. 1 Vibration - rotation in simple molecule

We are concerned, in the main, with vibration of two nuclei with respect to each other, connected by the electron cloud which forms the bond. The most elementary treatment is to liken the bonds to a spring and assume the two masses m_a and m_b oscillate in a simple harmonic fashion. Then, according to classical physics.

$$2\pi\nu c = (k/\mu)^{1/2} \qquad (1)$$

where k is the restoring force constant of the bond and μ the reduced mass of the molecules.

Stretching vibrations of individual bonds within more complex molecules may be considered similarly, though other vibrations become possible and absorption band frequencies are influenced by other factors.

Substitution in eqn. (1) of accepted numerical values of c, k and μ for the C-H bond gives a frequency of 3040 cm^{-1}, which is in tolerable agreement with found bond frequencies of 2975 - 2950 cm^{-1} and 2885 - 2860 cm^{-1} [89].

1. 2. 2 Bond vibration modes

Bond vibration modes are divisible into two distinct types: stretching and bending (deformation) vibrations, the former constituting the periodic stretching of the bond A-B along the bond axis. Bending vibrations of the bond A-B are displacements occurring at right angles to the bond axis.

Several different types of vibrations have been defined, these are represented diagrammatically in Fig. V.5 (stretching vibrations) and Fig. V.6 (deformation or bending vibrations) for both Ax_2 and Ax_3 groups.

1. 2. 3 Correlation charts:

Tables giving wave numbers for corresponding types of bonding between atoms are reported in the literature [89]. Since in this study we are interested in C-H and C-C configurations, Table V.1 taken from reference [90 - 92] is relevant to hydrocarbons only and has been used in interpretation of the infrared spectra studied in this work.

1. 2. 4 Absorption coefficient determination using Beer-Lambert law.

Beer's law and Lambert's law express, respectively, the relation of the intensity of absorption to changes in concentration and sample thickness. A general absorption law, which is a combination of Beer's and Lambert's laws, relates the absorption of incident

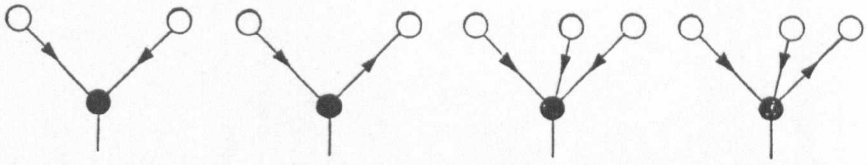

AX$_2$ symmetrical stretching

AX$_2$ asymmetrical stretching

AX$_3$ symmetrical stretching

AX$_3$ asymmetrical stretching

Fig. V. 5 Stretching vibration modes.

(Arrows indicate periodic oscillations in the direction shown.)

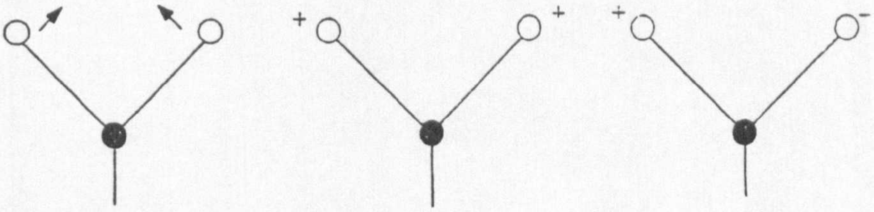

AX$_2$ in-plane deformation, or scissoring

AX$_2$ out-of-plane deformation, or wagging

AX$_2$ out-of-plane deformation, or twisting

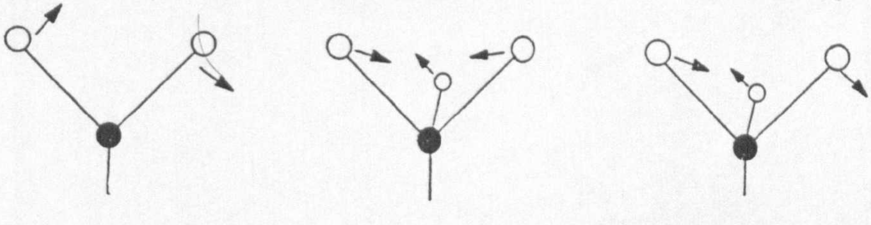

AX$_2$ rocking

AX$_3$ symmetrical deformation

AX$_3$ asymmetrical deformation

Fig. V. 6 Deformation (bending) vibration modes.

(The + and – signs represent, respectively, periodic motions above and below the plane of the paper.)

monochromatic radiation by a substance dispersed in a non-absorbing medium to both sample thickness and concentration, and is expressed [89] in the following equation :

$$I = I_O\ 10^{-kcd}$$

I and I_O are the intensities of the transmitted and incident radiation, respectively, k, is the extinction coefficient (absorptivity), c, the concentration of the substance (in g / l) and d the thickness of the sample (in cm)

In the case of solid sample (eg. thin film) (Fig. V.7)

The Lambert Law is used as:

$I = I_O \exp(-\alpha d)$ (α is the absorption coefficient.)

The transmittance, T, is defined as:

$T = I/I_O$

The absorbance, A, is defined as:

$A = \ln(1/T)$ (if the reflection can be neglected).

The absorption coefficient is therefore given by :

$\alpha = A/d$

TABLES V.1. GROUP ABSORPTION FREQUENCIES OF HYDROCARBONS [90-92]

ALKANES (SP^3)

		C-H Stretching Vibrations	C-H Deformation Vibrations
—CH_3—	**(asym.)**	2975 - 2950	1470 - 1435
	(sym.)	2885 - 2860	1385 - 1370
—CH_2—	**(asym.)**	2940 - 2915	1480 - 1440 (scissor.)
	(sym.)	2870 - 2845	
—CH—		2900 - 2880	1340

ALKENES (SP^2)

	C=C Streching Vibrations	**C-H Stretching and Deformation Vibrations**		
		stretch	**deformation**	
			in plane	**out of plane**
C=C	1680 - 1620			
$CHR=CH_2$	1645 - 1640	3040-3010 3095 - 3075	1420 - 1410 (CH_2) 1300 - 1290 (CH)	995 - 985 (CH) 915 - 905 (CH_2)
$CHR_1=CHR_2$ (sic.)	1665 - 1635	3040 - 3010	1420 - 1400 (CH)	730 - 665 (CH)
$CHR_1=CHR_2$	1675 - 1665	3040 - 3010	1310 - 1290 (CH)	980 - 960 (CH)
$CR_1R_2=CH_2$	1660 - 1640	3040 - 3010	1420 - 1410 (CH_2)	895 - 885 (CH)
$CR_1R_2=CHR_3$	1690 - 1670	3040 - 3010		850 - 790 (CH)

ALKYNES

Stretching Vibrations	
$RC\equiv CH$	3310 - 3300 C-H str 2140 - 2100 $C\equiv C$ str
$R_1C\equiv CR_1$	2260 - 2190 $C\equiv C$ str

AROMATIC COMPONDS

Stretching Vibrations	
=C-H	3080 - 3030 C-H str
C=C	1625 - 1440 C=C i.p. vib.
C-H In-plane Deformations and Benzene-Ring Substitution	
Monosubstitution and disubstititions	1225 - 1000

1. 3 Analysis methods:

The different techniques of quantitative and qualitative analysis of a material using infrared spectroscopy rely on classical absorption methods. The principles of some of these methods are briefly described below.

1. 3. 1 Absorption by transmission

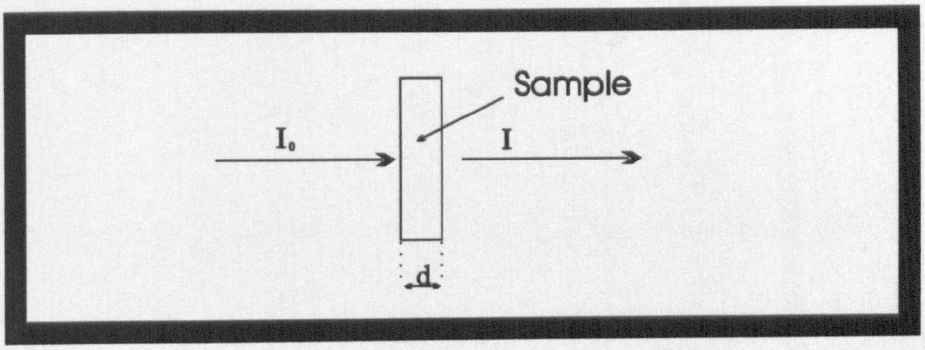

Fig. V. 7. Method of Absorption by Transmission

In this method a polychromatic beam (Fig. V.7) passes through the sample to be analyzed. The transmitted beam is then compared to the incident. A transmission spectrum is obtained from the ratio I/Io which is a function of the scanned wavenumber ν.

In the case of a thin film deposited on a substrate, the latter needs to be transparent in the wave number interval utilised.

1. 3. 2 Absorption by reflection

This method as shown in Fig. V.8 is used when the reflected beam intensity, R, is high enough to be detected. It is a very useful method for film deposited on reflecting surfaces. Substrate absorption and interference effects are however a disadvantage in this method, though the latter can be used for refractive index or thickness measurement as will be seen later. Powders are easily studied by reflection. The beam is reflected by scattering through the powder without reaching its support (Fig. V.9). Substrate effects and interferences are therefore non existent in this case.

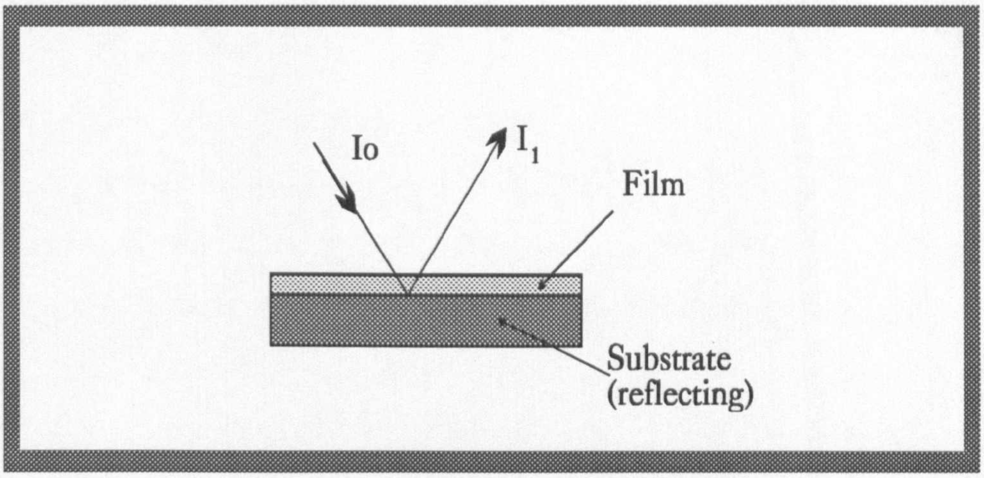

Fig. V. 8 **Method of Absorption by reflection**

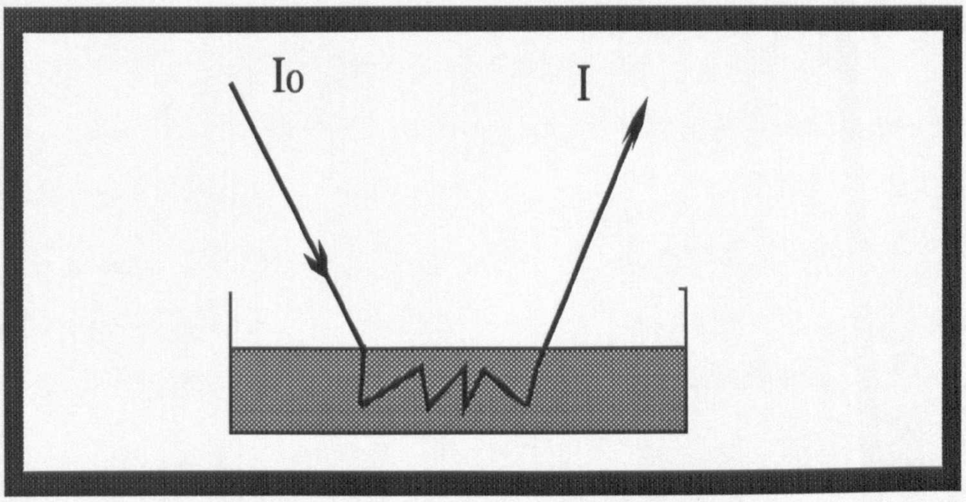

Fig. V. 9 **Method of Absorption by reflection from a powder**

2. Visible -UV absorption. (Electronic absorption)

2. 1 Principle

Because of the radiation-energy involved (1 -------►5eV) in the visible and ultra-violet, the absorption spectrum gives information about electronic excitation in the material studied. A sharp increase of the absorption coefficient, α, is the sign of photon energy absorption by electrons in the material.

The energy gained by the electron allows an electronic transition from the valence band to the conduction band. When an electron changes its state by collision with a photon, the energy and wave vector (k) conservation laws must hold. As a consequence of this selection rule, a transition can only occur between the two states belonging to the same k but to different energy bands, and any transition which changes k is forbidden. This is the main selection rule for optical absorption.

The energy corresponding to the absorption edge is the minimum value of the energy difference between two states for the same k; one in the conduction band and the other in the valence band. The absorption edge which is subject to the aforementioned selection rule (ie, transitions with constant k) corresponds to the transition from the state located at the top of the valence band to the state of $k = 0$ in the conduction band (Fig. V.10).

The wavelength of light which corresponds to a transition from the state located at the top of the valence band (A) to a state located at the bottom of the conduction band (B) is obviously longer than that of the above absorption edge (ie from A to C). But this transition cannot occur without the violation of the wave vector conservation law since k is not zero at the bottom of the conduction band.

The selection rule on k may be violated by the existence of imperfections in the crystal. For example, in optical absorption accompanying the emission and absorption of phonons, it is reasonable to allow k of the electron to change by q (the wave vector of the absorbed or emitted phonon), extending the law of wave vector conservation.

The sharp increase from A to B (Fig.V.10.a) corresponds to transitions due to light absorption accompanied by the emission or absorption of one phonon whose wave number is equal to the difference between the two wave numbers corresponding to $k = 0$ and $k = k_o$ (the bottom of the conduction band). The energy corresponding to this edge of the wave length is, therefore, the minimum value of the width of the forbidden band, and corresponds to the energy which governs the temperature-dependent characteristics of the conduction of electrons and holes in semiconductors.

2. 2 Optical band gap (definition & determination.)

Accordingly the energy corresponding to a sharp increase at the edge which satisfies the selection rule is called the optical band gap (E_{opt}) of the forbidden band, while the minimum value of the band-width of the forbidden band is called the thermal energy gap. A transition satisfying the selection rule is also called a direct transition, and a transition which does not satisfy the selection rule is called an indirect transition.

If a crystal is pure, the increase of α at the absorption edge is very sharp (vertical), the transition is direct, and the optical band gap is directly determined from the absorption coefficient spectrum, using

$$E_{opt} = h\,f = h\,c\,\nu$$

where ν is the wave number corresponding to the sharp absorption increase.

In practice the crystals are not always perfect. The absorption increase is not always very sharp and takes different shapes (eg parabolic or exponential). Therefore the optical band gap is not directly measured from the α spectrum. Some established equations linking the absorption coefficient and the photon energy are used for optical band gap determination. The theory leading to these equations uses Fermi-Dirac statistics in the study of photon, phonon and electron collision phenomena. The expressions involved in this theory are very complicated. For a more detailed description of the absorption process, the reader is referred to ref. [93].

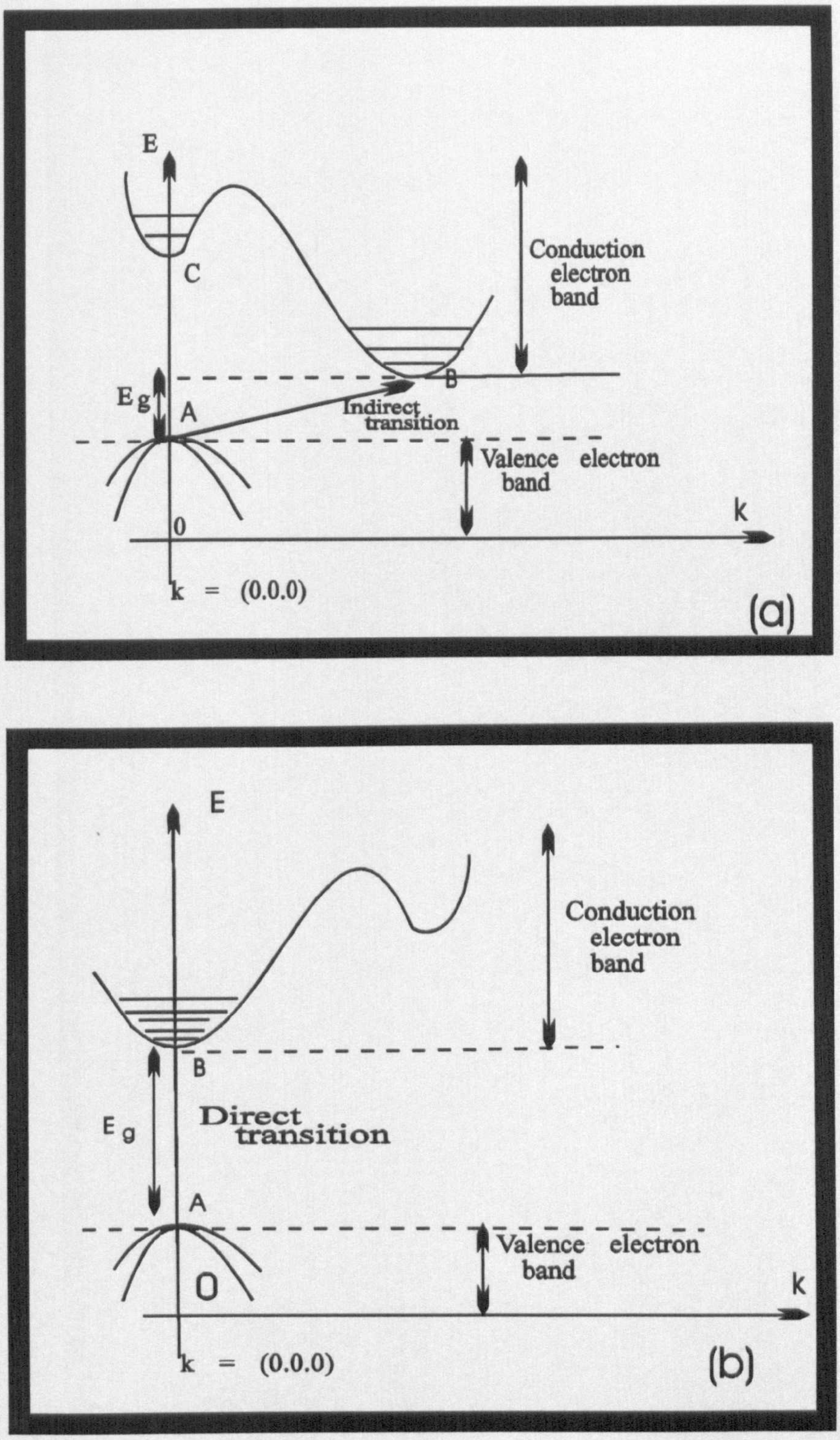

Fig. V. 10 Energy band diagram in a crystal.

(a) : Indirect transition, (b) : Direct transition

We shall therefore present only the final equations which are the most used for absorption coefficient determination:

a) Equation for direct transition in crystals.

b) Equation for amorphous materials.

a) Crystal material.

The expected variation of α with photon energy for direct transition is given by:

$$\alpha(E) = C(E - E_{opt})^{1/2}$$

where E is the photon energy and C essentially a constant [120]

A plot of α^2 as a function of E yields a straight line for a direct absorption. With an intercept on the photon energy axis equal to the direct band gap (E_{opt}) of the material. The equation relative to indirect transition due to phonons is slightly more complicated and is reported in the literature [94].

b) Amorphous material.

For amorphous materials, no sharp increase in α is observed, instead α increases gradually following a parabolic function. In this case, a number of procedures are in use to define the optical band gap. The simplest of these is to take E_{03} or E_{04} the photon energies at which the absorption coefficient reaches respectively 10^3 or $10^4 cm^{-1}$, as a measure of the position of the absorption edge [95]

A definition of E_{opt} that attaches more physical significance to the optical gap and the way it is derived was introduced by Tauc et al [96]. They found that the expected variation of α with photon energy at $\alpha > 10^4 cm^{-1}$ is:

$$(\alpha E)^{1/2} = B^{1/2}(E - E_{opt})$$

where B is constant.

When this relation is plotted in this form the linear extrapolation of $(\alpha E)^{1/2}$ versus E yields E_{opt}. Although the Tauc plot does not follow a straight line for all amorphous materials, it is however widely used and verified for amorphous materials. E_{opt} is sometimes called the Tauc gap and written as E_T.

3. Spectrophotometry for refractive index determination.

A relatively easier method for refractive index measurement than ellipsometry is usually used when interference fringes are obtained in a low absorption region of the absorption spectrum.

3. 1 Principle

For a thin film on a substrate we have to consider two interfaces:

Interface 1: The incident medium (complex refractive index Ni) / the film (complex refractive index N_f)

Interface 2: The film / substrate (complex refractive index Ns).

Taking into account the multiple reflections at the two interfaces (Fig. V.11), the reflectance and transmittance are given [4] by:

$$R = \frac{r_1^2 + 2\, r_1\, r_2 \cos(2\delta_1) + r_2^2}{1 + 2\, r_1\, r_2 \cos(2\delta_1) + r_1^2\, r_2^2}$$

$$T = (n_s/n_i)\, \frac{t_1^2\, t_2^2}{(1 + 2\, r_1\, r_2 \cos(2\delta_1) + r_1^2\, r_2^2)}$$

where $\delta_1 = (2\pi/\lambda)\, n_f\, d \cos\Phi_1$, d being the film thickness, $N_f = n_f + i\, k_f$, $N_s = n_s + i\, k_s$ and Φ_1 is the angle of refraction.

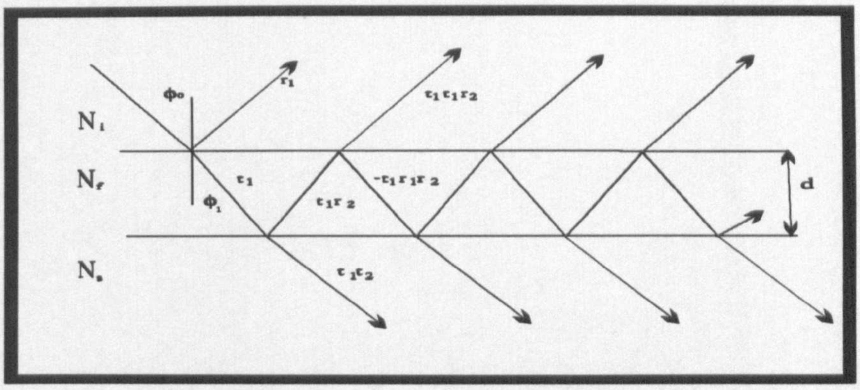

Fig. V. 11 Multiple reflections in a thin film

At normal incidence and at the spectrum region where the film is transparent, $\Phi_1 = 0$ and $k_f \simeq 0$, N_f becomes real. The transmittance and reflectance are oscillator functions of λ. The maxima (minima) in T_f and R_f occur when $(4\pi/\lambda)\, n_f\, d$ is even (odd) multiple of π. Therefore, the interference condition is used to derive values of n_f in the low absorption regime from the separation of transmittance or reflectance maxima when d is known. Therefore n_f may be calculated from the formula

$$n_f = \frac{p}{2d\,(\nu_1 - \nu_2)}$$

where p is the number of fringes between the maxima corresponding to ν_1 and ν_2.

NB. In the spectrum region where k_f is not null (ie $\alpha \neq 0$), this method can not be used and ellipsometry is used instead.

3 Spectrophotometry equipment utilised

The various types of spectrophotometer are double beam and single beam instruments. Spectra in the infrared regime were obtained using a modern single beam Fourier Transform Infrared Spectrophotometer (Nicolet SDX FTIR). Spectra in the near infrared, visible and ultra-violet were obtained using a Unicam SP 700 double beam spectrophotometer. All the measurement were done by the author in the Chemistry Department at Hull.

3. 1. Double beam.

(Fig. V.12) illustrates the optical path and principal components of a hypothetical double beam spectrophotometer. Technical details on the spectrometers components can be found in the literature [89].

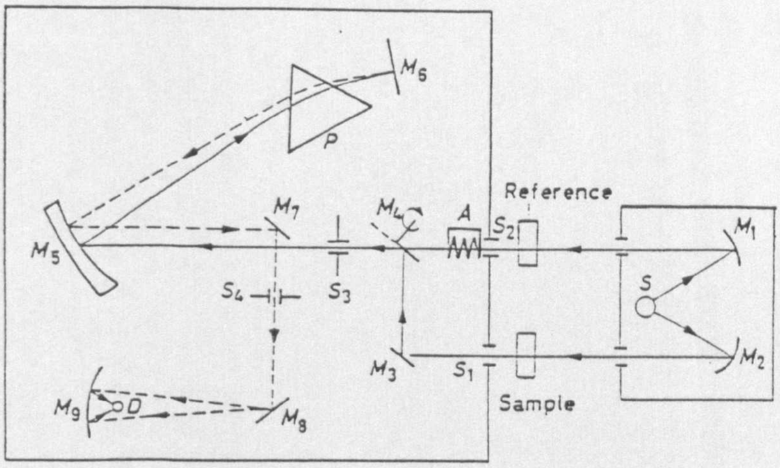

Fig. V. 12. Schematic diagram of a simplified double beam spectrophotometer

3.1.1. Procedure.

Two similar reference samples (identical glass slides for example) are put normal to the two beams in the sample and reference compartments (Fig. V.12). The spectrophotometer gives the ratio $I_1/I_2(\nu)$ on the paper chart. I_1 is then adjusted manually to match I_2. The spectrum obtained represents a 100% transmittance. Next, the coated sample (thin carbon film on glass slide) is put in the sample compartment after removing the non coated one. The spectrophotometer gives the ratio $Is(\nu)/Ir(\nu)$ (Fig. V.13).

Hence we have from Lambert's law,

$$I_r = I_o \, e^{-\alpha_r X}$$

where α_r and X are respectively the absorption coefficient and the thickness of the reference sample (substrate).

And for the coated sample we have:

$$I_S = I_O\ e^{-\alpha_r\ d}\ e^{-\alpha_r\ X}$$

where α_f and d are respectively the absorption coefficient and thickness of the film deposited on the same reference sample.

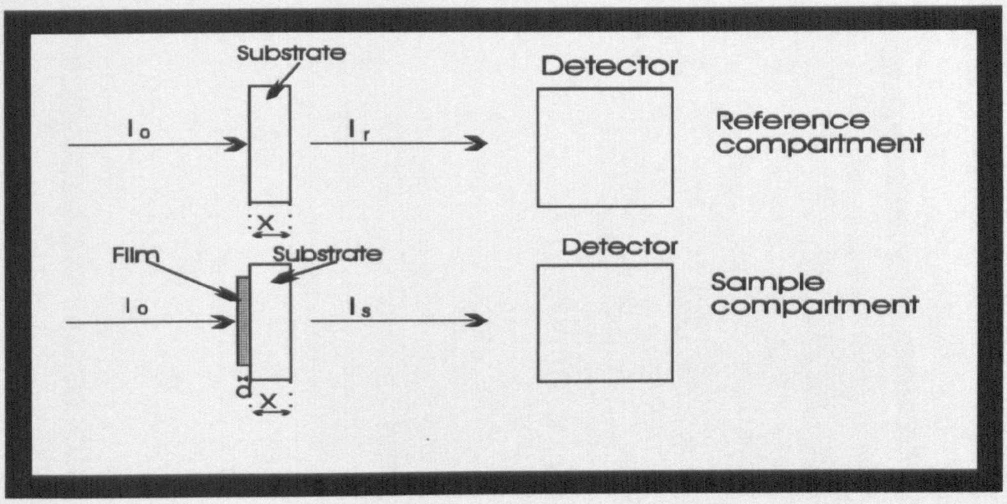

Fig. V. 13 Absorption by transmission procedure.

The spectrophotometer gives Is/Ir which can be written as:

$$I_S/I_r = \frac{I_O\ e^{-\alpha_r\ d}\ e^{-\alpha_r\ X}}{I_O\ e^{-\alpha_r\ X}}$$

$$= e^{-\alpha_r\ d}$$

Is/Ir is therefore the film transmittance, T_f:

$$T_f = e^{-\alpha_r\ d} = I_S/I_r$$

And the film absorbance A_f is given by :

$$A_f = \mathrm{Ln}\,(T_f)^{-1} = \alpha_f\ d$$

Finally α_f is obtained from:

$$\alpha_f = A_f / d$$

3. 2 Single beam.

Here the basic monochromator is linked to a suitable amplifier and recording system. The detector produces a square wave signal which is subsequently amplified, filtered and rectified electronically before display on the recorder. Figure V.14 shows a schematic layout of a single beam spectrophotometer.

Direct comparison of two materials is not possible using the single beam instrument. One sample only can be analyzed at a time.

3. 2. 1 Procedure

Without any sample in place, a background spectrum is first detected and recorded as $I_B(\nu)$ This spectrum contains CO_2 and H_2O absorption bands due to absorption in the air . A spectrum is then obtained from a reference sample (the substrate in our case) and recorded as $I_r(\nu)$. Finally the sample (substrate plus film) is analyzed and a spectrum is detected and recorded as $I_s(\nu)$. In the case of the FTIR used the recording system is a computer linked to a detector.

The computer uses software especially made for spectrophotometry measurement, and displays on screen the following spectra:

$T_r = Ir\ (\nu)\ /I_B\ (\nu)$:Transmittance spectrum of the substrate (reference)

$T_s = Is\ (\nu)\ /I_B\ (\nu)$:Transmittance spectrum of the sample, (film plus substrate)

$T_f = Is\ (\nu)\ /I_r\ (\nu)$:Transmittance spectrum of the film.

In the same way the absorbance is displayed by calculating respectively, $A_r = \ln(1/T_r)$, $A_s = \ln(1/T_s)$, and $A_f = \ln(1/T_f)$

The computer does the division of the absorbance by the film thickness and displays on screen the film absorption coefficient spectrum :$\alpha_f(\nu) = A_f / d$.

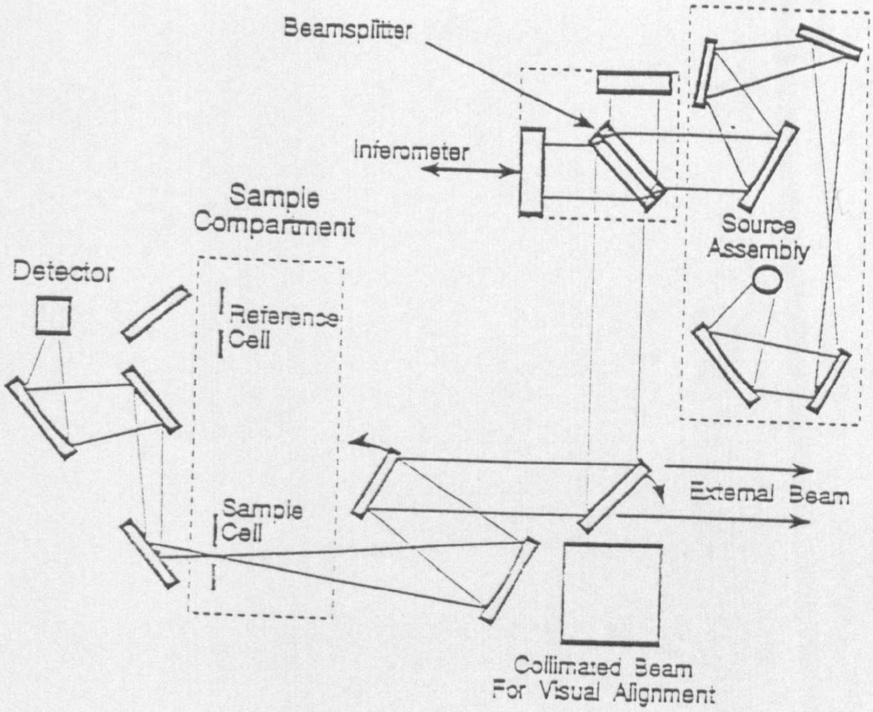

Fig. V. 14 **Schematic diagram of a simplified single beam spectrophotometer**

3. 3 Attachment for reflection-absorption analysis.

The spectrophotometers used in this study are equipped with reflection system accessories. Fig. V.15 shows the optical path in a reflection unit. This attachment does not work at normal incidence. Reflection has, however, to be done at normal incidence for quantitative measurements. For this purpose two identical reflection units have been built in the University workshop (Fig. V.16) which allow an incidence angle of 20°. This angle is a good approximation of normal incidence [97].

The spectrophotometer displays the ratio R_f/R_o where R_f and R_o are respectively the reflected light intensity obtained from the film on the substrate and a polished reflecting surface (metallic substrate or aluminium coated glass slide).

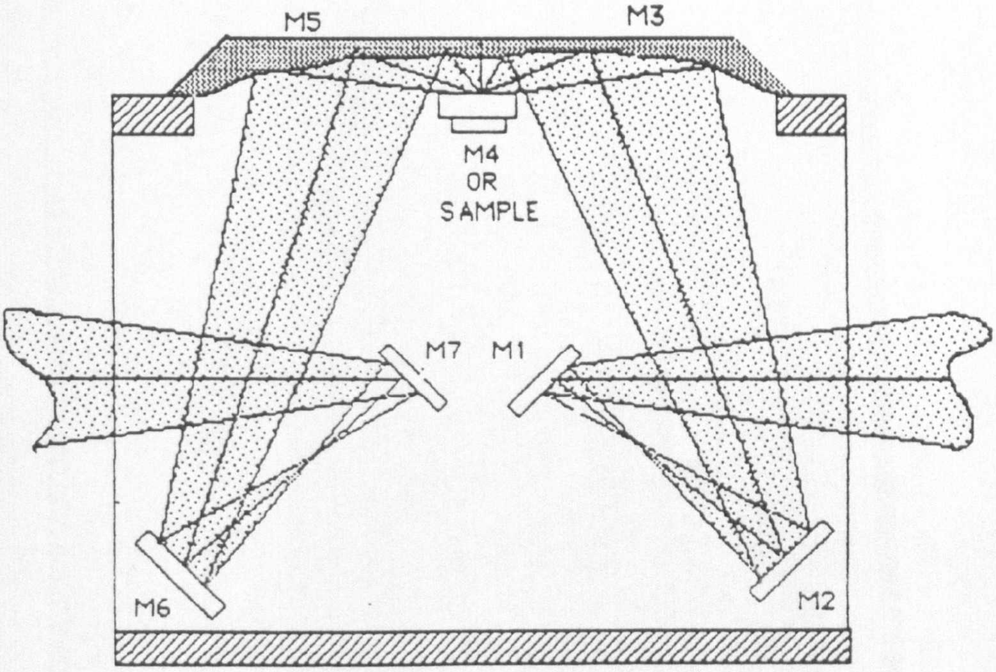

Fig.V.15 Optical system attachment for reflection analysis

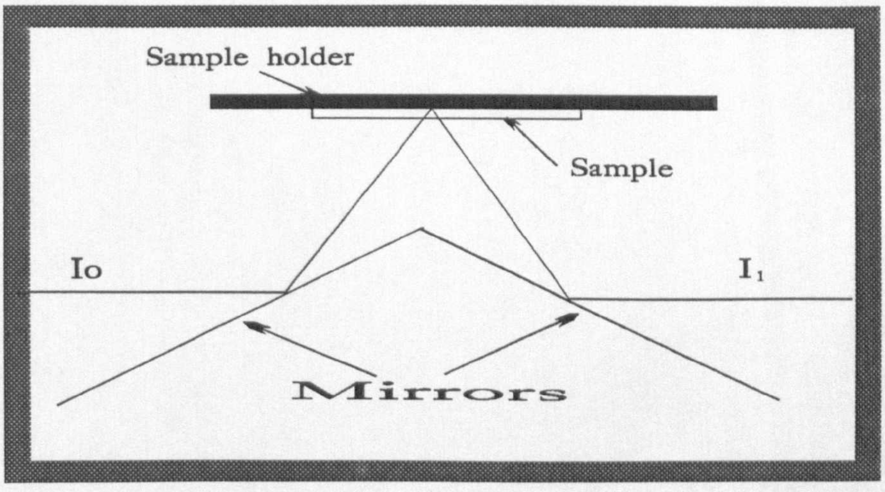

Fig. V. 16 Schematic layout of the attachment for reflection analysis at normal incidence

PART 3

EXPERIMENTAL, RESULTS, DISCUSSIONS AND CONCLUSIONS

CHAPTER VI

INVESTIGATION INTO FAB SOURCE FILMS

1. Introduction

The investigation in this chapter concerns carbon films produced by a Fast Atom Beam source. The work on this technique follows on from research reported elsewhere (eg [98]). Before starting this study it was known that the carbon films produced by the FAB source were very hard and semi-transparent in the visible (a 0.3μm film is brown and a 2 μm film is black and almost opaque); and transparency in the infrared regime is over 90% for films of 0.3μm. [7]. No quantitative values about their mechanical properties (hardness, adhesion, friction coefficient) were known. Their optical constants (optical band gap, refractive index), information on hydrogen content and type of C-H and C-C bonding had not been investigated. We, therefore, started this work by characterising the film properties. In a second step, an investigation on the effect of process parameters (effect of hydrogen, sample orientation, cathode voltage, annealing temperature and plasma parameters) on the film properties was carried out. Experimental details on the FAB. B93 source used are presented in the following section prior to the film properties investigation section.

2. Experimental details

2. 1. FAB B93 coating equipment:

The FAB B93 source used is a saddle field device [99], operated in the chamber of an Edwards E. 19A commercial evaporator. Fig. VI.1 shows a photograph of the unit. The construction details of the B 93 source are shown diagrammatically in Fig. VI.2.a & 2.b. Carbon films are prepared by introducing hydrocarbon gases into the source through a mass flow controller. A positive high voltage (1-3 kV) is applied to the anodes and a discharge is produced between the anodes and the internal walls of the source chamber. Depending on the anodes' voltage and the pressure inside the FAB source the discharge current varies from 0 to 300 mA. The plasma is in a source chamber which is lined with graphite, which is also the material used for the two anodes. The beam of particles emerges from a 25 mm aperture in the top of the source via an earthed graphite grid. In our work the samples were located at 30 cm in front of the grid (Fig VI.3). The pressure outside the FAB source is from 1 to 2×10^{-4} Torr and the substrate temperature is in the order of 35-50°C.

2. 2. Discharge mechanisms in the FAB source

The FAB B 93 source is a cold cathode device which operates at lower pressure than conventional cold cathode sources. This is due to the arrangement consisting of two positively biased parallel anode rods symmetrically disposed about the axis of a surrounding cathode cylinder, the electrostatic field has a saddle point midway between the two anodes. Electrons, originating from limited regions of the cathode wall by secondary emission, oscillate through this saddle point, describing long trajectories before being captured by an anode [100] The stable trajectories are concentrated about an axial plane normal to the plane of the anodes, but the envelope of trajectories does not include the anodes.

Fig. VI. 1 The Edwards E19 Chamber And The Fast Atom Beam Source.

All dimensions in mm.
Scale 1:2

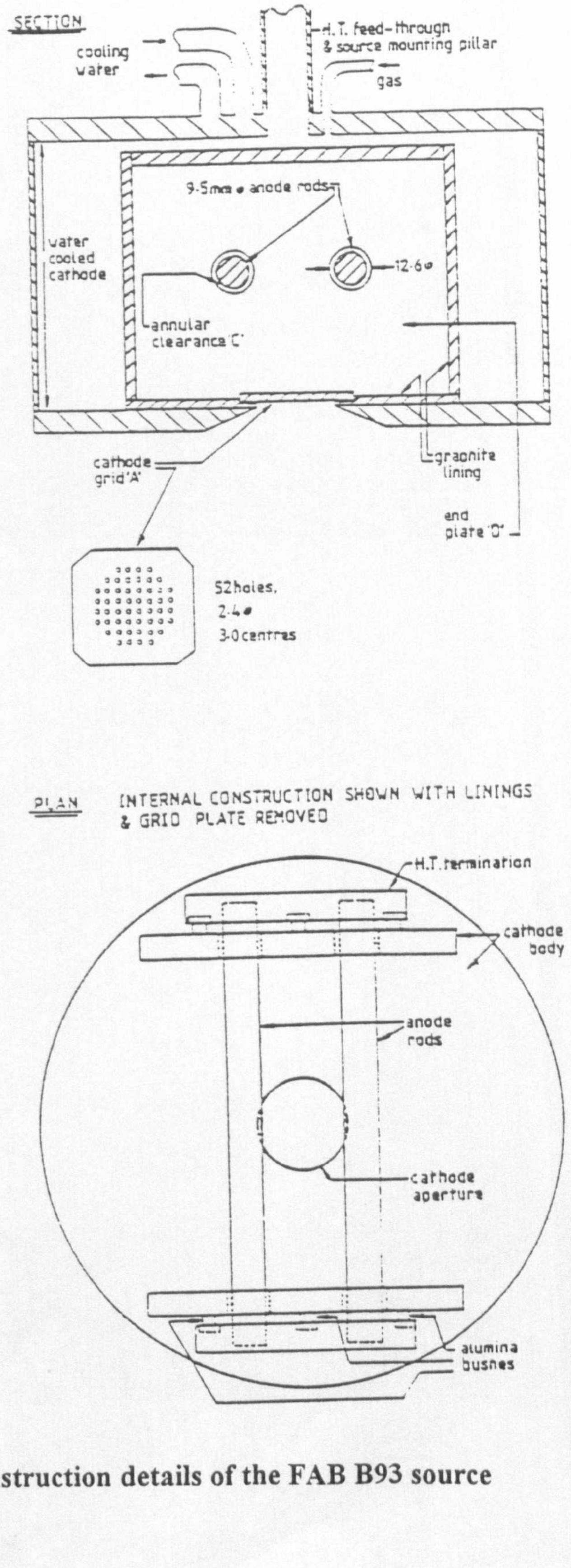

Fig.2.a Construction details of the FAB B93 source

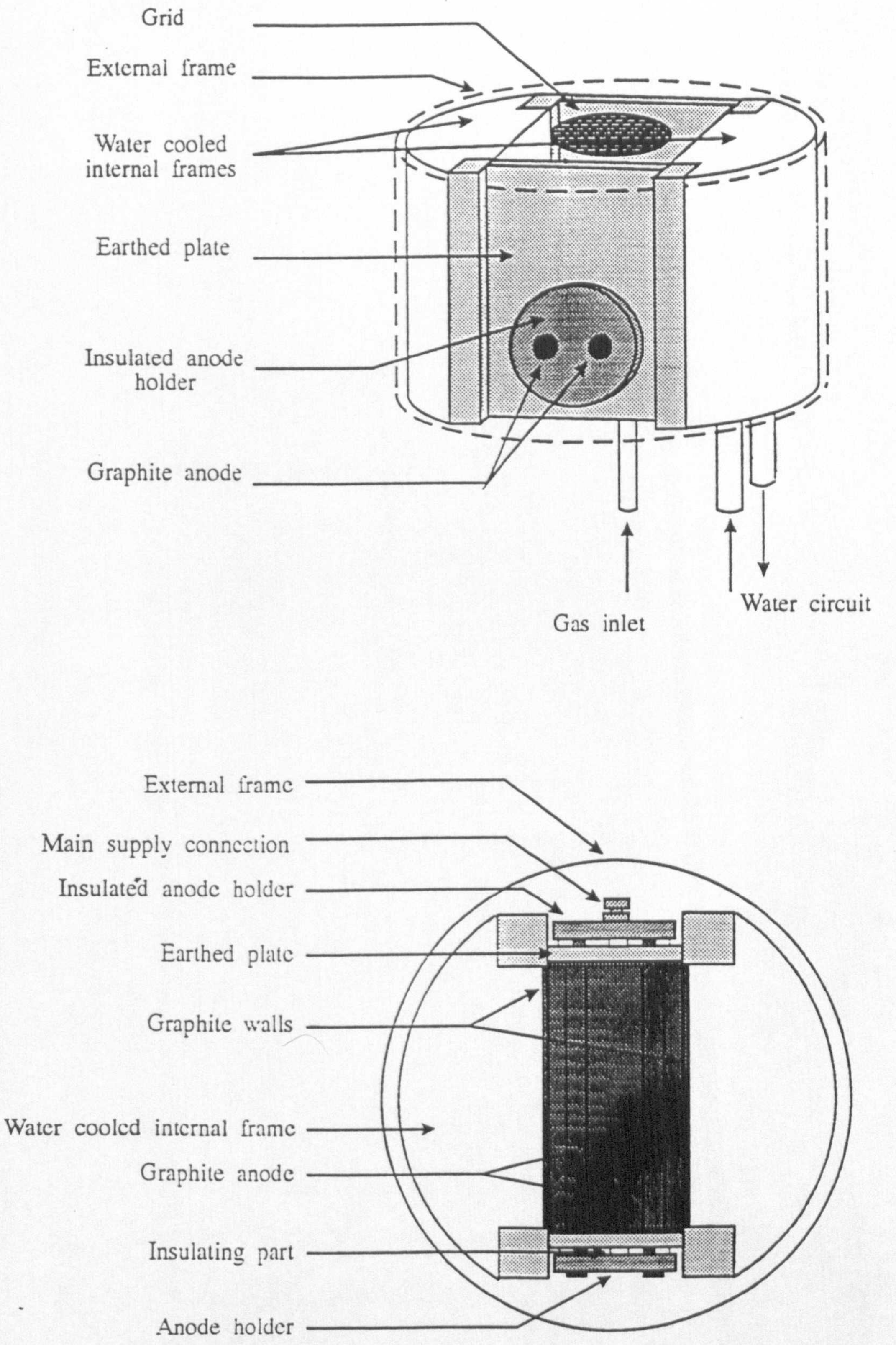

Fig VI.2.b FAB source diagram, top: in perspective, bottom; seen from above.

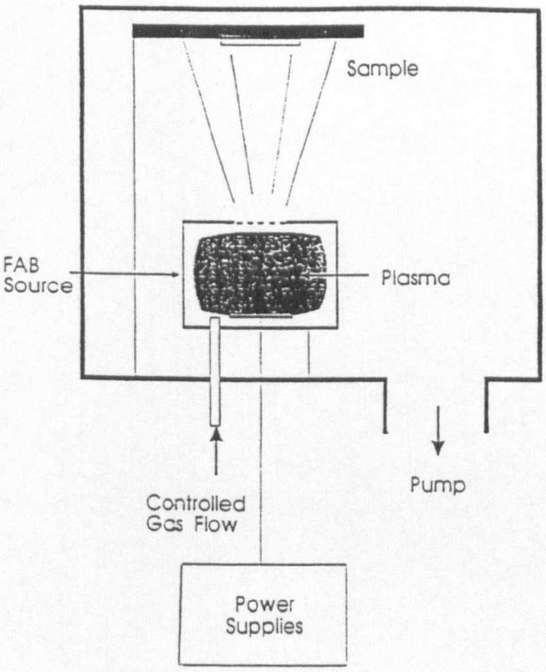

Fig VI. 3 Schematic diagram of a direct gas deposition using a FAB source.

In the presence of a gas, the positive ions formed in the discharge travel radially towards the cathode and emerge along straight paths when an aperture is introduced [100]. Extraction therefore does not present any problem when a gas is introduced, the probability of ionisation is high because of the long electron paths, so that a discharge can be maintained at relatively low pressure.

The mechanism of beam formation in saddle field sources lends itself to the production of almost wholly neutral beams without external charge exchange, in contrast to hot cathode sources. In such sources, the ions formed in the plasma assume random velocities and are extracted by an external field, the beam must therefore be wholly ionic. The reason why the beam from the FAB source is almost wholly neutral is not fully understood. Several hypotheses have been proposed on this subject eg: neutralisation by electrons created by secondary emission [99], or resonance transfer processes [101], whereby an electron is exchanged between an energetic ion and a slow gas atom.

2. 3. FAB source operating parameters

The discharge is maintained by direct current from a current-stabilised power supply unit. The discharge current I_D is variable over the range 0-300 mA. The anode potential (V_A) may not be controlled directly, but is dependent upon the plasma impedance. The impedance of the discharge is dependent upon the gas pressure within the source. This internal pressure may be varied by control of the flow rate into the source, provided the pumping speed is constant. In practice, V_A varies over the range 800 V to 4000 V at the maximum current drawn by the discharge. 800 V is considered the lowest operating voltage for this source (with an argon discharge) and is the threshold at which particles are extracted in significant quantities.

2. 4. Source instability

The FAB B93 source operated reliably with methane, acetylene, propane, or butane for more than 24 hours with little or no maintenance. Prolonged operation leads to discharge instability. The most frequent cause is carbon particulates sputtered from the plasma chamber or produced by the total dissociation of organic molecules becoming lodged in a region of high electric field. Regions most vulnerable to this form of tracking are the annular clearances between the anode rods and plasma chamber end plates (shown as "C" in Fig. VI. 2a) and to a lesser extent the space between the anode termination plates and plasma chamber ("D" in Fig. VI. 2a). The resulting low impedance in parallel with the discharge causes a rapid drop in V_A (as I_D is held constant) and a reduction in beam power. In severe cases the resistive paths may be sufficiently low to affect the operation of overload protection circuit.

Gradual deterioration of high voltage insulator bushes (alumina) usually results in voltage oscillations or short-circuit conditions. As these bushes are porous, organic material diffuses into the structure, and subsequent cleaning is ineffective.

Variation of beam power may also be caused by a change in the gas composition or flow rate into the source. Decreasing the flow will decrease the pressure inside the FAB source. The plasma impedance will therefore increase. As a result V_A increases (I_D constant). The length of time for stable operation decreases significantly when the source is operated at high power ($V_A > 2000V$, $I_D > 0.2A$)

Apart from beam power fluctuations as a characteristic of electrical malfunction, the presence of carbon particulates within the source may be observed as they are ejected at high velocity and are incandescent, indicating a particle temperature in the region of 1000°C.

In order to work in stable conditions, the FAB source was dismantled and cleaned up regularly. Carbon powder was found inside the source and removed during this cleaning operation. This powder results from bombardment of the carbon film grown on the cathode graphite plates (source internal walls). Therefore, the FAB source beam contains sputtered particles from this powder plus the particles coming directly from gas dissociation.

2. 5. Measurements

The hardness of the films was measured using a Knoop indenter at the lowest load producing a consistently measurable indentation (between 15 and 100g), taking an average of ten readings. The thickness was measured using a talysurf profilometer. Single-beam spectroscopy and ellipsometry were used for optical evaluations. The optical band gap was assessed from the visible wavelength absorption spectra, using the Tauc relationship, and refractive index was estimated from the interference fringes obtained by reflection in the low absorption regime. C-H and C-C bonding were identified using the IR Spectra. Details on these characterisation techniques have been given in Chapter V.

2. 6. Film preparation

The samples were located 30 cm in front of the grid. Three source gases were investigated: butane, propane and acetylene. The flow rates are listed in Table VI.1, together with voltage and current data. Three different substrates were used: glass, non coated polished tool steel (ASP 23, 64 Rc) and tool steel coated with titanium nitride. Precleaning was carried out initially with an acetone ultrasonic wash and then by hydrogen or argon bombardment using the FAB source for 20 minutes (2kV, 0.2 A on source anode). The substrate temperature in each case was about 50°C (this could be increased if the samples were closer to the source aperture).

2. 7. Deposition rate

One of the disadvantages of the FAB source and ion beams methods in general is the very low deposition rate: typically 0.3 μm/h. The deposition rate is a balance between the rate of arrival of the particles at the substrate and their rate of removal due to the sputtering effect of the energetic particles of the beam. With methane (CH_4), no deposition occurs and the substrate is etched, but as precursor gases are introduced with increasing carbon to hydrogen ratios the deposition rate increases. The rate for propane (C_3H_8) is 0.3μm h^{-1}, for butane (C_4H_{10}) it is 0.4μm h^{-1}, and for acetylene

(C_2H_2) it is 0.6μm h^{-1}. A similar progression was observed with a radio-frequency plasma [102]. The deposition rate was not constant. It reduced with time as the aperture in the grid became smaller. 10 hours or more are needed to deposit films of 2 μm thickness as shown in Table VI. 1.

Table VI.1

Summary of coatings deposited from the FAB source on glass, TiN and tool steel

Deposition parameters	Source gas		
	Butane	Propane	Acetylene
Flow rate (ml min^{-1})	11.6	15.7	12.8
Voltage (kV)	1.5	1.5	1.5
Current (A)	0.12	0.15	0.13
Pressure (Torr)	2×10^{-4}	1×10^{-4}	1.5×10^{-4}
Deposition time (h)	10	15	10
Thickness (μm)	2.2	2.1	1.8

2.7 Coating uniformity sample locations and

The thickness uniformity of FAB source fims is rather poor. When the sample is 30 cm above the grid the area coated represents a disc of 40 cm diameter. The thickness decreases with a rate of 10% at each location 10mm further from the centre to the edge of the coated area. This thickness decrease follows aproximately a gaussian law [103]. The substrates were always attached to the substrate holder in the center of the coating area and annalysed in their centre.

3. Results

A. Film morphology & Mechanical properties

A. 1. Film morphology

Under optical microscope observation, the film surface appeared to be covered with small grains which could be seen as small dots when observed with the naked eye. They can be considered as FAB source film signatures because similar grains were not observed in PVD or CVD films produced in this work. Under SEM observations these grains are found to have the appearance of hillocks (Fig. VI. 4). The film cross-section obtained by sample fracture after deposition shows in Fig. VI. 5 that FAB source coatings are very dense.

A. 2. Adhesion

The adhesion of FAB source films depended mainly on film thickness and substrate nature. the best adhesion was obtained on silicon and glass substrates. Films of 0.3 µm thickness on glass could not be scratched by a tungsten filament using hand pressure. This film could be scratched by a Knoop indenter using the microhardness tester. The critical load corresponding to film removal was 20g. Fig. VI. 6 shows scratch test tracks obtained for increasing loads 10g (each time) from 10 to 60g. (right to left in photo).

Adhesion on glass and silicon deteriorated with increasing thickness. Films of 2 µm or more showed debonding between the substrate and the carbon films. Optical microscope examination of these films revealed deformations and signs of high stress (Fig. VI. 7). Under optical microscope observation, stress deformation is sinusoidal or has complicated forms, and could be seen created at the substrate edges and at scratch tracks.

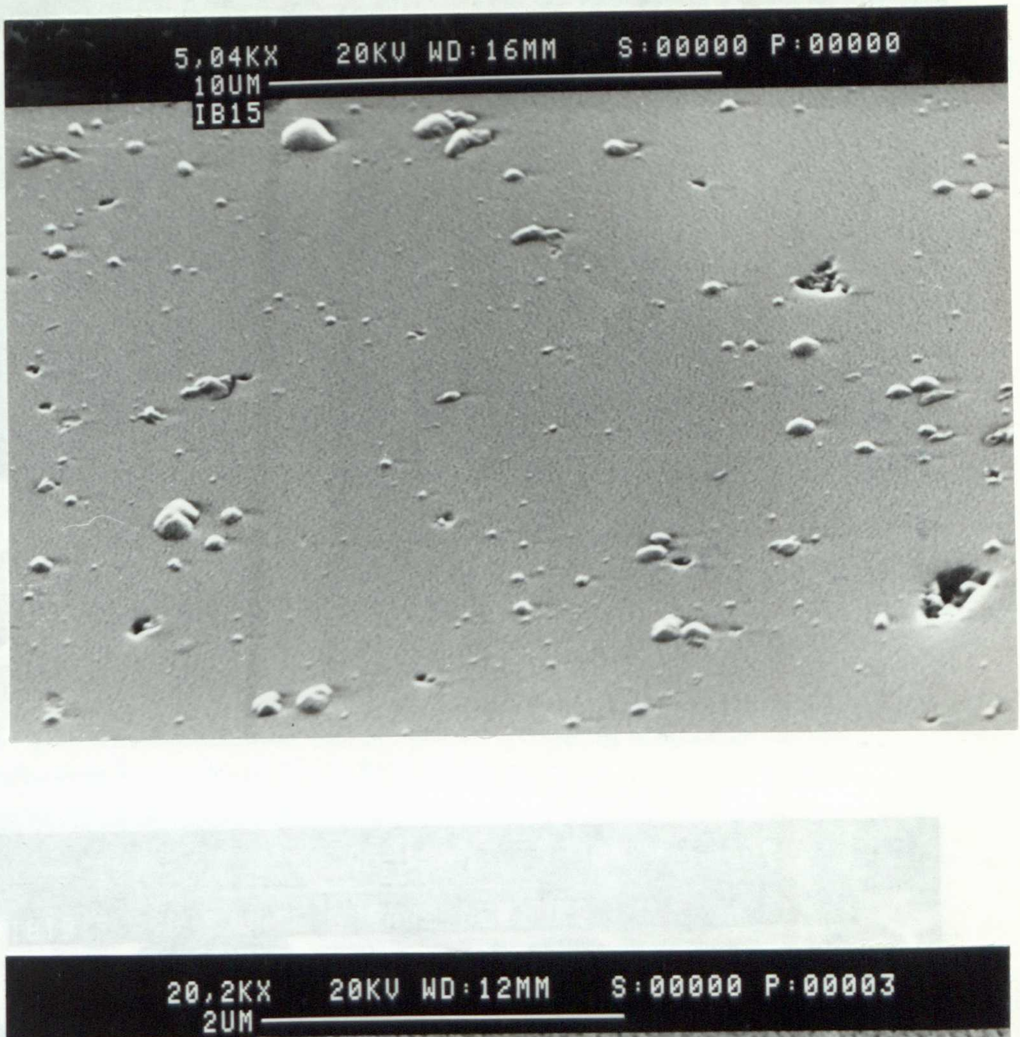

Fig. VI. 4. Scanning electron micrographs of hillocks observed on FAB source carbon films.

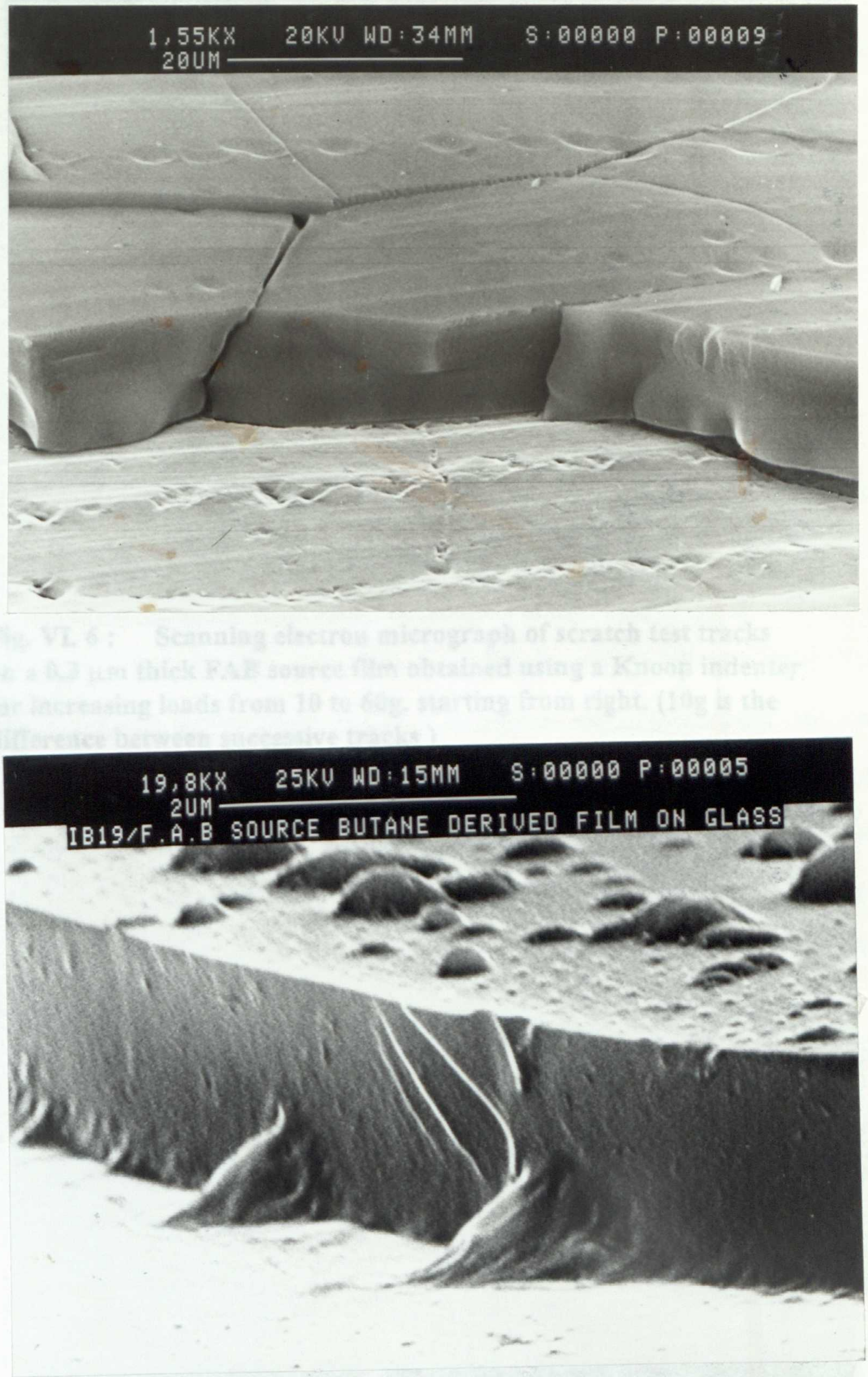

Fig.VI. 5 Scanning electron micrographs of FAB source carbon films; Top: Butane film on aluminium foil, bottom : on glass.

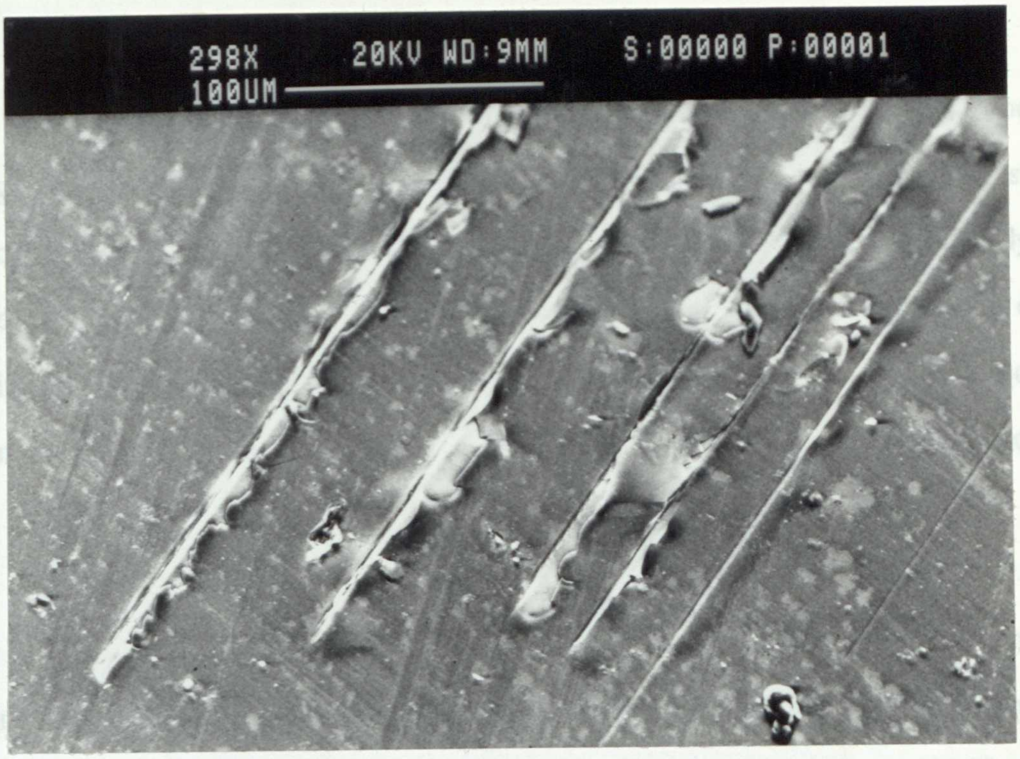

Fig. VI. 6 : Scanning electron micrograph of scratch test tracks on a 0.3 μm thick FAB source film obtained using a Knoop indenter for increasing loads from 10 to 60g. starting from right. (10g is the difference between successive tracks)

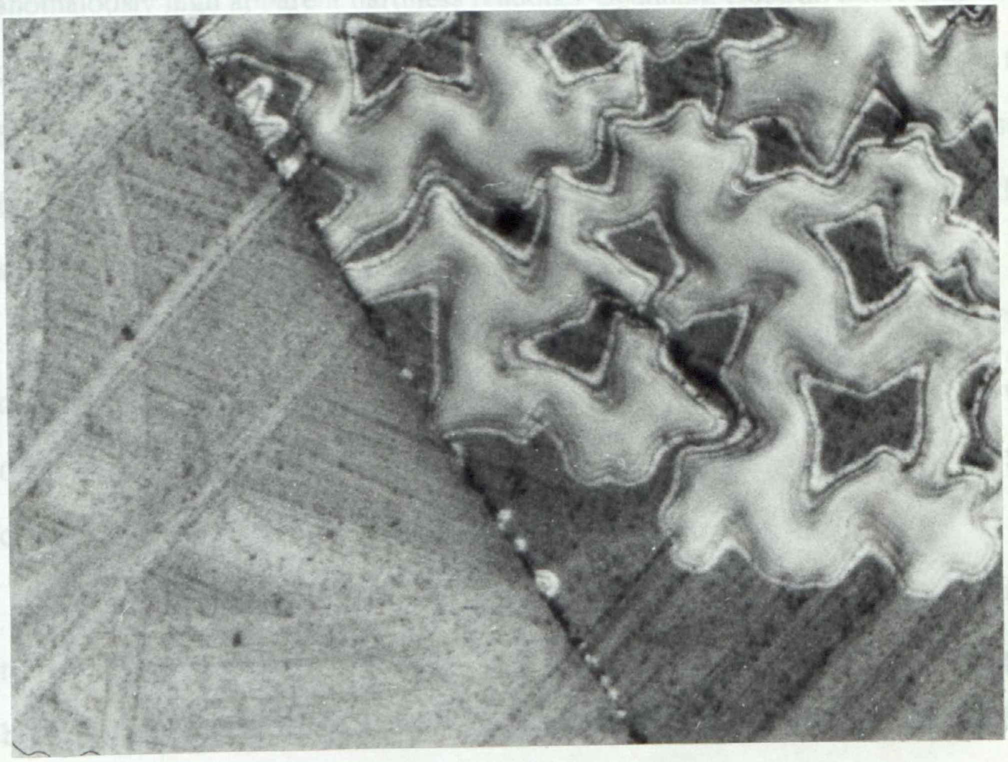

Fig. VI. 7 Optical micrograph of stress deformations observed in thick (> 2μm) FAB source carbon films .

On aluminium, mild steel and titanium nitride on steel, adhesion is as good as on glass slides as long as the film thickness is not more than 1.5 μm. On stainless steel and copper adhesion is very poor (the film debonded from the substrate immediately after deposition.). Good adhesion is generally obtained on a substrate that can form carbide interlayers. Precleaning, with argon bombardment of the substrate prior to deposition is necessary in order to obtain good adhesion, even if the substrate is glass or silicon.

A. 3. Hardness

The hardness of FAB source films which were of a sufficient thickness to permit micro-indentation hardness testing is around 2000 H_K. Very thin films (<0.3μm) gave lower hardness values; from substrate hardness at high load (25g) to 1500 H_K at low load (10g). Occasionally, some films show a hardness up to 8000 H_K (50g). These films, however, exhibit a high degree of elastic recovery of indentation. This can lead to anomalously high apparent hardness readings. Scanning electron micrographs of these ultrahard films show a higher number density of hillocks than is usual in FAB source films (Fig. VI. 8). However, it is clear from repeated tests that values in excess of 2000 H_K with a load of 25g are commonly achievable. This was observed with all three source gases used.

A very interesting exception was the film (0.5μm thick) deposited on TiN coated on steel. The hardness readings were around 5000 H_K (50g). No indentation was observed at 25g. Figure VI. 9 shows an SEM micrograph of its surface. This film is characterised by a high density of hillocks too.

Compared to the previous FAB source films, a relatively small elastic indentation recovery was observed in this film during microhardness testing . The film appeared to be brittle as noticed from the nature of the indentation deformation at higher loads (>50g). In order to resolve the elastic component from the plastic contribution, nanoindentation was performed for films with different hillock densities.

Fig. VI. 10, illustrates the hardness versus depth and the hysteresis curves obtained for ultra low loads (<5mN).

These measurements revealed that the hardness increased dramatically with increasing hillock density from 55GPa to 88GPa for the films on glass and to 100GPa for the film on TiN, (these values correspond to a load of 4.2mN). The percentages of elastic recovery at this load are respectively 31, 40, and 26 at %, as summarised in Table VI.2.

These hardness values are extremely high compared to the hardness of the usually produced FAB source films and PVD films which is around 20GPa. It is known that hardness versus depth curves often exhibit high apparent hardness values close to the surface (Fig. VI.10); this is because no diamond indenter will be perfectly sharp, and therefore a higher load than the theoretical will be required to initiate an indentation . Fig. VI.10 shows that the film on TiN exhibited the highest apparent hardness at the start of the indentation. The film on TiN is therefore more resistant than the others to the indentation penetration. This resistance could not be attributed to elasticity alone since its elastic recovery is not the highest (Table VI. 2).

Table VI. 2

Nanohardness and elastic recovery of typical FAB source films at a load of 4.2mN (V_A=1.5 kV, I_d = 0.1 A and Butane gas)

Substrate	hardness (GPa) at 4.2mN load	% indentation elastic recovery	hillock density
glass	55	31	low
glass	88	40	high
TiN on tool steel	100	16	high

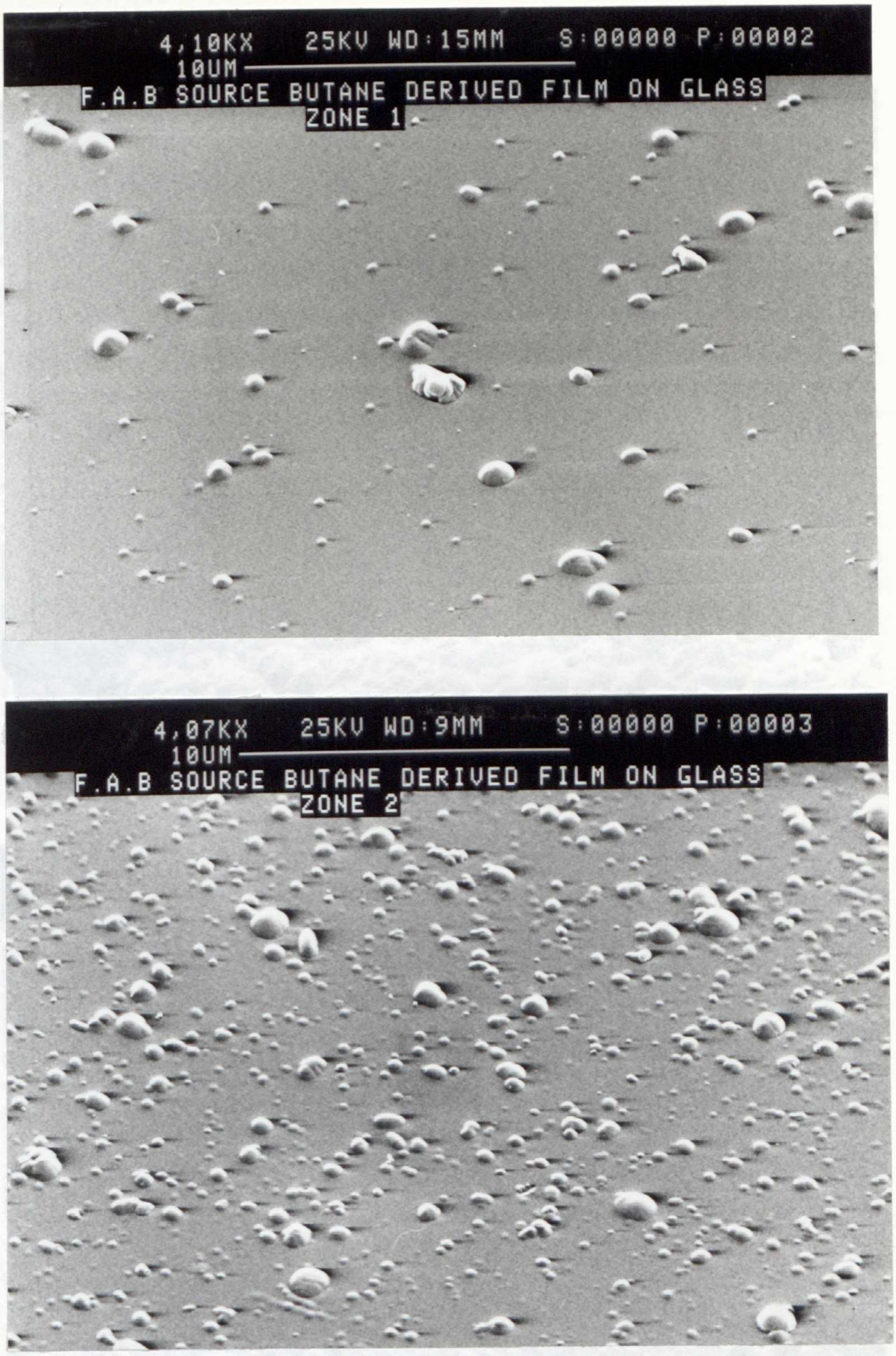

Fig. VI. 8. Scanning electron micrographs of hillocks on carbon films deposited on glass using FAB source B.93; (a) Hardness 2000 H_K at 25g load; (b) Hardness 8000 H_K at 50 g load

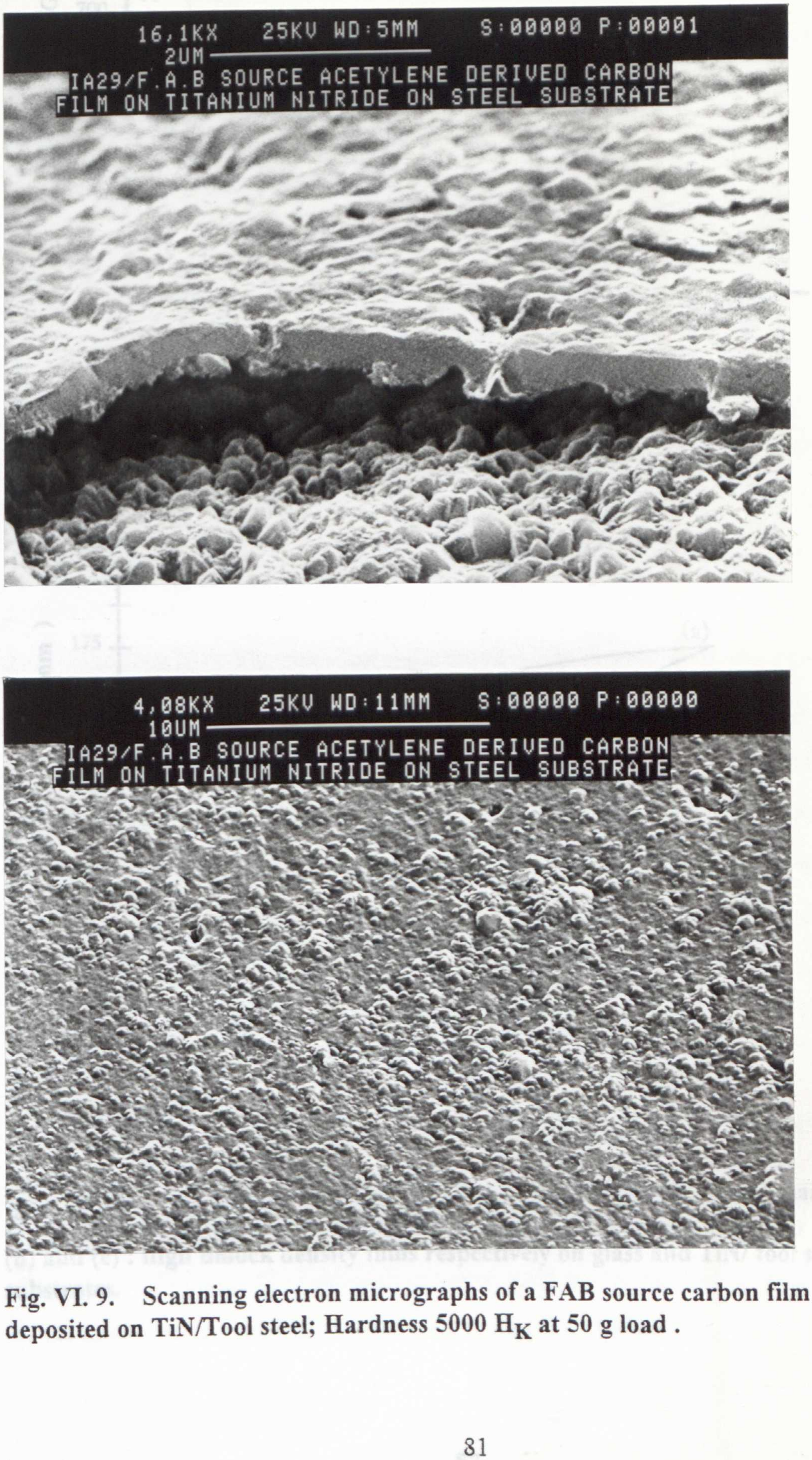

Fig. VI. 9. Scanning electron micrographs of a FAB source carbon film deposited on TiN/Tool steel; Hardness 5000 H_K at 50 g load .

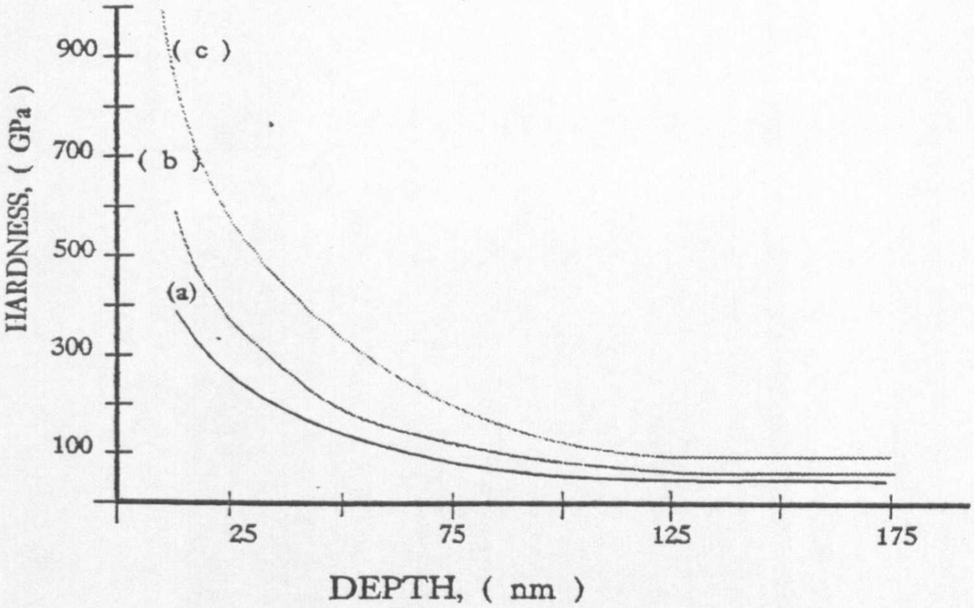

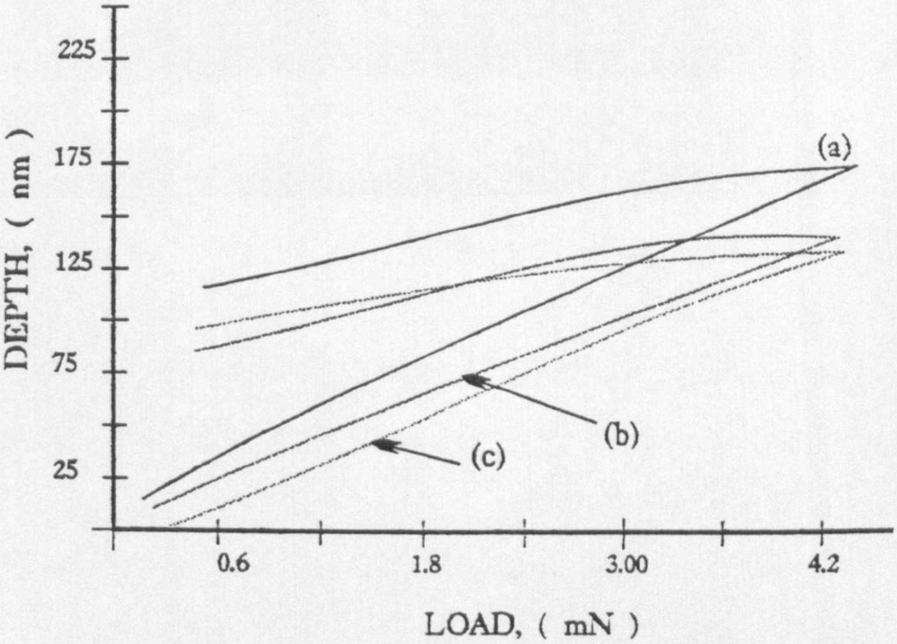

Fig. VI. 10 Nanohardness and elastic recovery of different FAB source carbon films; (a): low hillock density film on glass substrate.
(b) and (c) : high hillock density films respectively on glass and TiN/ tool steel substrates.

A. 4. Pin on disc test

Intensive tribological study of the FAB source films and the PVD films produced in this study was the main objective in Dr P. Holiday's research. In this section a brief summary of the performance of FAB source films in the pin on disc machine is presented; for more details on this subject the reader is referred to Dr P. Holiday's thesis [64].

For most of the films tested the friction and wear was excellent in comparison to the "standard" SAE 52100 pin material against an ASP23 tool steel substrate with no signs of cohesive failure after 100 metres sliding.

Testing exhibited a film wear of $9\text{-}10\times10^{-6}$ mm^3/Nm and the steady state coefficient of friction was recorded to be $\mu=0.10\text{-}0.15$ [64]. The best performance was obtained from the film deposited on TiN (described earlier). The combination of a hard coating and strong interfacial bond in this film provided the lowest frictional and wear partnership recorded for all the DLC films tested ($\mu=0.05$) and a film wear of 2×10^{-6}mm^3/Nm [64]. The reduction in the film wear, as determined by the size of the wear track, is approximately two orders of magnitude lower when coated with diamond like carbon on TiN compared to the non-coated specimen. The friction was reduced remarkably by an order of magnitude over that of the non-coated substrate and three times less than the majority of the DLC films [64]. The frictional behaviour was found to be largely insensitive to the humidity conditions although with the addition of a dry oxygen atmosphere a rapid increase in wear and friction was noted to occur immediately.

A. 5. Further studies on TiN as an interlayer for FAB source films:

The mechanical property results obtained when TiN was used as interlayer supporting FAB source films although excellent could not be taken as definitive, since only a small number of samples coated with TiN and DLC were tested.

The discussion in this section is focused on the reproducibility of DLC /TiN performance. For this study three thick (3μm) and three thin (1μm) TiN coatings were deposited on cobalt-chrome substrates. These films appeared to have excellent adhesive strength, with a surface roughness similar to that of the bare substrate. Vickers hardness tests on of these interlayers indicated average values of 1330kg/mm^2 (25g) compared to 500kg /mm^2 (25g) for the non-coated cobalt-chrome substrate. Optical observations of the titanium nitride films showed them to be highly reflective and gold in colour. These films were then coated with FAB source films of different thicknesses (thin and thick). All the films were tested by the pin on disc sliding wear test method. Microhardness indentation tests were carried out prior to the wear tests and revealed the layers to have values around 2000H_K (25 g). Observation of the DLC surface showed a low hillocks density. This result suggests that the high hardness (5000H_K) obtained for the earlier films deposited on TiN was due to the high hillock density and not to the TiN interlayer.

The DLC films deposited directly onto cobalt-chrome without the aid of TiN showed excellent wear resistance (3-9 × 10^{-6}mm^3/Nm) and friction (μ = 0.15-0.17) [104]. Surprisingly tribological tests revealed these multilayered films (DLC/TiN) to have poor wear resistance properties. Failure occurred within the first metre of sliding distance in every case and appeared to be a result of the weak adhesive strength between the DLC and the Titanium Nitride layers [104]. The thickness of TiN film and deposition conditions of the DLC did not have any effect on this poor tribological performance. The coefficient of friction however, remained low for the duration of this tests, showing an initial recorded value of μ =0.3 leading to a steady state value of μ =0.2. This phenomenon was observed to occur for all the multilayered films with no exception. All these TiN layers were yellow/golden in colour but the TiN layers that gave excellent results (section A. 3 and A. 4) were grey in colour. It is known that the colour of TiN is dependent on the film structure an composition which is itself dependent on TiN deposition conditions [105].

A second series of TiN was deposited onto tool steel and cobalt-chrome using deposition conditions known to lead to films of different structure and colour. The tribological performance of the DLC films deposited on this TiN was markedly improved compared to that of the previous test. Profilometry of the wear track showed no failure of the DLC film with evidence of a substantial amount of material being transferred from the pin to the wear track.

This second series of TiN films was dull grey or brown in colour, showing little optical reflection, similar in appearance to a rough surface. However, measurement of the surface finish showed the roughness value to be equal to Ra =0.03μm compared to 0.050 μm as recorded for the other multilayered samples. This suggests that the surface of these films has a different structure which is beneficial to the adhesion of DLC coatings deposited on this surface. SEM observations (Fig. VI. 11) showed that the dull surface was covered with hillocks, while the surface of the golden/yellow TiN layer showed no hillocks or any features that would be beneficial to the adhesion.

A. 6. Discussion

The finding of the study in this section indicate that the DLC films produced by the FAB source technique have good wear and friction properties with only a small sign of localised failure especially fo films thicker than 1.5 μm after pin on disc sliding tests for 100 metres.

Initial studies using titanium nitride/DLC multilayer films indicated poor tribological performance for various thicknesses of TiN and deposition conditions of DLC. The study showed that the failure was caused by poor adhesion at the TiN/DLC interface. This adhesion, and therefore the wear performance, can be improved by utilising an over-stoichiometric composition of titanium nitride.

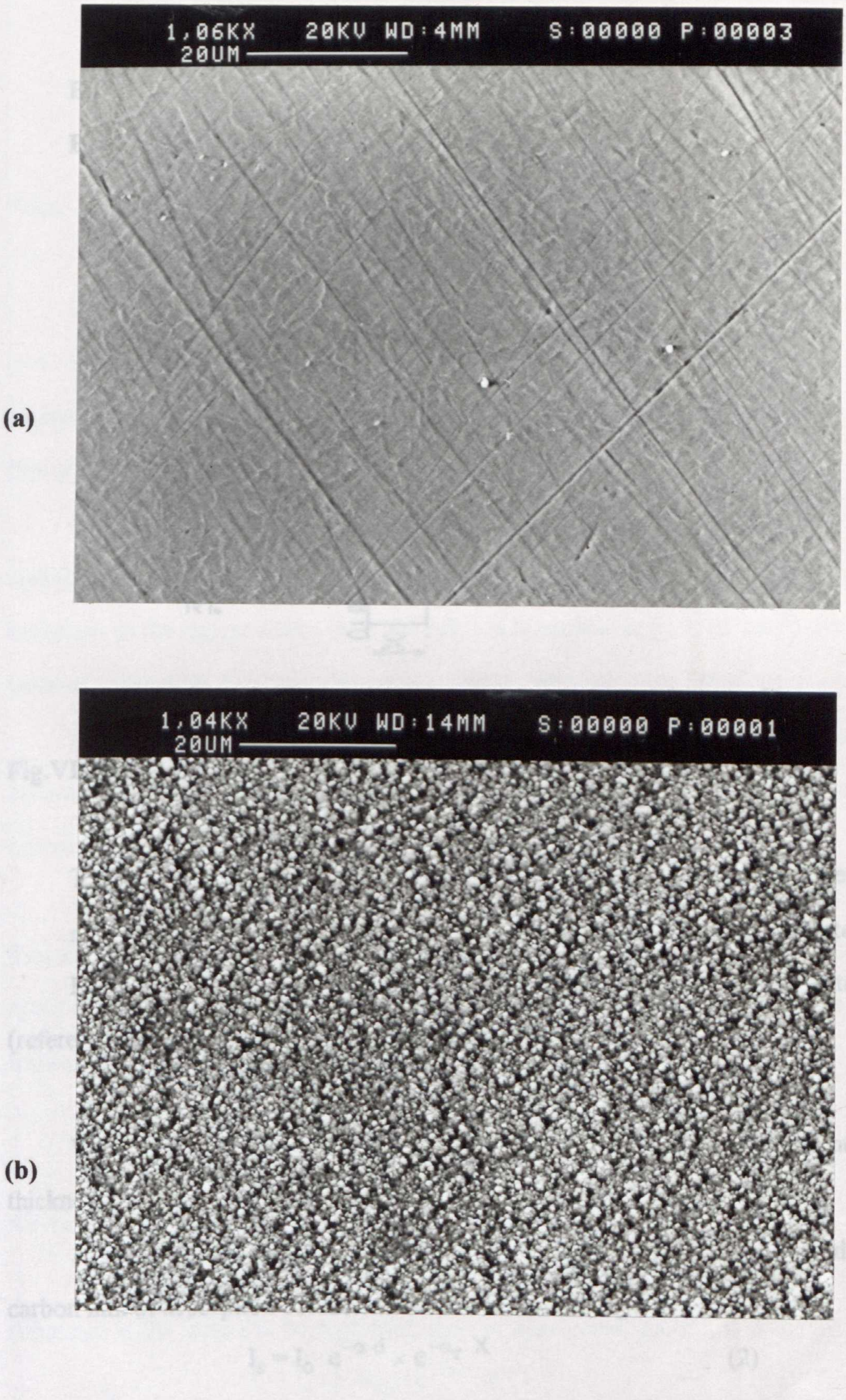

Fig. VI. 11. Scanning electron micrographs of two different TiN films used as interlayers for FAB source DLC films
(a) : shiny surface (golden)
(b) : dull surface (grey)

B. Optical evaluations.

B. 1. Absorption coefficient

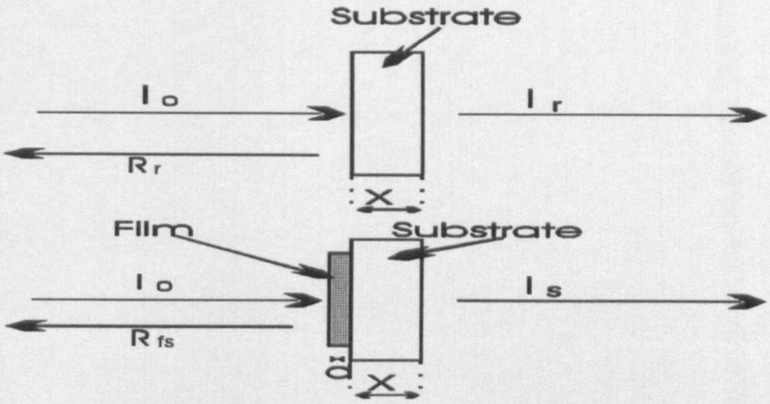

Fig.VI. 12a. Transmittance measurement procedure.

Two cases are to be considered in the measurement of the absorption coefficient:

a) Case where film absorption loss by reflection can be neglected.

In this case, the transmitted beam intensity I_r, through a non coated substrate (reference) is given by Lambert's Law:

$$I_r = I_o\, e^{-\alpha_r X} \qquad (1)$$

Where α_r and X are respectively the glass substrate absorption coefficient and thickness (Fig. VI. 12a).

And the transmitted beam intensity, I_s, through the same substrate coated with a carbon film of absorption coefficient α and thickness d is given by :

$$I_s = I_o\, e^{-\alpha\, d} \times e^{-\alpha_r X} \qquad (2)$$

The ratio I_s/I_r given by the spectrophotometer is therefore linked to α through :

$$(I_s/I_r) = e^{-\alpha\, d}$$

The film absorption is therefore given by:

$$\alpha = (1/d) \ln (I_r/I_s)$$

α measured by the spectrophotometer using the above expression will be labelled $\alpha_{mes.}$; and we can write if the absorption loss by reflection is neglected:

$$\alpha = \alpha_{mes}$$

b) Case where absorption loss by reflection is not negligible.

If reflection from the coated surface, during spectroscopy measurements, is not negligible compared to the transmitted light, α_{mes} would be an overestimation of the film absorption coefficient because part of it would be due to loss by reflection.

Reflectance of carbon films can be as high as 20% in the visible regime. The film absorption is high in the visible as well. Hence the relative error on α remains small especially in the region where the Tauc relation is applicable ($\alpha > 10^4 cm^{-1}$). For these reasons, correction from reflection is not always reported in the literature.

However since in this work accurate measurement of optical data is necessary for accurate correlation studies between optical properties and deposition parameters a correction for reflection loss has been carried out.

The theoretical expression of transmitted intensity through a coated sample as a function of reflection is in general not simple [93]. It can, however, be simplified in many cases. The transmitted intensity through a non coated substrate is given by the following simplified expression [94]

$$I_r = I_0 (1-R_r) e^{-\alpha_r X}$$

where R_r is the substrate reflectance.

And through a coated substrate, if absorption in the film is high and multiple reflection in the films can be neglected, then an approximation of I_s is given by

$$I_s = I_0 (1-R_{fs})^2 e^{-\alpha d} e^{-\alpha_r X}$$

where R_{fs} is the sample (film plus substrate) reflectance measured from the film side.

Therefore The new expression of the measured I_s/I_r ratio is:

$$\frac{I_s}{I_r} = \frac{(1-R_{fs})^2}{1-R_r} e^{-\alpha d}$$

and, the expression for α_{mes} ($\alpha_{mes} = (1/d) \ln (I_r/I_s)$) is :

$$\alpha_{mes} = \alpha + (1/d) \ln \frac{(1-R_{fs})^2}{1-R_r}$$

Finally, the corrected film absorption coefficient, α , is given by:

$$\alpha = \alpha_{mes} - (1/d) \ln \frac{1-R_r}{(1-R_{fs})^2}$$

Figure VI.12b. illustrates this correction in the visible regime for a 0.3 μm carbon film deposited on glass substrate using the FAB source.

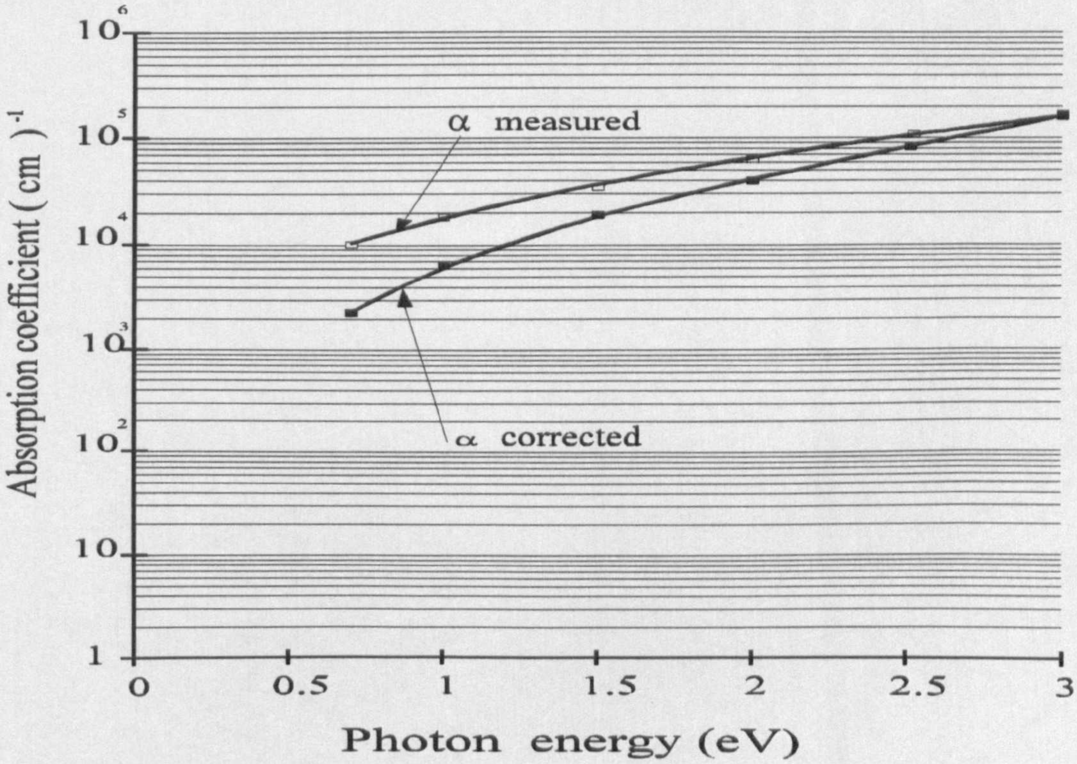

Fig. VI. 12b. Illustration of the effect of absorption loss by reflection on the measured values of the absorption coefficient in the visible regime.

B. 2. Absorption edge and Band gap

Measurement of the optical absorption in the visible regime (corrected for absorption loss by reflection) was performed using a double-beam spectrophotometer in the range 30000 – 4000 cm^{-1}.

Three films produced using the FAB source under the conditions shown in Table VI. 1 have been studied. The graphs of the absorption coefficient α obtained (Fig. VI.13) are similar to the parabolic curves reported for amorphous hydrogenated carbon (a-C:H) films [7] and do not appear to depend on the gas used. For the three films, α shows an increase from a background level of 10^2 cm^{-1} to $6x10^4$ cm^{-1}. Figure VI.13 shows that the E_{04}, the energy at which $\alpha = 10^4$ cm^{-1}, is around 1eV. This value is a low energy gap and a characteristic of all FAB source films.

The film transmittance of a 0.1μm film (Fig. VI.14) is ~40% in the middle of the visible regime and drops to less than 20% at higher wave numbers. Transmittance of an 8μm thick film drops sharply from 50% in the near-infrared to less than 1% at $\nu >$ 10,000cm^{-1} (Fig. VI.14). The former looks brown and the latter black.

The plot of the Tauc relationship ; $(\alpha E)^{1/2} = B^{1/2}$ (E-Eopt),(see Chapter V), where E is the photon energy and B a constant, produced a linear dependence for all the gases used (Fig. VI.15) as expected for amorphous materials [94]. The extrapolation of the straight lines to the abscissa yields the optical band gaps of the films. The values found are around 1eV (Fig. VI.15).

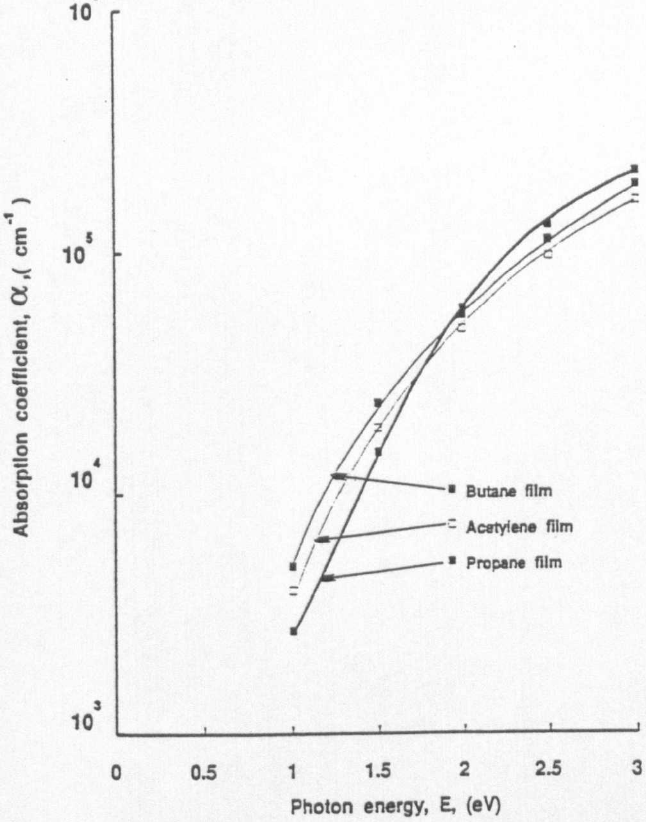

Fig. VI.13. Absorption coefficient versus photon energy for typical FAB source carbon films produced from different gases.

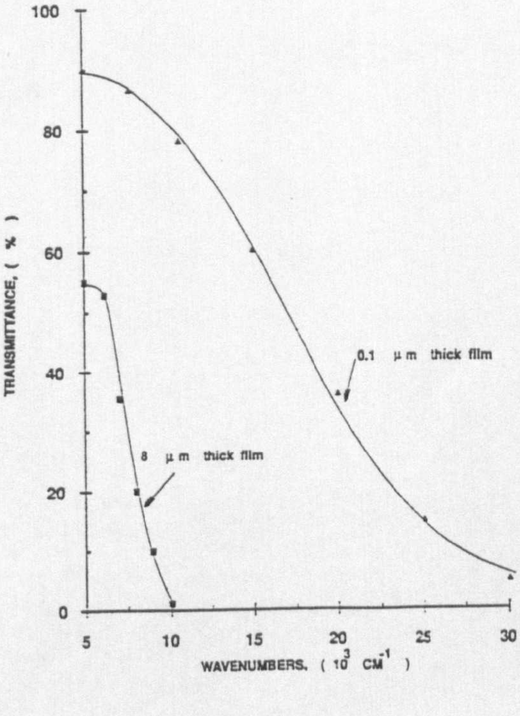

Fig.VI. 14. Typical transmittance in the visible regime of FAB source films deposited on glass substrates.

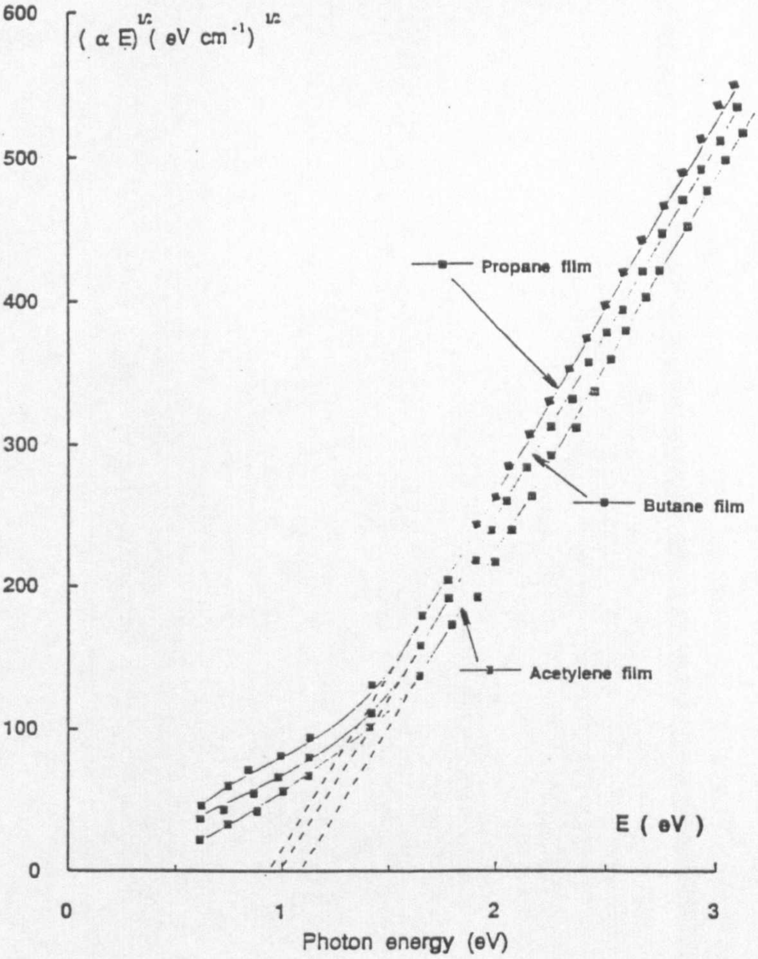

Fig. VI. 15 Optical absorption vs photon energy, plotted in the Tauc representation, $(\alpha E)^{1/2} = B^{1/2} (E - E_{opt})$, for typical FAB source films.

B. 3. C-H and C-C bonding configuration

The infrared optical transmission of FAB source carbon films on glass is illustrated in Fig. VI.16. The measurement was taken in the range 4,000 cm^{-1} to 2000 cm^{-1}, the region where the glass does not absorb and in which the C-H stretch bonds are usually detected (at around 3000 cm^{-1}).

Unusually the sp^3 C-H band at 2920 cm^{-1} and the sp^3CH_2 bands at 2850 cm^{-1} are very weak (Fig. VI.16). Moravec [106] has noted this feature in films produced by glow discharge decomposition of butane. Intense C-H bands are usually reported in this region of the spectrum for a-CH films at around the same thickness (2μm) [54].

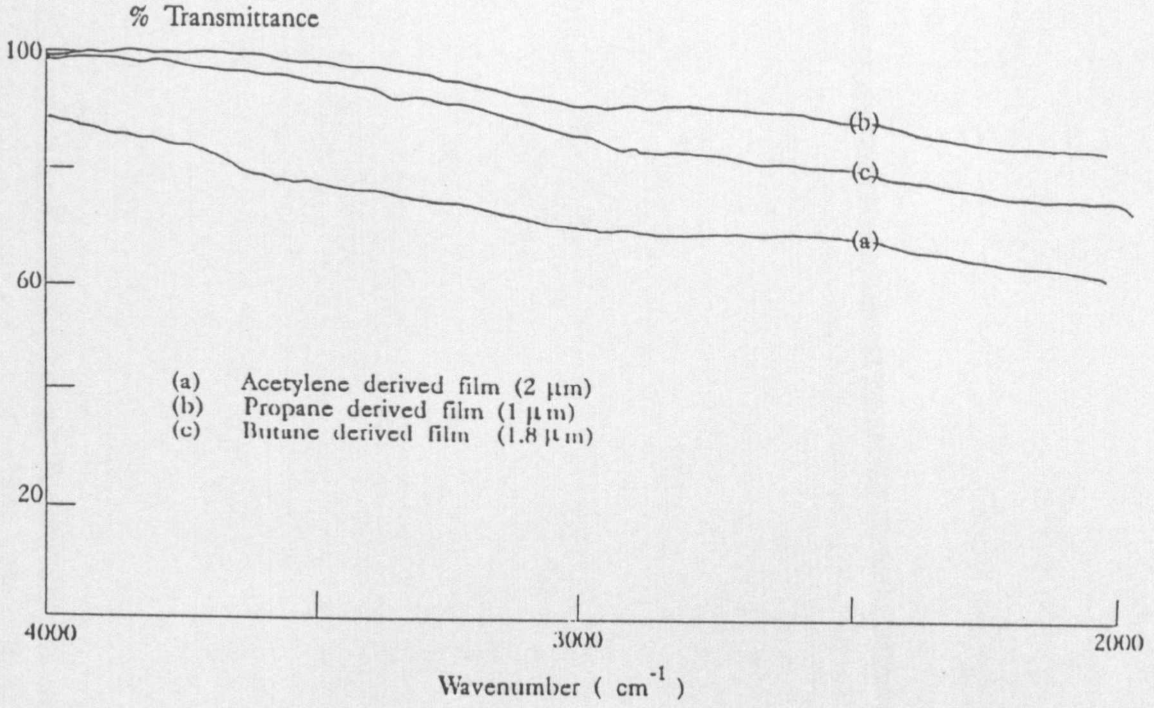

Fig.VI. 16 Typical infrared transmittance spectra from FAB source carbon films on glass.

The best resolution was obtained from free standing films (Fig. VI.17). These materials were removed for evaluation by abrading the substrate. The lines 1-13 (Fig. VI.17) are the observed C-H and C-C absorption bands. Details of these bonding types are given in Table VI.3 after comparison with standard charts of C-H and C-H frequencies (see Chap V).

Lines 5. 6. 9 and 12 confirm the presence of a graphitic structure; the other lines confirm the presence of tetrahedral C-C bonding characteristic of the diamond structure. The frequencies observed are usually associated with hard polymer films (a-C_xH_y.). Although only sp^3 bonding was detected around 3,000 cm^{-1}, the possibility of sp^2 bonding cannot be ruled out, since the sp^2 peak is usually weak in this region of the spectrum for organic materials.

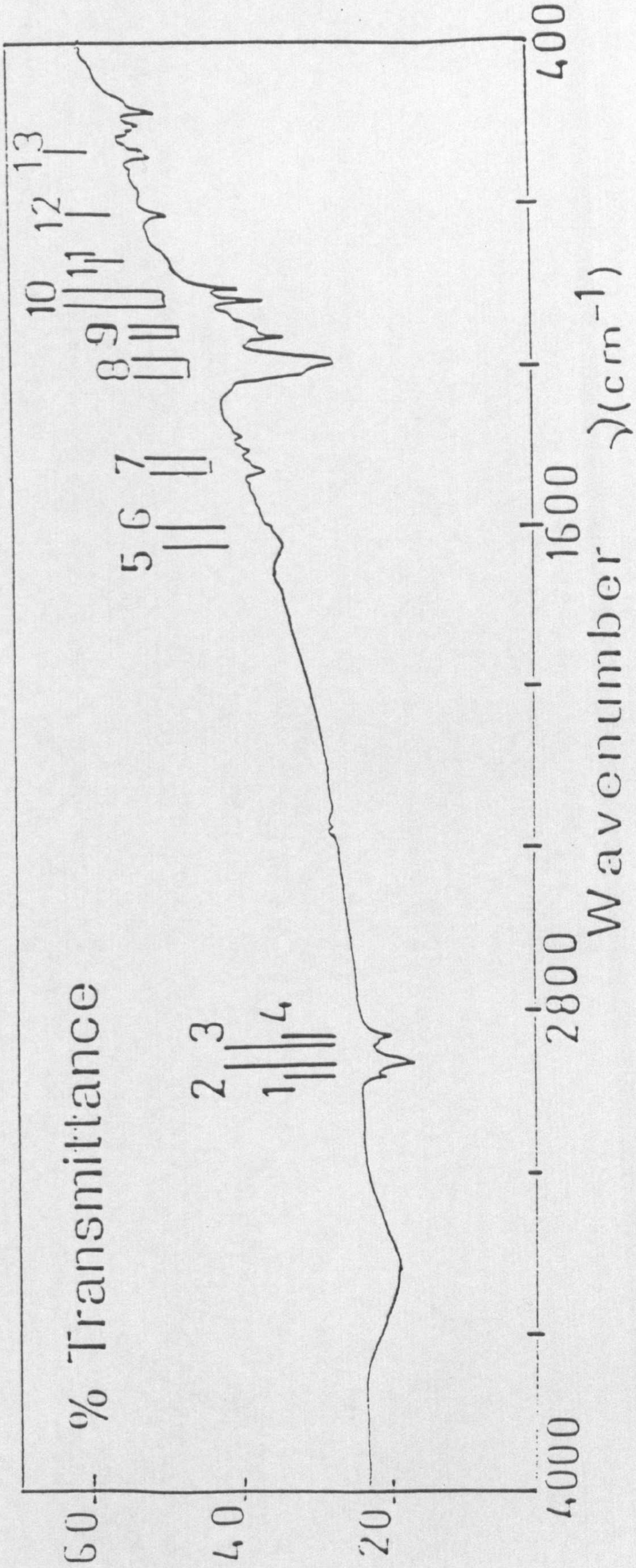

Fig.VI. 17 **Infrared transmittance spectrum from a compacted free standing carbon film produced using the FAB source and butane gas**

B. 4 Concentration of bonded hydrogen to carbon

The concentration of bonded hydrogen, N_H, in the films is given by:

$$N_H = k\,\alpha_s$$

Where α_s is the integration of the C–H stretch absorption band around 3,000 cm^{-1} ($\alpha_s = \int \alpha d\nu$; ν :wave number in cm^{-1}), and k is a constant. Since k is an unknown constant for a-C:H films, α_s is measured instead of N_H.

Band intensities or band width at half intensity are also proportional to N_H and are in common use. In this work, α_s has been measured from the expanded absorption coefficient spectra (Fig. VI.18). The integration was done using a computer linked to the FTIR. The α_s value is typically 34 x 10^3 cm^{-2} (Table VI. 4).

Since individual C-H bands are often overlapping, calculations based on deconvolution of the C-H bands intensities [102] have been used for $sp^3 : sp^2 : sp^1$ and $CH_3 : CH_2 : CH$ ratio determination. An sp^3:sp^2:sp^1 ratio of 70:30:0 and CH_3:CH_2:CH ratio of 39:31:30 are typical values found in this study for FAB source films produced in the deposition conditions listed in Table VI. 1. An example of deconvoluted C-H bands used in this work is shown in Fig. VI.19.

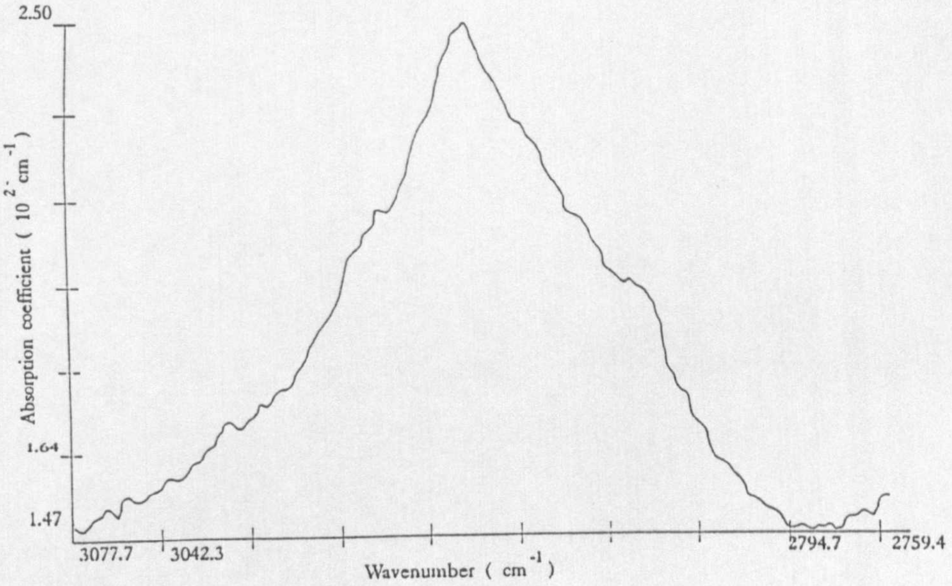

Fig. VI. 18. Typical C-H band (expanded around 3000cm^{-1} for α_s measurement) from a butane FAB source film on glass (1 μm thick)

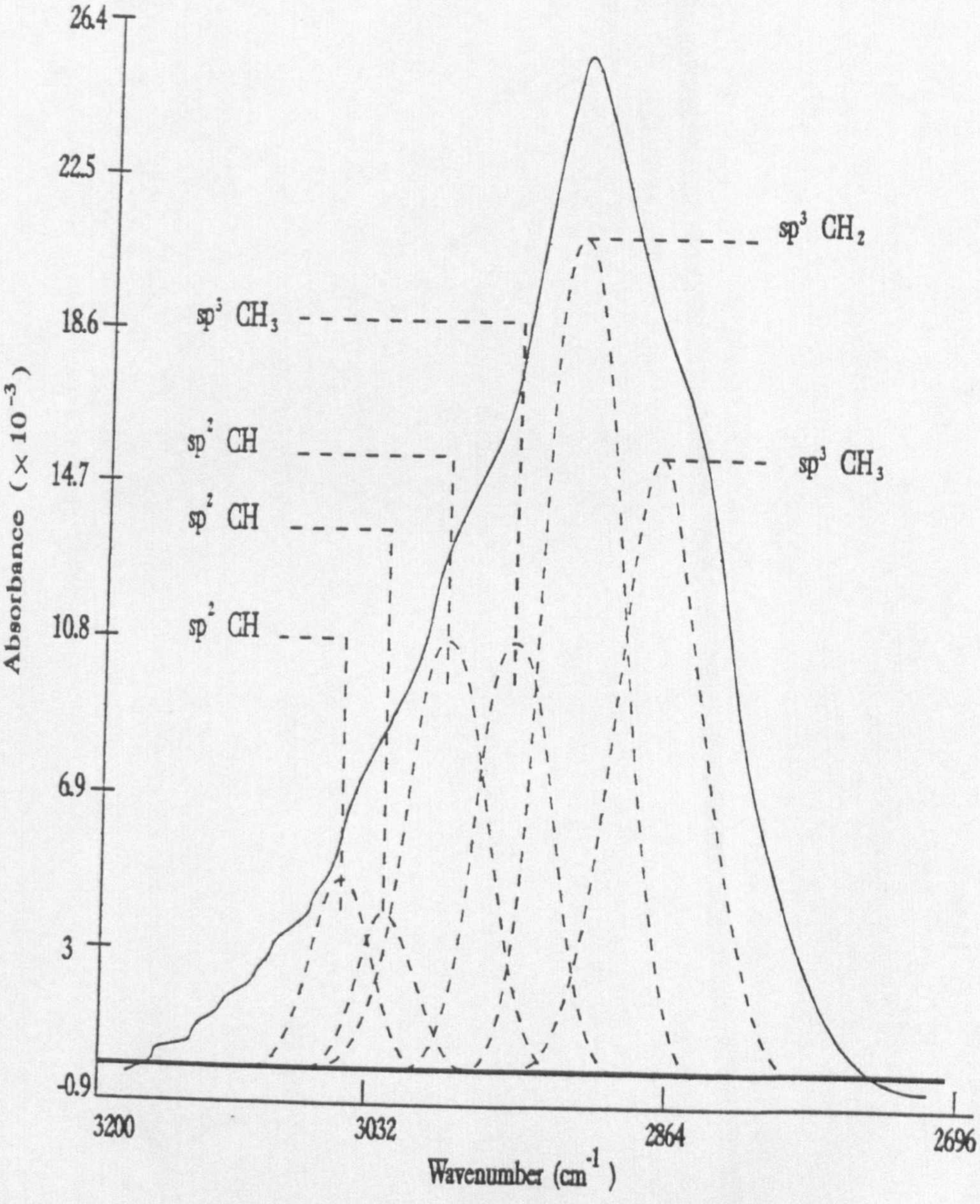

Fig.VI. 19. Deconvoluted C-H bands used for $sp^3 : sp^2 ; sp^1$ and $CH_3 : CH_2 :$ CH ratio determination obtained from a butane FAB source film (4μm thick)

Table VI.3
Carbon-carbon and carbon-hydrogen bonding types observed by transmission in a butane FAB source film

Line	Frequency (cm^{-1})	C-H	C-C	Nature
1	2957.7	sp^3 CH_3		Stretch
2	2924.8	sp^3 CH_2		Stretch
3	2871.1	sp^3 CH_3		Stretch
4	2854.6	sp^3 CH_2		Stretch
5	1620		sp^2 C=C olef.	Stretch
6	1580			Stretch
			sp^2 C=C arom.	
7	1440 - 1481	sp^3 CH_2 sp^3 CH_3		Deformation
8	1160 - 1192	C–H i.p.Benzene ring substitution		Deformation
9	1120 - 1132		sp^3 C-$(CH)_3$	Deformation
10	1000 - 1120			Deformation
11	885	sp^2 CH_2 o.o.p		Deformation
12	840	sp^2 CH o.o.p		Deformation
13	700	sp^2 CH o.o.p		Deformation

B. 5. Refractive index.

The real part of refractive index, n, was determined from interference fringes using the expression presented in Chapter V. Ellipsometry was used to determine n in very thin films which did not produce interference fringes. The n values obtained from the three films are around 2 (Table VI. 4). Example of interference fringes obtained in the I. R. regime from an 8μm thick propane derived FAB source film is presented in Figure VI.20

Table VI.4 Effect of anode voltage on FAB source film properties

(substrate: glass, Thickness: ~1μm)

Voltage (V)	800	1000	1500	2000
α_s (10^3cm^{-2})	42	40	37	34
E_{04} (eV)	1.33	1.30	1.25	1.23
Refractive index	1.9	1.9	2.2	2.2
Hardness (H_K) at (25g)	~ 2000	~ 2000	~ 2000	~ 2000

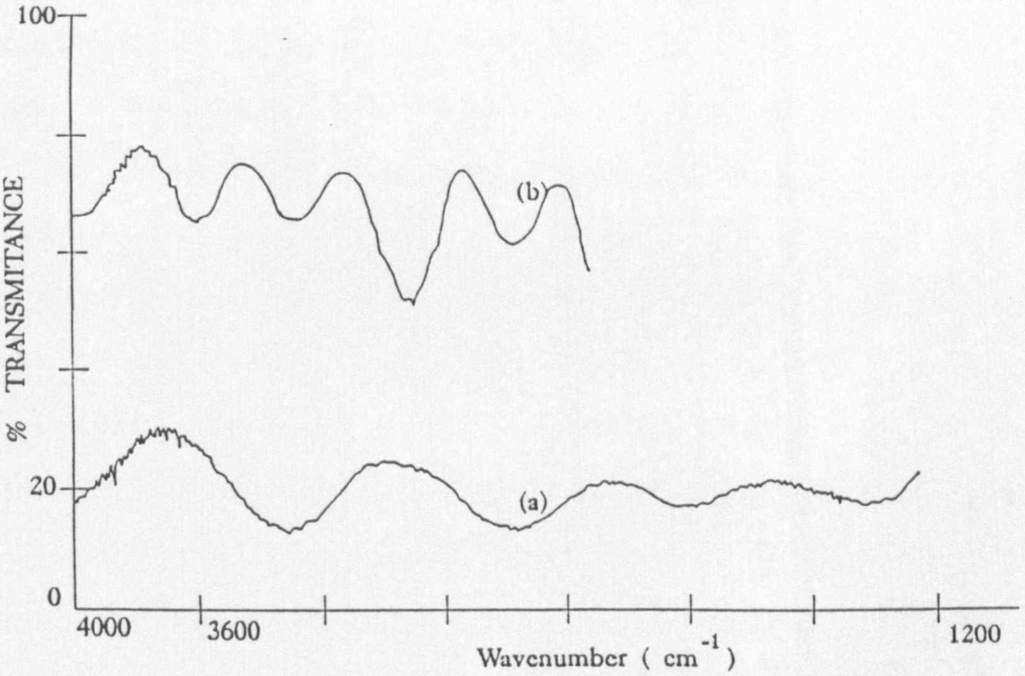

Figure VI.20. Example of interference fringes obtained in the I.R. regime from an 8μm thick propane derived FAB source film deposited on a glass substrate. (a) was obtained by reflection an (b) by transmission.

B. 6. Raman and further results

Analysis using Raman spectroscopy revealed the typical spectra of hard a-C:H films exhibiting a dominance of sp^3 fourfold co-ordinated carbon atoms (Fig. VI.21). The main features detected were a broad peak centred around 1515cm^{-1} and unresolved D (1350cm^{-1}) and (1600cm^{-1}) peaks which signify the presence of graphitic micro-crystalline sp^2 carbon sites [107]. The spectrum obtained from the film with high hillock density is an unusual spectrum in that the D band has moved to much higher wave number (>1400cm^{-1}) (Fig. VI.21). A similar shift was observed (Fig. VI.21) in the spectrum of a 3mm thick carbon residue film removed from inside the FAB source (a very hard residue grown on the anode). Microhardness of a polished surface of this residue gave values around 5000 H_K (50g). Large elastic indentation recovery was observed. Mr Garry Robinson (the laboratory technician) reported that polishing of this residue took more time than is usually required for hard materials (TiN, SiC,..). In fact pieces of this residue have been used by the author as glass slide cutters. Infrared spectroscopy revealed that this residue is hydrogenated (Fig. VI.22). SEM observation of this residue (Fig. VI.23 & 24) revealed a cauliflower structure and that bigger hillocks are themselves sets of smaller hillocks and so on .

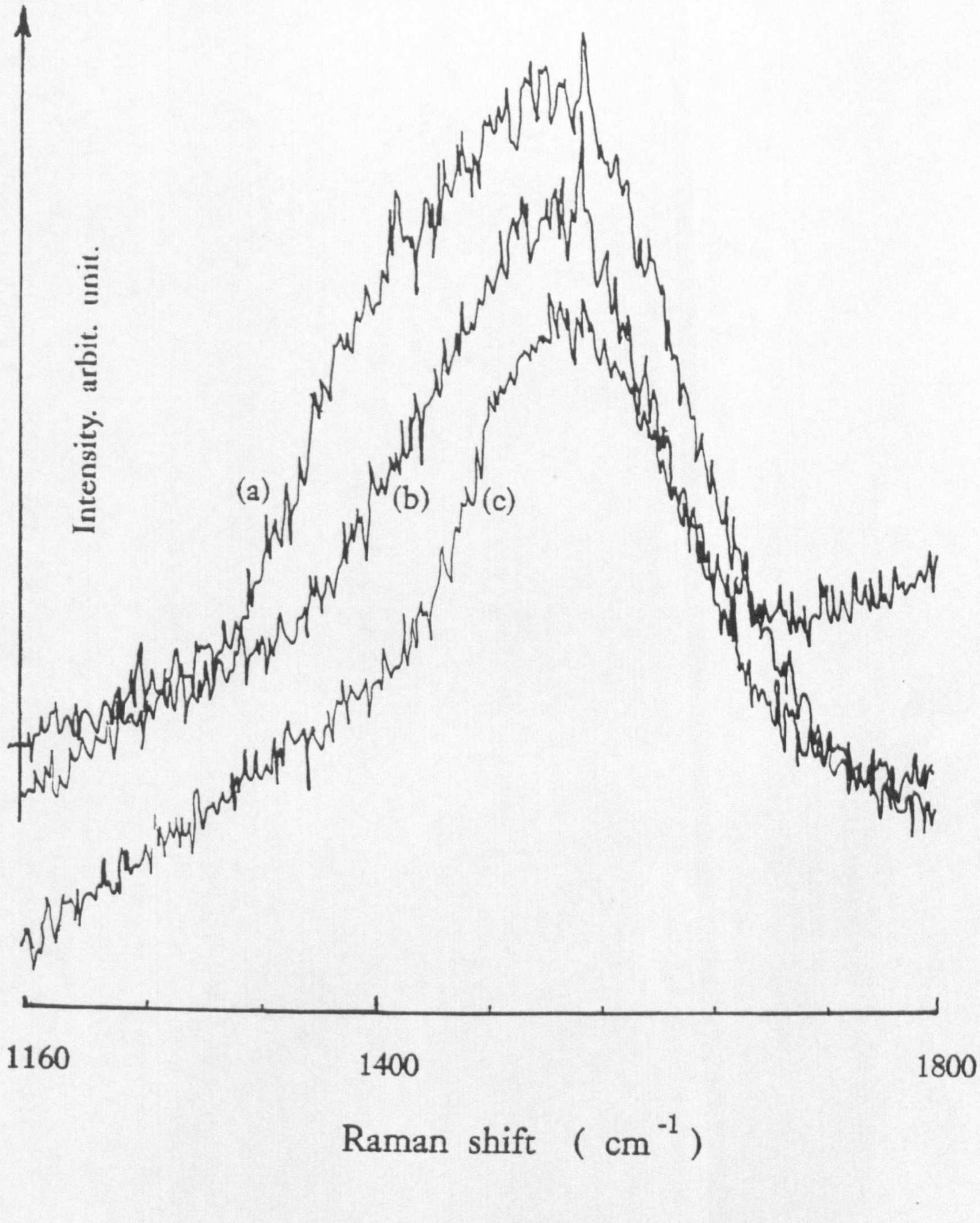

Fig. VI. 21. **Typical Raman spectra of different FAB source films;**
(a) : film with low hillock density on glass substrate.
(b) : film with high hillock density on glass substrate.
(c) : hard carbon residue grown on the FAB source anode rods.

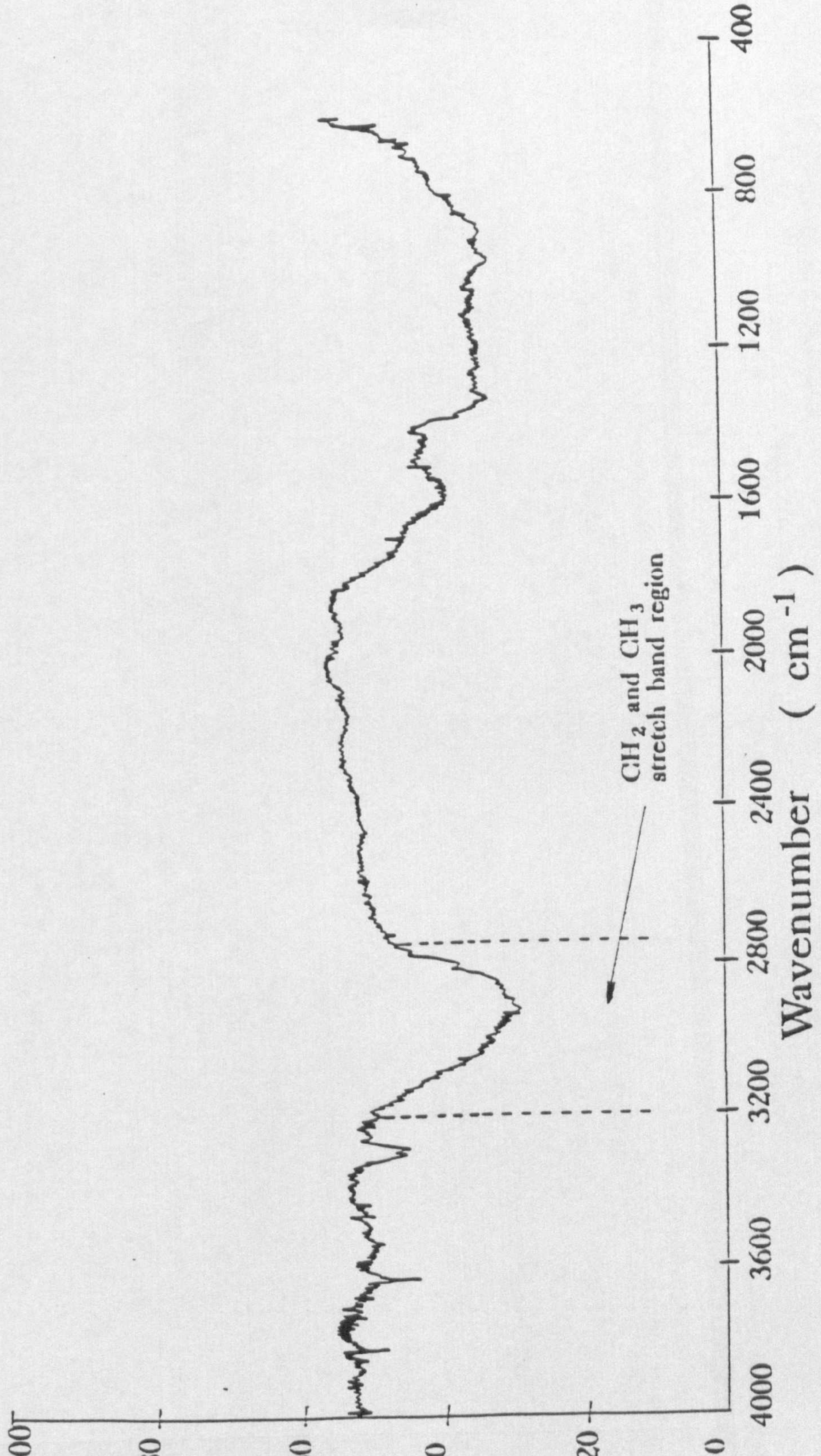

Fig.VI.22. Transmittance by reflection from the FAB source carbon residue showing that it is hydrogenated

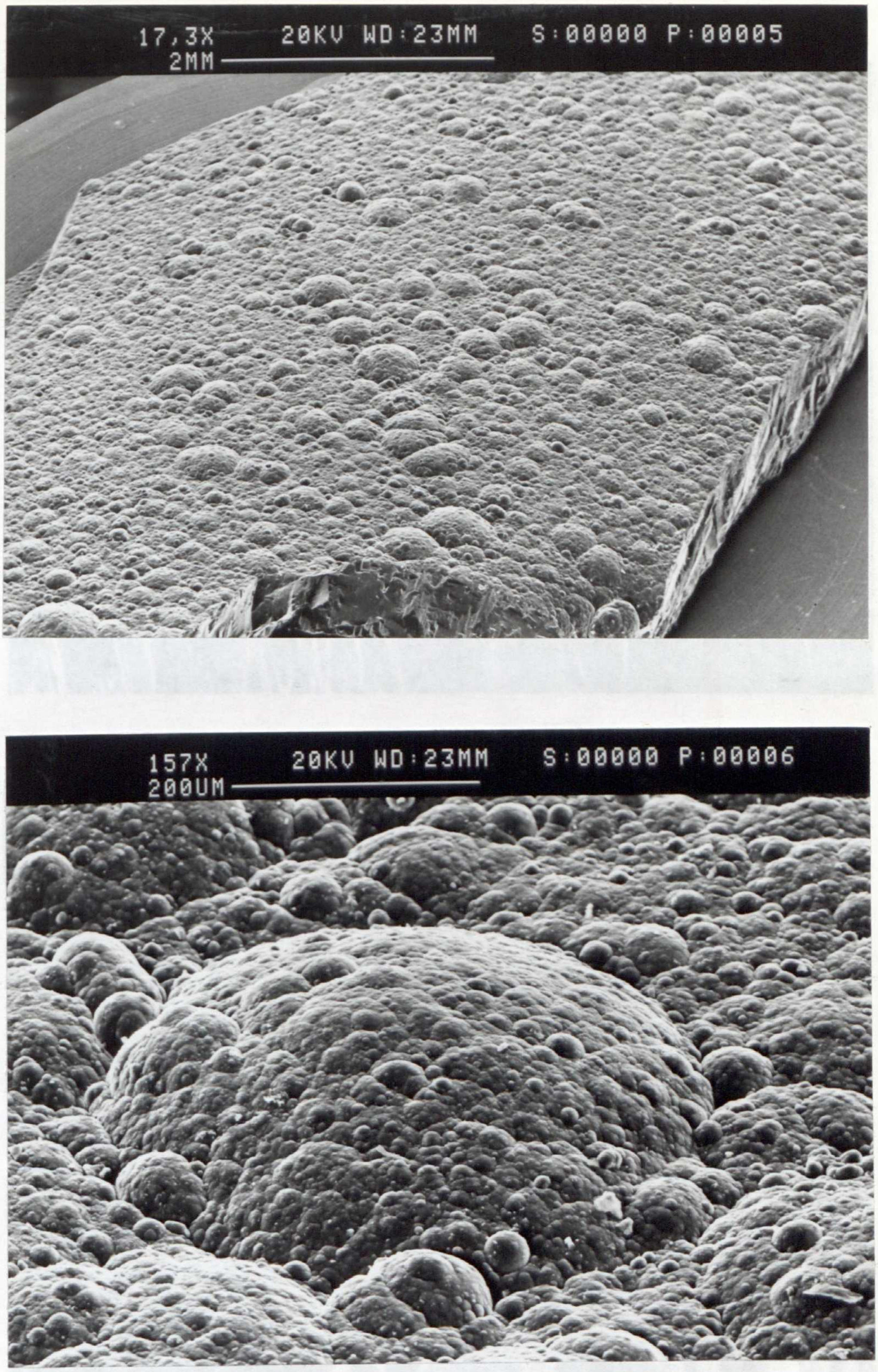

Fig. VI. 23. :Scanning electron micrographs of a carbon residue film removed from inside the FAB source (showing that bigger hillocks are themselves sets of smaller hillocks)

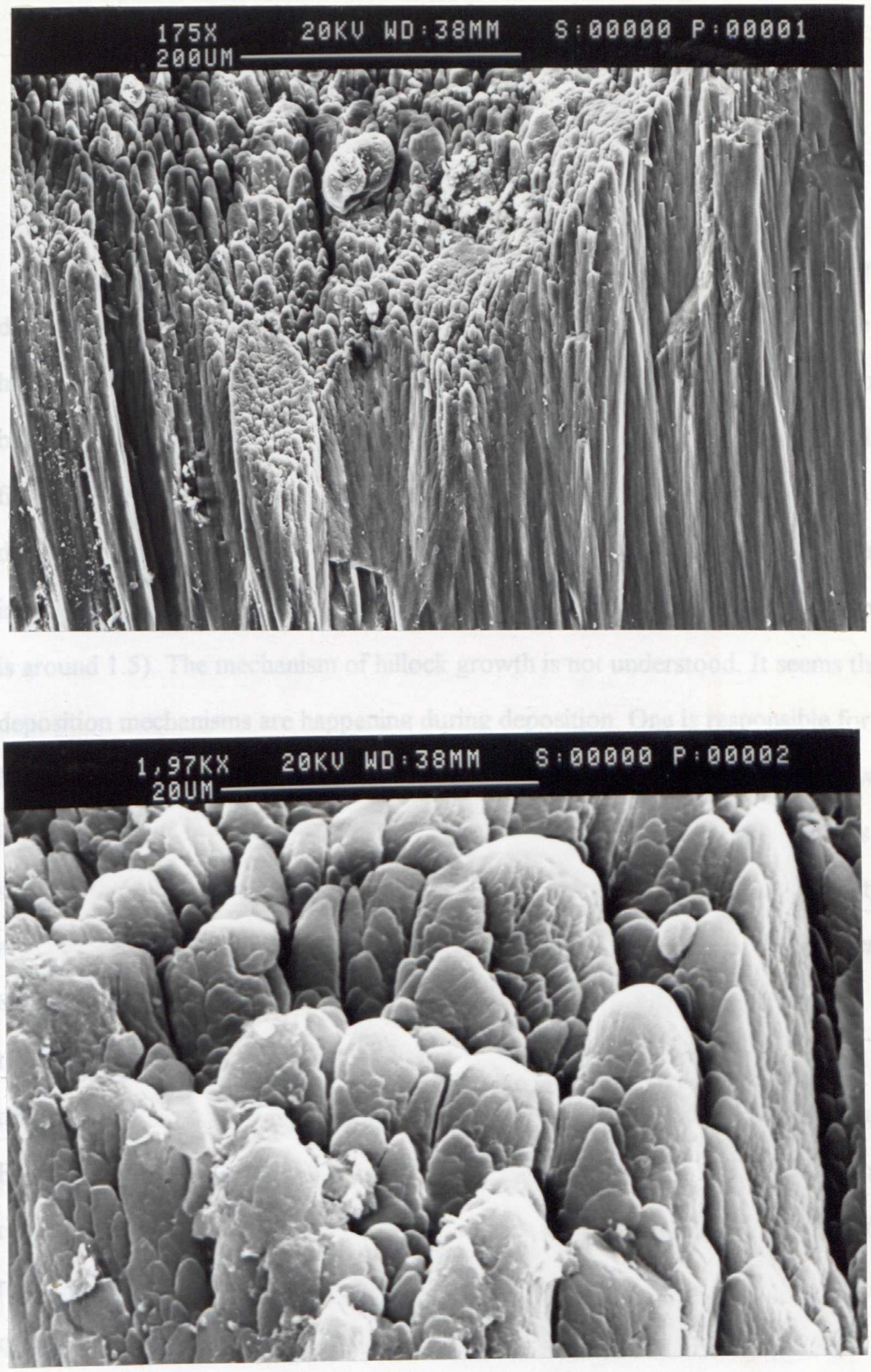

Fig. VI. 24.:Scanning electron micrographs of a carbon residue film removed from inside the FAB source.

B. 7. Discussion

The FAB source can provide films which exhibit extremely high hardness levels due, in part, to elastic recovery during testing. This behaviour appears to relate to the hydrogen content (much of which is not bonded) and to the high density. The optical band gap is about 1eV and does not depend on the type of gas used in our studies. The films are brown in colour. However, for films thinner than 0.1μm, the colour is dependent on the thickness (complete transparency is never attained). The refractive index (2.2) suggests that the films are not polymeric.(refractive index of bulk polymers is around 1.5). The mechanism of hillock growth is not understood. It seems that two deposition mechanisms are happening during deposition. One is responsible for the hillocks the other for the smooth appearance. Particles sputtered from the growing film inside the source (on the walls) could be contributing to hillock growth. This is supported by the similarity found between Raman spectra of high hillock density films and that of the FAB source residue. The temperature inside the source is higher than 600 °C. The film grown inside the source must be of graphitic structure at this temperature [7]. Hillocks might therefore be of graphitic structure. They might be the cause of poor transmission in the visible and the low optical band gap. The structure of FAB source films can be described as a matrix of smooth carbon film in which the hard residue particles are deposited in the early stage of growth. During deposition the residue particles would be very hot, and the coating is at room temperature. A quenching process accompanies the deposition of these particles. The resulting film is much harder than the matrix alone. Further investigation is needed to support this hypothesis.

C. Effect of process variables on FAB source films properties

C. 1. Introduction

The FAB source technique offers a convenient means of investigating the influence of process variables on diamond like carbon film formation (e.g. gas composition, energy, flux, and substrate temperature). This section is an investigation into this influence especially on the films' optical properties, looking for an improvement of the transparency in the visible regime.

C. 2. Effect of hydrogen

In the mechanism growth of carbon films, hydrogen is believed to be a solvent agent for graphitic structure (Chap. III) and favours sp^3 bonds. As a result Eopt increases, α decreases, and the transparency increases.

In order to see to what extent hydrogen will affect FAB source films properties high proportions of hydrogen in the FAB sources gas were investigated (99%, 98% and 97%, based on the relative flow rates of hydrogen to hydrocarbon). The deposition conditions were otherwise as listed in Table VI. 1.

The first observation was the reduction of deposition rate to about 100 nm h^{-1} owing to the lower flow rate of hydrocarbon gas and hydrogen etching effect (physical or chemical).

The mechanical properties of the films have not been improved, they were softer than the earlier films (typically 1500 H_K at 25 g load). They were also more brittle and less adherent to the glass substrate, although they showed good adhesion to silicon.

The types of C-H bonding observed around 3000 cm^{-1} were the same as those produced with no hydrogen mixture. The concentration of bonded hydrogen increased linearly with the proportion of hydrocarbon gas input as revealed by α_s that increased from 34×10^3 cm^{-2}.to around $80 \times 10^3 cm^{-2}$ (Fig. VI.25).

The absorption in the visible range decreased but not very much (Fig. VI.26 curves 1, 2, 3), and the films remained brown. The optical band gap increased from 1eV to 1.5eV and the refractive index decreased slightly to around 1.9.

Based on the IR C-H bonding intensities, it could be deduced that the $sp^3:sp^2:sp^1$ proportions changed to (typically) 90:10:0. Others have reported an increase in optical band gap with an increase in $sp^3:sp^2$ ratio or with an increase in hydrogen [109]

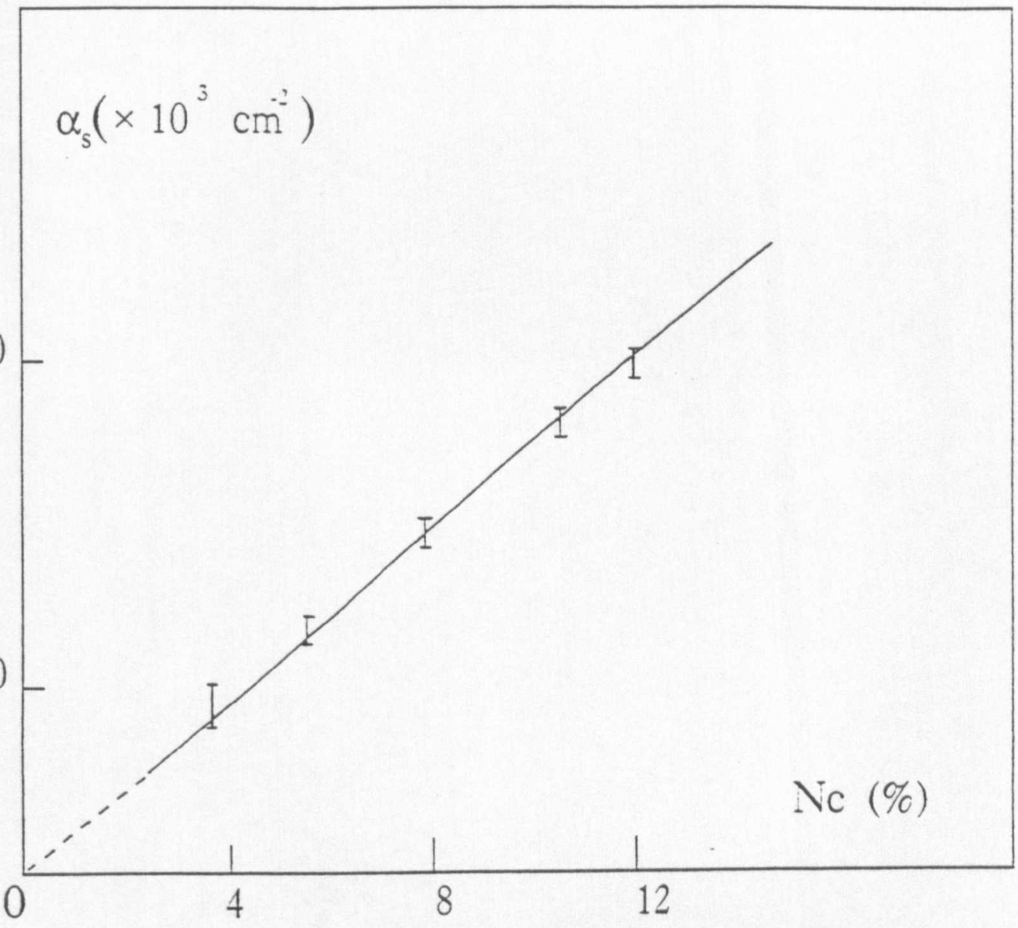

Fig. VI. 25 Dependence of the integrated C-H stretch absorption (α_s) on the carbon content (N_c) in different butane-hydrogen gas mixtures (V = 1.8 kV, I = 0.1 A)

$$N_c = \frac{n(n+m)^{-1}\phi(C_nH_m)}{n(n+m)^{-1}\phi(C_nH_m) + \phi(H_2)}$$ where ϕ is the gas flux.

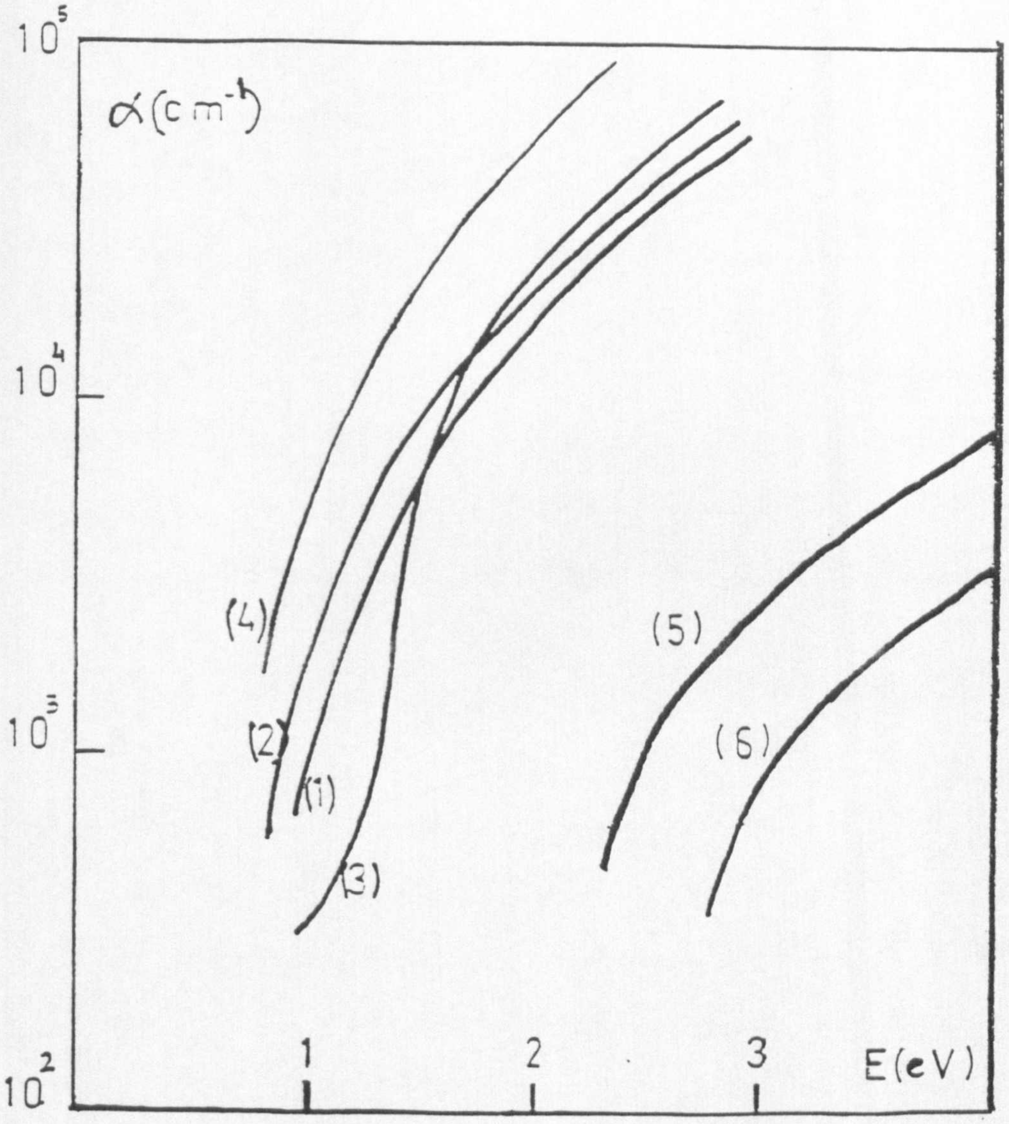

Fig. VI.26
Absorption coefficient versus photon energy for carbon films produced in different conditions using the FAB source;

-(4): butane only,

-[(1): 1% butane, (2): 2%butane, (3): 3% butane] in hydrogen.

-(5) and (6): samples tangentially oriented to the FAB source beam.

C. 3. Effect of particle energy

C. 3. 1. Introduction

The fact that the substrate position is outside the FAB sources, the beam particles are not subject to collisions during their path from grid to substrate (the pressure outside the FAB source is around 10^{-4} Torr; the mean free path is of the order of substrate to FAB source distance). The impact energy is therefore directly affected by the FAB source anode voltage since the energy of the extracted particles is due to this voltage. However, the voltage acts on the degree of ionisation of the FAB source discharge as well. The voltage effect is therefore not a purely energy effect. On the other hand sample orientation influences the normal impact energy of the arriving species independently of the discharge ionisation degree. The effect of these two parameters on film properties has been studied in this work and is described below.

C. 3. 2. Effect of anode voltage

For this study several films have been produced at different voltages using butane. The voltage effect on film properties is summarised in Table VI. 4. The films remained hard; small variations could not, however, be detected because of the large reading error due to indentation elastic recovery. However, it is clear from repeated tests that the interval of voltage (800 - 2000V) studied has no big effect on the hardness reading. It is believed that voltages less than 800 V should affect the hardness [7]. Verification of this hypothesis was not possible because the FAB source beam could not be extracted at voltages lower than 800 V .

The optical band gap and α_s increased slightly with decreasing voltage. and the refractive index decreased but remained close to 2 (Table VI. 4). The films remained brown.

C. 3. 4. Effect of sample orientation

Fig. VI.27, shows the sample orientations studied. The most important result was that the films grown in positions B, C, E and F were transparent in the visible range (Fig. VI.26 curves 5 and 6 demonstrate the low absorption). The optical band gap of these films was between 3.5 and 4.0 eV. The α_s value is typically 12x 10^3 cm^{-2}. This value is ten times less than that found for typical hydrogenated films [110]. Therefore, they contain a low amount of bonded hydrogen, and this transparency could thus not be attributed to "polymer-like" behaviour. These films show no C-H sp^2 or sp^1 content in the IR stretch region.

The main disadvantage of the films grown at grazing incidence to the beam was that they were relatively soft (at about 900 H_K (25 g)), though further work is needed to characterise fully their mechanical behaviour (e.g. with a nanoindentation method). Also, the deposition rates in positions B and C were low (typically 100 nm h^{-1}, even if 100% hydrocarbon gas was used). The deposition rate on the insides of samples E and F was, however, higher with the cap G in place (up to 0.6µm/h).

Figure VI.28 shows the variation of sp^3 and sp^2 concentrations (based on band intensities) with substrate orientation angle Θ. The sp^2 / sp^3 ratio decreases from around 33% at normal incidence to zero at grazing incidence (Fig. VI.28). A scanning electron micrograph of a typical film is shown in Fig. VI.29; it can be seen that the film is dense and its surface is not covered with hillocks as is the case at normal beam incidence.

Some problems remain unsolved however : transparent films thicker than 0.6µm could not be achieved at tangential substrate orientation even after 4 hours deposition time. They also showed, a few month after deposition, adhesion deterioration and changes in colour (from clear transparent to slightly yellow).

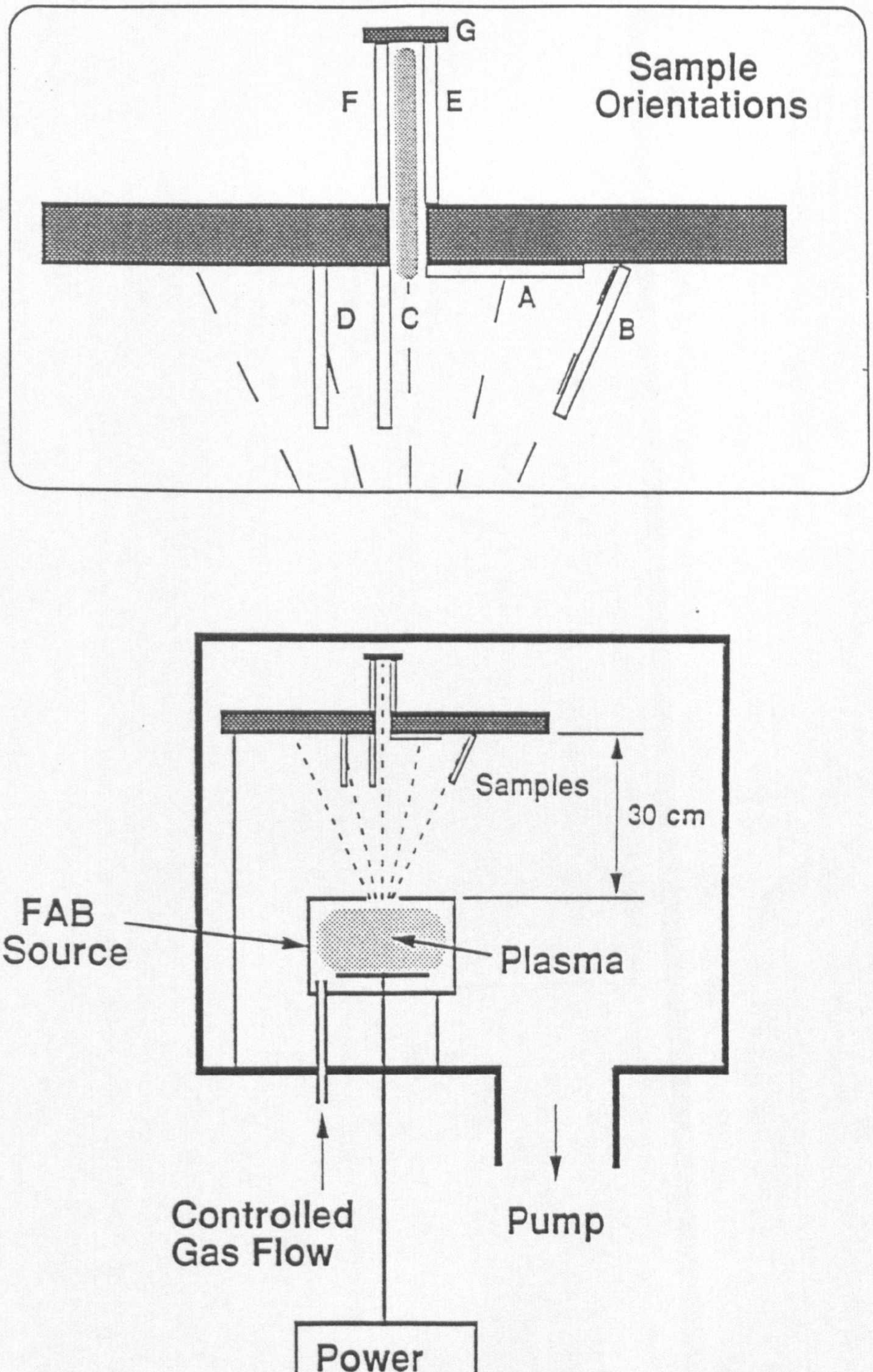

Fig. VI. 27 Schematic of system layout

(sample orientations shown enlarged)

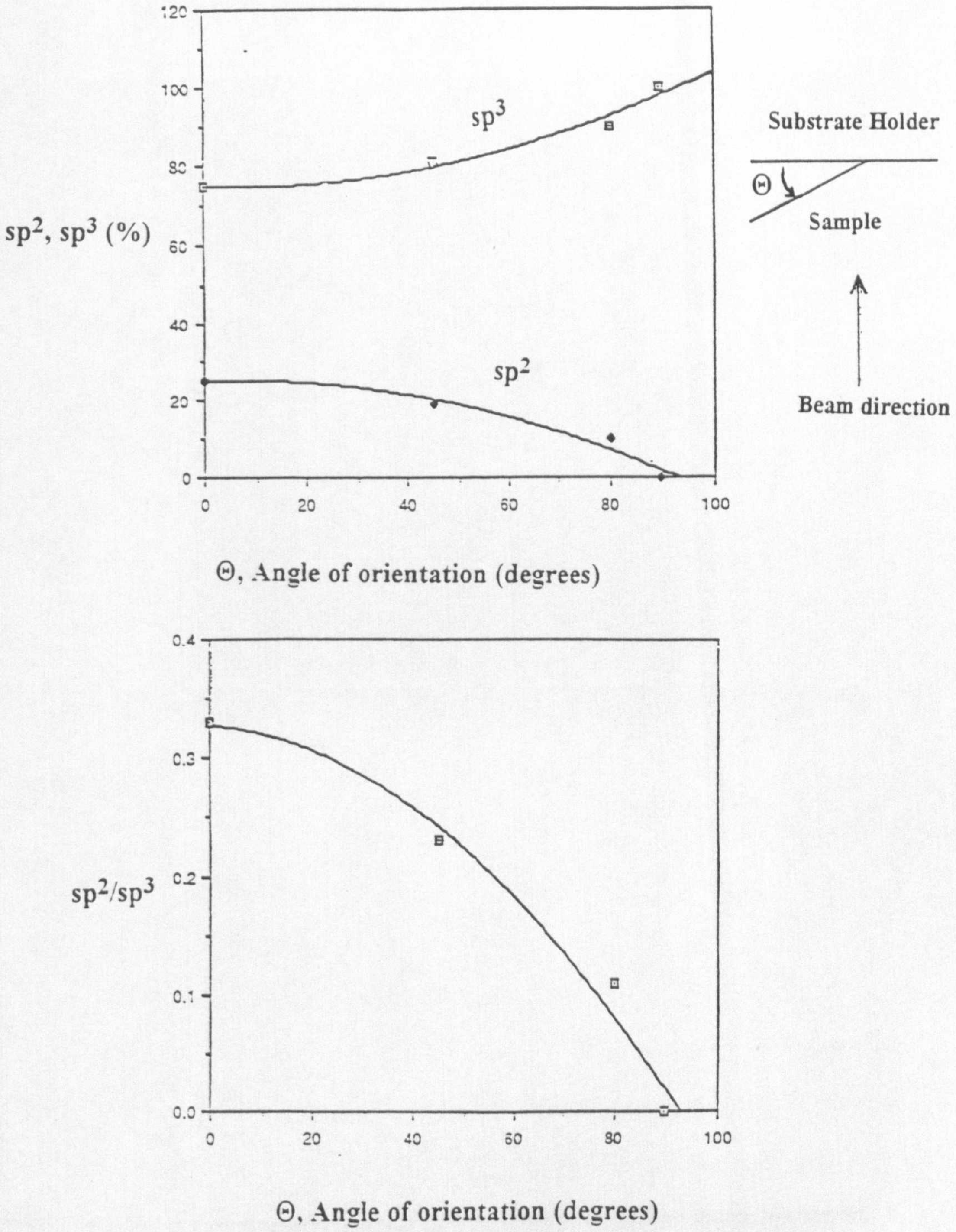

Fig. VI. 28 Effect of sample orientation on sp^2 and sp^3 concentration in FAB source films

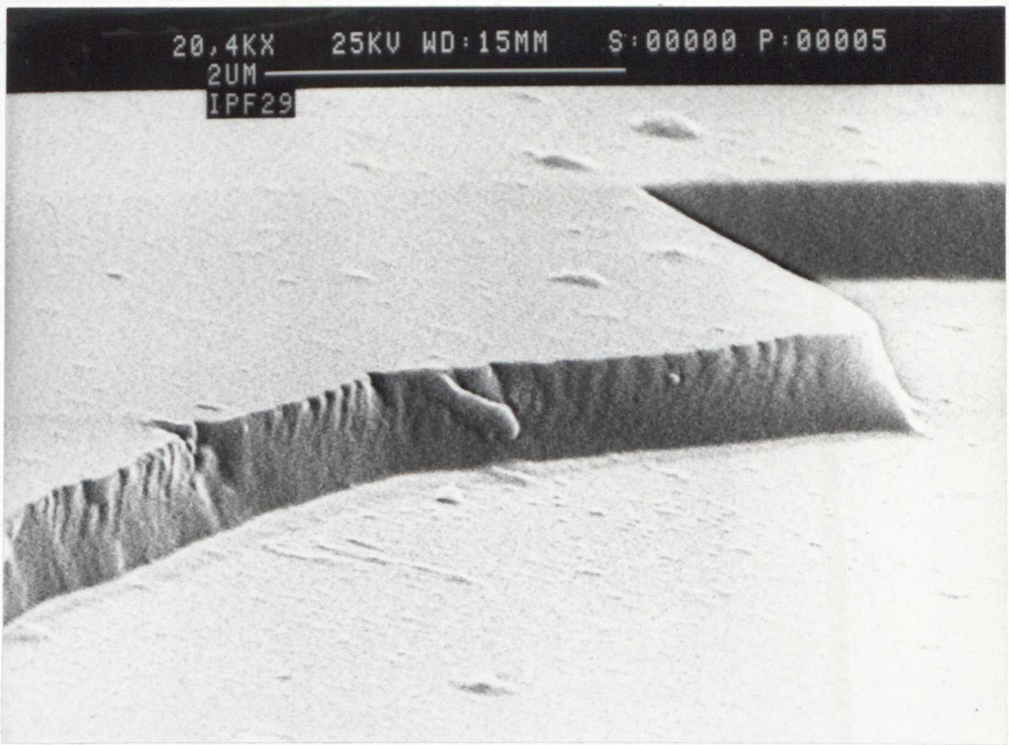

Fig. VI. 29 **Scanning electron micrograph of propane derived film grown on glass substrate oriented tangentially to the FAB source beam.**

C. 4. Effect of annealing.

C. 4. 1. Posts deposition annealing

In section 3. 3. 2 we described how some films gave anomalously high hardness readings, owing to elastic recovery. We believed that this was due in part to hydrogen [111]. Our view was that this must be non-bo~~u~~nded, since we did not detect a large amount of C-H bonding. Annealing the films was seen as one method to determine the influence of hydrogen on hardness. Somewhat unexpectedly when we raised the temperature (in air) to 300°C and then cooled to ambient, the hardness increased, and no impression was left by a Knoop indenter even at 50 g load. Higher loads led to spallation of the film around the indenter. One effect noticed was that the number density of the hillock structures increased after annealing. (Fig. VI.30). Films on glass became black and opaque.

Figure VI.31 shows the influence of temperature on C-H bonding in the film. At temperature higher than 400°C the film turned into particles which jumped a few centimetres above the substrate. SEM examination of the substrate surface (Fig. VI.32) from which the film debonded revealed small particles (approximately 1μm diameter) located mainly on the substrate surface scratches.

C. 4. 2. Annealing during deposition

One of the advantages of the FAB source technique is its low deposition temperature (50°C). However the temperature can play a fundamental role in the growth mechanism. For example in PVD techniques the temperature (~200°C) improves coating diffusion into the substrate which improves the adhesion. And in diamond technology if deposition temperature is not around 900°C only graphite is produced. Trying to produce diamond using an ion beam or FAB source by adjusting the substrate temperature and the proportion of the methane in hydrogen is the first thing one might consider . However, let us not forget that the energy involved in an ion beam is too high. The reason of our annealing study is not diamond production but an investigations on ways of improving the film properties. A substrate holder equipped with resistive elements (tungsten wires) has been made for this investigation. The temperature controlled by the electric current producing the heating was measured by a thermocouple. Temperature could be varied from 0 to 600°C.

To our surprise no improvement of the film properties was observed. At temperature above 200°C the coating adhesion deteriorated. At temperature between 100°C and 200°C the films remained adherent to the substrate but were black and soft. The deposition rate also decreased dramatically. This was observed for all hydrocarbons used and also when hydrogen was mixed with hydrocarbon. Films deposited on silicon showed better resistance to debonding from the substrate but were black and soft as well.

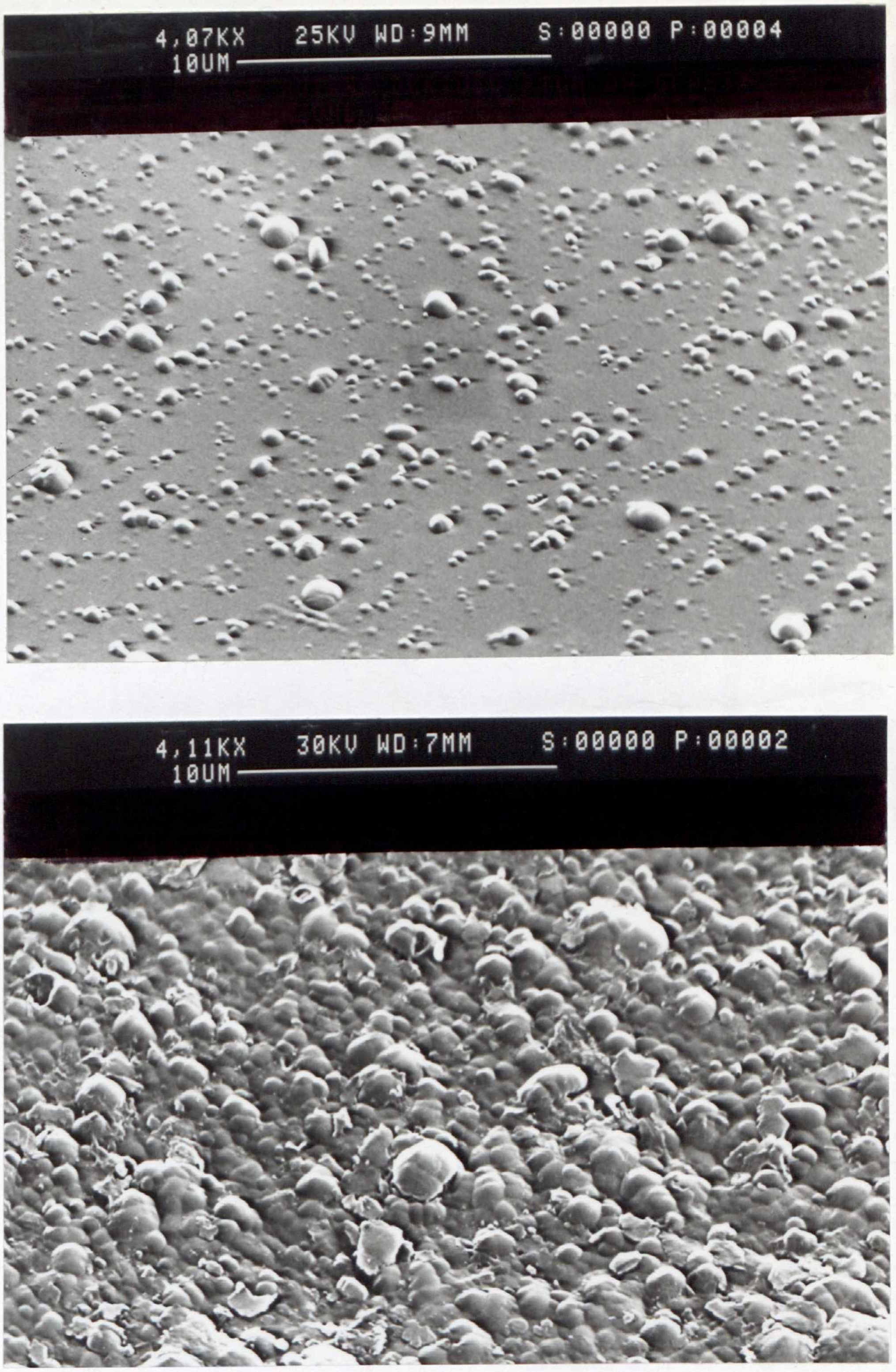

Fig. VI. 30 : Scanning electron micrograph illustrating the effect of annealing temperature on the surface morphology of a FAB source film on TiN.

Top: As prepared **Bottom : Annealed 300°C**

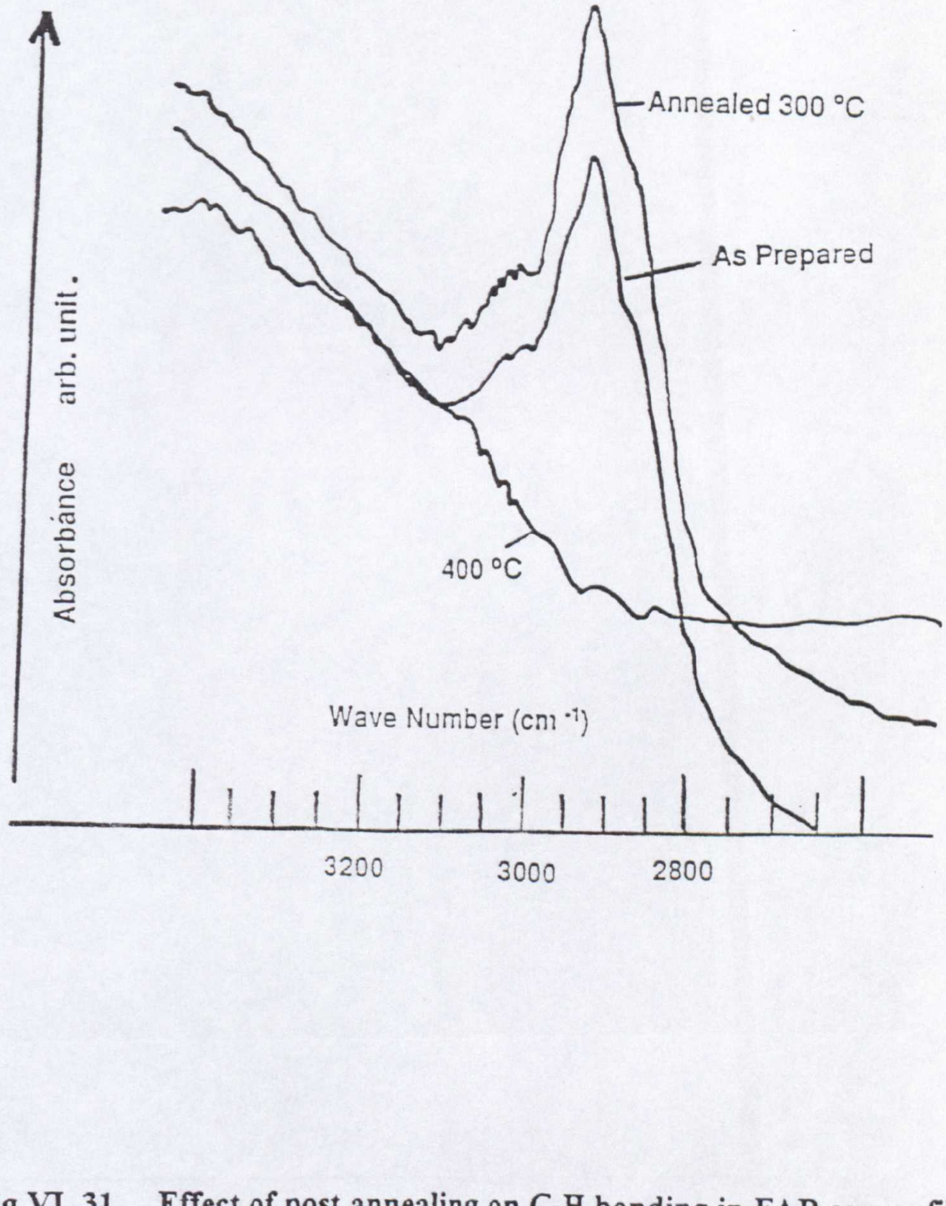

Fig VI. 31. Effect of post annealing on C-H bonding in FAB source films

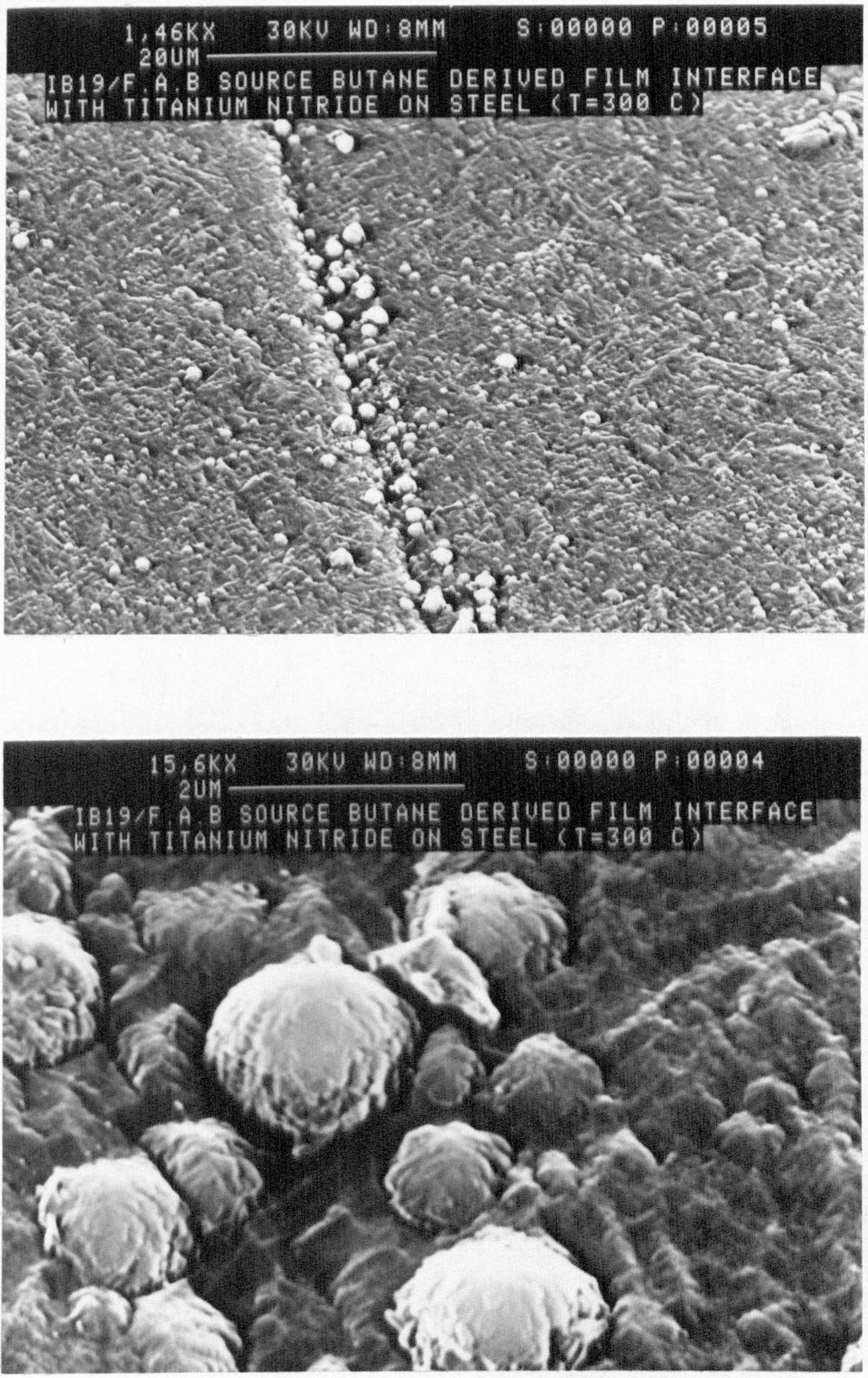

Fig. VI.32 : Scanning electron micrographs of particles observed on the interface TiN after debonding of DLC due to the annealing effect .

C. 5. Discussion

It has been shown that the sample orientation has a dominant influence on the properties of films produced using an FAB source. This is most probably related to the normal impact energy of the beam and its interaction with the surface. Possible explanations lie in the changed sputtering mechanism and/or the change in energy when one moves from a normal "impact" situation to a "flow" situation, where there is a ready availability of species moving over the surface. This has further consequences in terms of the optimisation of impact energies and the coating flux. Certainly the results whereby transparent films with low hydrogen content can be grown at grazing incidence, suggest that the normal incidence is the preferred route when hardness is the main requirement.

The absence of hillocks on the surface of the clear films produced at grazing incidence supports the earlier hypothesis on hillock origin (section B .7). The fact that thick clear films could not be achieved is probably due to bonding saturation mechanism: All the free carbon sites available on the surface become occupied by hydrogen atoms. This saturation effect is not observed at normal incidence because the growth mechanism in this case is physical (i.e. the arriving species do not need to be chemically bonded to the growing film; they are implanted in the first film layers due to high energy impact). This forced growth mechanism yields to disorder which is responsible for the low band gap. Trapped non-bonded hydrogen is believed to be responsible for the stress in the film [111].

D. Evaluation of FAB source films deposited on PET

D. 1. Introduction

Many potential applications of DLC films are currently limited by its relatively poor light transmission in the visible range, low deposition rates and high deposition temperature. Since the FAB source technique operates at room temperature, its application to coat low melting temperature materials such as plastics will be of great interest to industrialists. FAB source films and DLC in general do not, however, adhere to many kinds of plastics. Polyethyleneterephalate (PET) is a polymer which is used under magnetic media [112] and for encapsulation applications because of its good mechanical properties and high transparency in the visible regime. Its permeability to oxygen is however relatively high compared to other encapsulating materials such as aluminium foil. The idea of coating PET with a DLC layer was therefore suggested and the FAB source technique is a candidate for this application. Since this had never been done before the adhesion of FAB source films on PET was still an open question. On the other hand transparency of the coated PET would change from clear to semi-transparent (Chap. VI.). Nothing was known to us about the permeability of FAB source films to oxygen. Their high mass density should be beneficial to low particle diffusion into the coating.

In this section we report the results of our evaluations on this subject and ways of improving some of DLC on PET properties.

D. 2. Experimental details

D. 2. 1. Direct gas deposition using FAB source

The FAB source technique has been described earlier. Polymer substrates were 12 μm thick PET sheets, clamped to a substrate holder. Precleaning was carried out, first with an acetone wash and then by hydrogen bombardment using the FAB source. The temperature during deposition was approximately 50°C, which caused no visible damage to PET substrates. Acetylene alone or mixed with hydrogen in different proportions has been used as the FAB source gas. The pressure outside the FAB source was kept around 2×10^{-4} Torr in all experiments. The substrate to FAB source distance was 30cm.

D. 2. 2. Measurements

Film thickness was measured using a Talysurf profilometer, and by SEM observation. Transmittance in the visible regime was measured using double beam spectrophotometer. Scratch tests were performed with an adapted microhardness tester (Leitz Miniload 2). A stylus with a Rockwell C diamond insert was employed, the tip being ground to a radius of 200μm.

D. 3. Results and discussion

D. 3. 1. Adhesion

The adhesion measurement have been carried out at Hull by Mr B. Ollivier. A summary of the results obtained is presented in this paragraph; for more details the reader is referred to refs. [113 & 103.]

The first adhesion characterisation showed that none of the films deposited on PET could be removed by adhesive tape testing, although low carbon content (i.e. high hydrogen content) DLC films deposited on glass during the same run were easily removed by this method. The adhesion of DLC films deposited on PET is better than on a glass substrate.

Semi-quantitative results have been obtained using the scratch test method. In this case the PET substrate was bonded to a glass slide with an epoxy resin [103], and the scratch test was performed on the coated polymer. While the load was applied, the sample was moved at a constant speed of 0.1mm/sec. The load was then incrementally increased for a new scratch on an adjacent area. The critical load was defined as the load for which debonding occurred in the film. Debonding was associated with the DLC failure. Tests have been carried out on 70nm and 200nm thick films. The film thickness seemed to have no influence on the critical load value for films produced in similar deposition conditions . No correlation between adhesion and gas carbon content has been found, nor with voltage (the films studied were however very thin (< 0.2μm)). Critical loads for the DLC films deposited on PET are around 130 g. For comparison, the critical load for sputtered gold on PET is 120g (sputtering is generally considered to give adherent coatings on plastics [114]), and the value for evaporated titanium is between 50 and 60g (low adhesion).

D. 3. 2. Transmission in the visible regime of DLC on PET

When acetylene only was utilised as the FAB source gas, the PET coated with DLC was semi-transparent as expected. The DLC films obtained on PET were typically brown beyond 300nm thickness.

In section VI.C.2, we showed that mixing high proportions of hydrogen with the FAB source hydrocarbon gas was a way to increase the transparency of DLC films deposited on glass substrates. Since transparency is an important parameter in encapsulation applications (in order to retain the benefit of using PET), new experiments have been carried out to improve the optical properties of DLC films deposited on PET using acetylene-hydrogen mixtures at different deposition conditions.

The results obtained with different proportions of hydrogen for a constant set of voltage and current values are given in Fig.VI.33, the corresponding deposition conditions being gathered in Table VI.5. As we can see, transmittance of the coated PET has been relatively improved. For example at $\nu = 15000\ cm^{-1}$, transmittance increased by 40.2% when the carbon content in the FAB source gas was reduced from 50 to 6.5 %.

Table VI.5 : Summary of film deposition conditions using the FAB source technique.

Film	(1)	(2)	(3)	(4)
Carbon content (atom %)	50	36.25	20.25	6.55
Flux C_2H_2 (ml/min)	40.8	54.4	27.7	6.5
Flux H_2 (ml/min)	0	40	82	85.5
Current (A)	0.1	0.1	0.1	0.1
Voltage (kV)	1.3	1.3	1.3	1.3
Thickness (nm)	75	70	70	75
Deposition rate (nm/hr)	300	200	130	55

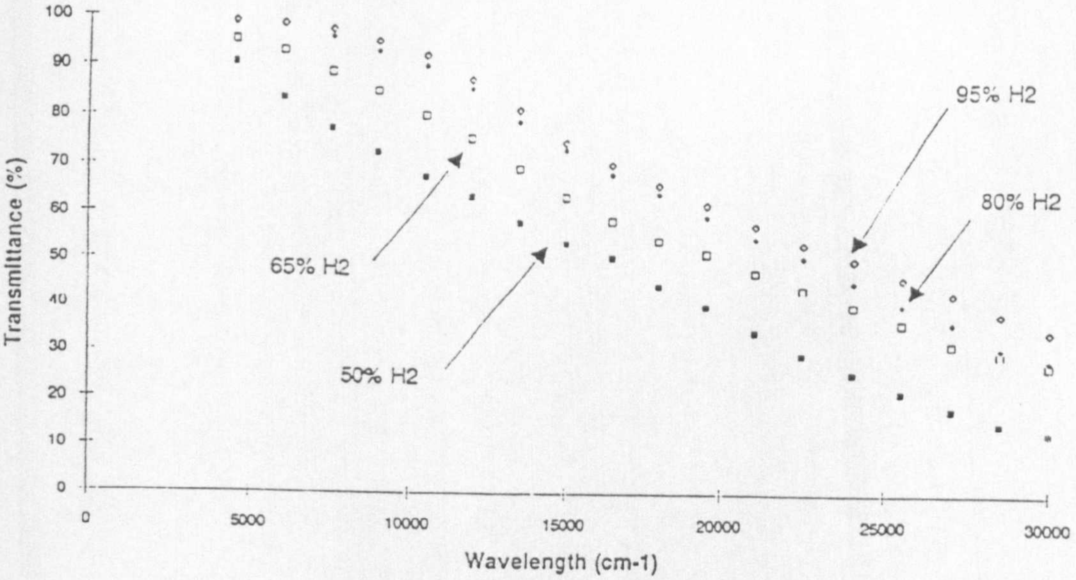

Fig.VI.33 **Influence of hydrogen on the transmittance of PET coated with a FAB source film.**

D. 3. 3. Further increase in transmittance

The impact energy of the beam has been demonstrated to influence the hardness and transparency of DLC films deposited on glass substrate by the FAB source technique (Chap. VI). Experimental conditions have been chosen to achieve highly transparent films. When the FAB source voltage was decreased, transparency of the coated PET film increased dramatically (Fig.VI.34). Transparency of film (1) and (5) has been improved as expected when the carbon content in the FAB source gas was reduced. Despite this, film (6) showed more transparency than film (5) although its corresponding carbon content is higher,(Table VI.6), but this is due to a lower voltage and a higher discharge current (i.e. a higher degree of ionisation which is also beneficial for transparency) (see Chapter VIII). A big improvement in the transparency of DLC films can be achieved under optimum deposition parameters (low carbon content, low voltage and high discharge current).

Table VI.6: Experimental conditions of DLC films on PET

Film	(1)	(5)	(6)
Carbon content (%)	50	6.6	12.4
Flux C_2H_2 (ml/min)	40.8	6.6	15
Flux H_2 (ml/min)	0	90.4	91.2
Current (A)	0.1	0.1	0.18
Voltage (kV)	1.3	1.3	0.7
Thickness (nm)	75	75	70
Deposition rate (nm/hr)	300	210	60

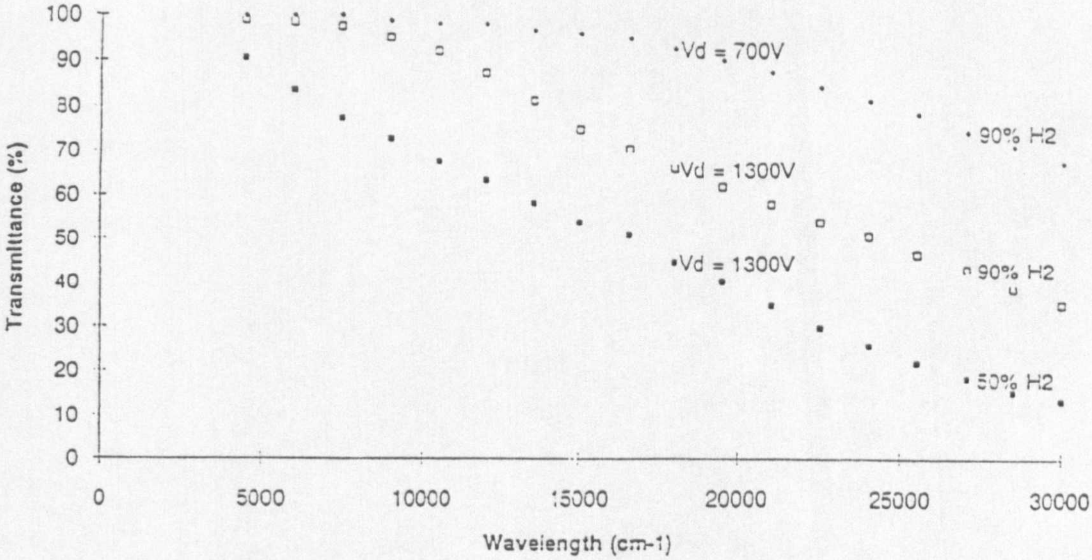

Fig.VI.34 Influence of hydrogen and voltage on the transmittance of PET with a FAB source film.

D.4. Conclusions

Adhesion of DLC on PET has been shown to be as good as that of sputtered gold on PET, and very superior to evaporated titanium on PET.

It has been shown that FAB source DLC films deposited on PET at room temperature were more transparent when a low carbon content source gas, high discharge current and low voltage were used. However, low carbon content leads to low deposition rates; the FAB source technique does not operate at very low voltages and discharge current is also limited to 0.3A. Modified FAB sources operating at low voltages and higher discharge current could permit better results; for example the latter could be achieved using an electron-emitter or magnetic field in the source.

CHAPTER VII

INVESTIGATION INTO R.F. AND D.C. EBPVD CARBON FILMS.

1. Introduction.

Carbon films deposited by many different PVD an CVD techniques have been the object of many studies. In these works the carbon source is, however, often a hydrocarbon gas, and when graphite is the carbon source it is often sputtered rather than evaporated. Most works in which graphite was evaporated in vacuum or in a plasma were unsuccessful in producing DLC films. The films were soft, black, conducting and graphitic. An investigation into EBPVD carbon films was therefore needed.

Normally in order to coat insulating samples rf plasma is needed to overcome substrate charging effect (Chap. IV). In this study insulating samples have been coated with carbon films in the dc regime as well when the glow discharge was assisted with an electron emitter (tungsten filament). The effect of this filament on the discharge mechanisms will be discussed in this Chapter.

Deposition conditions in the PVD techniques are different from that of FAB source process. The main differences are that in the PVD process the substrate is biased and immersed in the plasma, the deposition pressure is higher, the particles bombarding the substrate are not monoenergetic and it is possible to decrease this energy to very low values (<100 eV). A comparison between the properties of EBPVD films and FAB sources films was therefore, expected to reveal interesting differences.

2. Experimental

This experimental unit comprised a 450 mm cube stainless steel chamber, in which a differentially pumped 225° bent beam gun was located on the base for the evaporation of solid graphite. The unit was evacuated to high vacuum by means of both a 9" oil diffusion pump connected directly to the chamber via a throttling part and a 6" oil diffusion pump situated in the plenum chamber, to provide differential pumping of the electron gun. Both oil diffusion pumps were simultaneously backed by a single two stage rotary vane pump. Figure VII.1 shows a photograph of the r.f./d.c. EB PVD unit.

In general the substrate holder was a stainless steel rod (1 cm diameter , 50 cm long) mounted vertically in the chamber. This served as the cathode in the system as it was directly connected to the power supply, The samples were fixed horizontally to this central column at a distance of 30 cm and 40 cm above the source (Fig. VII. 2a & 2b). In order to overcome sputtering edge effects [115] on the samples for some of the work especially at high discharge intensity, it was necessary to modify the jigging arrangement. A stainless steel disc (24 cm diameter and 0.5 mm thick) was mounted perpendicularly to the rod and the samples were fastened to the bottom and the top of this disc at different distances from its centre. The effect of this distance on the film properties will be discussed in this Chapter.

The negatively biased filament used to enhance the plasma was located about 5 cm above the base. This filament provided control of the specimen current, supported the discharge at low pressures and permitted the coating of insulating substrate in the d.c. regime. The substrate assembly could be operated as a cathode via a 3 kV d.c. power supply or alternatively a low frequency 380 kHz r.f. power supply.

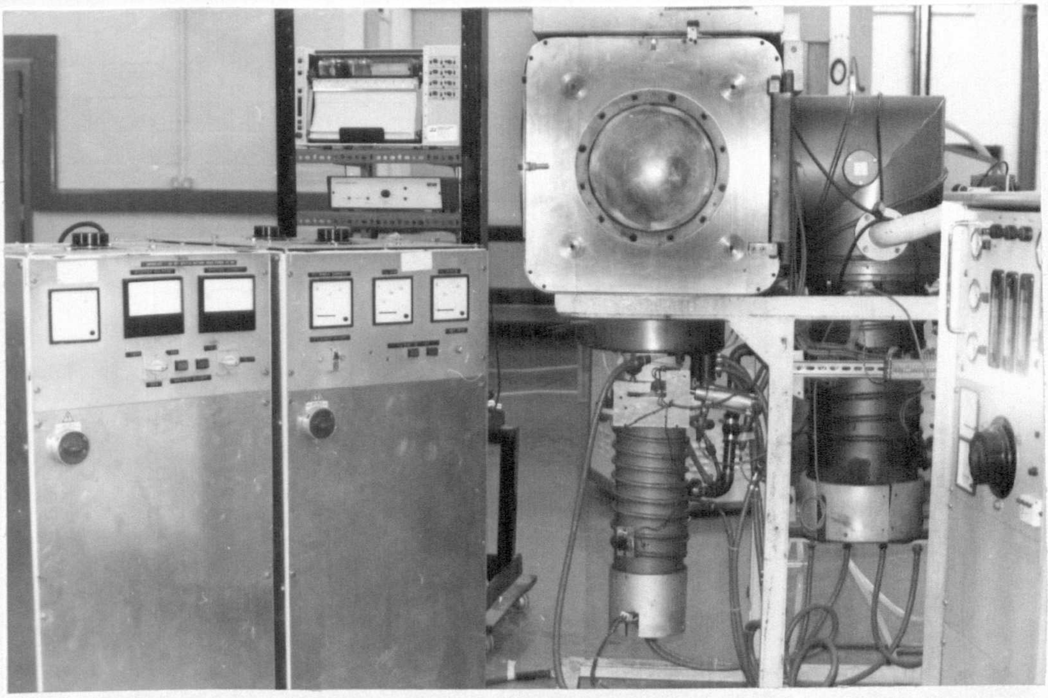

Fig.VII.1 Photograph of the Experimental Hybrid DC/RF Electron Beam PVD Deposition Equipment.

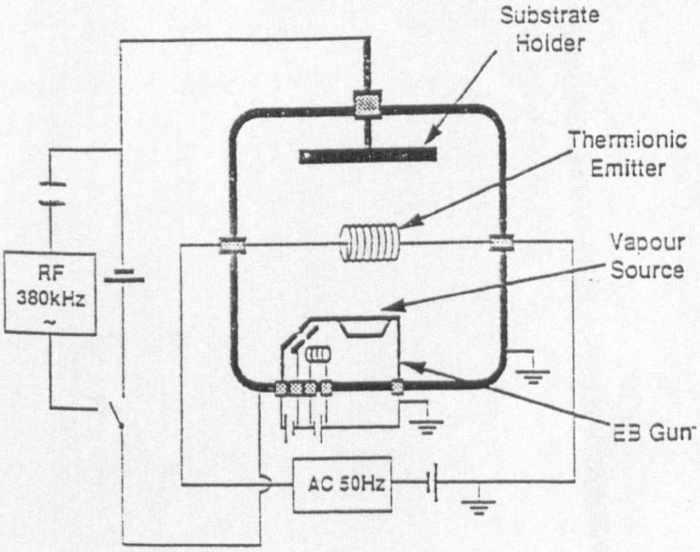

Fig.VII.2a Schematic Layout of Thermionically Enhanced Plasma

Gas monitoring was accomplished using a mixture of glass "Rotometer"flow tubes and mass flow controllers. Argon, hydrogen and hydrocarbons (methane, propane, butane and acetylene) have been used to support the discharge or as a carbon source. The system was used also as a hybrid technique in which the carbon source was, simultaneously, evaporated graphite and butane. The deposition temperature increased during coating, due to bombardment, but was never greater than 400°C.

3. Coating procedure

3. 1. First approach

A first series of carbon films was produced by evaporation of graphite in an argon discharge. Two substrate materials were investigated: glass and polished tool steel (ASP23, 64 Rc).

It was clear from the first produced films that the DLC production by the EBPVD technique is not a trivial procedure as was relatively the case in the FAB source technique. In fact the films produced were almost all black and soft as is usually reported for carbon films produced by graphite evaporation. Some important observations were, however, made:

-Films produced at lower evaporation rates were less dark and slightly harder.

-At very high discharge currents no film was produced and the substrate was etched.

-Deposition rate depended on evaporation rate, discharge current and pressure.

3. 2. Second Approach.

Taking into consideration these observations, a second series of films was produced, during which electron beam power was kept low and the discharge current was varied during coating until growth of brown or transparent films was observed. (Film growth could be observed by the eye through the chamber window). Hydrogen and argon were investigated using dc and r.f. EBPVD techniques in deposition conditions as summarised in Table VII.1.

In order to work in conditions where only carbon and hydrogen are present in the plasma, evaporation of graphite in r.f. or d.c. hydrogen or butane discharges was investigated. The presence of argon in this later hybrid system was thereby avoided, which could be a further variable in nucleation and growth kinetics. Deposition conditions in the d.c. hybrid system are summarised in Table VII.2.

TABLE VII.1

Deposition conditions of the (r.f.) EBPVD system.

(pressure, 0.6 Pa; electron beam gun power, 1.4 kW).

Run	**Gas**	**D.C. offset (kV)**	**Peak current (A)**	**Coating rate (μm h^{-1})**	
				Glass	Steel
RF1	Ar	1.3	0.6	0.4	Etched
RF2	Butane	1.1	0.6	0.6	1.4
RF3	H2	1.1	0.6	0.5	Etched

Two substrate materials were investigated: glass and polished tool steel (ASP23; Rockwell C hardness, 64 HRC).

Table VII.2
Hybrid d.c. electron beam physical vapour deposition conditions

(I_{em} = 5A; V_F = -100V)

Run	**Voltage (V)**	**Current (mA)**	**Gas flow (butane) (ml min^{-1})**	**E.B.gun power (kW)**	**Pressure (mTorr)**	**Coating rate (μm h^{-1})**
DC1	200	28	17.9	2.1	10.37	2
DC2	200	30	17.9	1	7.9	2
DC3	500	43	17.9	1	7.9	1.3
DC4	1000	51	17.9	1	7.9	1.2
DC5	500	31	17.9	0.8	7.1	1.8
DC6	500	29	32.2	1	8.47	2.8

4. Results.

4.1. Effect of sample holder shape and sample locations on the coating uniformity

For both rf and dc EBPVD substrate edge effect was important. Substantial etching of the edge of the samples was observed especially at high voltages and current densities. In the situation where the sample holder was a vertical rod axis (Fig VII.2b), the films grown in the vicinity of the rod were thicker, and were thinner or etched at the other end of the glass slides substrates which were (7 × 2.5)cm . This suggests that the particles bombarding the rod near the substrate were re-ejected and deposited on the adjacent glass region The etching on the other end of the substrate is believed to be caused by a non-uniform dark space length at the sample edge [115]. This problem of uniformity was overcome by changing the rod to a disc holder (FigVII.2c). The substrate edge effect remained but 2cm from the edge the films were uniform. The deposition rate decreased with increasing substrate-crucible distance. All the properties carried out on the films were measured in the thicker and uniform regions of the samples.

4. 2. Effect of cathode voltage on the impact energy in the dc mode.

In the dc regime, When the filament was not used, V_S had to be at least 3kV to create a glow discharge. In this case only graphitic coatings were produced on conducting substrates. This is often reported for carbon films produced at high impact energy . On insulating materials no coating was produced due to charging effects (Chap. IV). When the process was assisted with the filament the discharge could be maintained at very low

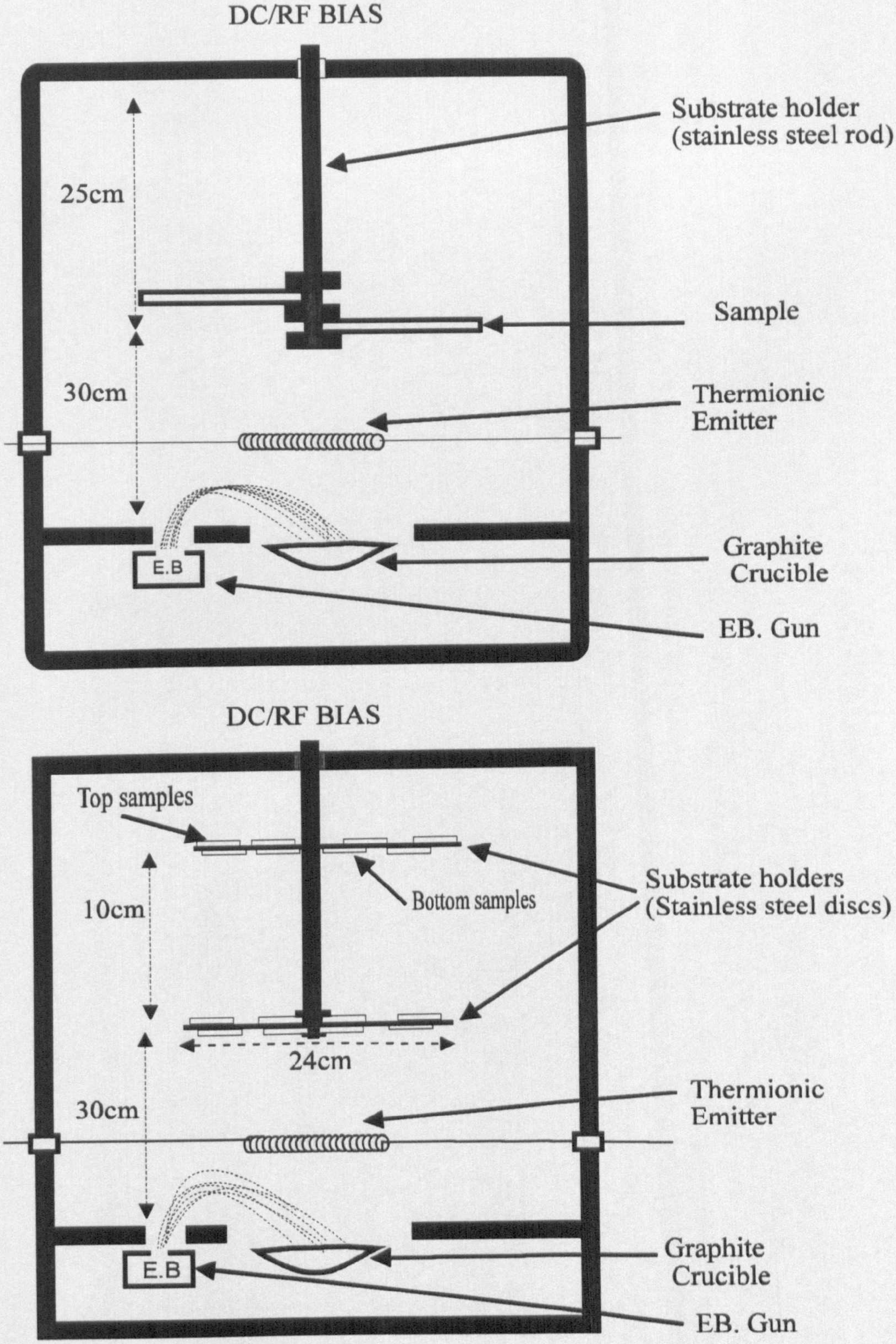

Fig.VII.2b Schematic of different sample locations and substrate holders in dc/rf EBPVD

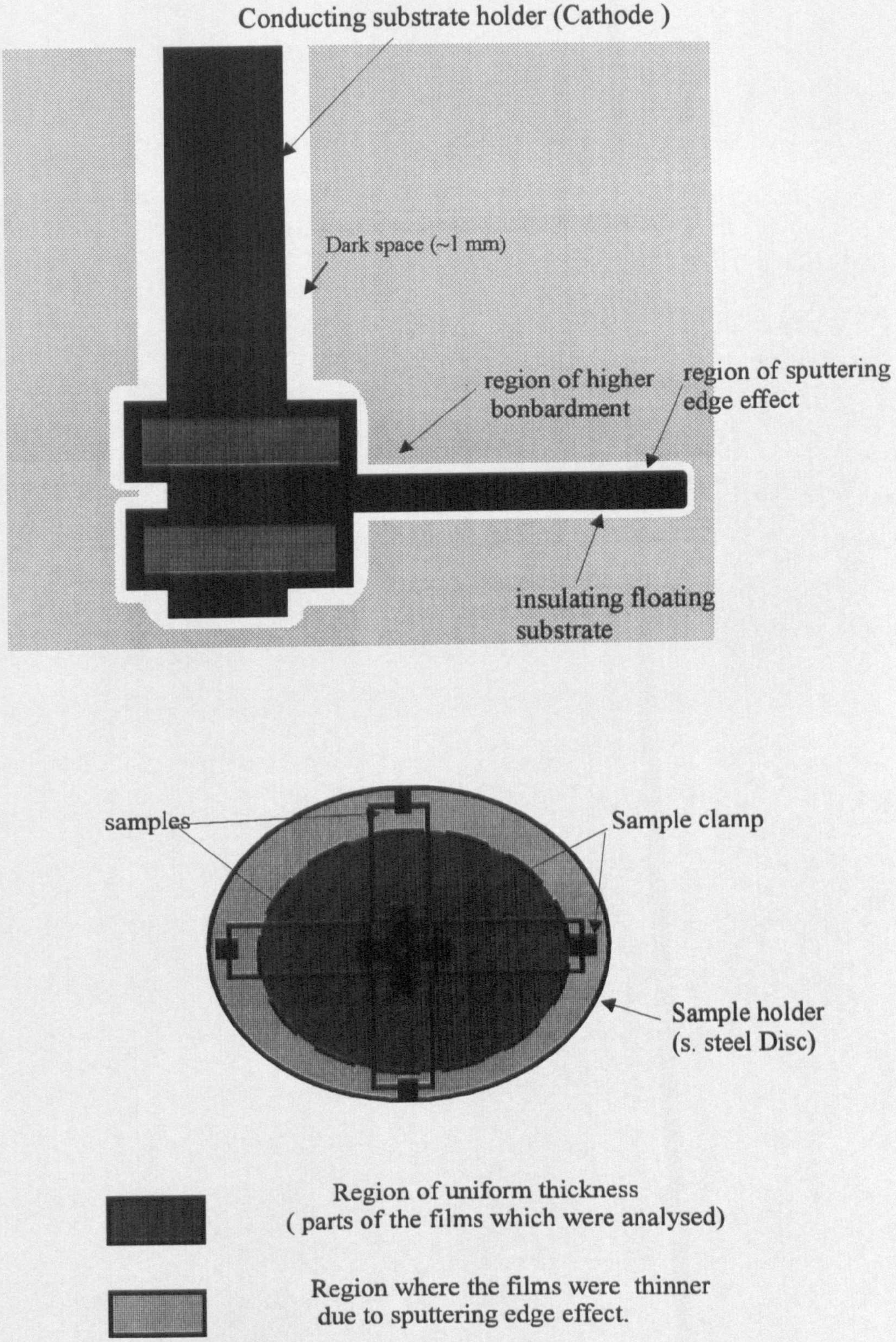

FigVII.2c Schematic of substrate assembly and sputtering edge effect in rf and dc EBPVD systems.

voltages (Table VII.2) and insulating substrates (glass and silicon) have been coated with a rate at high at 4μm/hr. The problem of the charging effect has therefore been removed by the filament. The electrons are accelerated towards the plasma due to the electric field existing between the filament and the plasma. (the plasma potential is around 1 or 2 eV [78] and the filament is negatively biased at -100V with respect to the chamber). The plasma electron density will therefore increase. The building up of positive surface charges will be neutralised by electron bombardment coming from the plasma. The substrate will develop a small negative potential with respect to the plasma due to the higher mobility of the electrons with respect to the ions. Since the dark space is of the order of a millimetre, ions existing at the edge of the negative glow region are very close to the substrate and can therefore be deposited on the insulating material with out losing much of their initial energy E_0. This energy was reported to be not always zero [78]; some ions may return to the negative glow with a substantial energy E_0 after being accelerated towards the cathode (conducting substrate holder in our case) and re-ejected. Decreasing the dark space increases E_0 and was found to be as high as 100eV at V_S =3kV and L = 4cm, where L is the dark space length in a triode system. In our case although V_S was less than 1kV, L is forty times smaller. Therefore we believe that these ions or neutrals are contributing to an increase of impact energy on insulating materials and therefore will be dependent on the cathode voltage. This also could explain the decrease of the optical band gap and α_S when V_S increases since it was similar to the one related to the impact energy. The higher thickness obtained in the region of the substrate which was close to the rod axis (Fig VII.2b&2c) and the more uniform thickness obtained in the case of the disc sample holder goes in line with this proposed growth mechanism.

4. 3. Mechanical evaluations

The film growth mechanism in the EBPVD coating depended considerably on the process parameters used (Tables VII.3& 4). In some cases, for example, no net deposition was observed. The reason for this could have been carbon diffusion into the (steel) substrates, or debonding could have occurred during deposition. The coating method giving the best adhesion and hardness results was graphite evaporation in an r.f. butane plasma. The average hardness level was 4000 H_K (25g) on tool steel . The structure was dense, as seen in Fig. VII. 3. The coating on glass, produced in the same run, was much thinner (0.6μm cf. 1.4μm); this coating was completely transparent whereas that on tool steel was brown. When this deposition process was repeated using argon, rather than butane, no coating was produced on the steel (due to sputter-removal), but again a completely transparent film was produced on glass (typically 0.4μm thick). We tried to increase this thickness by repeated coatings, but for reasons which are not known to us further growth did not occur. Similar transparent films were produced when graphite was evaporated in a hydrogen (alone or mixed with argon) plasma. At high discharge current a hydrogen plasma caused severe etching to the glass and steel substrates.

TABLE VII.3

Summary of r.f. EBPVD coating properties

Run	Plasma Gas	Knoop Hardness (H_K)		E_{opt} (eV)	Refractive index	α_s ($\times 10^3$ cm^{-2})
		Glass substrate	Tool steel Substrate			
RF1	Argon	1000 (10g)	Etched	3.5	1.5	0
RF2	Butane	1000 (10g)	4000 (25g)	2.6	1.8	46
RF3	Hydrogen	1500 (10g)	Etched	3.5	1.7	20

Fig.VII. 3 **Scanning electron micrograph of a carbon film deposited on tool steel using r.f. EBPVD in butane plasma**

D.C. plasma films were all transparent (from yellow-to brown) in a butane plasma. The structure was less dense than rf films , as seen in Figs VII.4 and VII.5. Some porosity which is thought to be a result of hydrogen effusion during coating under the effect of temperature (300-400°C) was observed by SEM.

These films were brittle, and attempts to measure the hardness were unsuccessful. The net deposition rate in the d.c. plasma case was higher than for r.f., presumably due to a lower resputtering rate. This was on a glass substrate while no deposition was obtained on a metallic substrate. The reason of this is could the combination of high impact and high temperature as it was found for FAB source films when they were annealed to 300°C during coating.

TABLE VII.4
Summary of d.c. EBPVD coatings properties

Run in butane plasma	Knoop hardness (H_K)		E_{opt} (eV)	α_S ($\times 10^3$ cm^{-2})	Refractive index
	Glass substrate	Tool substrate			
DC1	Brittle	Poor adhesion	1.1	144.6	1.7
DC2			1.9	160	1.7
DC3			1.6	120	1.8
DC4			1	45	1.9
DC5			2.3	162	1.6
DC6			2.8	180	1.7

Nanoindentation testing was performed on r.f. deposited a-C:H films. Fig. VII.6 illustrates the hardness versus depth and the hysterisis curves obtained for typical r.f. EBPVD films deposited respectively in argon and butane at voltages of 1500 V and 2000 V. The hardness results and deposition conditions are summarised in table VII.5. The results show that r.f. EBPVD films are extremely hard (33-44 GPa) and the lowest elastic recovery was obtained for the non-hydrogenated film (11% against 44% for the a-C:H film).

Pin on disc testing was carried out by P.Holiday [64] who reported that r.f. a-C:H films exhibited a film wear of 48 × 10^{-6}mm^3/Nm which when compared to the standard SAE 52100 pin on ASP23 disc material (64-87×10^{-6}mm^3/Nm) represents only a modest reduction in wear. The coefficient of friction was however greatly reduced to a value of μ =0.16 compared to the "standard"(μ =0.45-0.54) for steel against steel. These results correspond to the best coating in term of hardness and adhesion obtained. D.C EBPVD films and the films obtained by evaporation of graphite in vacuum had poor adhesion and hence poor performance in the pin on disc machine. More details on the mode of coating failure and SEM observation of the wear tracks are reported in P. Holiday's thesis [64]

Table VII. 5

Nanohardness and elastic recovery of typical (a-C:H and a-c) r.f. EBPVD films

Film type	a-C	a-C:H
Plasma	Argon	Butane
Voltage (V)	1500	1500
Current (A)	0.6	0.6
Hardness (GPa)	44 (2.7mN)	33 (2.7mN)
% Indentation elastic recovery	11% (4mN)	44% (2.7mN)

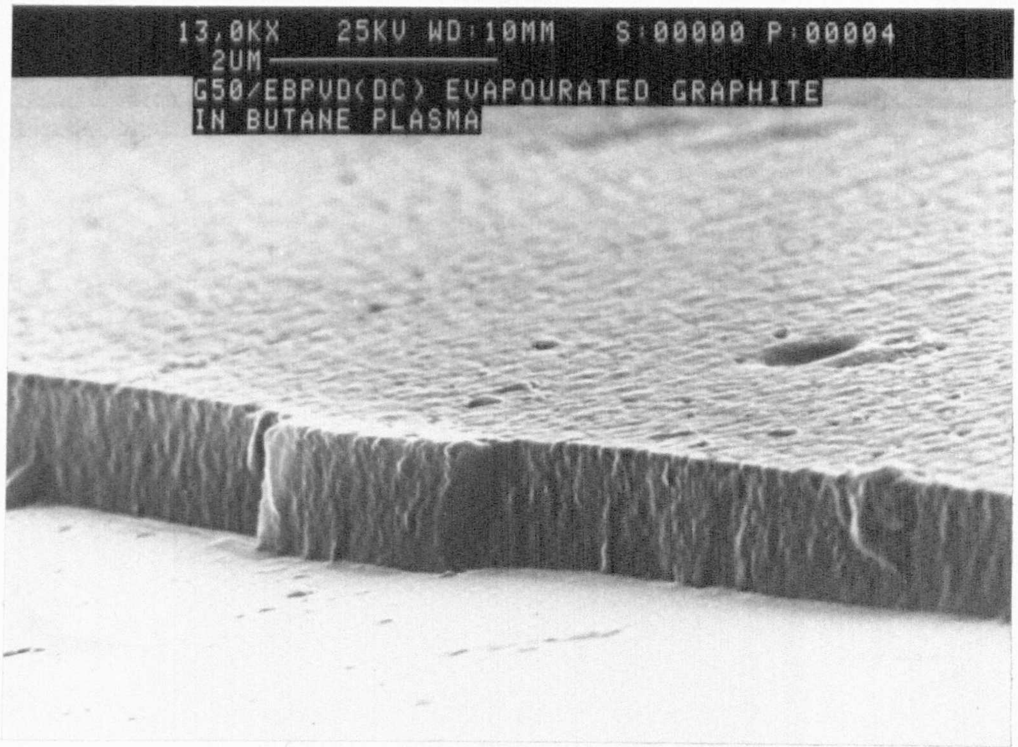

Fig.VII.4 Scanning electron fracture micrograph of a carbon film deposited on tool steel using d.c. EBPVD (butane + graphite evaporation).

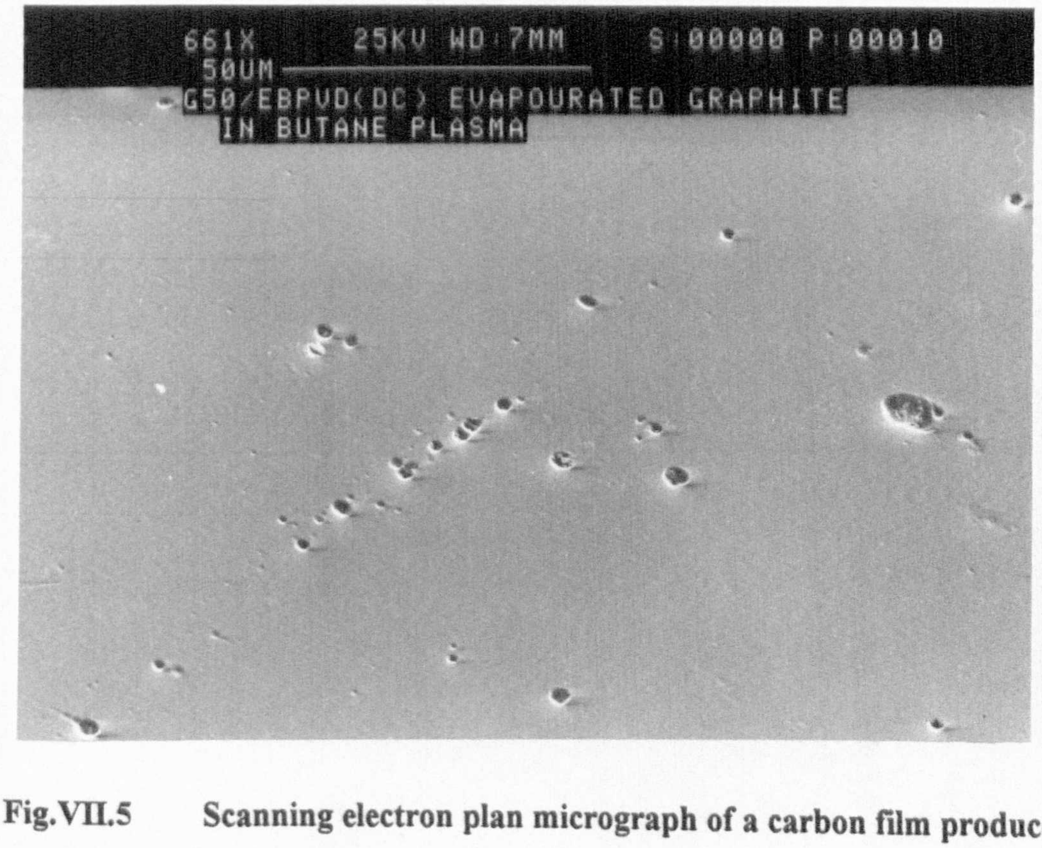

Fig.VII.5 Scanning electron plan micrograph of a carbon film produced on tool steel using d.c. EBPVD (butane + graphite evaporation).

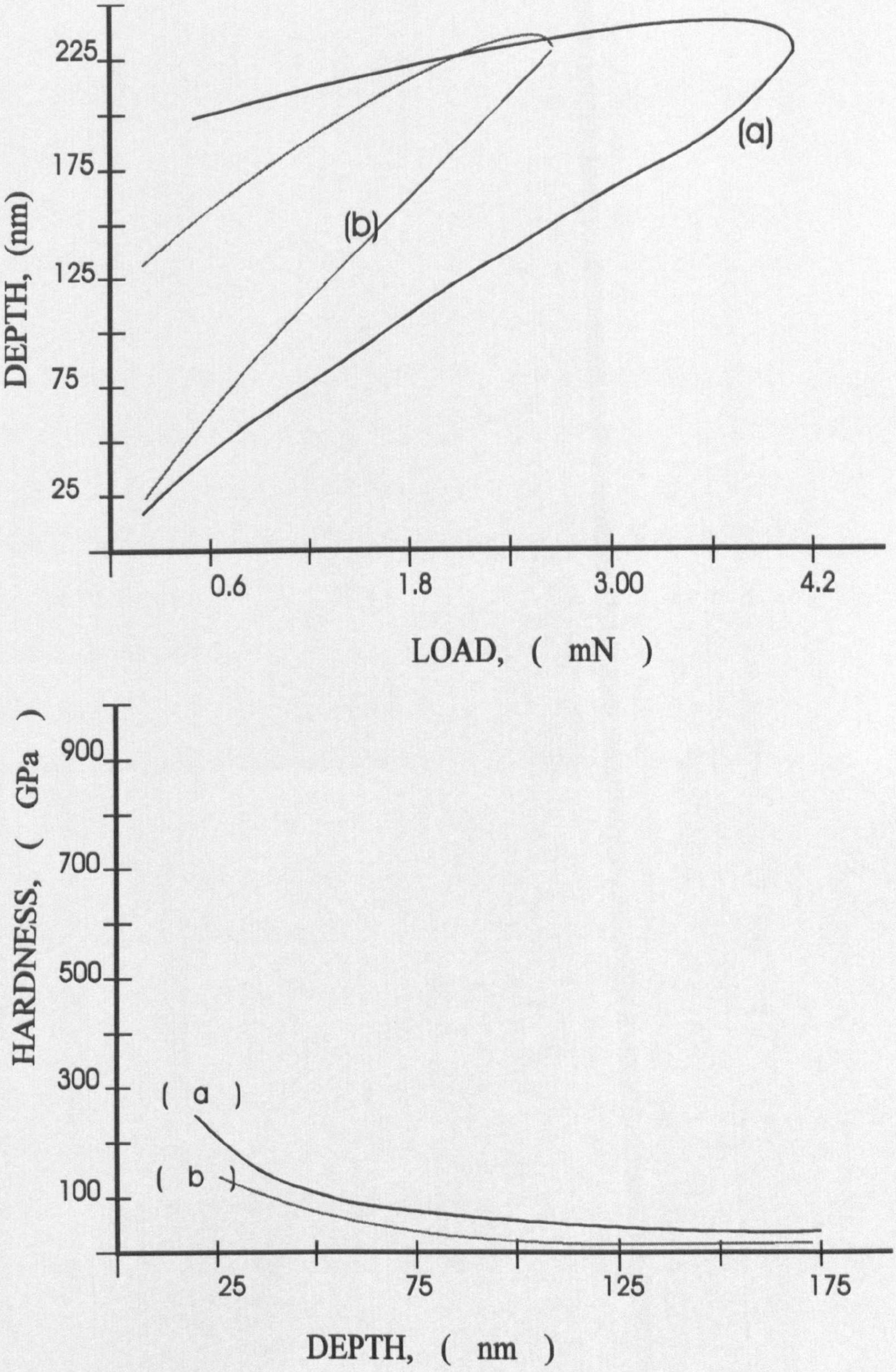

Fig.VII.6 **Nanohardness and elastic indentation recovery of different r.f. EBPVD carbon films;**

(a) non-hydrogenated (argon plasma) on tool steel.

(b) hydrogenated (butane plasma) on tool steel.

4. 4. Optical evaluations.

4. 4. 1. Visible regime.

The absorption of the films produced by the r.f. and d.c. EBPVD methods is considerably different and depends on the process parameters used. The deposition method which gave the best transmission was evaporation of graphite in an r.f. argon plasma. These films were completely transparent. Their optical band gap was measured and found equal to 3.5 eV. (as a glass substrate is not suitable for the measurement of such a high photon energy, these transparent films were deposited on a quartz substrate). The substitution of argon by butane under the same r.f. conditions also gave transparent films with E_{opt} = 2.6 eV (Table VII 3).

In the d.c method, the E_{opt} value varies in the range 2.8-1.0 eV(Table VII 4) depending on the process parameters used. The optical band gap decreases dramatically with increasing d.c. voltage (Fig. VII. 87) up to 1000 V (at 1500 V there was no net deposition because of sputter removal). A similar correlation has been reported for r.f. plasma chemical vapour deposited (CVD) films using C_6H_6 [109,116] when the r.f. voltage is increased. The refractive indices of the films are listed in Table VII.3&4. Some of the d.c. films have a refractive index as low as 1.5. This is a low value when compared with FAB source films. The decrease of the refractive index with the increase of the voltage is related to the increase of the film density (Chap.III).

4. 4. 2. Infrared regime.

The IR transmission spectra obtained from the r.f. and d.c. films are presented in Figure VII.8 together with a FAB source spectrum for comparison. It can be seen in this figure that d.c. films contain a considerable amount of bonded hydrogen. Some of these films show the water absorption band usually reported for a-C:H films at around 3300 cm^{-1}. The type of C-H bonds observed around 3000 cm^{-1} are shown in Figs.VII.9 & 10. The frequencies observed are usually associated with hard a-C:H films. The proportions CH_3:CH_2:CH are found to depend on deposition conditions. The absorption coefficients were calculated in the region 4000 - 2000 cm^{-1} and are presented in Figure VII.11. The concentration of bonded hydrogen in the coatings as obtained by integration of the C-H stretch absorption around 3000 cm^{-1} is reported in Table VII.3&4 ($\alpha_s = \int \alpha d\nu$; ν is the wave number in cm^{-1})

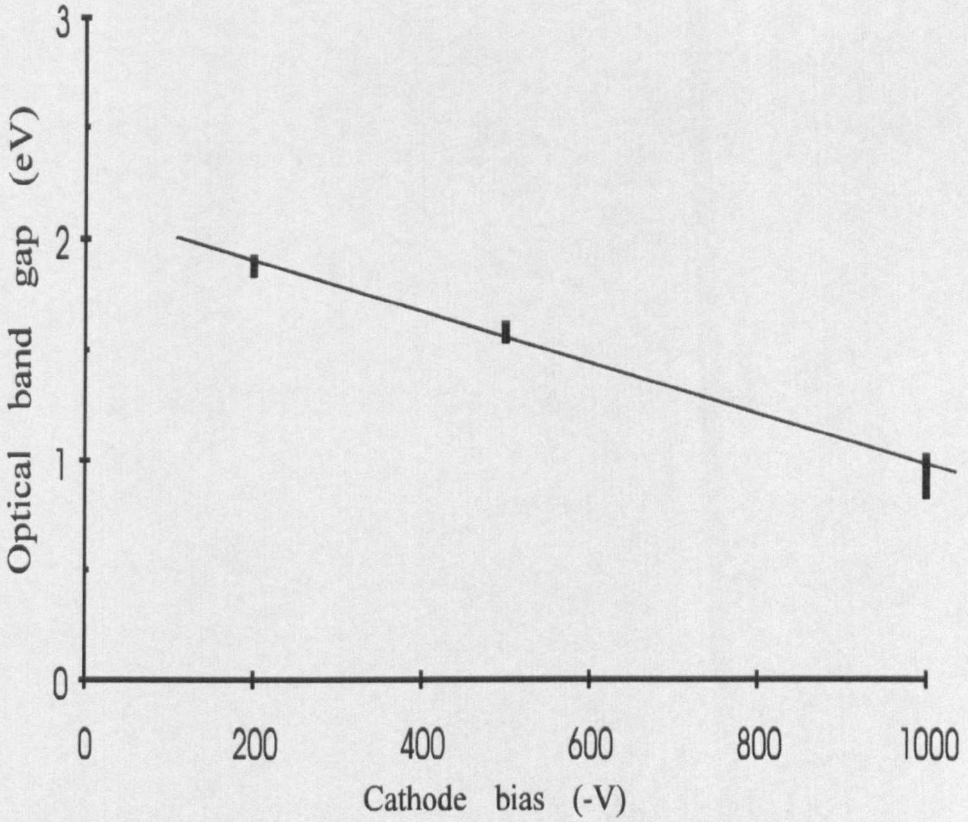

Fig.VII.7 **Effect of cathode voltage on the optical band gap of d.c. EBPVD films.**

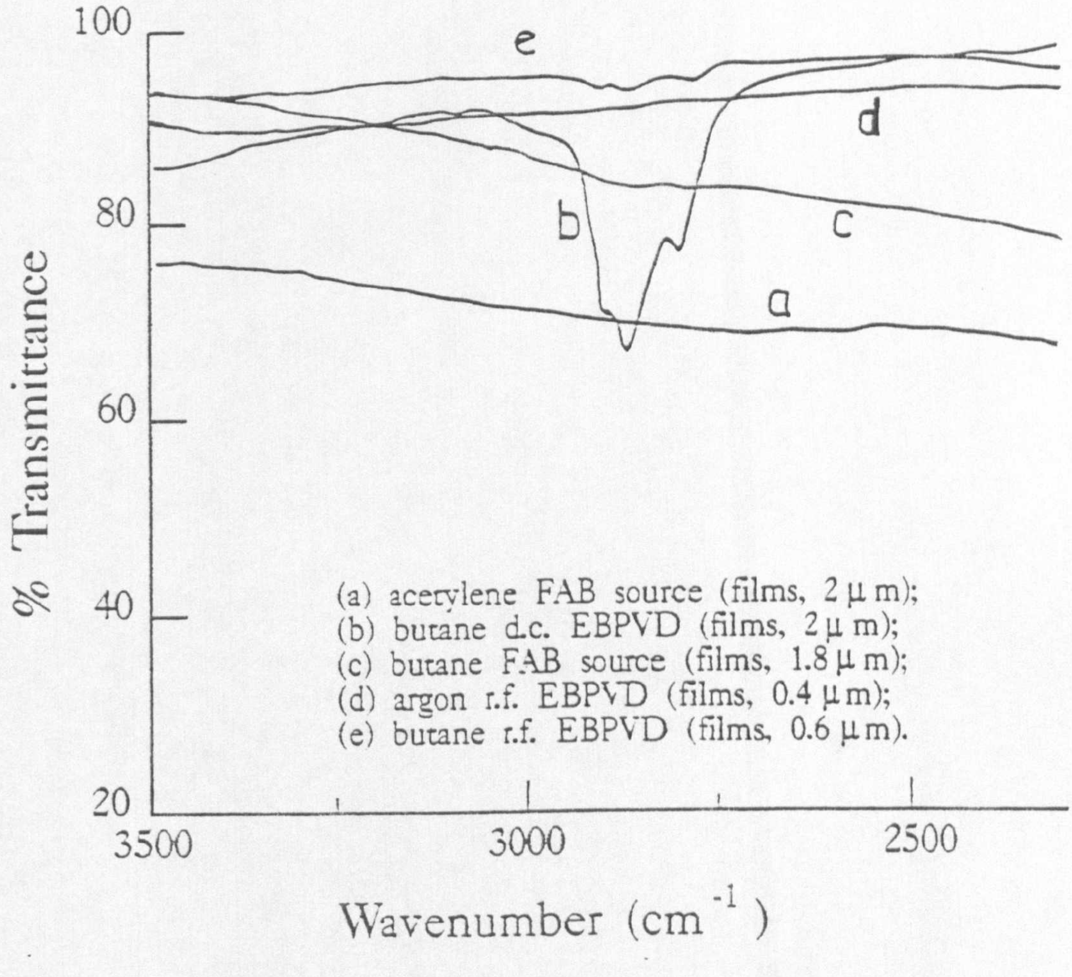

Fig. VII.8 **Typical IR transmission spectra from carbon films produced on glass using different techniques and conditions.**

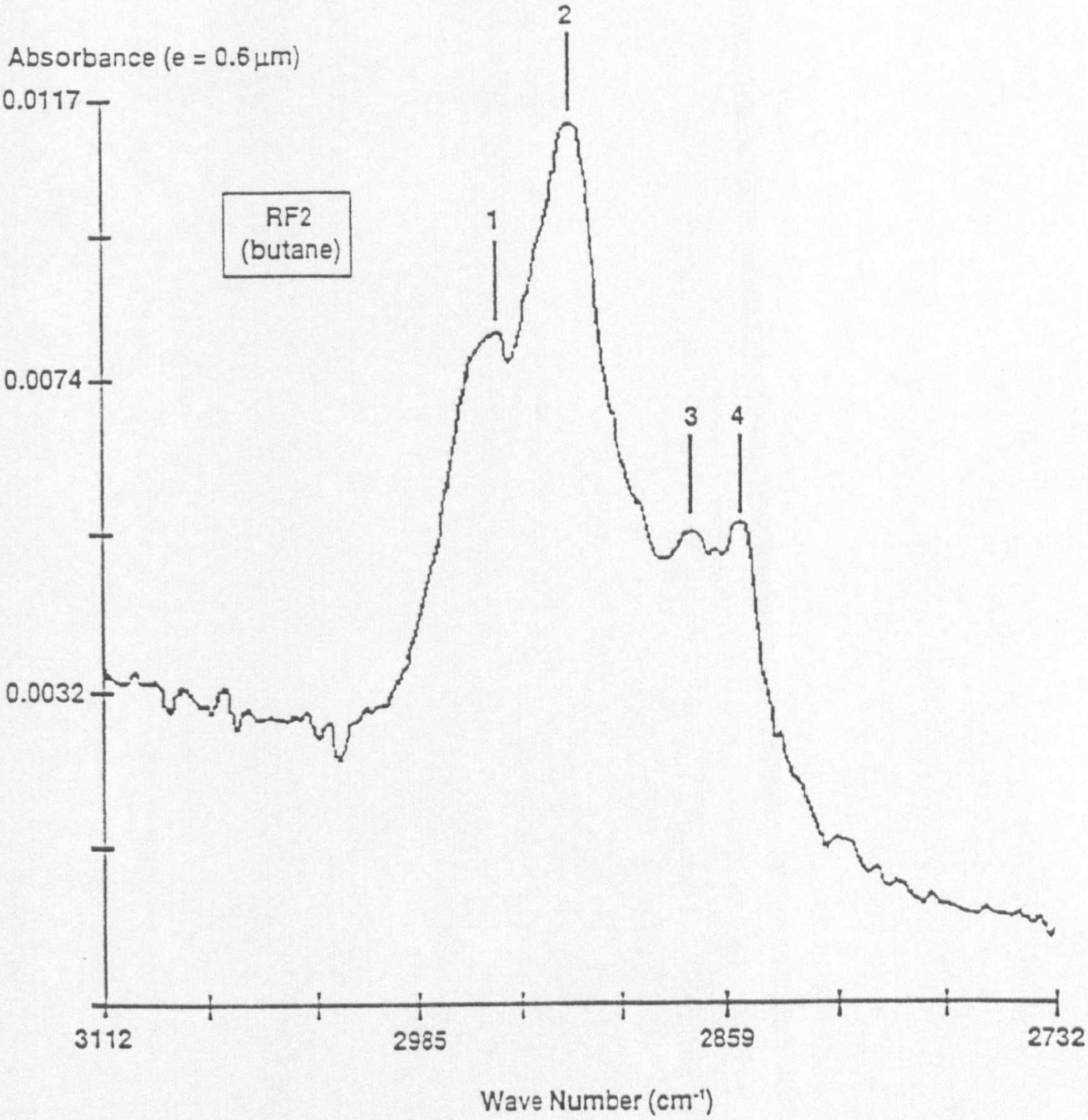

Line	Wave Length (cm⁻¹)	Assignment
1	2957.7	sp^3 CH_3
2	2924.8	sp^3 CH_2
3	2871.1	sp^3 CH_3
4	2854.6	sp^3 CH_2

Fig. VII.9 **C–H bonding types observed by transmission (run RF2; butane).**

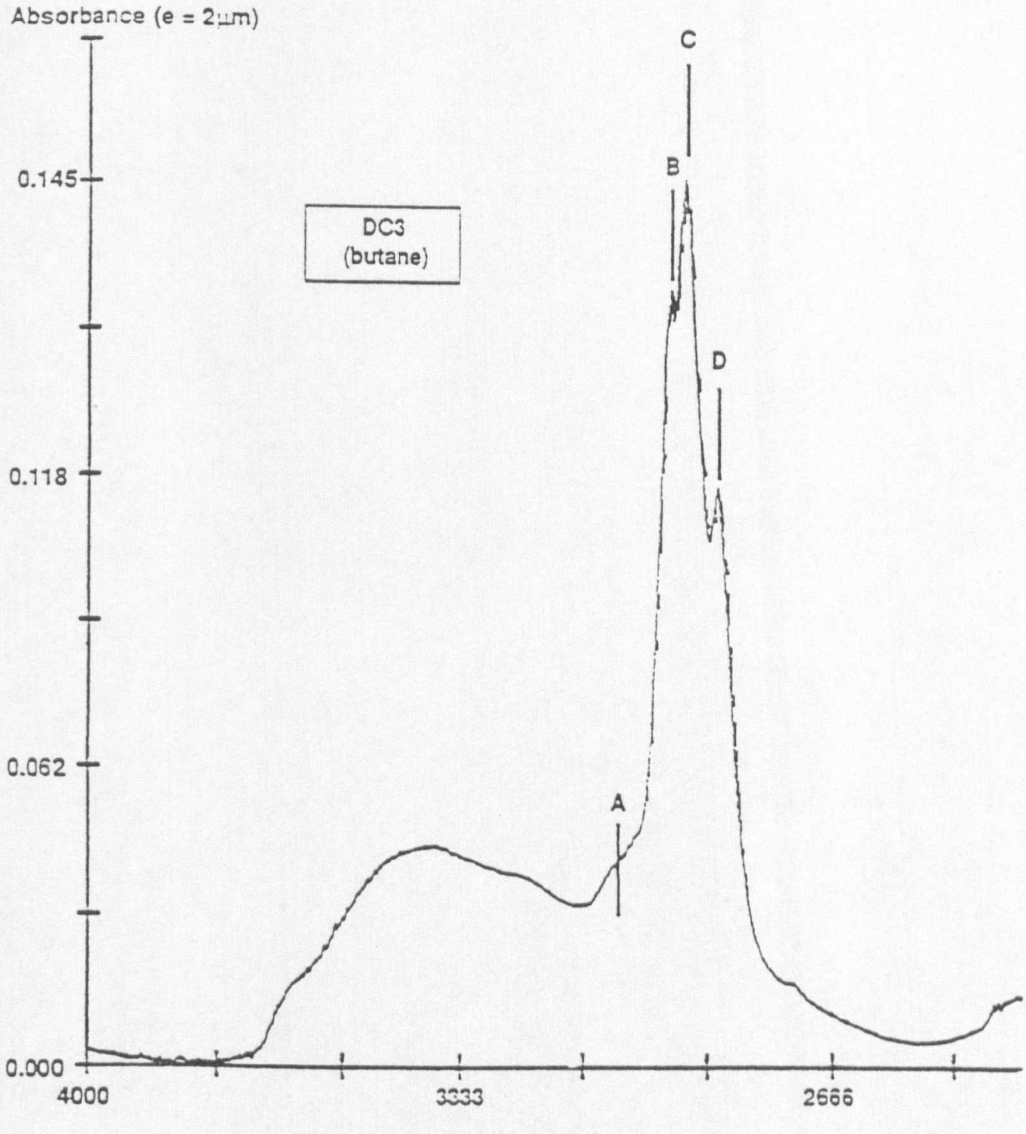

Line	Wave Length (cm^{-1})	Assignment
A	3025	sp^2 CH
B	2950	sp^3 CH$_3$ asym
C	2920	sp^3 CH$_2$ asym
D	2875	sp^3 CH$_3$ sym

Fig. VII.10 C–H bonding types observed by transmission (for DC3; butane).

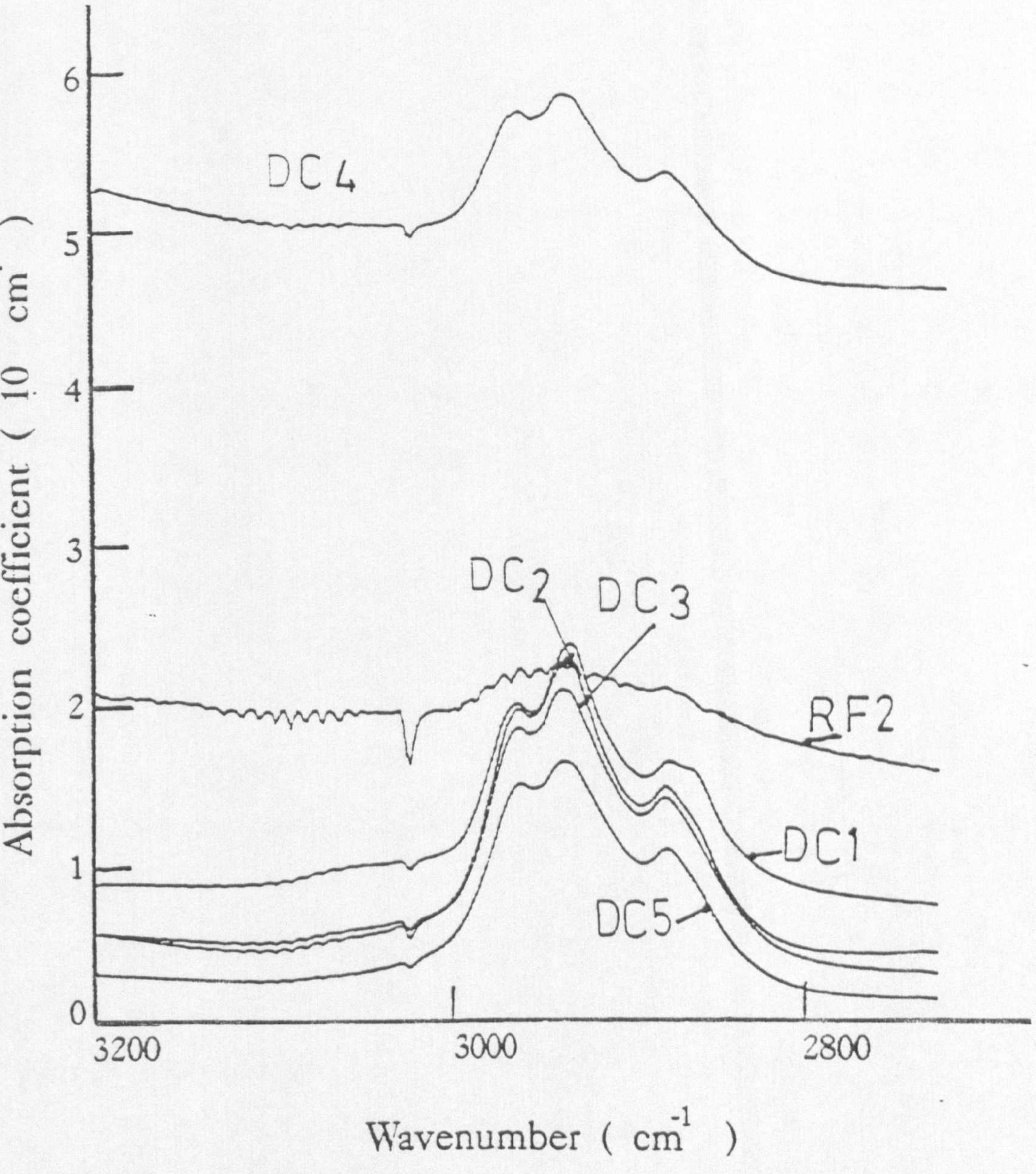

Fig. VII.11 Plots of absorption coefficient *vs.* wavenumber ν from carbon films produced using d.c. and r.f. EBPVD in butane plasma.

4. 5. Correlation between E_{opt} and α_S

In has been reported that there is a linear relationship between E_{opt} and α_S in r.f. plasma decomposition of C_6H_6 gas [109]. For our d.c. films only runs DC2, DC3 and DC4 could be fitted to a straight line (FigVII.12). DC1 is slightly below this line and DC 5 is above it. However it can be seen in Table VII.2 that in all these four runs the butane flux was kept constant but the electron beam power corresponding to these runs was the highest for DC1, the lowest for DC5 , and the same for DC2, DC3 and DC4. On the other hand when the electron beam power is constant increasing the butane flux increases the optical band gap for DC6. Therefore it appears that a linear relationship between E_{opt} and αs is obtained only when the carbon to hydrogen flow input ratio (r_c^H) was kept constant(Fig. VII.12).

The ratio r_c^H is kept constant by acting on the electron beam power and the gas flux. We therefore believe that each r_C^H ratio will have its own linear relationship. The relationship is of the form:

$$E_{opt} = A_1\alpha_S + f(r_c^H) \qquad (2)$$

A_1 is the gradient found when E_{opt} is plotted against α_S; $f(r_c^H)$ is the intercept on the E_{opt} axis.

Therefore we believe that the Dischler group [109] reported a linearity between E_{opt} and α_S for all their films, it is because they were working in a system where the relative carbon flow input to hydrogen input could not be changed. (rf discharge in one gas only (benzene)). It is not surprising to find that E_{opt} depends on the relative carbon flow input to hydrogen since for FAB source films at a constant voltage we have been able to increase E_{opt} by reducing the butane flux input to hydrogen. Also reducing the relative input of methane to hydrogen 1% in diamond synthesis is a necessary condition (Chapter II).

Therefore in order to correlate E_{opt} and α_S with an empirical expression a new parameter is needed. Ideally this parameter should be the $N_C/(N_C+ N_H)$ ratio where

N_C an N_H are respectively the number of carbon and hydrogen particles per unit of volume in the plasma near the substrate during deposition. However since access to this ratio is very difficult, the ratio of gases flux input is often used as an indirect measurement for this parameters. For example when C_nH_m is mixed with hydrogen the following expression is used as a parameter to follow the evolution of the real carbon to hydrogen in the plasma.:

$$n(n+m)^{-1}\Phi_g)\,[(n(n+m)^{-1}\Phi_g+\Phi_H]^{-1}$$

Where n Φg andΦ_H are respectively the C_nH_m and hydrogen fluxes. In Chapter VI we used this ratio when butane was mixed with hydrogen .The good linear relationship obtained in that case suggest that the input ratio is a valuable parameter for correlation studies. Furthermore all the important process parameters are often measured indirectly (eg the cathode voltage for the impact energy and the current density for the degree of ionisation).

Since in the hybrid dc EBPVD case the gas C_nH_m flux of the evaporated carbon is difficult to measure an expression as above was not possible. We had therefore to look for another parameter that increases when we increase manually the electron beam power. During deposition it was observed that the total pressure was responding instantaneously to the variation of the electron beam power. This suggests that the increase of carbon was the predominant factor acting on the pressure. We therefore decided to use this pressure increase in our estimation of the relative carbon flow input ratio r_c^H . The means of calculating r_c^H was first to measure the initial pressure prior to evaporation (P_0) corresponding to a fixed gas flux. The number of hydrogen atoms introduced into the chamber is a function, f, that depends on P_0 . It can be written as f(P_0) or f($(n(n+m)^{-1} P_0)$ since only a fraction of P_0 is related to hydrogen. After evaporation P_0 increased to P_t. The total number of hydrogen and carbon atoms introduced into the chamber is a function of g, which depends on P_t. It can be written as g (P_t).

The relative hydrogen input flow ratio, $N_H/(N_C+N_H)$, is therefore given by:

$$f[\,m(n+m)^{-1}P_0]\,/\,g\,(P_t)$$

But

$$N_H/(N_C+N_H) = 1 - N_C/(N_C+N_H)$$

Therefore

$$N_C/(N_C+N_H) = 1 - f[\,m(n+m)^{-1}P_0\,]\,/\,g\,(P_t)$$

Since the functions f and g are not known, in order to study the effect of the increase of C/(C+H) with the evaporation rate on the film properties we have used the ratio.

$$r_c^H = 1 - m(n+m)^{-1}P_0\,/\,P_t.$$

This is because we assumed that the latter ratio (r_c^H) increases as the former in the same way when the evaporation rate increases. This is justified by the fact that during deposition, P_0 was kept constant and therefore $f(\,m(n+m)^{-1}P_0)$ was constant too. Also the increase of P_t is caused manually by an increase in the evaporation rate which must increase with g. P_t could describe the increase in the function g.

When $f(\,r_c^H\,)$ was plotted against r_c^H our initial results suggest that a linear relationship exists (Fig. VII.13). This implies that the equation relating the optical band gap to the bonded hydrogen in the film and the r_c^H value is :

$$E_{opt} = A_1\alpha_s + A_2\,r_c^H + A_3 \qquad (3).$$

The result of increasing the voltage is to reduce α_s (Fig. VII.14). This relationship also confirms the previously reported observation, that to increase the optical band gap (eg by producing diamond films) one should increase the ratio of hydrogen to carbon, and also reduce the bias voltage; [109] though clearly there are limits to the extent to which these routes can be followed (eg based on desired deposition rates).

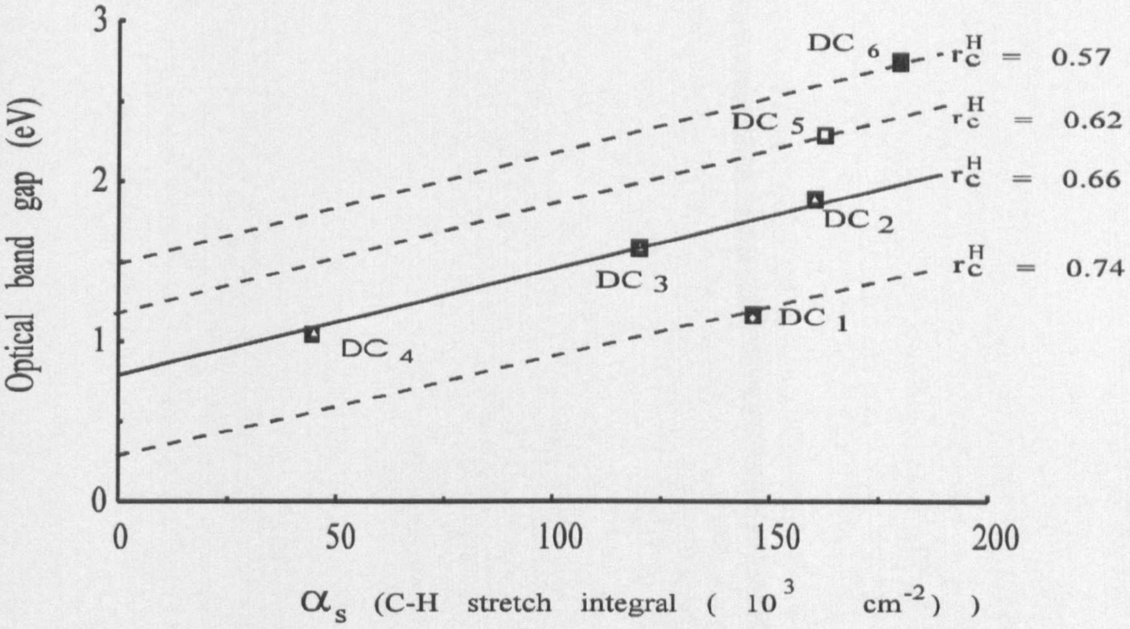

Fig. VII.12 Plot of E_{opt} vs. the integration of the C-H stretch band ($\alpha_s = \int \alpha \, d\nu$).

DC2, DC3 and DC4 were produced in conditions where r_c^H was kept constant; DC1 corresponds to a higher r_c^H ratio (higher evaporation rate); DC5 and DC6 correspond to a lower r_c^H ratio (higher butane flux for DC5 and lower evaporation rate for DC6 see Table VII.2)

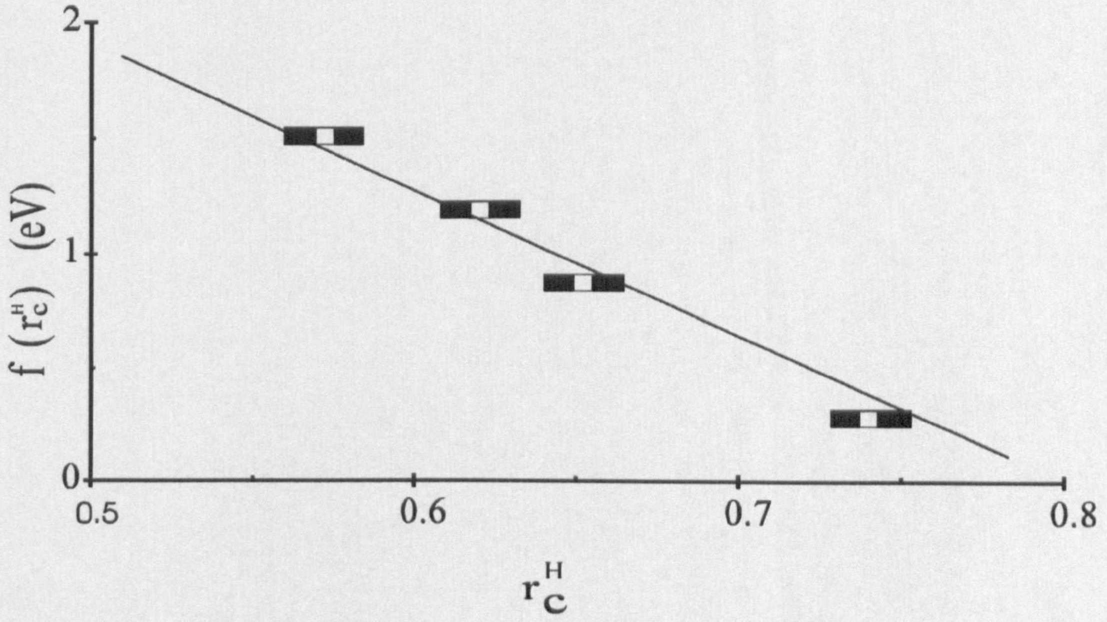

Fig. VII.13 Plot of $f(r_c^H)$ *vs.* the r_c^H ratio.

($f(r_c^H) = E_{opt} - A_1\alpha_s$ at $\alpha_s = 0$ ie the intercepts in Fig. VII.12))

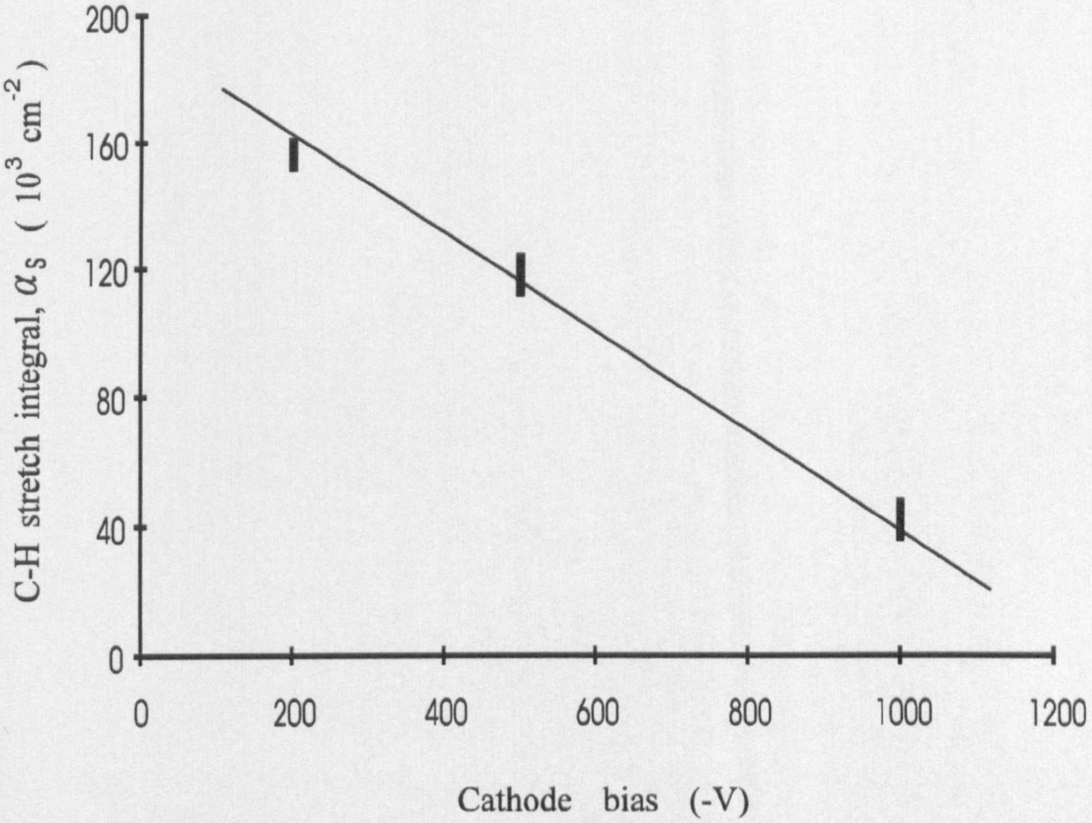

Fig. VII.14 Effect of cathode voltage on the relative content of bonded hydrogen in d.c. EBPVD films.

4. 6. Effect of post deposition annealing.

Post deposition annealing was carried out in air at temperatures up to 600°C. All the films turned black at temperatures higher than 200°C, and at around 500°C the films debonded from their substrate in the form of particles. The effect on the optical properties is summarised in Figs. VII.15 & 16, which demonstrates the reduction of E_{opt} and α_S with increasing annealing temperature.

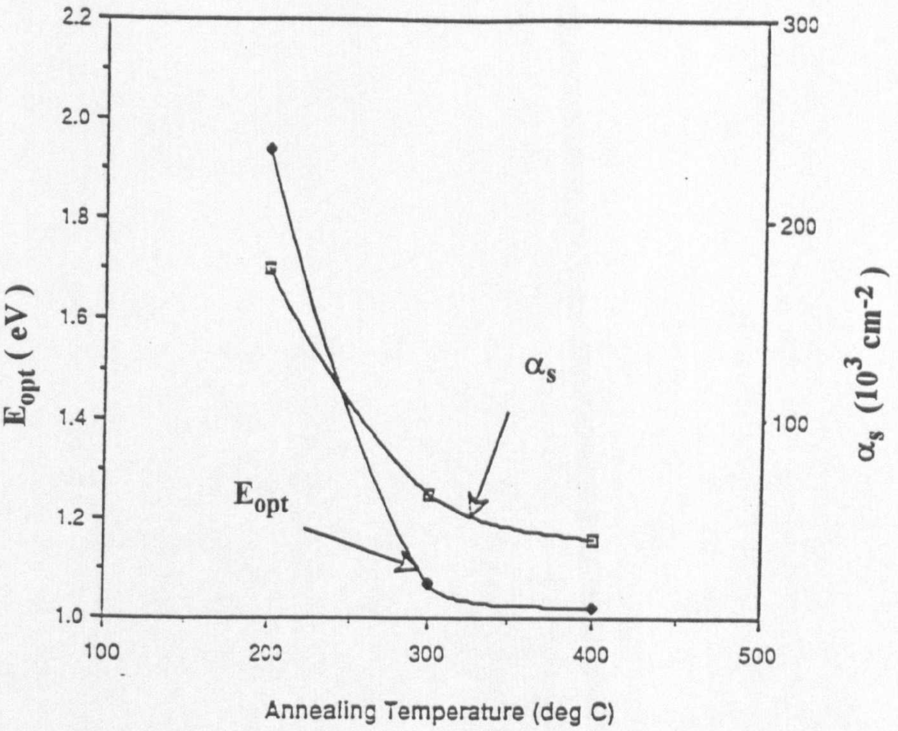

Fig. VII.15 Effect of annealing temperature on the optical band gap E_{opt} and integrated C–H stretch absorption α_s ($\alpha_s = \int \alpha \, d\nu$).

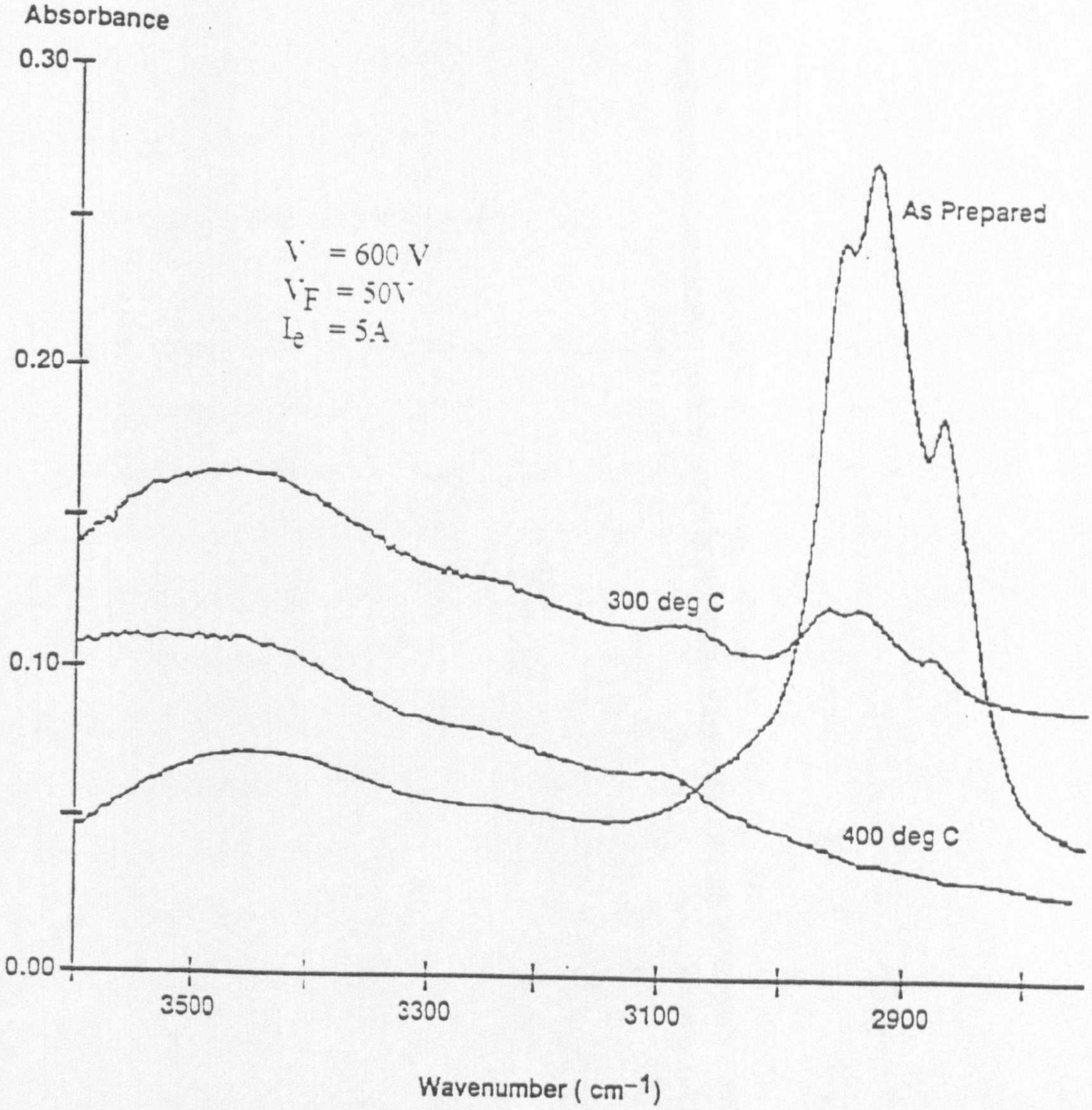

Fig. VII.16 Effect of annealing temperature on C−H bonding in d.c. EBPVD evaporation of graphite in butane plasma.

4.7 Further results and discussions

After this study it has become clear that hard carbon films (DLC) can be produced with the FAB source or rf EBPVD systems and soft films by dc EBPVD. In order to investigate further the differences between these two types of films, a series of FAB source films and d.c. EBPVD films were characterised in Paris using several complementary techniques (Appendix) which were applied both to the as deposited samples and to the same samples after controlled annealing cycles at increasing temperatures [117]. All their measurements were performed on as-deposited samples prepared simultaneously for each series, and on the same samples after controlled annealing cycles under vacuum (10^{-7} Pa) during two hours at increasing temperatures up to 600°C. Only the results relevant to our discussion are presented here, more details on the characterisation techniques used and the results obtained can be found in the thesis of Dr Y. Bounouh [117].

The optical measurement (spectrophotometry and PDS (Appendix)) confirmed our previous results on optical band gap, refractive index and absorption coefficient. The concentration of total hydrogen (bonded or eventually non-bonded) in our films, has been measured by Dr J.P. Stoquert (Laboratoire PHASE du Centre de Recherches Nucleaires de Strasbourg) using the ERDA [117]) and reported by Dr Y. Bounouh in his thesis to be 33% in dc EBPVD films and 25% in FAB source films. No correlation between the total hydrogen and the cathode voltage was found. However they confirmed the decrease of the concentration of bonded hydrogen in the films with the cathode voltage in dc/EBPVD an FAB source films. This result is evidence of the presence of non bonded hydrogen in the films. This non bonded hydrogen must increase with the voltage to compensate the decrease of the bonded hydrogen. This supports the argument that the increase of stress with voltage observed in all the films is due to the increase of non bonded hydrogen in the films.

Electron energy loss spectra (Appendix) carried out by the Paris group in the energy range corresponding to transitions between the C 1 s core level and the bottom of the conduction band indicates very clearly that both series contain an appreciable proportion of sp^2 C sites, although smaller in FAB source films [117]. This is in agreement with our results obtained from infrared spectrophotometry. They reported also the presence of a characteristic peak related to π^* states at the bottom of the conduction band which demonstrates unambiguously that both series contain a large amount of sp^2 C sites, FAB source films being however more "graphite-like". But in both series, and especially in dc films, the proportion of sp^2 C sites bonded to hydrogen is rather small. On the other hand, several other features of the XPS and EELS spectra indicate the presence of sp^3 C sites [117].The Paris group came to the following conclusion: All the results are in agreement with a two-phase model consisting of π-bonded clusters embedded in an amorphous sp^3 C:H matrix [118]. In FAB source films, the sp^2 C sites must be gathered in rather large clusters, which explains the small gap values and in dc. EBPVD films on the contrary, the sp^2 C sites should agglomerate into smaller clusters (probably with a broad size distribution), in agreement with the large band gap values. These clusters must be highly isolated from each other by the sp^3 C:H matrix which forms wider barriers.

5. Conclusion.

The properties of films grown by plasma-assisted evaporation of graphite depends on the carrier gas used, substrate type and bias voltage (under both d.c and r.f. conditions). Specific results are reported, the most important ones are summarised here. Films grown on tool steel in a butane r.f. plasma have a hardness around 4000 H_K (25g).The growth rate on glass under similar conditions is very low, but the film is completely transparent with an optical band gap of 2.6 eV. When argon is used as the carrier gas, no film is formed on tool steel, but on glass a completely transparent film is produced, with an optical band gap of over 3 eV.

Nanohardness measurement showed that r.f. EBPVD films on tool steel are extremely hard (33-44 GPa) and the lowest elastic recovery was obtained for the non-hydrogenated film (11% against 44% for the a-C:H film). This result confirms that hydrogen in the film is the main cause of film stress which is responsible for high elasticity in the film.

Pin on disc tests of r.f. a-C:H films exhibited a film wear of 48 × $10^{-6}mm^3/Nm$ which represents only a modest reduction in wear. The coefficient of friction was however greatly reduced to a value of μ =0.16 compared to the "standard" (μ =0.45-0.54) for steel against steel. Poor performance was shown by d.c. EBPVD films in the pin on disc machine due to their poor adhesion.

Films grown by graphite evaporation in a d.c. plasma exhibited higher growth rates than those in r.f.. There is also a greater amount of bonded hydrogen present when butane is used as the carrier gas, compared to the r.f. plasma or FAB source films. The concentration of bonded hydrogen (α_S) in d.c. films is up to five times more than that of FAB source films. Their relatively low refractive index reflects a polymeric type of film. d.c. plasma coatings were more brittle and usually less well adhered than those produced by other methods, though increased cathode voltage improves adhesion in d.c. deposited coatings. The optical band gap decreases with increasing voltage from around 1.9 to 1.1 eV. With higher H/(C+H) input ratios, the maximum band gap in a low voltage situation was found in some cases to be as high as 2.8 eV. A relationship for the variation of band gap with concentration of bonded hydrogen in the films and the relative carbon to hydrogen Input ratio has been derived.

A study on dc. EBPVD and FAB source films carried out by co- workers in Paris, showed that the structure of the two kind of a-C:H films studied is well described by a two phase model. The two series differ essentially by the sizes of the clusters and by the degree of confinement of the π electrons within the clusters. The electronic density of states depends, not only on the respective proportions of sp^2 and sp^3 C sites, but also on the size of the π-bonded clusters and on the properties of the amorphous sp^3C:H matrix, which both determine the degree of confinement of the π electrons within the clusters.

CHAPTER VIII

PROCESS PARAMETERS AND DIRECTIONAL EFFECTS ON THE OPTICAL PROPERTIES OF CARBON FILMS GROWN BY (D.C.) PLASMA ASSISTED PVD.

1. Introduction.

In the previous Chapters, we discussed the optical properties of hard and soft carbon films produced by various PVD and direct gas deposition methods. A critical factor with many of the available techniques is in scaling-up for commercial deposition purposes. This may involve not only achieving coating coverage on larger components but also ensuring uniformity of composition and physical properties on all surfaces. The optical properties of films are important, not only for applications where these are needed; they also provide information about the nature of the films, eg whether they are diamond, diamond-like or polymeric, their chemical bonding type and hydrogen content. We therefore chose to utilise the optical properties (in particular the optical band gap) as a means of establishing the consistency and uniformity of coatings produced in a thermionic dc plasma enhanced physical vapour deposition system. It is clear that there has been comparatively little work carried out to investigate the influence of plasma process parameters (such as the carbon to hydrogen ratio, pressure, applied voltage and the degree of ionisation) on the film properties. We report work on this subject within this chapter.

2. Empirical background.

In chapter VII, we postulated a relationship between the optical band gap E_{opt}, the relative content of carbon bonded to hydrogen in the film (α_S) and the relative carbon to hydrogen flow input ratio (r_c^H). The form of the relationship suggested was:

$$E_{opt} = A_1\alpha_S + A_2 r_C^H + A_3 \qquad (1)$$

In the present work, we sought to establish values for A_1, A_2 and A_3, and to determine the influence of process variables on this relationship, including the location and orientation of the sample surface.

3. Experimental.

3. 1. The process system

The system used was as shown in Fig. VII.1, and described in Chap.VII. The vapour source material was graphite, evaporated using a bent-beam electron beam gun, augmented with butane to establish the operating pressure and permit control of the carbon to hydrogen ratio. The filament was biased negatively with respect to the earthed stainless steel chamber. Electrons emitted support and enhance the plasma. In this work the specimens were glass slides, clamped to a stainless steel holder which was biased negatively from 100V to 1000V as described in Chap.VII (Fig. VII. 2b). The specimens were located at a distance of 30cm above the source, offset from the vertical axis by 10 cm. The tungsten filament was located 5 cm above the source.

3. 2. Measurements taken

The optical absorption in the visible regime was assessed as described in the previous chapters. The optical band gap was determined using the Tauc relationship. In the infrared regime, we have already reported that most of the C-H bonding observed around 3000 cm^{-1} is sp^3, (CH_2, CH_3). The integration of the C-H stretch absorption gives α_S.

4. Results and discussion

In table VIII.1, the values of E_{opt}, α_s and r_c^H at constant filament bias are listed. Figure 2 shows E_{opt} versus α_s for different r_c^H ratios. The value of A_1 is the gradient of the lines, which was found to be about 7×10^{-6} eV cm^2. When the negative specimen bias is increased, the E_{opt} value decreases along the corresponding line in Fig. VIII.1. This means that the specimen bias can be used to reduce the amount of bonded hydrogen in the film. However, this also leads to a reduction in E_{opt}, which is usually not desirable. Also, it can be seen that reducing the r_c^H value leads to an increase in E_{opt}; however, the quantity of bonded hydrogen will not necessarily decrease.

TABLE VIII.1. Values of E_{opt} and α_s obtained for different r_c^H ratios and V_S values.

r_c^H %		V_S (V)				
		100	200	500	600	1000
74	α_s (10^{-3} cm^{-2})	174	140	108	70	--------
	E_{opt} (eV)	1.92	1.63	1.44	1.2	--------
64	α_s (10^{-3} cm^{-2})	210	174	145	129	70
	E_{opt} (eV)	2.5	2.2	2	1.8	1.52
44	α_s (10^{-3} cm^{-2})	230	210	190	170	--------
	E_{opt} (eV)	3.6	3.5	3.3	3.1	--------

In order to reduce α_s without reducing E_{opt} we need to operate on another variable. Considering A_2 and A_3; these together are part of the function making up the remainder of equation (1), i.e.

$$E_{opt} = A_1\alpha_s + f(r_C^H)$$

The value for $f(r_C^H)$ can be determined from the intercept of Fig.VIII 1 (i e where $\alpha_s = 0$)

Figure 3 shows that these intercept values vary with r_C^H and filament bias. It can be seen that $f(r_C^H)$ defines a family of parallel lines, the location of each one being determined by the filament bias voltage. Thus:

$$f(r_C^H) = A_1 r_C^H + g(V_F)$$

i.e. $A_3 = g(V_F)$, and V_F is the filament bias.

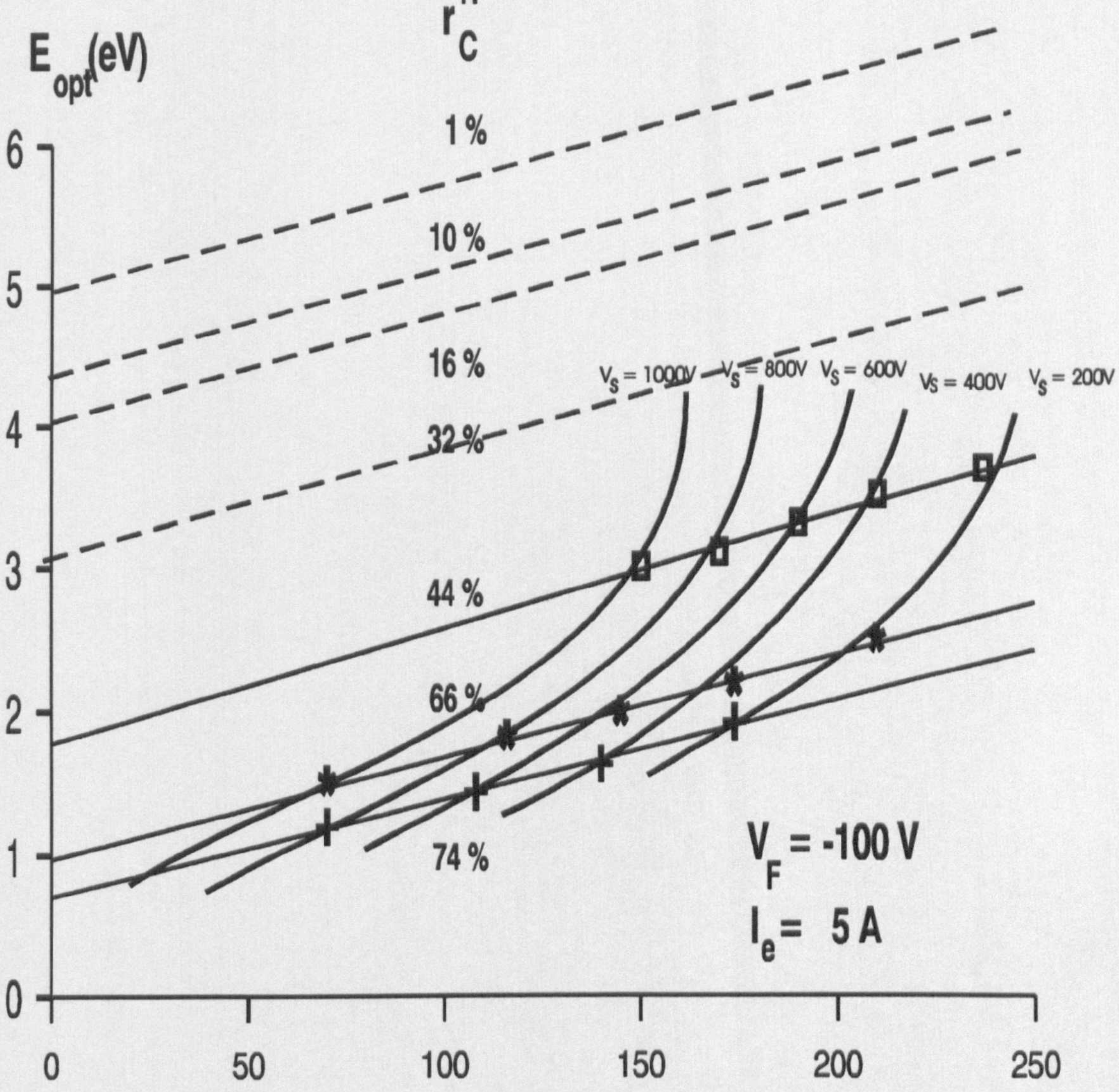

Fig. VIII.1 E_{opt} versus α_s for different r_c^H ratios (solid lines denote actual readings. Dotted lines are predicted from equation (1)) [note: We should now strictly write $f(r_C^H, V_F)$ as the function operating on the second part of eqn. (1), knowing that V_F also influences E_{opt}. We had previously found that A_3 is a constant (chap. VII), but in that case V_F was constant].

The gradient of the lines in Fig. VIII.2 allow us to determine A_2, which was found to be about –6.2eV.

Figure VIII. 3 shows how $g(V_F)$ varies with filament bias. This function is of parabolic form, and an equation can be fitted to it as follows:

$$g(V_F) = 5.2\times10^{-4}(V_F + 50)^2 + 3.7 \qquad (3)$$

The full form of eqn.(1) now becomes:

$$E_{opt} = 710^{-6}\alpha_S - 6.2\ r_C^H + 5.2\times10^{-4}(V_F + 50)^2 + 3.7 \qquad (4)$$

This equation, and the results leading to it, are of considerable significance for the optimisation of thermionically enhanced plasma-based processes, in terms of process parameters and specimen location/orientation aspects. Some of these consequences are outlined below.

First of all, in Fig.VIII.2 we can see that $f(r_C^H)$, which is ($E_{opt} - A_1\alpha_S$), is maximised for each V_F by decreasing r_C^H. For instance, when V_F=-100V, by reducing r_C^H to zero we should be able to achieve a value of 5eV for the function ($E_{opt} - A_1\alpha_S$). If the film has no bonded hydrogen, the E_{opt} value would be 5eV, since α_S would then be zero. However, if V_F is less than -100V, then it is impossible to achieve an E_{opt} value of 5eV for a non hydrogenated film (ie α_S=0). Thus the filament bias is crucially important.

Furthermore, if V_F is less than -100V (i.e. less negative) the E_{opt} value can be high, but only by increasing α_S (i.e. the amount of bonded hydrogen), an effect which is known to lead to "polymeric" films. If the r_C^H. value is high, even with a suitable filament bias, this can give a low optical band gap (i.e. as typified by a highly "carbonaceous" deposit). Conversely a reduction in carbon and increase in hydrogen will increase ($E_{opt} - A_1\alpha_S$); therefore if α_S can be reduced under these conditions then we have a means of obtaining high E_{opt} and a low amount of bonded hydrogen.

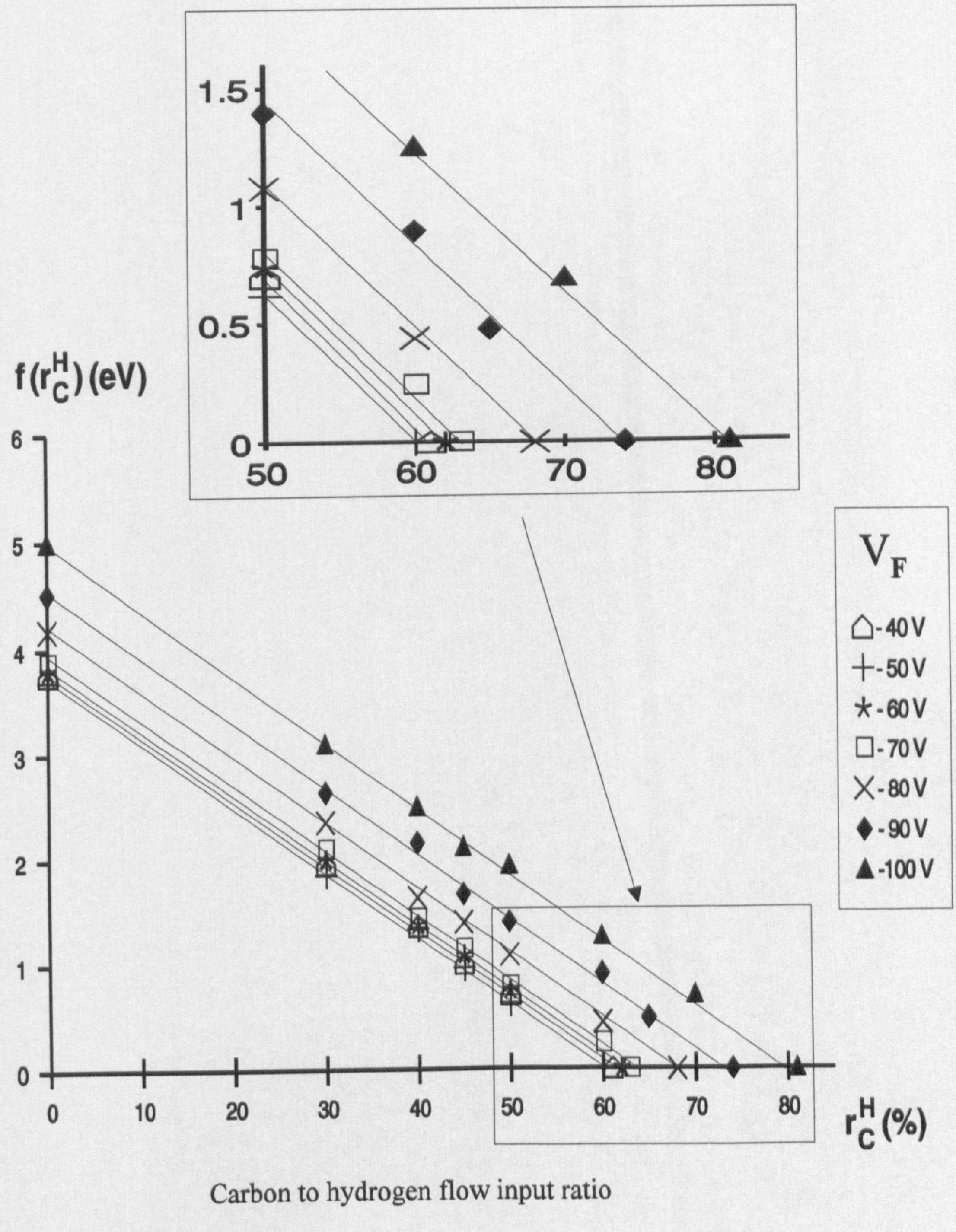

Fig. VIII.2: **$f(r_c^H)$ versus r_c^H for different V_F values, $E_{opt} = A_1 \alpha_s + f(r_c^H)$.**

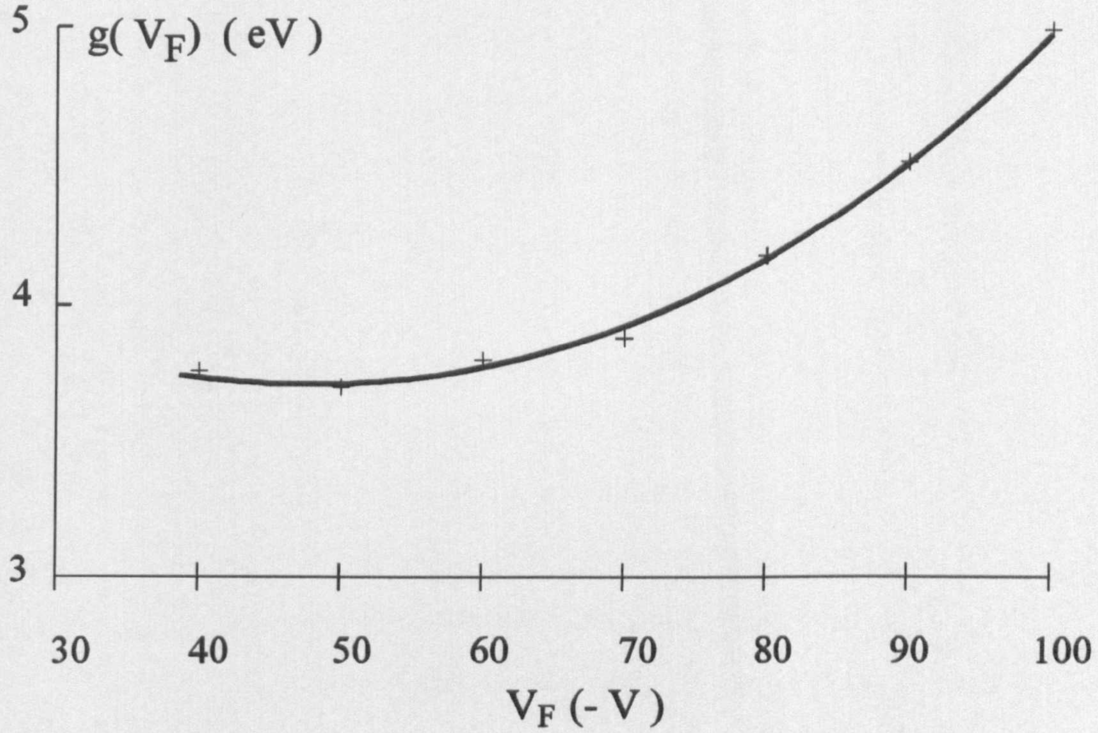

Fig. VIII.3: Graph showing that g (previously called A_3) is not a constant when V_F varies. The solid line is theoretical and the crosses show the experimental values.

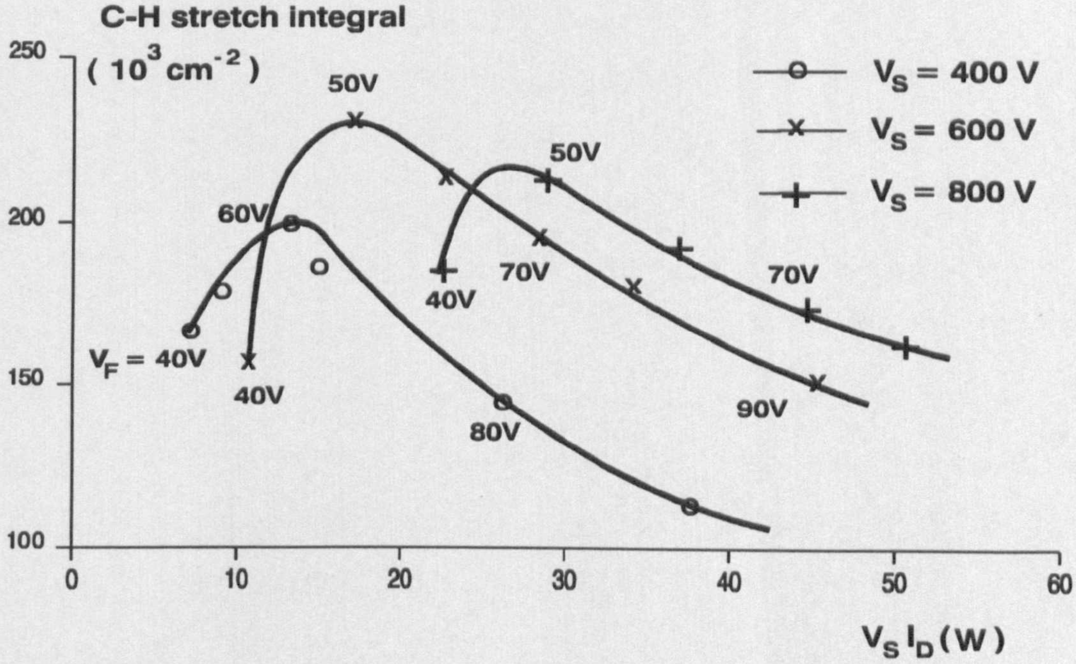

Fig. VIII.4: Graph showing that when V_S is fixed, V_F increases I_D and decreases α_s

The question arising is thus how to reduce α_s. We have already said that increasing the cathode voltage (V_S) can reduce α_s, but this approach suffers from the drawback that E_{opt} decreases at the same time. In order to investigate further means of reducing α_s we have therefore studied the influence of V_F, V_S and I_D (the discharge current to the sample) on α_s.

In Fig VIII.4, α_s is plotted against $V_S I_D$, for different V_F values. It can be seen that for each V_S, α_s starts to increase, for V_F up to about 60V, (negative) after which it starts to decrease. This signals a way of reducing α_s independently of V_S and without decreasing E_{opt}. Fig VIII.5 shows that when α_s is reduced E_{opt} can be increased, without increasing V_S. Together these observations guide us to a means of increasing E_{opt} in a truly optimal way, i.e. by increasing the filament emission (eg by increasing the filament current I_F) and thereby increasing the ion current to the cathode (Fig.VIII.6), whilst maintaining other parameters, such as V_S and r_c^H at the appropriate level.

There are a number of consequences of what has been stated above. In the context of the original aim of study (i.e. to investigate scale-up and geometrical factors in coating) we can say that the location of the sample should influence the type of film obtained. This is because not only will the carbon to hydrogen ratio vary on surfaces facing or remote from the vapour source, but also the ionising electrons will be non uniformly distributed and therefore the rate of dissociation of CH_n radicals will vary from plasma region to another.

Evidence for this is in Fig. VIII 7, which shows the α_s values on the "front" and "back" surfaces of samples, i.e. facing towards and away from the vapour source (and electron emitter). The model developed in this work was found to apply for all surfaces, with similar values for the constants, as given in equation (4). The E_{opt} and α_s values for the back surfaces are higher than for the front, confirming that they correspond to a lower r_c^H value, as expected, since they are not facing the carbon source.

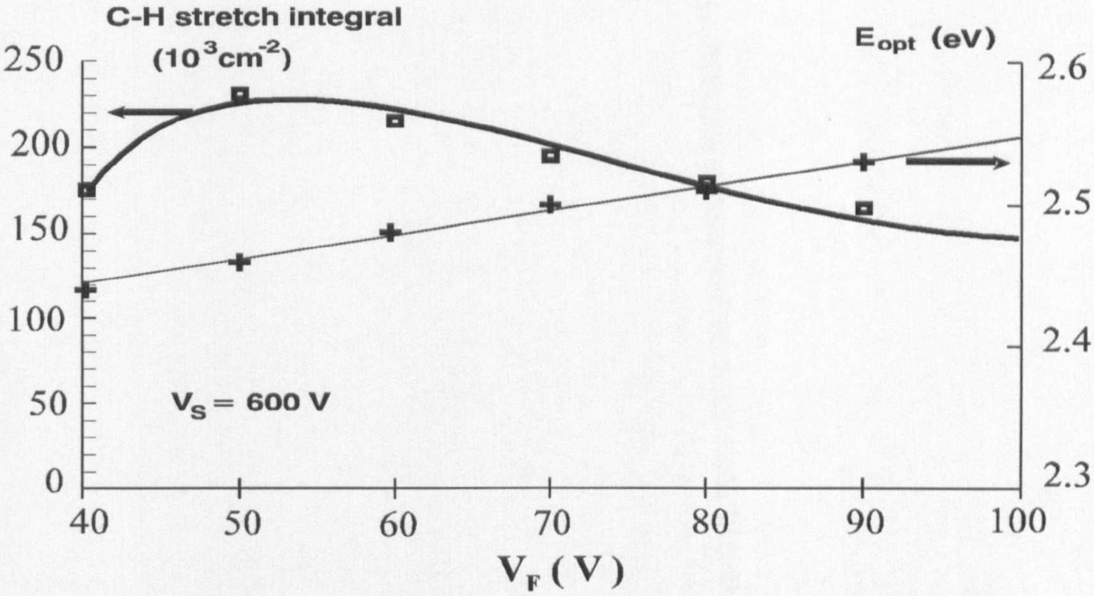

Fig. VIII.5: Graph showing that varying V_F provides a means of decreasing α_s without decreasing E_{opt} when V_S is fixed.

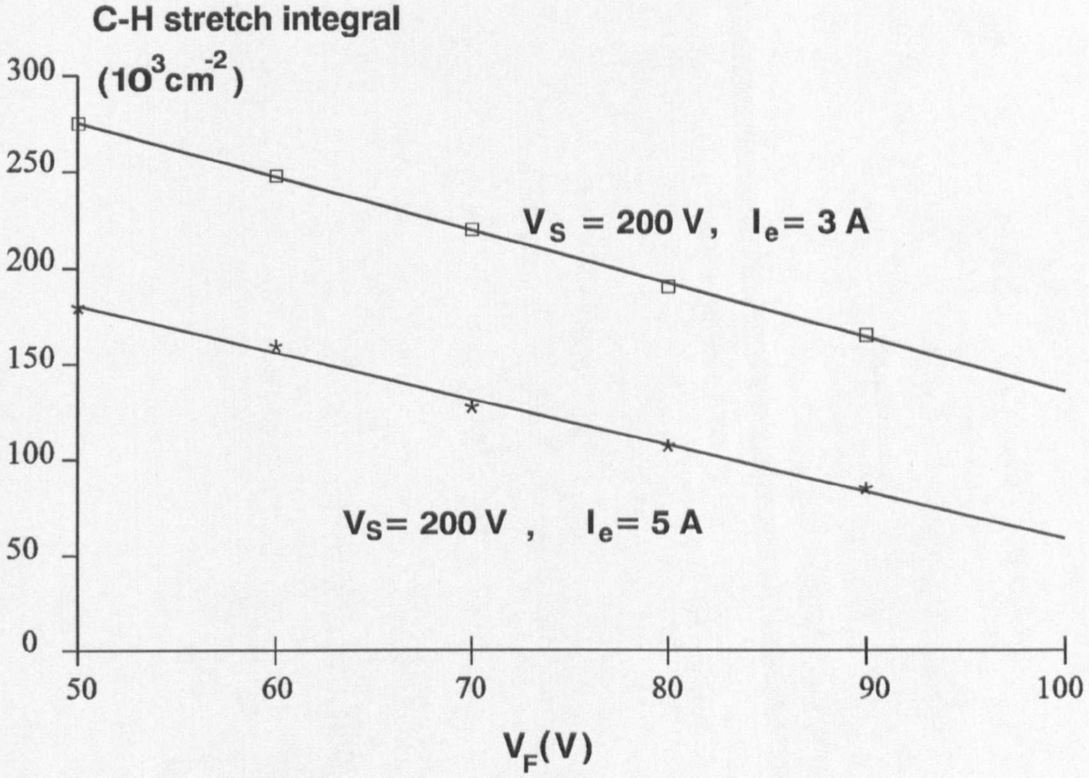

Fig. VIII.6: Graph showing that the filament current emission is also an important variable which can be used to decrease α_s without decreasing E_{opt}

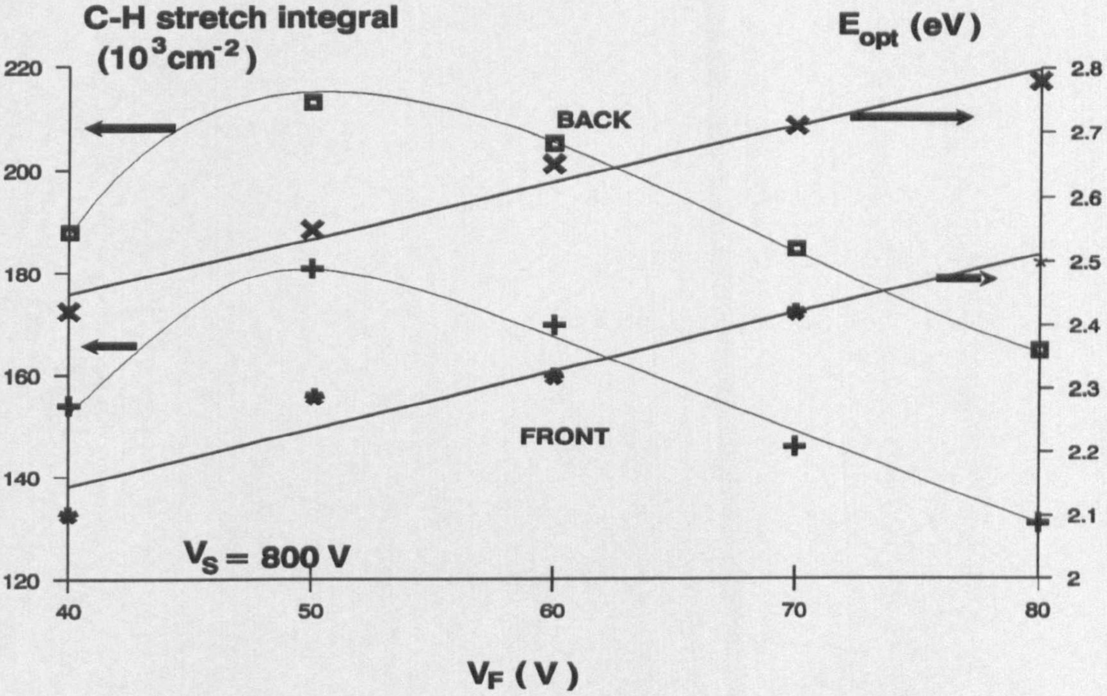

Fig. VIII.7: Graph showing that the back of the samples have higher E_{opt} and α_s values than the front when produced under the same conditions.

5. Results interpretation

The fact that the r_c^H ratio was well correlated with the optical properties although it is not the exact value of the carbon to hydrogen in the plasma suggests that the effect of graphite evaporation rate on the pressure was dominant relatively to other thermodynamic effects like particle temperature. The reason for this might be the high evaporation rates used (r_C^H from 30% to 70%). Also the linear lines obtained in Fig VIII.1 should be taken as linear only in the region of experimental values.

On the other hand even in the simplest case where V_F and I_e are constant, the expression of E_{opt} in eqn.(1) is not as simple as it may seem. The relationship linking E_{opt} and r_C^H is not linear because α_S is a function of r_C^H and V_S, therefore we have

$$E_{opt}(r_C^H, V_S) = A_1\alpha_S(r_C^H, V_S) + A_2 r_C^H + A_3$$

If we had the mathematical expression of α_S as function of r_C^H and V_S we could express r_C^H as a function of α_S and V_S if it is possible. (from the Implicit Functions theory). Therefore r_C^H could be eliminated from the expression above and E_{opt} would be written as

$$E_{opt} = Q(\alpha_S, V_S)$$

where Q is a non linear function.

For each fixed V_S the expression of E_{opt} would be:

$$E_{opt} = Q_{V_S}(\alpha_S) \qquad (5)$$

If the degree of plasma ionisation is not constant, the expression (5) becomes

$$E_{opt} = Q_{V_S}(\alpha_S(V_S, r_C^H, \delta).) \qquad (6)$$

where δ is a function of the parameters that act on the degree of plasma ionisation (V_F, I_e and V_S)

The fact that these three variables V_S, r_C^H and δ are not independent makes the problem even more complicated. V_S acts on the current density (which acts on the degree of plasma ionisation) and on the impact energy. This latter acts on the rate of implantation of bonded hydrogen in the film and the rate of dissociation of CH_n radicals in the plasma ; the magnitude of these two effects will depend on r_C^H .

In Fig VIII. 1 it can be seen that E_{opt} is a set of curves of parabolic shape and each curve corresponds to a fixed value of V_S . Therefore since these curves were experimental results, the function Q_{V_S} exists and corresponds to the equation describing these curves.

It is important to note that the parabolic curves of Fig VIII.1 are experimental results that have been found independently of r_C^H , (for each V_S fixed a film was deposited, then its E_{opt} and α_S were measured). Eqn.(1) shows that r_C^H can be used to illustrate the effect of the evaporation rate on the film properties and expression 6 show that r_C^H can be kept implicit in the expression of E_{opt}. However although it can be eliminated from the equations it cannot be ignored by the producer of carbon films because what is happening in the plasma depends strongly on the input functions. The substrate temperature is also a valuable parameter that exists implicitly in the expression of E_{opt} (in Chap. VI α_S and E_{opt} decreased dramatically with increasing temperature when FAB source films were annealed during deposition or after deposition).

We believe also that at a given degree of ionisation the density (d) of the films could be expressed as function of V_S and r_C^H and therefore we would have :

$d = f(V_S, r_C^H)$ and $\alpha_S = g(V_S, r_C^H)$

If these expressions could be changed to :

$V_S = h(\alpha_S, d)$ and $r_C^H = k(\alpha_S, d)$

V_S and r_C^H could therefore be eliminated from in eqn (5) and a new intrinsic relationship linking E_{opt} to the films properties could be found:

$$E_{opt} = Q(d, \alpha_S) \text{ or } E_{opt} = Q(n, \alpha_S)$$

where n is the refractive index.(d an n are proportional and increase with V_S for a-C:H films (chap.III). The film density is however not an easy parameter to measure.

6. Inter-relationship between deposition techniques , process parameters and film properties

The effect of the process parameters on E_{opt} and α_S is illustrated geometrically in Fig.VIII 8. where a carbon film is represented by a vector OM (E_{opt}, α_S).The modulus of OM ($E_{opt}^2 + \alpha_S^2$) and its argument (Φ) are functions of process parameters.

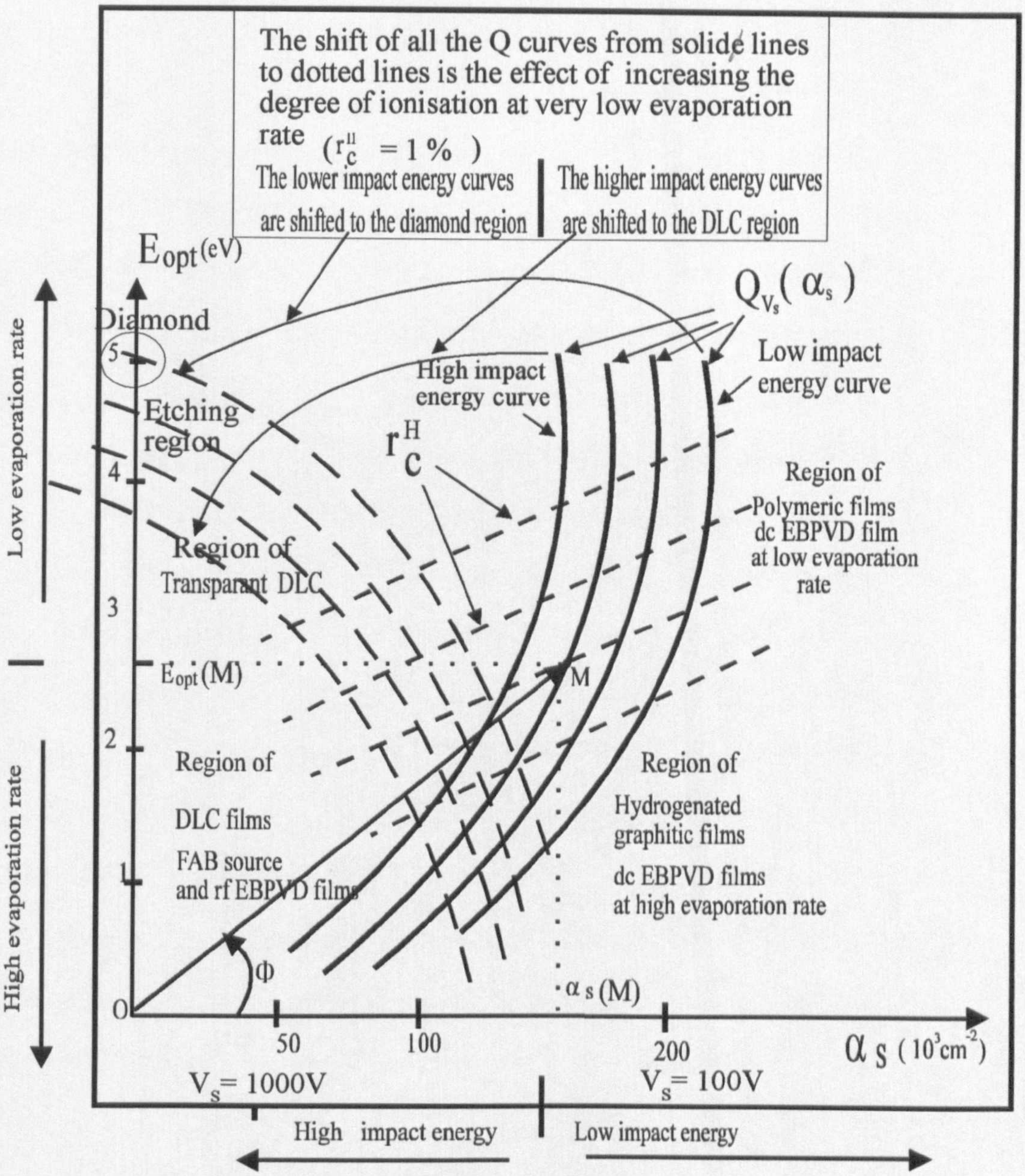

The shift of all the Q curves from solide lines to dotted lines is the effect of increasing the degree of ionisation at very low evaporation rate ($r_c^{H} = 1\%$)

The lower impact energy curves are shifted to the diamond region | The higher impact energy curves are shifted to the DLC region

Fig. VIII.8 Schematic interelationship between deposition techniques, process parameters and film properties.

For a given degree of plasma ionisation, increasing r_C^H while V_S is kept constant will move the point M down along the parabolic curves. During this movement E_{opt} increases and α_S decreases. If this movement is on the curves to the right side (low V_S), the film will move from a polymeric to a hydrogenated graphitic type and if the movement is on the left side (high impact energy curves), the film will move from transparent DLC films (rf EBPVD at low evaporation rate) to hard DLC films with a low optical band gap (FAB source films or RF EBPVD films at high impact energy)

Increasing V_S while r_C^H is kept constant will move the point M from one curve Q_{V_S} to another along the r_C^H lines. On the highest lines the film will move from a polymeric region to an etching one (ie no net deposition) and on the lowest lines the film will move from hydrogenated graphitic films to DLC films with low bonded hydrogen content and low band gap(FAB source films or RF EBPVD films).

If both r_C^H and V_S are fixed the point M cannot move unless its support (ie the curve Q) is moved as well. A shift of all these curves from right to left is possible by increasing the degree of plasma ionisation. This shift will rotate OM from right to left and during this rotation E_{opt} increases and α_S decreases. If the point M is in the intersection of a very low r_C^H line (eg 1%) and a very low Vs curve (low impact energy and very low evaporation rate region), the shift of these curves will move the point M to the region of films with high optical band gap and very low hydrogen content. This last movement is the route to diamond films.

6. Conclusion

We have developed an empirical relationship linking the optical band gap with the amount of bonded hydrogen in the film, the carbon to hydrogen ratio in the plasma, and other plasma electrical parameters for carbon coating produced using a thermionically enhanced plasma-assisted d.c. PVD process. This relationship explains observed properties in terms of process parameters and highlights the difficulties in obtaining consistent coatings on sample surfaces at different locations and orientations in the deposition chamber. These problems can be overcome by appropriate process modifications, e.g. by using multiple vapour sources and electron emission sources, and/or placing these in closer proximity to the samples, so as to achieve the appropriate vapour flux/ion flux distribution [115], within the temperature constraints of the sample to be coated.

CHAPTER IX

DIAMOND-LIKE CARBON FILMS GROWN BY A HOT FILAMENT ENHANCED PLASMA ASSISTED CVD

1. Introduction

In Chap.VIII we have investigated the influence of plasma process parameters on the film properties produced in a thermionic d.c. plasma enhanced hybrid physical vapour deposition system. In that hybrid technique carbon films were grown by evaporation of graphite in different hydrocarbon gas d.c.plasmas enhanced by a negatively biased heated filament. When graphite is not evaporated during coating, the system becomes a Filament Enhanced Plasma Assisted CVD. In both cases an empirical relationship linking the optical band gap with the bonded hydrogen concentration in the film, the carbon to hydrogen ratio in the plasma, the degree of ionisation and other electrical parameters has been developed (Chap. VIII) .

In the present work, we have improved the Filament Enhanced Plasma Assisted CVD technique in order to work in the optimum conditions drawn from this empirical relationship (low bias voltage, low carbon to hydrogen ratio and very high degree of ionisation).

There have been several reports on work to improve the hot filament CVD technique. For example an investigation into different ways of biasing the filament with respect to the substrate has been reported [119]. The classical hot filament

CVD technique that relies on thermal decomposition of the hydrocarbon gas used (no glow discharge is produced during coating) suffers from a very low deposition rate (0.01-1μm hr^{-1}), a small deposition area (2-4cm^2), and a relatively high working pressure (20 to 40 Torr) [Chap.II]. In this chapter we report on means to act on the emitted electrons from the filament in order to improve their ionisation efficiency.

2. Empirical Background

A hard carbon film that has a high optical band gap, Eopt, is not necessarily a Diamond-Like carbon (DLC) film, since, for instance hard polymeric films can have an optical band gap as high as 5eV. However, such a hard carbon film cannot be polymeric if its concentration of bonded hydrogen to carbon (α_S) is very low. Hence E_{opt} and α_S are two important parameters used in distinguishing films.

In Chap. VIII we presented an empirical relationship between these two parameters and deposition conditions. This relation is of the form:

$$\mathrm{Eopt} - A_1\alpha_S = A_2 r_c^H + g(V_F)$$

where r_c^H is the C/(C+H) ratio in the plasma and $g(V_F)$ is a parabolic function of the filament bias V_F. We also showed that α_S can be decreased by increasing the sample bias Vs; however this leads to a decrease in E_{opt} which is not desirable. The best way to decrease α_S was found to be to increase the filament bias V_F and most importantly to increase the filament emission current I_e. The consequence of a high V_F and I_e is a high discharge current density, J at the cathode.

In our earlier CVD process, the highest J we could obtain was 0.13mA/cm^2. This value was low because we had to keep the cathode bias Vs as low as possible in order to achieve films with a high E_{opt}.

From Chap. VIII we know that in order to decrease α_S and keep V_S low, the degree of ionisation should be increased by two orders of magnitude compared to that mentioned above. This was practically impossible in previously reported techniques. Therefore we have developed a new system, which ensures a very effective use of ionising electrons, by confining the deposition volume.

3. Experimental

3. 1. Limits of the previous system

In earlier hot filament CVD systems, as described in Chap. VII, the emitted electrons were accelerated to the walls of an earthed stainless steel chamber by means of a negative d.c. voltage applied to the filament. During their path they ionise the hydrocarbon gas (methane, propane, butane, or acetylene) when it is at the appropriate pressure, and thus produce a glow discharge. However this discharge is very weak and almost invisible to the eye. Samples located at 10 or 30cm from the filament can be coated at a maximum rate of 4µm/h. The films obtained are soft, brittle, poorly adherent to the substrate and contain up to 50% Hydrogen. They are polymer-like in their properties when the samples are further from the filament and no hydrogen is used. Biasing the cathode at a voltage up (in modulus) to 1000V enhances the discharge, producing a higher current density (Fig. IX.1). However the films continue to be polymer-like and their optical band gap decreases from 3.5eV (at Vs = - 100V) to 1eV (at Vs = -1000V) (Chap. VII). Increasing (in modulus) the sample bias to 2000V or 3000V creates a discharge with a current density of 1mA/cm^2 which is an improvement by a factor of 10 on the case where Vs = -100V or 0V; the films obtained are more adherent to the substrate with properties closer to DLC than polymers. However, they contain a considerable amount of hydrogen and have a very low optical band gap (1eV). If 1% of methane, butane, acetylene, or propane in hydrogen is

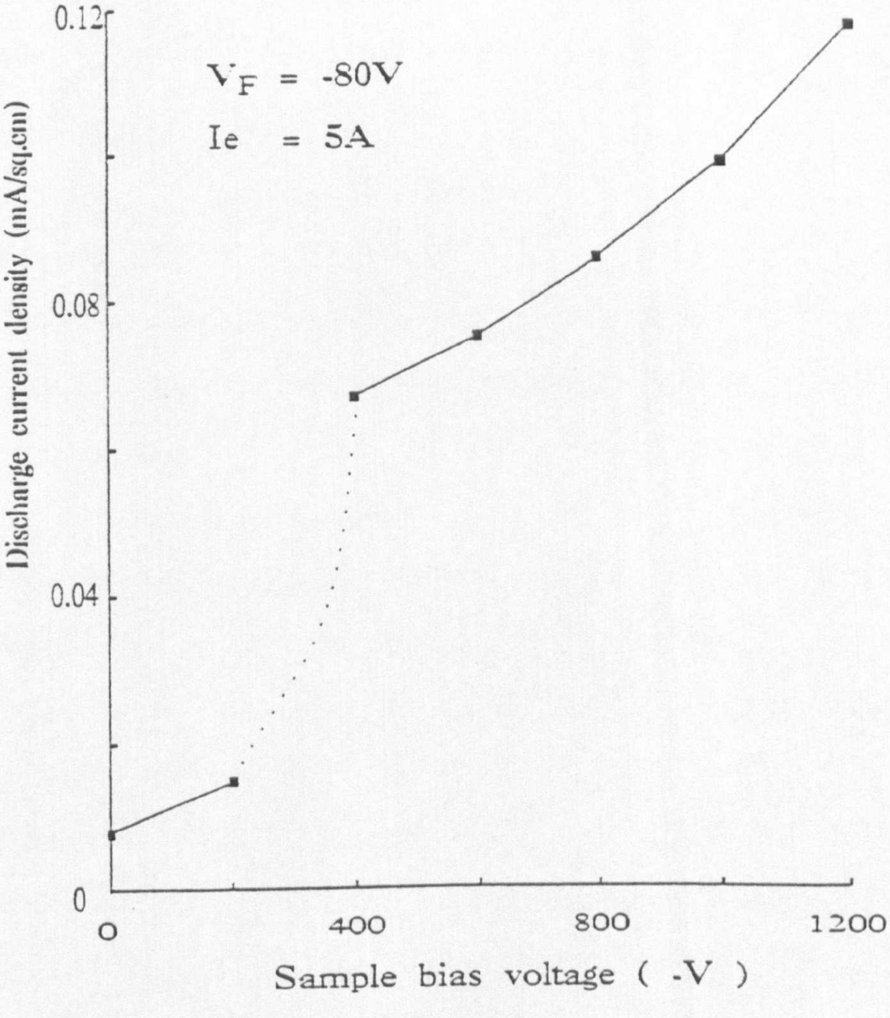

Fig. IX.1: Discharge current density versus samples bias in a thermionically enhanced hot filament CVD system.

used, no detectable coating is obtained in a 1h deposition time. Therefore it was necessary to change our system in order to obtain better quality films (lower amount of hydrogen, better mechanical properties, and higher optical band gap), and higher deposition rate especially when the carbon to hydrogen ratio in the plasma is very low (eg: 1% methane in hydrogen). This can be achieved with a process which can work with low particle energies (low sample bias) and a high degree of ionisation. A system achieving this is shown in Figure IX.2.

3. 2. Description of the new system

This involves biasing the filament negatively, and almost completely surrounding it with surfaces, biased at the same negative voltage, on which the samples are mounted. This ensures that electrons emitted are trapped, and can achieve their maximum extent of ionising collisions. Naturally this requires that the electrons have sufficient energy and this can be achieved by making the plasma positive by means of a third electrode, analogous to a triode system. This third electrode, is shown in Fig. IX.2 as (a). Points to note are that the internal surfaces of the coating chamber are made of graphite, to avoid contamination of the coating with metallic species. Also the filament is normally made of tungsten but experiments have also been made with a graphite emitter. The coating enclosure shown in Fig. IX.2 is housed in a large vacuum chamber in which the pressure was measured. We assumed that this pressure is the same in the enclosure chamber since the two chambers communicate through two holes A and B of 2cm diameter each (Fig. IX.2). The currents, I_s, I_a, and I_e, arriving respectively at the surfaces surrounding the filament, the anode (the third electrode), and the filament were measured during deposition. The average value of the current density on the samples, J, was calculated using : $J = I_s/S$, where $S = 160cm^2$ (S is the surface of the internal walls of the enclosure). A gas flow controllor was used to introduce the gases in the chamber with desired proportions. Stainless steel, mild steel, and silicon were used as substrates.

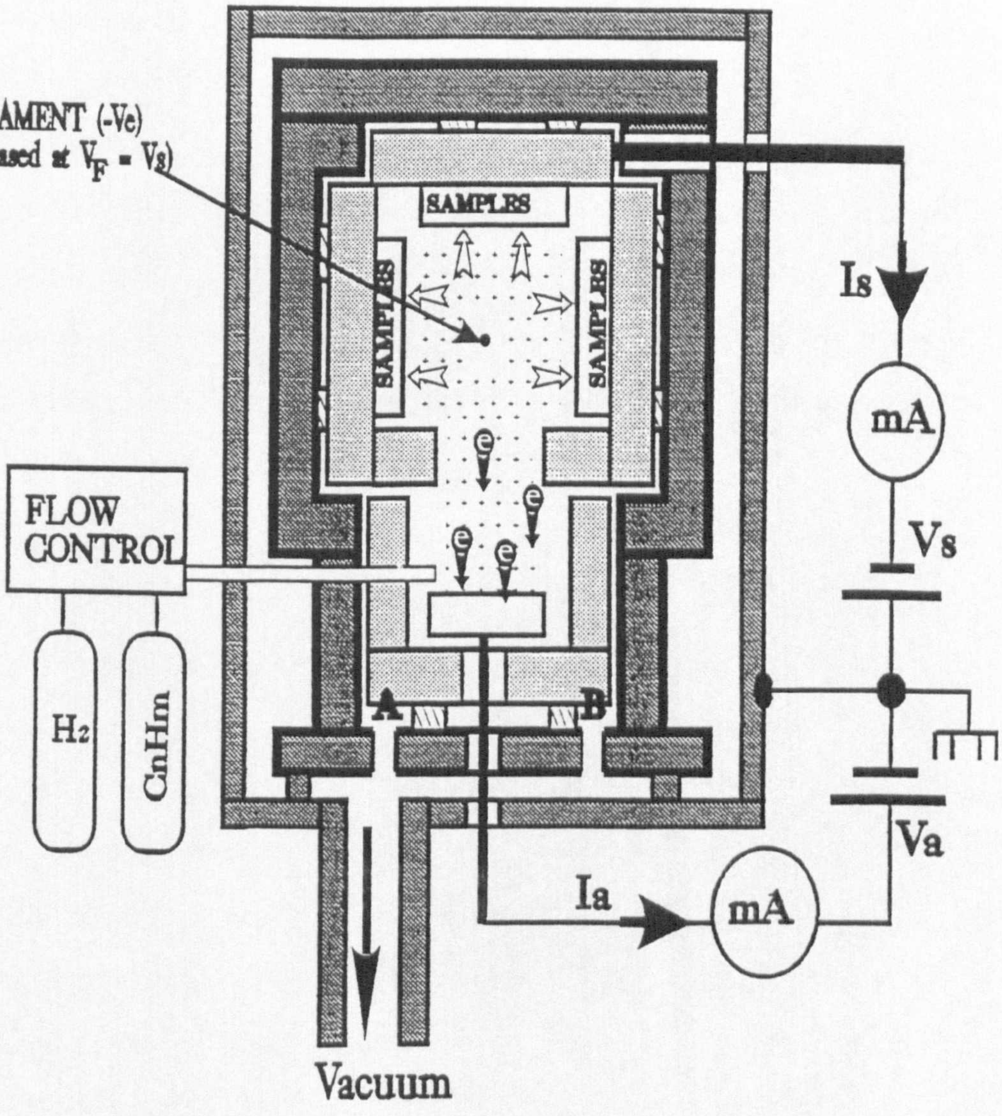

Fig. XI.2: Schematic layout of the improved hot filament-enhanced plasma assisted CVD system.

4. Results and Discussion

4. 1. Plasma Characteristics.

The filament typically consists of a straight wire of tungsten 0.5mm in diameter and 6cm long, and carrying a current of 25-35A. A bias (V_S) of -50V on the filament and surrounding surfaces, with anode at 0V, produced a weak discharge with an electron current of a few milliamperes arriving at the surfaces surrounding the filament. (C_4H_{10} pressure 10^{-3}Torr). Increasing (in modulus) Vs to -80V led to no net current being monitored on the surrounding surfaces (Is =0A) (Fig. IX.3) (ie we believe the ion and electron currents were balanced). Increasing the anode bias (V_a) resulted in a reduction in the negative bias needed on the filament and the samples to produce an intense discharge. Further increase in the bias to -120 V produced a more intense discharge (Fig. IX.3). When the modulus of V_S is higher than 200V the discharge reaches the Arc regime. In this case I_a can be higher than 10A. The current density could be intensified by increasing the filament current or the gas flow (Fig. IX.4). Control was important since sample heating could be excessive (eg to > 800°C with uncontrolled bias and current levels). Similar plasma characteristics were observed when other gases such as methane, propane, acetylene, argon, or hydrogen were used. The pressure range in which a discharge could be maintained varied from 1 mTorr to 3 Torr. The working pressure during coating was kept as low as possible in order to minimise film contamination. The summary of process parameters in the earlier system and the new one is given in Table IX.1.

4. 2. Coating Characteristics

Initial trials were carried out using a plasma in which the carbon to hydrogen ratio is relatively high. For this, butane, propane, acetylene, and methane were tried separately with no hydrogen mixture. The deposition conditions were kept the same for each gas used, and were as follows: $V_S = -120V$, $V_a = +50V$, $V_F = V_S$, and $I_F = 35A$ at

Table IX.1. Summary of process parameters.
(a), earlier hot filament CVD system, (Chap.VII)
(b), improved hot filament CVD system.

Process	Cathode Voltage, V_s(V)	Anode Voltage, V_a (V)	Filament Voltage, V_F (V), (negative)	Current Density, J, (mA/cm^2)	Pressure (mTorr)	Deposition Temperature (°C)
(a)	100 - 1000	0 - 70	50 - 100	0 - 0.14	5 - 10	up to 300
(b)	50 -200	0 -50	$V_F = V_S$	0 - 14	$5 - 3\times10^3$	up to 900

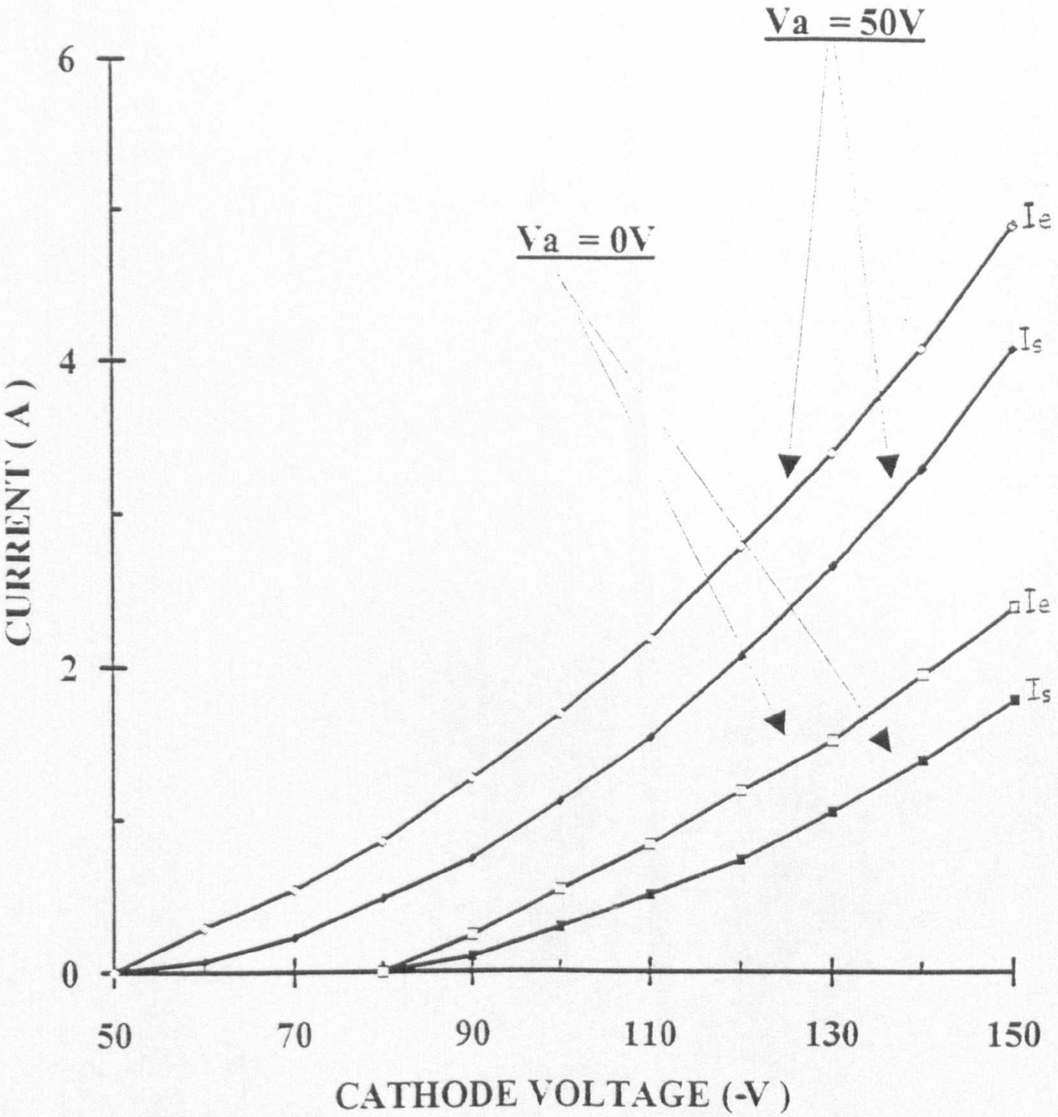

Fig. XI.3: Effect of anode voltage, V_a, on the current arriving at the samples, I_s, and at the filament, I_e, for different cathode voltages in the improved hot filament CVD system

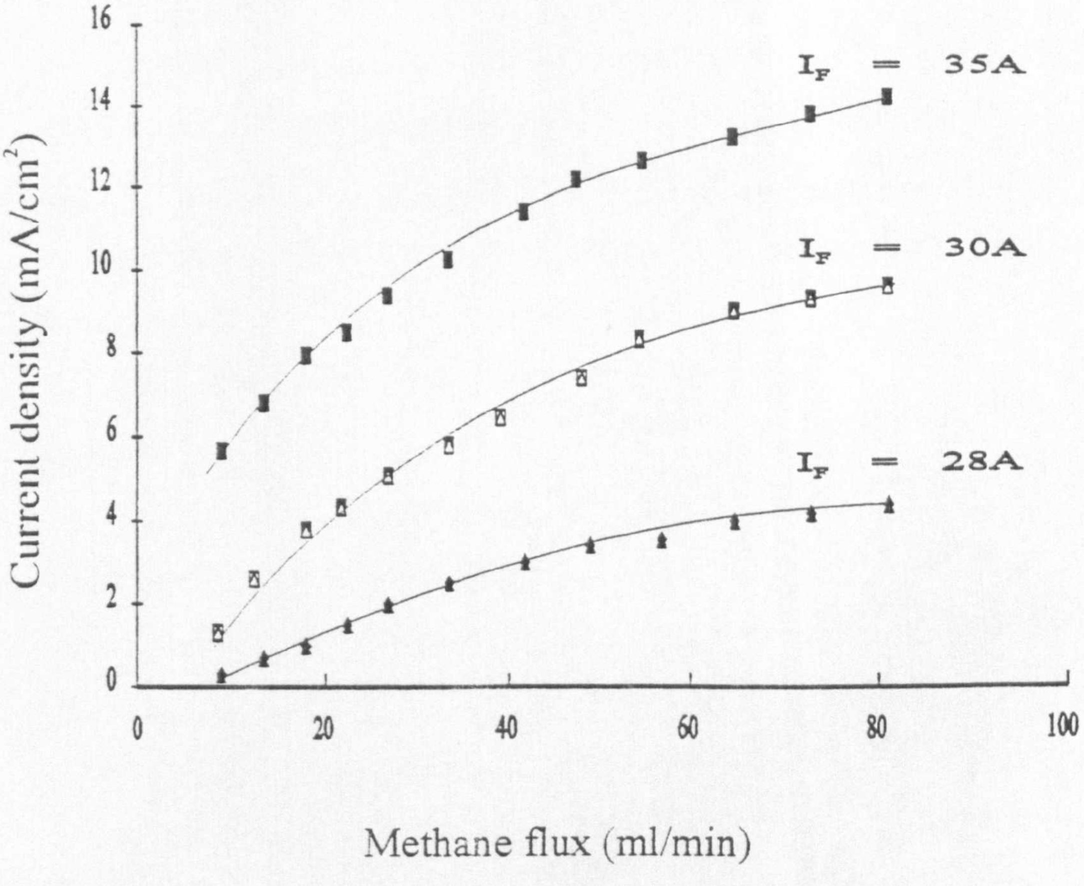

Fig. XI.4 Current density on samples versus methane flux for different filament current, I_F, in the improved hot filament plasma assisted CVD system.

5×10^{-3} Torr. The discharge current density, J, on the samples was equal to 14mA/cm^2. Theses values were chosen as they correspond to the best discharge in terms of stability. The deposition rate on stainless steel substrates varied from 10μm/h for methane to 20 μm/hr for acetylene. The films in all these cases were graphitic. They were black and had poor mechanical properties. Changing the discharge intensity, the pressure, or the gas flow did not improve the film qualities.

Next a low carbon to hydrogen ratio was utilised (1%CH_4 in H_2). The deposition conditions were kept the same as above. The film growth rate was 2-3 μm/hr on stainless steel and silicon substrate. The film colour was grey when thick (~2μm) and exhibited interference colours when thin. (~0.3μm). They had such a high hardness that under a 200g load no indentation was visible in a Knoop microhardness test in several of the coatings; others produced in the same conditions gave a reading of over 8000 H_K Further increase in the load in the higher hardness films led to brittle spallation of the film. The summary of coating properties produced in the earlier system and the new one is given in Table IX.2.

Raman studies indicated that these films were DLC with a disordered graphite component (Fig. IX.5). SEM studies showed particles with an octahedral shape which were particularly evident in thinner films deposited at low carbon concentrations (0.5% CH_4 in H_2) (Fig. IX.6). Viewed from above, some of the thicker films (>2 μm) exhibited a dimpled appearance (Fig. IX.7a). Other workers [34] have described this as a "smoothed diamond" appearance, achieved after argon ion bombardment of diamond films. The films are very dense as shown in fracture cross-section (Fig. IX.7b).

The transmittance spectrum of a 2μm thick film on tool steel obtained by reflection (Fig.IX. 8) showed very weak sp^3 C-H stretch bands around 3000 cm^{-1} and sp^2 C=C stretching vibration bands around 1600 cm^{-1} and 1000 cm^{-1} and an aromatic C-H in-plane deformation band is observed around 1225 cm^{-1}. The intensity of these bands is usually higher in hydrogenated a:C-H and polymeric films.

The band gap mesurement has been performed on a 2 μm thick film which was deposited on a silica substrate. The optical band gap obtained using the Tauc relationship is 2.2 eV. This film was not however, similar to the films deposited on tool steel; it was less hard (2000H_K at 25g) and less transparent.

Table IX.2. Summary of coating properties
Process (a) Previous hot filament (d.c.) CVD system, (Chap.VII)
(b) Improved hot filament CVD system.
CnHm: (butane, propane, acetylene, or methane)

	CnHm : 100% **H_2 : 0%**		**CnHm : 1%** **H_2 : 99%**	
Deposition rate	**(a)**	**(b)**	**(a)**	**(b)**
Glass.–	**up to 5μm/hr**	**---------------**	**no coating in 1 hour deposition time**	**-------------------**
S. steel-	**no coating**	**up to 20 μm/hr**	**no coating in 1 hour deposition time**	**up to 3μm/hr**
Hardness	**100H_K (25g) on glass substrate**	**700H_K (25g) on s. steel substrate**	**----------------**	**>8000H_K (200g) on s. steel and silicon.**
Type	**Polymeric**	**Graphitic**	**----------------**	**-DLC** **-Particles with octahedral shapes in the early stage of growth.**

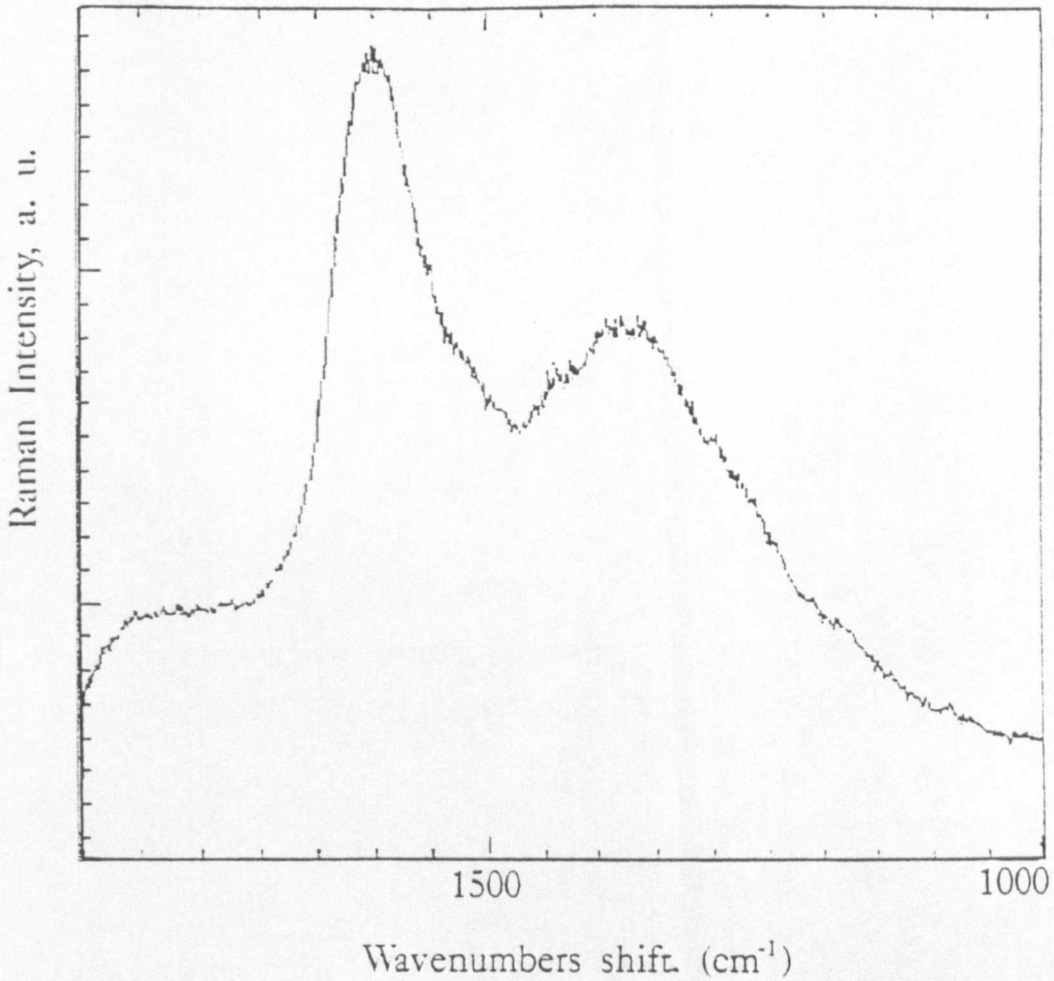

Fig. XI.5: Raman spectrum of a DLC film (2. 5 μm) produced in the improved hot filament-enhanced plasma assisted CVD system.

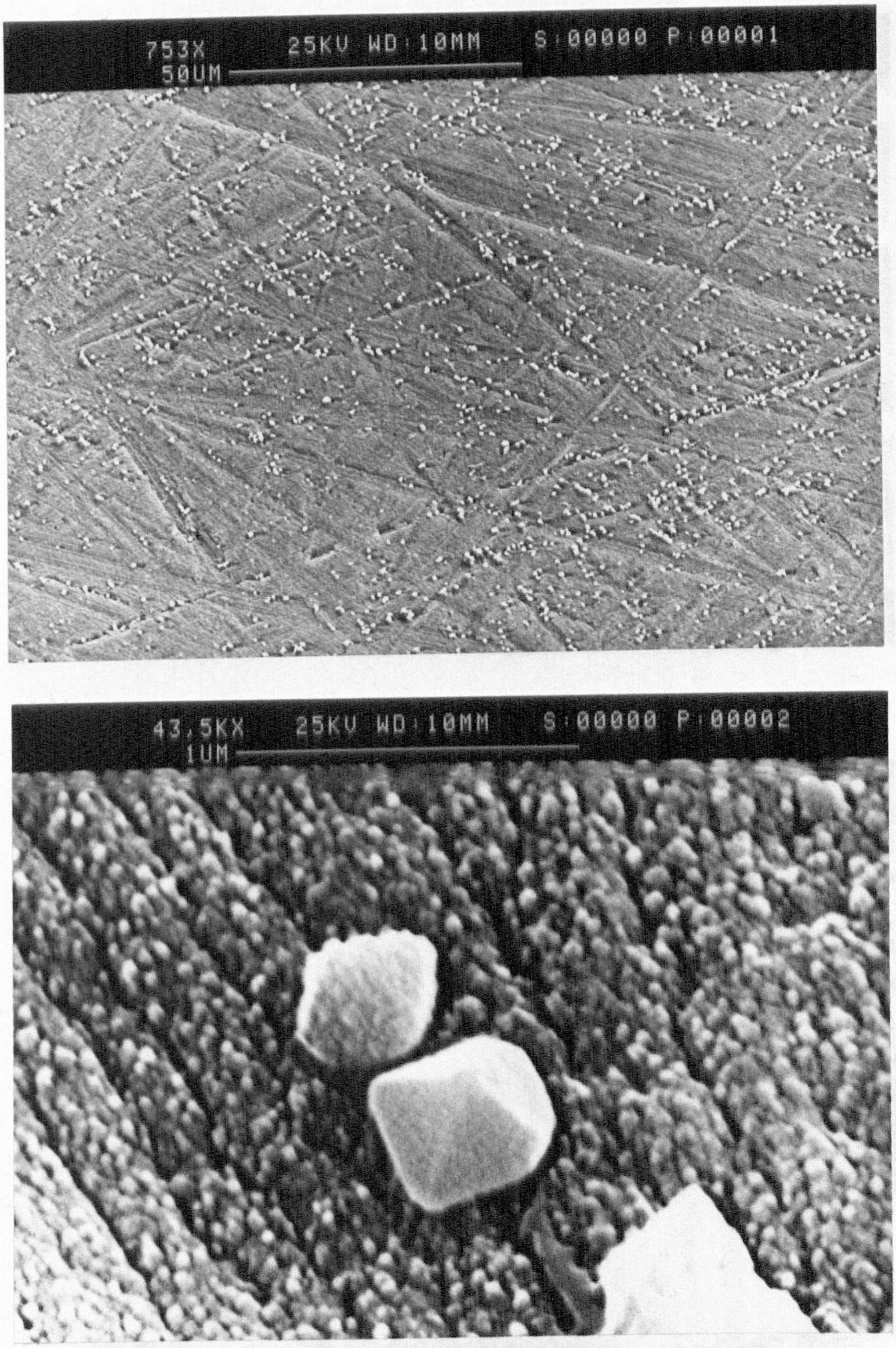

Fig. IX.6: SEM micrographs of a DLC film surface grown by the improved hot filament enhanced plasma assisted CVD system;
(a) showing particles at the early stage of growth.
(b) showing particles having octahedral shapes.

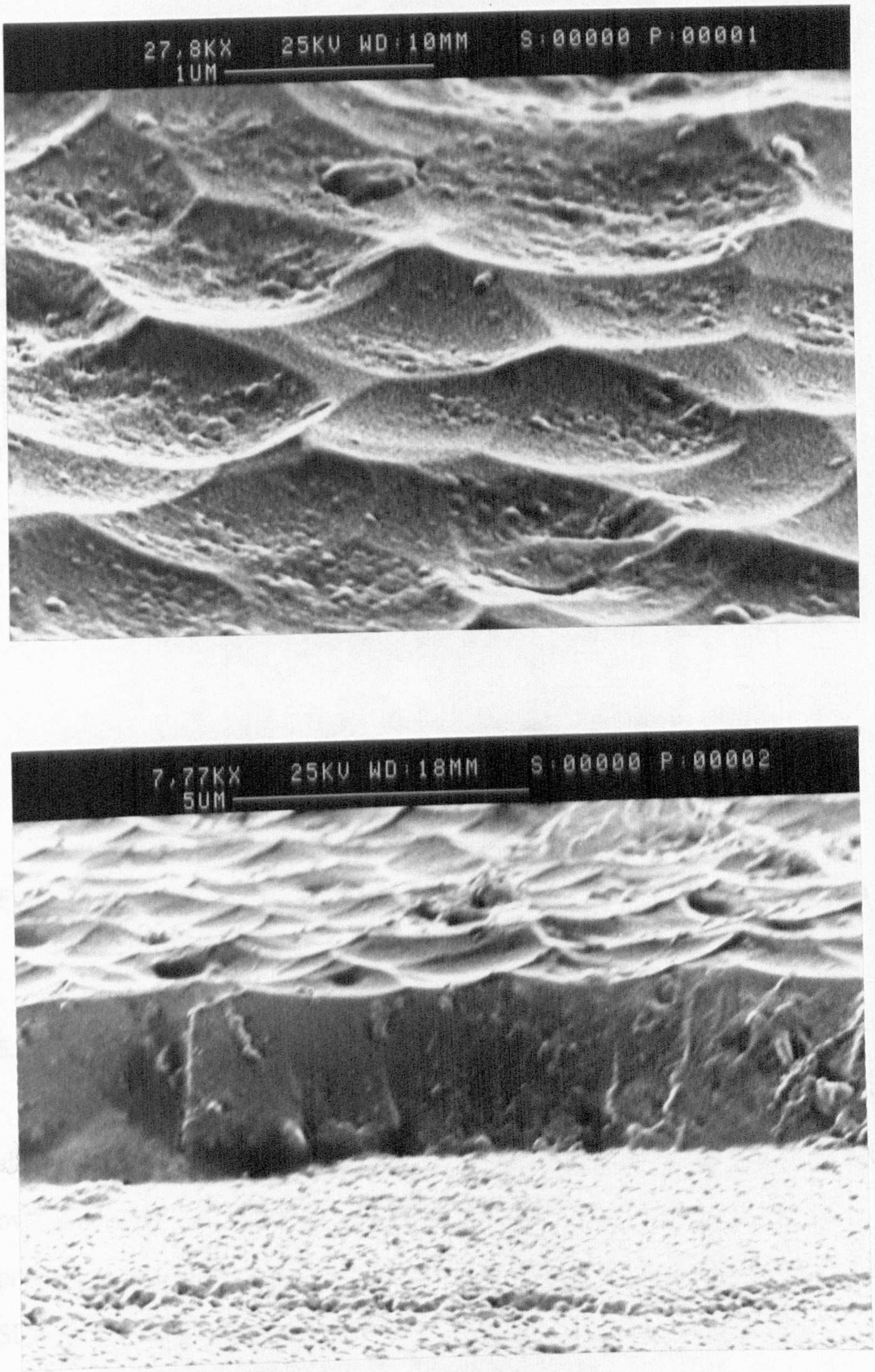

Fig. XI.7: SEM micrographs of a 2 micron thick diamond-like carbon film grown by the improved hot filament enhanced plasma assisted CVD system;(a) is showing the surface morphology, (b) is showing a cross section illustrating a high density

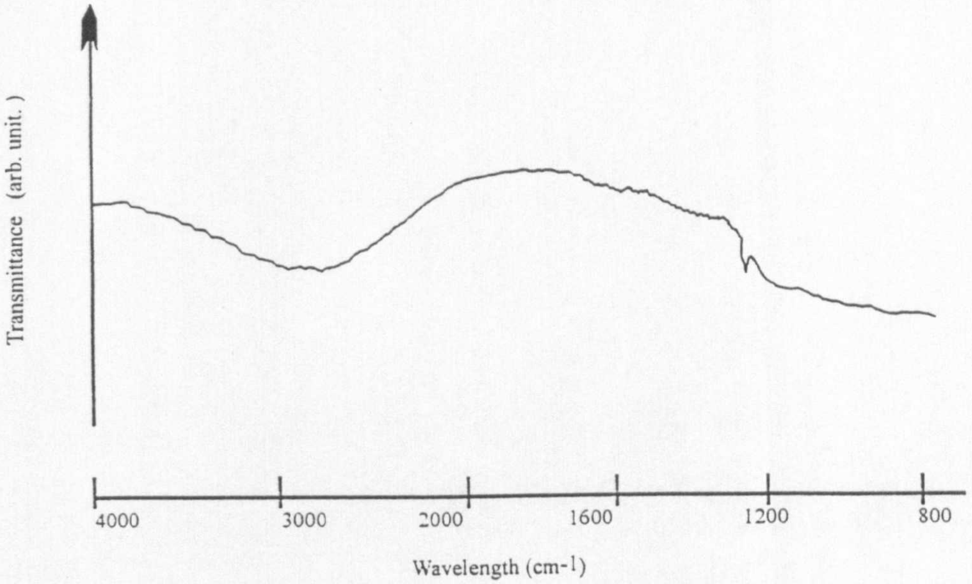

Fig. XI.8: Infrared transmittance spectrum obtained by reflection from a 2µm thick film deposited on tool steel by the improved hot filament technique.

5. Conclusion

We have described a new system for the deposition of hard carbon films, which allows the generation of very high ionisation levels and produces films with hardness over 8000 H_K (200g) (thickness ≈ 2.5µm). The deposition rate is higher than previously reported for such hard films (2-3 µm/hr) in a 0.5-1% CH_4 in H_2 plasma. SEM microscopy showed particles having octahedral shapes. Raman spectroscopy indicates a DLC structure with some disordered graphite present. Infrared spectrophotometry revealed that the content of bonded hydrogen in the films is very low compared to the previous films produced in this project. This low hydrogen content was expected because of the high deposition temperature involved in this process.

CHAPTER X

CONCLUSIONS AND DISCUSSIONS

1. Summary of results from each deposition technique

The research reported here has led to many findings, concerning several deposition systems, as follows :

DLC films produced by the FAB source technique can exhibit extremely high hardness levels (up to 8000 H_K at 25g) due, in part, to elastic recovery during testing. This behaviour appears to relate to the hydrogen content and to the high density of the coatings.

The optical band gap is about 1eV and does not depend on the type of gas used in our studies. The films are brown in colour, however, for films thinner than 0.1µm, the colour is dependent on the thickness (although complete transparency is never attained). The refractive index of 2.2 proves that the films are not polymeric (the refractive index of polymers is around 1.5).

The structure of FAB source films can be described as a matrix of smooth carbon film in which the hard residue particles are deposited in the early stage of growth. During deposition the residue particles would be very hot, wilst and the coating is at room temperature, a quenching process may therefore accompany the deposition of these particles. The resulting film is much harder than the matrix alone. Particles sputtered from the growing film inside the FAB source (on the walls) could be contributing to the growth of the hillocks observed in the films. This is supported by the similarity found between Raman spectra of high hillock density films and that of the FAB source residue.

It has been shown that the sample orientation has a dominant influence on the properties of films produced using the FAB source. This is most probably related to the normal impact energy of the beam and its interaction with the surface. Possible explanations lie in the changed sputtering mechanism and/or the change in energy when one moves from a normal "impact" situation to a "flow" situation tangential to the surface, where there is a ready availability of species moving over the surface. This has further consequences in terms of the optimisation of impact energies and the coating flux. Certainly the results whereby transparent films with low hydrogen content can be grown at grazing incidence, suggest that the normal incidence is the preferred route when hardness is the main requirement.

The absence of hillocks on the surface of the clear films produced at grazing incidence supports the earlier hypothesis on hillock origin. The fact that thick clear films could not be achieved is probably due to a bonding saturation mechanism. This saturation effect is not observed at normal incidence because the growth mechanism in this case is physical. This forced growth mechanism yields to disorder which is responsible for the low band gap. Trapped non-bonded hydrogen is believed to be responsible for the stress in the film.

The films have good wear and friction properties with only a small sign of localised failure after pin on disc sliding tests for 100 metres. Indications appear to suggest that thicker films (1.5 μm) gave better tribological performance.

Initial studies using titanium nitride/DLC multilayer films indicated poor tribological performance for various thicknesses of TiN and deposition conditions of DLC. The study showed that the failure was caused by poor adhesion at the TiN/DLC interface. This adhesion, and therefore the wear performance, can be improved to produce excellent results by utilising a different structural composition of titanium nitride. Nanohardness measurements revealed that the hardness increased dramatically with increasing hillock density from 55GPa to 88GPa for the films on glass and to 100GPa for the film on TiN, (these values correspond to a load of 4.2mN). These hardness values are extremely high compared to the hardness of the usually produced FAB source films and PVD carbon films which is around 20GPa.

Adhesion of DLC on PET has been shown to be as good as that of sputtered gold on PET, and much superior to evaporated titanium on PET. It has been shown that FAB source DLC films deposited on PET at room temperature were more transparent when a low carbon content source gas, high discharge current and low voltage were used. However, low carbon content leads to low deposition rates; the FAB source technique does not operate at low voltage and the discharge current is limited to 0.3A.

The properties of films grown by plasma-assisted evaporation of graphite depends on the carrier gas used, substrate type and bias voltage (under both d.c and r.f. conditions).

Films grown on tool steel in a butane r.f. plasma have a hardness of around $4000H_K$ (25g). The growth rate on glass under similar conditions is very low, but the film is completely transparent with an optical band gap of 2.6 eV. When argon is used as the carrier gas, no film is formed on tool steel, but on glass a completely transparent film is produced, with an optical band gap of over 3eV.

Nanohardness measurement showed that r.f. EBPVD films are extremely hard (33-44 GPa) and the lowest elastic recovery was obtained for the non-hydrogenated films (11% against 44% for the a-C:H film). This result confirms that hydrogen in the film is the main cause of film stress, which is responsible for high elasticity in the film and poor adhesion.

Pin on disc tests of r.f. a-C:H films exhibited a film wear of $48 \times 10^{-6} mm^3/Nm$ which represents only a modest reduction in wear. The coefficient of friction was however greatly reduced to a value of μ =0.16 compared to the "standard" (μ =0.45-0.54) for steel against steel.

Due to their poor adhesion, d.c. EBPVD films showed poor performance in the pin on disc tests. Films grown by graphite evaporation in a d.c. plasma exhibited higher growth rates than those in rf. There is also a greater amount of bonded hydrogen present when butane is used as the carrier gas, compared to the r.f. plasma or FAB source films. The concentration of bonded hydrogen (α_S) in d.c. films is up to five times more than that of FAB source films. Their relatively low refractive index reflects a polymeric type of film. They were more brittle and usually less well adhered than those produced by other methods, though increased voltage improves adhesion in d.c. deposited coatings. The optical band gap decreases with increasing voltage from around 1.9 to 1.1 eV. With higher plasma H/(C+H) ratios, the maximum band gap in a low voltage situation was found in some cases to be as high as 2.8 eV.

In Chapter VIII an empirical relationship is developed, linking the optical band gap with the amount of bonded hydrogen in the film, the carbon to hydrogen ratio in the plasma, and other plasma electrical parameters for carbon coatings produced using a thermionically enhanced plasma-assisted hybrid d.c. EBPVD process. This relationship explains observed properties in terms of process parameters and highlights the difficulties in obtaining consistent coatings on sample surfaces at different locations and orientations in the deposition chamber. These problems can be overcome by appropriate process modifications, e.g. by using multiple vapour sources and electron emission sources, and/or placing these in closer proximity to the samples, so as to achieve the appropriate vapour flux/ion flux distribution, within the temperature constraints of the sample to be coated.

Finally a new system is described for the deposition of hard carbon films which is a direct consequence and application of the ideas drawn from the empirical relationship mentioned above and developed in ChapterVIII. This new system allows the generation of very high ionisation levels and produces films with hardnesses of over 8000 H_K (200g) (thickness ~ 2.5μm). The deposition rate is higher than previously reported for such hard films (2-3 μm/hr) in a 0.5-1% CH_4 in H_2 plasma. SEM microscopy showed particles having octahedral shapes. Raman spectroscopy indicates a DLC structure with some disordered graphite present. The optical band gap is 2eV for a film deposited on silica. The optical band gap of the films deposited on stainless steel and tool steel could be higher because they look more transparent. More work on the characterisation of these films is in progress in collaboration with co-workers.

2 General Classification of the films produced in this study

It is clear from this study that many different type of carbon films can be produced depending on the process parameters and the deposition technique used. Looking at all the results obtained, it can be seen that in general the best films in terms of the optical properties (dc EBPVD films) had poor mechanical properties and the hardest films obtained with FAB source and rf EBPVD had poor optical properties. The optical and mechanical properties tend thus to vary in opposite directions.

For this reason the films produced in this study have been classified depending on their hardness and optical band gap values. Six types have emerged from this classification :

Optical band gap	high	low
Ultra-hard (DLC)	type 1	type 2
Hard (DLC)	type 3	type 4
Soft	type 5 (polymeric)	type 6 (graphitic)

Table X.1 summarises the film properties of these six types.

Table X.1 Film properties of the different type of films produced in this study.

	Transparency (Visible regime)	Hardness (H_K)	high E_{opt} (eV)	low E_{opt} (eV)	α_s (10^3 cm^{-2})
Type 1 **Ultra hard**	Semi-transparent (1 μm)	Over 8000 (200g)	~2		~ 0
Type 2 **Ultra hard**	Semi-transparent (1 μm)	Over 8000 (50g)		~1	~ 30-40
Type 3 **Hard**	Clear- transparent (0.5 μm)	(1000 - 1500) (15g)	~2.6		~ 0 - 46
Type 4 **hard**	Semi-transparent (1μm)	(~2000) (25g)		~1	~ 30-40
Type 5 **Soft**	Transparent (1 μm)	(1000 - 100) (15g)	(2 - 3.5)		120 - 230
Type 6 **Soft**	Brown-black (1μm)	(1000 - 100) (25g)		< 0.6	(0 - 100)

2. Main process parameters and their effect on film properties.

Although there are so many parameters that can affect the films properties, four have been found to be the most important:

i) Impact energy of the particles on the samples during growth.

ii) Degree of ionisation of the plasma.

iii) Relative content of carbon to hydrogen in the plasma.

iv) Substrate temperature.

Impact energy has been related to the rf or dc voltage, accelerating the particles to the substrate , pressure, length of dark space and the sample orientation. Degree of ionisation has been related to the filament current emission , and its voltage, the cathode voltage and the discharge current density . Relative content of carbon to hydrogen in the plasma has been related to the carbon flow input ratio, r_C^H, (This ratio was controlled by the electron beam power and the gas flux). Substrate temperature was measured during deposition.

2.1 Effect of impact energy:

High impact energy is expected to cause the $C_nH_m^+$ radicals to dissociate as soon as they are deposited [7], this is probably why the bonded hydrogen in the film decreases. High impact energy increases sp^2 over sp^3 bonding in the films (Chap. VI) and this may explain the decrease of the E_{opt} . The films are harder with high stress which is believed to be caused by an increase in the concentration of non-bonded hydrogen.

2. 2. Effect of degree of ionisation of the plasma.

Increasing the degree of ionisation tends to increase the dissociation of radicals and clusters present in the plasma and thereby favours deposition of single particles or smaller clusters containing less hydrogen. As a result the film is less polymeric; E_{opt} increases and α_s decreases.

2.3 Relative content of carbon to hydrogen in the plasma.

Increasing the carbon flow input ratio favours an overgrowth of graphitic structure and minimises the effect of hydrogen etching . The films properties move towards a more graphitic structure.

2.4 Substrate temperature

The substrate temperature increases during coating as a result of particle bombardment. Temperatures higher than 300°C may contribute to an increase of the $sp^2 : sp^3$ bonding as found in the post deposition annealing experiment. Annealing FAB source films during deposition turned the films graphitic.

Tables X.2-4 summarise how the film properties relate to the process parameters for the six type of films, and demonstrate the inter- relationships amongst the systems studied . These inter- relationships are developed in the next paragragh.

3. Inter-relationships amongst the systems studied

Type 1 : Ultra-hard and high optical band gap
(Conditions: low impact energy , very high degree of ionisation and 1% CH4 in H_2*)*

This is the only case where ultra hard carbon films were produced at low impact energy. High impact energy is normally needed to compensate for the relatively low degree of ionisation of rf EBPVD and dc EBPVD. The energetic particles help to break the radicals that could not dissociate in the plasma due its low discharge intensity. In the case of the improved hot filament CVD system (IHFCVD), because of the very high degree of ionisation all the radicals can be dissociated before they reach the substrate .The high surface temperature (900 °C) and the high hydrogen content in the plasma are contributing to the same effect. Therefore high impact energy was not necessary and IHFCVD was the only process suitable for this type of film.

Type 2 Ultra-hard and low optical band gap
(Condition: high impact energy and high degree of ionisation 100% CnHm)

This type of films were produced occasionally using the FAB source technique. Their unusual hardness has been related to the particles sputtered from the growing film inside the FAB source. The high elastic recovery observed in these films has been related to the high impact energy. The rf EBPVD , dc EBPVD and IHFCVD did not produce films of this type probably due to their lower impact energies and higher substrate temperatures.

Table X.2 Deposition techniques and process parameters for ultra hard DLC films

IHFCVD: Improved Hot Filament CVD system (Chap.IX)

Type 1 Ultra hard Over 8000 H_K (200g), dense and semi-transparent in the visible regime (very low bonded hydrogen content)

Process	Impact energy	Degree of ionisation	Carbon flow input ratio	Substrate temperature	max.deposition rate μm/hr	
					silicon	Steel
IHFCVD	Low cathode voltage 200V	Very high $J = 14$ mA/cm^2	Very low 1% methane in hydrogen	Very high up to 900 °C	2	3
FAB source ,dc EBPVD, and rf EBPVD	Not suitable (Degree of ionisation not high enough)					

Type 2 Ultra hard Over 8000 H_K (25g) (30% indentation recovery), dense and semi-transparent in the visible regime

Process	Impact energy	Degree of ionisation	Carbon flow input ratio	Substrate temperature	Max.deposition rate (μm/hr) on glass , tool steel and TiN on steel
IHFCVD	High Cathode voltage (1000-2000)V	High $I_D = 0.15$ A	High 100% C_nH_m	Low 50 °C	0.3
dc EBPVD and rf EBPVD	Not suitable (Impact energy not high enough)				

Type 3 Hard and high Optical band gap
(Condition: high degree of ionisation, high impact energy and low carbon flow input)

In this case the degree of ionisation was not as high as for Type 1 films, as a result α_s was not minimised. High impact energy was therefore needed to decrease α_s, but this has a side effect of decreasing the E_{opt} due to the increase of sp^2 bonding as a result of high particle bombardment. Therefore dc EBPVD is not the appropriate deposition roue to use because of its low impact energies. FAB source and rf EBPVD were suitable for producing this type of film. Ultra hard films up to 8000 H_K with low E_{opt} and α_s were obtained occasionally on TiN deposited on tool steel using the FAB source with the same process parameters as in this case. High indentation recovery was observed in these films (16 - 45%). This is due to a high content of hydrogen in the films, most of which must be non bonded.(Chap.VII).

Type 4 (Hard and low optical band gap)
(Conditions: high degree of ionisation, high impact energy ,and lower carbon flow input than in type 3 situation)

These films were the only films that combine good mechanical properties with excellent optical properties. The films were not soft (1500H_K) and had high E_{opt} (2.6-3.5) eV and low α_s (20 - 46 $\times 10^3$)cm^{-2}. They were obtained by optimising the process parameters for the type 2 films. The carbon flow input was decreased (lower graphite evaporation rate in maximum hydrogen , argon or butane flux). Only rf EBPVD has produced such films . The FAB source was not suitable because of its higher impact energies compared to rf EBPVD where there is substantial rduction of impact energy loss due to charge exchange collisions in the dark space region.

The problem in this case is that films thicker than 0.2 μm could not be obtained due to the etching and saturation effect. This could not be avoided due to the combination of high impact energy and low carbon imput levels. The films produced in argon were non hydrogenated, showed lower indentation elastic recovery and were very thin.

DC EBPVD and IHFCVD do not correspond to these conditions because of their lower impact energies.

Table X.3 Deposition techniques and process parameters for hard DLC films

Type 3 (1000 - 1500 H_K) (15g) Hard , dense and clear -transparent in the visible regime (low bonded hydrogen content)

Process	Impact energy	Degree of ionisation	Carbon flow input ratio	Substrate temperature	Max. deposition rate (μm/hr)	
					Glass	Steel
rf EBPVD	High D.C. offset 1.1 kV	High Peak current ~ (0.6 - 1)A	Low low evaporation rate in H_2 or argon r_c^H ~ (20%)	Medium ~200 °C	0.5	etched
FAB source	not suitable (Degree of ionisation near the substrate surface not high enough)					
dc EBPVD	not suitable (impact energy too low).					
IHFCVD	not suitable (impact energy too low and substrate temperature too high)					

Type 4 (~2000) (25g)H_K Very hard, dense and semi-transparent in the visible regime (low bonded hydrogen content)

Process	Impact energy	Degree of ionisation	Carbon flow input ratio	Substrate temperature	Max. deposition rate (μm/hr)	
					Glass	Steel
FAB source	High V_a = (1000-2000)V	High I_D = 0.15A	High (CnHm) 100%)	50 °C	0.3	0.3
rf EBPVD	D.C. offset 1.1 kV	Peak current ~ 0.6A	Butane and graphite evaporation r_c^H ~ (30% - 60%)	~200 °C	0.6	1.4
DC EBPVD	not suitable (impact energy too low).					
IHFCVD	not suitable (impact energy too low and substrate temperature too high)					

Type 5 : soft and high optical band gap
(Conditions: low impact energy, low degree of ionisation, low carbon flow input)

For soft films deposition, low impact energy deposition techniques were needed, dc EBPVD was therefore suitable. Decreasing the carbon flow input, increases E_{opt} whereas increasing the impact energy or the substrate temperature will produce the opposite effect.

A FAB source operated under normal conditions can not produce polymeric films as the impact energy is too high. They can be decreased by either orienting the substrate tangentially to the beam or by increasing the pressure outside the FAB source (eg the introduction of C_nH_m into the vacuum chamber containing the FAB source). In these two situations polymeric films have been obtained. IHFCVD can be suitable for this type of film at low degrees of ionisation (low current emission and sample voltage). but the enclosure chamber should be water cooled in the latter case.

Type 6 Soft and low optical band gap
(Conditions: High carbon flow input, low impact energy and low or high degree of ionisation)

Here the main cause of the very low E_{opt} is the high carbon flow input (> 70%). The films are soft because of the low impact energies . The level of hydrogenation of these films can be modified by acting on the degree of ionisation and the surface temperature. Therefore the rf EBPVD and FAB source techniques were not suitable due to high impact energies. IHFCVD and dc EBPVD have produced this type of film when a high carbon flow rate was used.

Finally we can say that depending on the films properties needed a process can be chosen and its parameters adjusted for an optimum production. Thick and hard transparent films are not easy to produce as we saw in this study. More research is needed on the deposition techniques studied in this project . In the next chapter recommendations for future work are suggested.

Table X.4. Deposition techniques and process parameters for soft films

Type 5 (100 - 1000) H_K(15g) (soft, and semi-transparent in the visible regime (high bonded hydrogen content) polymeric.

Process	Impact energy	Degree of ionisation	Carbon flow input ratio	Substrate temperature	Deposition rate μm/hr Glass and Steel
FAB source	Low -substrate tangential to the beam	High (I_D 0.15 A)	High (C_nH_m 100%)	50°C	0.1 - 0.2 Thickness saturation 0.5 etched
	Low -High pressure (5 10^{-3} Torr) in the substrate region.	as above	as above	50°C	1 - 3
dc EBPVD	Low Substrate insulating and floating (Cathode voltage (0 - 1000)V	Low J up to (0.14 mA/cm^2)	10% - 60%	up to 300 °C	up to 4
rf EBPVD	Not suitable (too high impact energy).				
IHFCVD	Not suitable (too high substrate temperature)				

Type 6 (100 - 1000) H_K (25g) Poor mechanical and optical properties (graphitic)

Process	Impact energy	Degree of ionisation	Carbon flow input r	Substrate temperature	Max. deposition rate (μm/hr)
dc EBPVD	Low Substrate insulating and floating (Cathode voltage (0 - 1000V)	Low J = 0- 0.14 (mA cm^{-2})	Very high r_C^H >70%	Medium up to 300 °C	4
IHFCVD	Low Cathode voltage 200V	Very high J = 0 - 14 (mA cm^{-2})	High100% butane in hydrogen	Very high up to 900 °C	20
rf EBPVD	Not suitable (too high impact energy).				
FAB source	Not suitable (too high impact energy).				

CHAPTER XI

RECOMMENDATIONS FOR FUTURE WORK

1. Process limitations

The most fundamental limitations of the FAB source relate to the very low deposition rate (0.3 µm/h). The cause of this low deposition rate is in the design of FAB source; the beam is not focused in one direction but projected in all directions within the source. Therefore only particles directed towards the grid holes can reach the substrate when these small holes are not narrowed with carbon. An experimental study carried out by the author after the PhD programme, showed that the deposition rates on molybdenum, tool steel, and chromium cobalt substrates which were clamped on the walls cathodes inside the FAB source were around 20 µm/h. These film were of graphitic appearance probably because of the high carbon /hydrogen ratios in the plasma used (butane). This was confirmed when a lower carbon content plasma (5% butane in hydrogen) gave better quality films in terms of hardness and transparency and were produced with the same high deposition rate. These results show clearly that there is enough dissociated carbon inside the FAB source that needs to be extracted to the outside of the source. A new FAB source configuration in which all the particles created inside it are focused towards the grid is required. A magnetic field or an electron emitter should be added to assist the discharge and compensate any eventual decrease in the discharge intensity which may occur in a new configuration. This is an area where there is a strong requirement for further, more detailed, development work. Another cause of the low deposition rate is the fact that not all the particles bombarding the substrate will stick on it. A non negligible proportion is ejected due to a sputtering effect as a result of the high voltage used. (It should not be forgotten that the FAB source was initially built for etching processes). To see more clearly this effect, glass slides were put outside the beam area in the path of the ejected particles and the deposition rate obtained was around 0.1μm/h. In order to investigate this effect further a small chamber of the FAB source size was put 1 cm above the grid. In this situation when the beam emerges from the FAB source plasma it enters immediately a new plasma formed by the particles re-ejected from the walls of this second chamber and trapped in it . As a result the deposition rate was increased to 3μm/h for the films obtained on the surface inside chamber facing the beam and to 1μm/h on its walls. The former coatings proved to be very hard (5000H_K at 50g) with a very high hillock density, and the latter were soft polymeric films. The substrate temperature increased to 150 °C in this new configuration. These investigations need further development.

The following FAB source limitations have been discussed in this work and should also receive further attention:

i) Poor coverage due to the narrow beam width. Rotation of the sample is a possible solution in this case, the surface to be coated has however, to remain normal to the beam during its rotation in order to obtain uniform coating properties.

ii) The need to dismantle so often the FAB source and clean the electrodes from the deposited carbon residue is a time consuming procedure.

iii) the non reproducibility of the film properties (e.g. some films are hard and others are ultra hard due to the occasional high hillock density in the films)

iv) The impossibility to work at voltages less than 800V.

v) The voltage and the degree of ionisation are not independent (decreasing the voltage is desirable in order to increase the band gap but this also decreases the discharge intensity which leads to a decrease in the dissociation rate of C_nH_m radicals.). Introducing an electron emitter will help to increase the discharge intensity without having to increase the voltage. Tungsten electron emitter is not desirable because of contamination of the film. This problem can be solved by using a carbon electron emitter or a magnetic field.

In the (d.c./r.f.) EBPVD processes DLC films have been produced only in the r.f. mode , in the d.c. mode only soft films have been produced. The reason for this has been demonstrated to be the low degree of ionisation in the d.c. mode. This was confirmed in the new configuration of the hot filament CVD system. Therefore in the d.c. EBPVD mode a further investigation employing other means of assisting the discharge (increasing the number of tungsten filaments, biasing positively the crucible, or adding a magnetic field) is needed.

The reason why in the d.c. mode no coating was produced on the conducting materials while polymeric films have been deposited at a rate of 4µm/h on the insulating ones remain an open question. A further investigation on this subject using plasma spectroscopy is needed to study the different radical species present in the d.c. mode and also in all the other processes utilised in this work.

The effect of substrate temperature during coating has not been studied systematically for all the processes. All these deposition techniques should be equipped with an in-situ substrate cooling and heating attachment. It would be very interesting to see the substrate temperature as an explicit parameter in the empirical model presented in Chap. VIII. instead of being implicit .

The hot filament CVD process presented in Chap. IX is a very promising technique which could be switched to diamond deposition. It was however very quickly designed and produced by the author with the help of the workshop technicians, towards the end of the programme. Further work, employing appropriate power supplies delivering high current and low voltage (typically 300V, 20A) is required. The enclosure surrounding the filament should be water cooled. Scaling up this technique is worth considering and would probably overcome the processing difficulties encountered in this work to produce thick and very hard transparent films.

2. Film properties and Characterisation techniques

In this work very hard DLC films have been produced but the most important problem remains only partially solved; improving the adhesion of DLC on many metals (stainless steel, tool steel, copper, chromium cobalt .etc..). The tribological properties of DLC film depends extremely on its adhesion to the substrate. The best resistance to wear failure in the pin on disc machine of all the carbon films produced in this work was obtained from a FAB source film deposited on a glass substrate. This is because of the excellent adhesion obtained on glass. Unfortunately glass is not suitable for mechanical applications. Nitrogen rich titanium-nitride(over-stoichiometric) has been demonstrated to be an excellent inter-layer between DLC and substrate (stainless steel, tool steel and chrome-cobalt). A recent study showed that a relatively soft titanium substrate inter-layer is improves the adhesion [120]. Further studies on other inter-layers such as Si, SiC,...etc. ... are required. Characterisation of the carbon film at the early stage of growth using in-situ photon and electron spectroscopy would give valuable information on the interface substrate/coating structure which would allow a better understanding of the adhesion mechanism.

The high stress observed in the films causes adhesion failure and a decrease in the hardness. Quantification and correlation between these parameters is required. Since hydrogen has been demonstrated to be contributing to this stress, investigations into non-hydrogenated carbon films should be further studied. Evaporation of graphite in an inert gas using (d.c./r.f.) EBPVD or by sputtering graphite by the FAB source (an inert gas being the gas source) is a further work that could produce transparent hydrogen free films. (We have produced clear films by evaporation of graphite in argon using r.f. EBPVD, these films were however very thin and not very hard (Chap.VII)).

Microhardness evaluation has been shown to be almost inappropriate for the evaluation of DLC films, due to the interdependent effects of elastic recovery, substrate load support and the load-indentation size effect. However it was used in this work as a simple and quick means of classifying films. Nanoindentation should be adopted as the means for probing the hardness on a nanometer level.

The comparison study done in Paris on the optoelectronic properties has been performed only on FAB source and d.c. EBPVD films. A similar study is required for the carbon films produced by the r.f. EBPVD, and the improved hot filament CVD method.

References

1. S. Aisenberg, and R. J. Chabot, Appl. Phys. , 42 (1971) 2953.
2. E. G. Spencer, P. H. Schmidt, D. C. Joy, and F. J. Sansalone, Appl. Phys. Lett., 29 (1976) 118.
3. L. Holland and S. M. Ojha, Thin Solid Films, 38 (1976) L17.
4. L. Holland and S. M. Ojha, Thin Solid Films, 58 (1979) 107.
5. G. Gautherin and C. Weissmantel, Thin Solid Films, 50 (1978) L 135
6. Weissmantel C. , Proc. IX Int. Vacuum Cong. and V. Int. Conf. on Solid Surfaces J. L. de Segovia, Ed. Assoc. Espanola de Vacio y Aplicacions. Madrid, 1983, 299.
7. C. Angus, P. Koidl, and S. Domitz, in J. Mort and F. Jansen (eds.), Plasma Deposited Thin Films, CRC Press, Boca Raton, FL, 1986. pp. 89-125.
8. Diamond Films Evaluating the Technology and Opportunities. Emerging Technologies n° 25. Published by Technical Insights, Inc. Englewood/Fort Lee, NJ.
9. B. V. Derjaguin, D. V. Fedoseev, Diamonds Wrought by Man, Mir Publishers Moscow, 1985. (translated from the Russian)
10. J. E. Field, The properties of Diamond, Academic press, London, 1979.
11. J. E. Field, Phil. Mag. 43 (1981) 595-618.
12. M. Seal: Industrial Diamond Review 38 (1978) 130.
13. M. Seal and W. J. P. van Euchevort: "Applications of Diamond in Optics" , vol. 969 Diamond optics (1988), p. 114.
14. A. T. Collins "Visible light emission from diamond" Proceeding of the second International symposium on New Diamond materials, in press (1991).
15. B. D. Cullity, Elements of X-ray Diffraction, Addison-Wesley

Publishing Co. Inc., Reading, Massachusetts, 1978.

16. J. J. Cuomo, J. P. Doyle et al. in Applications of Diamond Films and Related Materials eds., Y. Tzeng M. Yoshikawa and A. Feldman (Elsevier Science Publishers B. V. Amsterdam, The Netherlands, 1991) pp. 169-180.

17. M. G. Peters, J. L. Knowless, M. L. Breen and J. J. Mc Carthy: "Ultra thin diamond films for X-ray window applications" SPIE Vol. 1146, Diamond Optics II (1989) pp. 217-224.

18 K. Suzuki and T. Inuzuka, Appl. Lett, 53 (1988) 1818.

19 K. Kurihara, K-Sasaki, M. Kawarada and N. Koshino,
Appl. Phys. Lett., 52 (1988) 437.

20 F. Akatsuka, Hirose and K. Komaki, Jpn, J. Appl. Phys. 27 (1988) L 1600.

21 N. Ohtake and M. Yoshikawa, J. Electrochem. Soc. 137 (1990) 717.

22 K. Saito, K. Sato, H. Tanaka, K. Fujita and S. Matsuda,
J. Mater. Sci, 23 (1988) 842.

23 C. P. Chang, D. L. Flamm, D. E. Ibbotson and T. A. Mucha,
J. Appl. Phy. 63(1988) 1744.

24 K. Ito, T, Ito and I. Hosoya, Chem. Let, 4 1988 588.

25 A. Inspektor, K. Lion, T. Mc kenna and R. Messier,
Surf. Coat. Technol., 39-40 (1989) 211.

26 L. Kostadinov and D. Dobrev.
Surf. Coat. Technol., 47 (1991) 623-627.

27 Y. Matsui, H. Yabe T. Sugimoto and Y. Hirose
Surf. Coat Technol., 47 (1991) D69

28 T. Nakamura, F. Naori, J. Nakai and S. Nakatani, In super-abrasives 91, Chicago, Illinois, June 1991, Society of Manufacturing Engineers, Dearborn, Michigan, pp. 15-15 to 15-29.

29 P. M. Stephan, R. A. Hay and C. D. Dean
Diamond and Related Materials, I (1992) 110-116.

30 M. S. Wong, R. Meilunas, J. P. Ong and R. P. H Chang,
Appl. Phys. Lett, 54 (20) (1989) 2006.

31 K. Enke, H. Dimigen and H. Huesch,
Appl. Phys. Lett., 36 (4) (1980) 291.

32 N. Yoshino, Y. Shibuya, K. Naoi and T. Nanya,
Surf. Coat. Technol., 47 (1991) 84.

33 T. P. Ong and R. P. H Chang, Appl. Phys. Lett, 58(4) (1991) 358.

34 M. Yoshikawa, Diamond Films and Technology vol. 1, N. 1 1991 MYU. Tokyo
pp.1-29.

35 S. R. P. Silva et al. Diamond and Related Materials, 1 (1992) 612-618

36 H., Z. Schmellenmeier, Phys. Chem., 205, 349, 1955/56

37 S. M. Ojha, and L. Holland, Thin Solid Films, 40, L31, 1977

38 L. Holland, and S. M. Ojha, Thin Solid Films, 48, L15, 1978.

39 C., Weissmantel, C. Schurer, R. Frohlich, P. Gran and H. Lehmann,
Thin Solid Films, 61, L5, 1979

40 C., Weissmantel, K., Bewilogna, and C. Schurer,
Thin Solid Films, 61, L1, 1979.

41 C., Weissmantel, Thin Solid Films, 58, 101, 1979

42 C. Weissmantel, J. Vac. Sci. Technol., 18, 179, 1981.

43 C. Weissmantel, K. Bewilogua, K. Breuer, D. Dietrich, U. Ebersbach, H. J.
Erler, B. Ran and G. Reisse, Thin Solid Films, 96, 31, 1982.

44 B. Huck, E. Jaeschke, W. Kratshmer, R. Repnow and H.Wirth,
Nucl. Instrum. Methods, 184, 215, 1981.

45 S. Iida and S. Ohki, Jpn. J. Appl. Phys. 2 Lett., 21, 262, 1982.

46 A. R. Nyaiesh and W. B. Nowak, J. Vac. Sci. Technol, A1, 308, 1983

47 J. R. Reimer, R. W. Vaughan, T. C. Knights, and R. A. Lujan,
J. Vac. Sci. Technol., 19 (1981) 53.

48 J. C. Angus, J. E. Stultz, P. J. Shiller, J. R. Mac Donald, M. J. Mirtich and

S. Domitz, Thin solid Films, 118 (1989) 311.

49 R. H. Bragg, Synth. Met., 1 (1983) 95.

50 S. Craig and G. L. Harding, Thin Solid Films, 97 (1982) 345.

51 A. Bubenzer, B. Dischler, G. Brandt and P. Koidl, J Appl. Phys., 54 (1983) 4590.

52 T. Miyazawa, S. Misawa, S. Yoshida, and S. Gonda,
J. Appl. Phys., 55 (1984) 188.

53 J. J. Zelez, Vac Sci., Technol., A1 (1983) 305

54 J. J. Zelez, RCA Rev., 43 (1982) 665

55 D. Mori, R. Kalish, and G. Lewin, Thin Solid Films, 117 (1984) 125.

56 C. Weissmantel, K. Bewilogua, K. Brewer, D. Dietrich, V. Ebersbach, H. J. Erler, B. Ran. and G. Reisse, Thin Solid Films, 96 (1981) 179.

57 Z. Marinkovic, and R. Roy, Carbon, 14 (1976) 329

58 F. Jansen and M. A. Machonkin, Thin Solid Films 140 (1986) 227.

59 N. H. Cho., K. M. Krishnan, D. K. Vries., M. D. Rubin, C. B. Hopper, B. Bruschan, D. R. Bogy, J. Mater Sci 5 25 43 (1990).

60 P. G. Turner, R. P. Howson, and C. A. Bishop. Inst. Phys. Conf. Ser.,
54 (1980) 229.

61 D. S. Whitmell, and R. Williamson, Thin Solid Films, 35 (1976) 255.

62 X. Jiang, J. W. Zon, K., Reichelt, and P. Grumberg, J App. Phys 66 (4) (1989) 729

63 B. Dischler, A. Bubenzer, and P. Koidl, Appl., Phys. Lett., 42 (1983) 636.

64 Dr P.Holiday PhD Thesis, Hull University 1993.

65 L. P. Anderson, S. Berg, H. Norstrom, R. Olaison, and S.Towta,
Thin Solid Films, 58 (1979) 155.

66 T. J. Hauser, J. Non. Cryst. Solids 23 (1977) 21

67 J. Fink, T. M. Heinzerling, J. Phluger, B. Scheerer, B. Dischler, P. Koidl, A. Bubenzer, R. F. Sah, Phys., Rev., B. 30 (1984) 4713

68 F. W. Smith, J. Appl. Phys., 55 (1984) 764.

69 B. Dischler, A. Bubenzer, and P. Koidl, Solid State Commun., 48 (1983) 105

70 T. J. Moravec, and J. C. Lee, J. Vac. Sci. Technol, 20 (1982) 338.

71 B. Dischler, R. E. Sah, P. Koidl, W. Fluhr, and A. Wokaun, Proc. 7th Int. Plasma Chemistry, Schramm, D. C., Ed., Eindhoven, pp. 45-52, 1985

72 J. Robertson, Advances in Physics, vol., 35, No 4 (1986) 317-374.

73 S. Kaplan, F. Jansen, and M. Machonkin, Appl. Phys. Lett., 47 (1985) 750.

74 C.Weissmantel, K. Bewilogua, D. Dietrich, H. J. Erler, H. Hinneberg, S. Klose, W. Nowick, and G. Reisse, Thin Solid Films, 12 (1980) 19 .

75 T. Mori and Y. Namba, J. Appl Phys 52 (1981) 6151 .

76 D. R. Mc Kenzie, R. C. Mc Phedran, N. Savvides, and L. C. Botten, Phil. Mag., B48 (1983) 351.

77 D. E. Carlson and C. R. Wronski, in: Amorphous Semiconductors (Ed. M. H. Brodsky), Topics in Applied Physics, Vol. 36, Springer-Verlag, New York (1979), p.287.

78 A. Dehbi-Alaoui Doctorate Thesis, University of Limoges, 1983, Limoges, France.

79 R. S. Nelson, J. A. Hudson, and D. J. Mazey V. S. Patent 4,191,735, 1980.

80 D. M. Mattox, Sandia Corp. Rep., sc. DR.63, 1963.

81 B. Zega, Le Vide, Les Couches Minces, n° 193, 1963.

82 W. D. Davis, T. A Vanderslice: Phys. Rev, 131 (1963) 219 .

83 A. Dehbi-Alaoui, P. Saulnier, and J. Machet, Vacuum/Volume 34/number 8/9 (1984) 765-769

84 A. Matthews and D. G. Teer, Thin Solid Films, 80 (1981) 41 .

85 P. Koidl. Proc. 1st Int. Symp. on Diamond and Diamond-like Films, J.P.Dismukes Ed, Electrochemical Soc. Proc. 89-12 (1989). pp. 237-249.

86 B. Dischler, EMRS Meeting, June 1987, vol. xvii, pp. 189-201.

87 T. I. Conn and D. G.Avery, Infrared Methods, Principles and Applications Academic Press: New York, 1960.

88 R. N. Jones, and C. Sandorfy, in Technique of Organic Chemistry, vol.ix, Chemical Applications of Spectroscopy, Ed. A. Weissberger; Interscience: New York, 1956, p. 332.

89 A Course in the Principles and Practice Infrared Spectroscopy. Edited by W. J. Price, Published by Pye Unicam Ltd, York Street, Cambridge CB1 2PX, England. Edition June 1970.

90 P Fleury, J. P. Mathieu, Lumiere, Ed. Eyrolles, Paris, 1961.

91 N. J. Harrick, Internal Reflection Spectroscopy, John Wiley, New York, 1967.

92 A. Celerier Doctorate, University of Limoges. July 1985.

93 Optical Properties of Solids, ed. by F. Abeles (North- Holland, Amsterdam 1972)

94 R. A. Smith, (1968). "Semiconductors".
Cambridge Univ. Press, London and New York.

95 E. C. Freeman, W. Paul; Phys. Rev. B 20 (1979) 716

96 J. Tauc, R. Grigorovici, A. Vancu : Phys. Stat., 15 (1966) 627

97 Discussion with Dr Howson Director of Laboratory of Optics of Thin Films. Loughbourough University. UK.

98 J.Franks, J. Vac. Sci. Technol. A, 7(3) (1989) 2307

99 J.Franks, Vacuum, 34 (1984) 259-261.

100 G. H. Rushton and R. K. Fitch, Vacuum 21 (1971) 449 .

101 R. K. Fitch, M. Khorassany, and T. N. Mawlood, Proc. 7th Int. Vac Conf. and 3rd Int. Conf. on Sol. Surf., p. 285. Vienna (1977).

102 C. Wild, P. Koidl, and J. Wagner, EMRS symp. Proc, 17 (1987), 1374.

103 B. Ollivier Msc Thesis, Hull University, 1993.

104 A. Dehbi-Alaoui, A. Matthews, and P.Holiday, a project report on the Characterisation of DLC films for Howmedica International, RCSE, EDM department, University of Hull, HU6 7RX, UK.

105 Dr A. Leyland, PhD Thesis, Hull University, 1992

106 T. J. Moravec, Final Technical Report, SERI contract N° XS-O-9010-3, 1981.

107 Private communication, AEA Technology

108 Dr T. J. Dines private communication, Department of Chemistry, University of Dundee, Dundee DD1 4HN,U.K.

109 A. Bubenzer, B. Dischler, G. Brandt, and P. Proc., Int. Conf. on Metallurgical Coatings, San Diego, CA, April 1990 in Surf. Coatings Technol, 43-44 (1990) 88.

110 A.Dehbi-Alaoui, A.S. James, and A. Matthews,
Surf. Coat. Technol. 43/44, 88, 1990.

111 J. B. Pethica, P. Koidl, J. Gohrecht, and C. Schuler,
J Vac. Sci. Technol-A. 3 (6) (1985).

112 H. Nakaue, T. Mitani, H. Kuorokawa, T. Yonezawa, and H. Yoshio, Thin solid Films, 212 (1992) 240 - 244.

113 A. Dehbi-Alaoui, B. Ollivier, A. Matthews,
Le Vide, Les Couches Minces-Suplement au N° 261- Mars- Avril 1992.

114 K. M. Anetsberger, "Metallized Plastics 1, Fundamental and Applied", Mittal and Susko editors, Plenum Publishing Corporation, 1990, p.43.

115 Dr K.Fancy PhD Thesis, Hull University, 1990

116 Z. Has, S. Mitura, M. Clapta, J. Szhidt, P. Pieta, A. Balasinski. Archuwum Nauki O. Materiatach 1986 t.7 z.2 str. 131-137. International Conference on Diamond

117 Dr. B. Yahya PhD Thesis University of P. et M. Curie, Paris, 1993.

118 J. Robertson and E. P. O' Reilly, Phys. B, 35 (1987) 2946.
Crystallisation under reduced Pressure Warsawa, Poland June 27-30, 1985.
J. Vac. Sci. Technol A7(3) (1989) 2315.

119 W. Banholzer and R. Kehl, Surf. Coat. Technol, 47 (1991), 51-58.

120 B. Ollivier and A. Matthews, RCSE, to be published in J. Adh. Sci. and Technol.

APPENDIX

STANDARD CHARACTERISATION TECHNIQUES USED IN THIS STUDY

1. Optical microscopy.

Optical microscopy for topographic observation or detailed measurement was performed using a Nikon Optiphot Microscope. Observation of samples could be undertaken at magnifications of between x10 and x400 with an additional facility to record the image using a UFX-IIA photographic attachment. A Nikon Filar Micrometer eyepiece was used to measure dimensions down to 1μm with a vernier resolution of 100 nm. Optical microscopy was used during microindentation testing, wear scar examination, adhesion assessment and topographic studies. All these activities were performed routinely with further detailed work being performed using by the scanning electron microscope (SEM).

2 SEM

Scanning electron microscopy is an analytical technique commonly used for studying the surfaces of solids at high magnification (109). Its most immediate advantages relative to optical microscopy are improved resolution and depth of field, additional advantages accrue from the fact that electron bombardment of a surface results in a much wider range of phenomena which may be exploited for analysis.

The SEM available in the EDM. department capable of providing photo-micrographs of x 100,000 on suitable specimens has been used for carbon films morphology characterisation.

3. Thickness measurement and profilometry

For film thickness measurement and surface topography, a Rank Taylor Hobson Talysurf was utilised. The Talysurf 50 uses a standard conispherical diamond stylus (tip radius 1.5-2.5 µm) on the end of a pivoted arm, the deflection of which was measured by means of a sensitive interferometric helium neon laser transducer. Traversing of the stylus is achieved by a precision stage which rides on an optically flat reference surface to give a scan length of 120 mm.

The step needed for film thickness measurement is produced by masking a region of the sample during deposition, the non coated area is used as a reference surface. The sample surface should have an optical quality finish, since the accuracy of this method decreases rapidly with surface roughness.

This method is sufficiently accurate only if the film is not very thin. Films of submicron level (≤ 50 nm) pose problems as their thickness approaches that of the surface roughness.

4. Adhesion

The main factor which has prevented the more widespread use of many coating processes has been poor adhesion. The true adhesive strength of a coating is related to the amount of energy which is required to separate it from the substrate at the interface. This energy is however difficult to measure. .

Many techniques are used for adhesion assessment. The scratch test appears to be the most acceptable technique in adhesion assessment. This method has been used in this project in order to obtain an idea of the adhesion of the different carbon films produced. A detailed study of adhesion is, however, not among the obectives of this work.

4. 1 Scratch test procedure

Typically, an indenter is pulled across the coating surface, under increasing normal load, until detachment occurs, the load corresponding to failure gives a guide to adhesion strength and is sometimes known as the critical load. Coating detachment is determined by tangential force measurement, acoustic emission and optical microscopy. The failure can be either cohesive (lower critical load) or adhesive (upper critical load). Cohesive failure (fracture) is recognised by an increase in acoustic emission and variations in tangential force. Adhesive failure which results in the complete removal of the coating is characterised by large increases in tangential force (often accompanied by heavy acoustic emission). The normal procedure consists in making a series of parallel scratches with different loads applied on the stylus. Optical microscopy or SEM are used to examine the nature of the coating failure.

5. Microhardness

One of the most common tests for assessment of the mechanical properties of materials is the hardness test. The hardness of a material is generally defined as its resistance to permanent indentation.

Various techniques have been developed to measure the hardness of materials using different indenter materials and geometries. The tests the most suitable for thin films are Knoop and Vickers. These are the tests used in this study.

5. 1. Vickers test

The Vickers hardness test, also known as the diamond pyramid hardness test, uses a square based pyramidal diamond indenter. Loads range from 5 g to 2000 g for thin films and 1 kg to 120kg for bulk material. The Vickers hardness number (H_V) is given by the formula:

$$H_V = \frac{189 \times F \times 10^3}{d^2}$$

where

H_V = Vickers hardness in (Kg/mm^2)

F = Test force in Newton (N)

d = Length of the indentation diagonal in (µm.)

5. 2 Knoop test

This test uses a diamond indenter in the shape of an elongated pyramid with loads generally from 5g to 5000g . It is a microhardness test because of the light loads it employs and hence is suitable for very small or thin specimens and for brittle materials such as carbides and glass. The size of the indentation is generally in the range of 10 µ m to 100 µm. Because the hardness number obtained depends on the applied load, test results should always cite the load employed.

The Knoop Hardness number (H_K) is given by the formula

$$H_K = \frac{1450.5 \times F \times 10^3}{I^2}$$

where

H_K = Knoop Hardness in (kg/mm^2)

F = Test force in (N)

I = Length of longer diagonal in (µm.)

The measurement of Knoop microhardness was performed on a Leitz Miniload microindenter instrument. Due to thickness of the films which was often around 1 µm, loads from 10 to 25 g were used, although the tester can be used with a range of loads from 10 to 2000 g. Diagonal length was measured using the Nikon Optiphot. 400 x magnification microscope and an average of ten readings were taken at every load used.

5. 3 Factors affecting the microhardness test

There are many factors which could affect the hardness measurement: loading variations, substrate support effect, penetration depth, surface roughness effect and elastic recovery of the indentation.

For these reasons the hardness reading in this study were used only as a comparison between films deposited on the same kind of substrate and having the same thickness. During measurement we tried to satisfy the requirement that the film thickness must be several times greater than the indentation depth in order to avoid substrate effect. The knoop indenter was preferred because of its relatively small indentation depth. Elastic recovery of the indentation however, could not be avoided for films having high internal stress. Over estimated values are often reported for this kind of film. Up to 30% can be the error of over estimating [1].

6. Sliding wear and friction measurement

The pin on disc test has been used for the evaluation of sliding wear and friction coefficient measurement in our Laboratory. A schematic diagram of the pin on disc tribo-tester is shown in Fig. 1. Loads are applied at the pin through the action of weights positioned at the end of a lever arm. SAE 52100 tool steel balls are the pin material used. Specimens are clamped to a holder table and precisely mounted on an horizontally rotating table so as to provide movement in the rotational plane only. By means of the normal load and the friction force measured by a load cell mounted perpendicular to the lever arm, the friction coefficient is calculated. Temperature and humidity stabilisation was achieved by a system of water evaporators, cooling elements and heating lights to provide the injection and extraction of water vapour and a source of heat respectively.

After the sliding wear tests, the physical condition of the film track and pin scar is examined. The quantity of material removed from the pin, although relatively small, can be measured. The degree of pin water indicates fundamentally the level of Hertzian pressure to which the film/substrate combination is subjected.

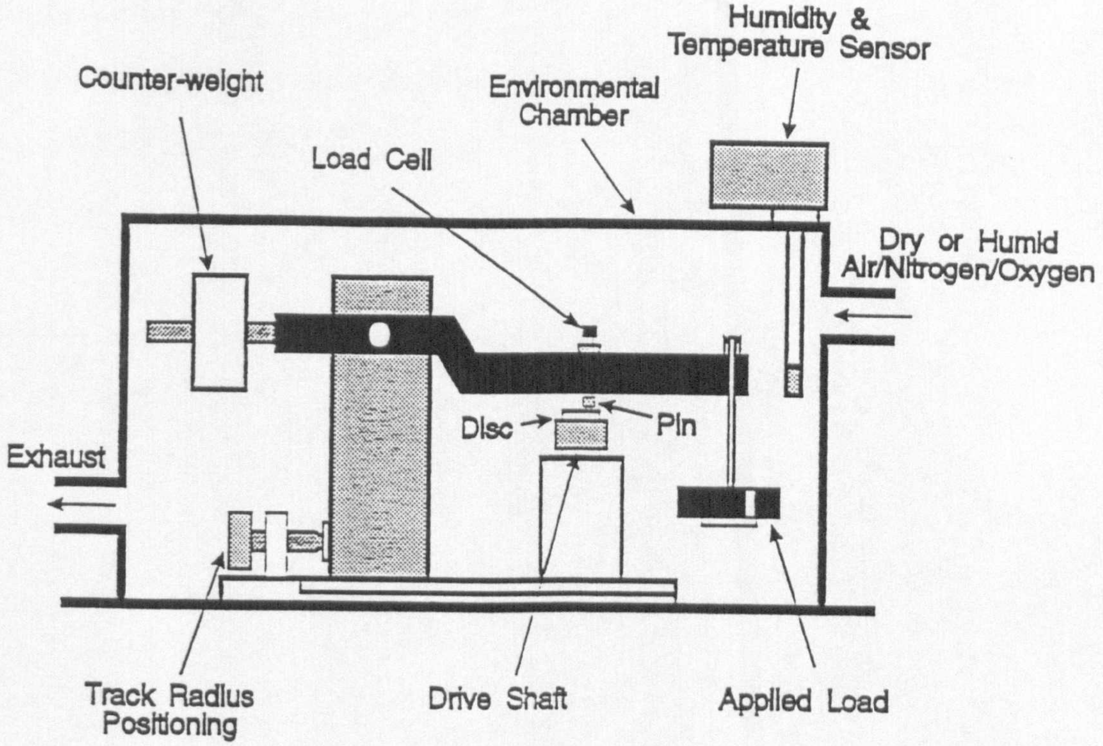

Fig. 1 A Schematic Diagram of a Pin On Disc Tribotester

7. Nanohardness

Nanohardness testing is a sophisticated technique that measures the hardness during the penetration of the indenter. A schematic diagram of a nanohardness tester is shown in Fig. 2. True values of the hardness are obtained as a function of depth penetration. The hardness and the Young modulus can be derived from the hysteresis curves corresponding to indenter depth versus applied pressures during penetration and removal of the indenter. The depth values therefore contain both plastic and elastic contribution. The elastic recovery parameters (ERP) [1] is determined from the unloading branch of the hysteresis curve where the intercept at zero load represents the plastic depth.

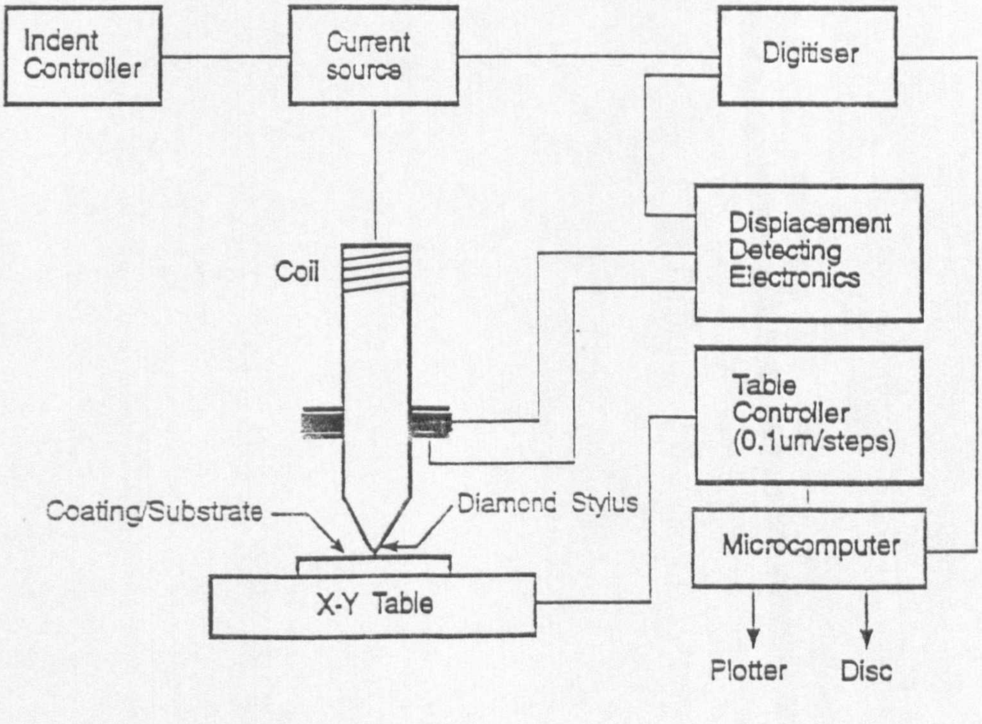

Fig. 2 A schematic diagram of a nanohardness tester.

8. Ellipsometry .

Ellipsometry is a convenient and accurate technique for the measurement of thickness and refractive indexes of very thin films on reflecting surfaces.

This technique is concerned with the measurement of changes in the state of polarisation of light upon reflection from a surface.

For the purpose of characterisation and subsequent examination, media can be divided into two groups:

i- Non absorbing media.

ii- Absorbing media.

The refractive index, n ,of a non absorbing medium is given by :

n = wave velocity in vacuum / wave velocity in the medium.

For a medium which is absorbing, the refractive index n is replaced by a complex quantity:

$$N = n - i\,k$$

The real part, n, and imaginary part, k, are calculated from the relative attenuation, ψ, and phase shift, Δ, of the parallel component of the incident beam, with respect to the perpendicular, that occur upon reflection using the classical theory of Drude [2].

When a surface is examined using an ellipsometer, Ψ and Δ are determined at a given angle of incidence Φo. In turn the optical constants n and k for the reflection surface can be calculated for the corresponding light wavelength using [3]well established equations giving $n^2 - k^2$ and nk as functions of Ψ, Δ and Φo in a form suitable for computation:

$$n^2 - k^2 = \sin^2 \Phi_0 \left[\frac{\tan^2 \Phi_0 \,(\cos^2 2\Psi - \sin^2 2\Psi \sin^2 \Delta)}{(1 + \sin 2\Psi \cos \Delta)^2} + 1 \right] \qquad (2)$$

$$2\,n\,k = \sin^2 \Phi_0 \quad \frac{\tan^2 \Phi_0 \sin 4\Psi \sin \Delta}{(1 + \sin 2\Psi \cos \Delta)^2}$$

Detailed accounts of the theory of ellipsometry methods may be found in refs. [2, 4, 5]

9. Photon Spectroscopy (Raman and PDS)

9.1 Raman Spectroscopy

Raman spectroscopy is a technique involving the inelastically scattering of light from vibrational excitations within the sample. The frequency shift of incident photons (from a laser source) after inelastic scattering due to collisions with the molecules of interest is measured. This frequency shift yields molecular vibration information which can provide structural, orientations and chemical details about the specimen being probed. The peak location (ie wave numbers cm^{-1}) identifies the phase.

Fig.3, shows typical Raman spectra obtained from different carbon phases [6]. Raman spectroscopy allows easy identification of film carbon phases. It is a powerful tool in providing strong evidence in favour of graphite bonding. The 1550 cm^{-1} G peak is close to the mode in graphite and well above any mode frequency possible in an sp^3 -bonded lattice. It has however a relatively poor sensitivity due to the low intensity of the inelastically scattered light. Fluorescence of the substrate can complicate the Raman spectrum. A schematic diagram of conventional Raman spectrometer is shown in Fig. 4.

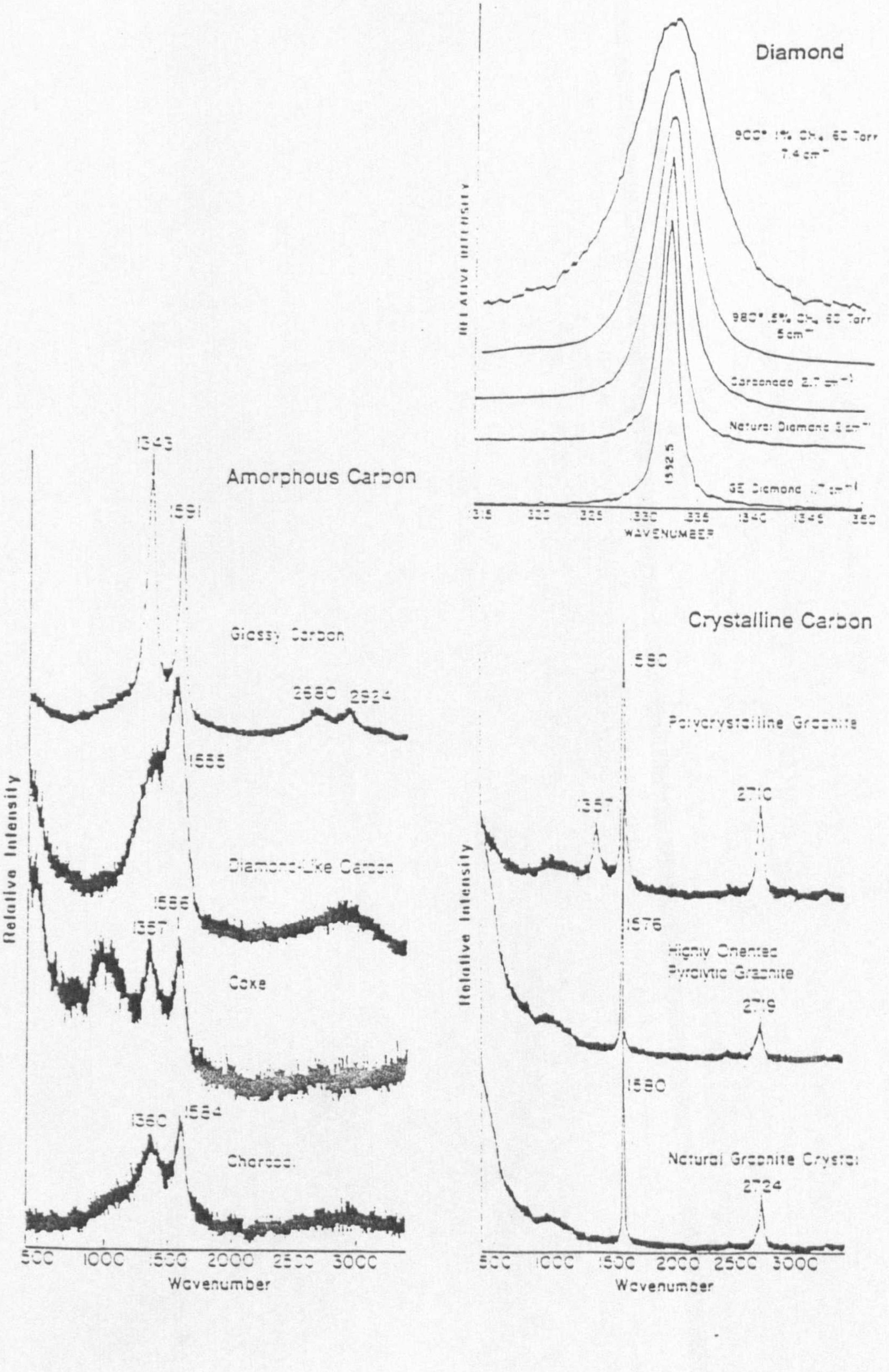

Fig.3 Characteristic Raman Signatures For Diamond and Amorphous / Crystalline Forms of Carbons.

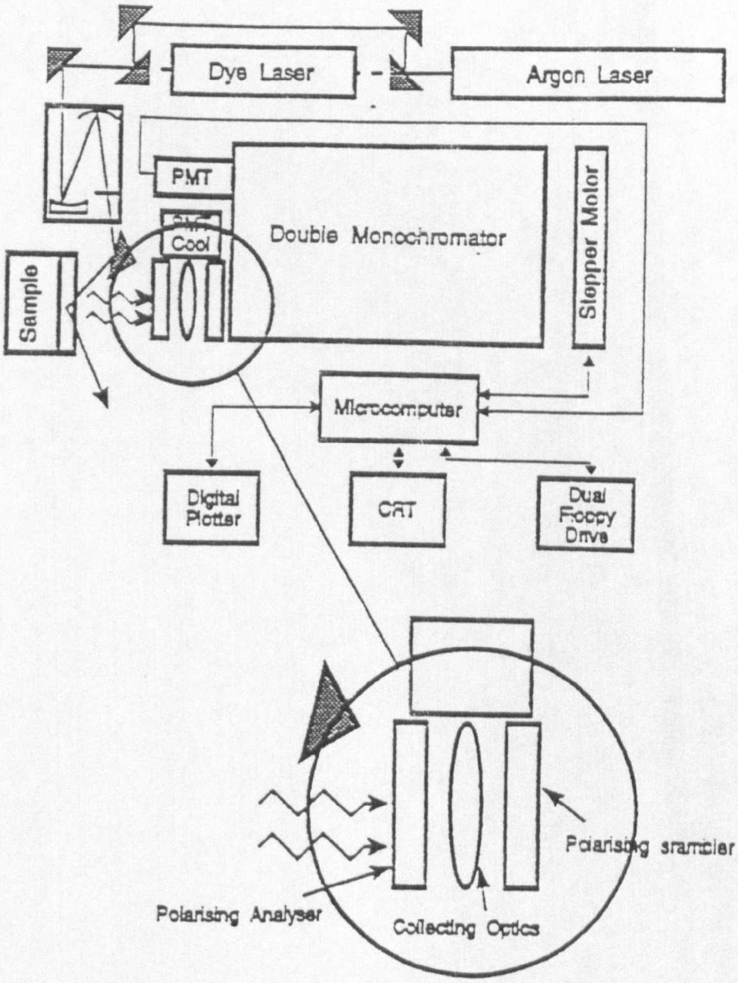

Fig. 4. A Schematic Diagram of Conventional Raman Spectrometer

9.2 Photothermal Deflection Spectroscopy (PDS)

Because the optical band gap is one of the most basic parameters of a semiconductor, there are many measurement techniques for optical absorption in amorphous semiconductors. In the absorption spectrum region, corresponding to absorption coefficient α above 10^3 cm^{-1}, the optical band gap is determined using the Tauc relation as described in chapter V.

The second part of the absorption spectrum is the region around the fundamental edge with absorption coefficients from 10 to 10^3 cm^{-1}. Below this is the third region of extrinsic absorption. An immediate problem with measurements is that direct absorption measurements rapidly become inaccurate at or below the absorption edge when $\alpha d \ll 1$ and so substantial effort has gone into finding better measurement techniques. Photothermal Deflection Spectroscopy (PDS) method seems to be the most promising technique [7]. This measures the absorbed power P, rather than transmitted power as in the conventional optical measurements. When αd is small, $P \sim P_0 \times \alpha d$, where P_0 is the incident illumination power. The measurement gives αd directly and the lower limit on αd depends on the detection sensitivity. The PDS method uses the change in refractive index of a fluid in contact with the sample to deflect a laser beam. This technique has a sensitivity limit for a-C:H films down to $\alpha = 10$ cm^{-1}

10. Elecltron Spectroscopy (AES, ADP, XPS and EELS)

10.1 Auger Electron Spectroscopy (AES).

Incident electrons knock a low level electron out of its shell, causing the ejection of a higher level "Auger" electron. The energy of the Auger electrons yield information about the sample. The mechanism of Auger emission is illustrated [8] for an iron atom in Fig.5. In the solid state, of course, energy bands of finite width may replace some of the discrete energy levels shown and consequently lead to broadening of the Auger lines.

Since ultra high vacuum apparatus and sophisticated electron optics are required, equipment for Auger analysis is expensive.

10.2 Auger Depth Profiling (ADP)

This is the most popular technique for thin film analysis. Here, composition variations in layers adjacent of a surface are revealed by sequential inert ion sputtering and AES. The surface is simply eroded away in a controlled fashion by ion bombardment and the composition of the freshly exposed surface determined by AES. In practice, several Auger peaks can be monitored continually while sputtering away the surface layer by layer.

10.3 X-ray photoelectron spectroscopy (XPS)

Auger techniques generally yield little information on the chemical bonding of surface atoms. In XPS, the specimen surface is irradiated with a monoenergetic X-ray beam which causes ejection of both low level and valence electrons. Since the incident energy is well defined, energy analysis of the emitted photoelectrons enables their binding energy to be accurately determined from the principle of conservation of energy: $E_k = h\nu - E_B - \Delta\Phi$, in which E_k is the kinetic energy of the liberated electron, E_B is the binding energy, $h\nu$ is the photon energy, and $\Delta\Phi$ is the difference in work function between the sample and spectrometer. XPS, then, may be used to identify surface constituents, to measure binding energies, and to indicate the way in which a particular element is combined. The large secondary electron background accompanying AES is absent in XPS, sensitive specimens can be studied without electron beam damage; and specimen charging effects are minimised. The same electron spectrometer may be used for both AES and XPS.

10.4 Electron Energy Loss Spectroscopy (EELS)

The energy of the primary electrons are measured after the electrons pass through, or reflect off the sample. The loss processes the electrons undergo are determined by transitions specific to the sample. Typical EELS spectra obtained from different carbon phases are shown in Fig. 6.

10.5 Secondary ion Mass Spectroscopy (SIMS)

The most sensitive analytical technique for determining trace impurities in thin films is secondary ion mass spectroscopy. In this technique, a focused beam inert or reactive gas ions is used to bombard the surface of the specimen. This causes fractions of the material to be sputtered from the surface in an ionised state, the proportions depending on the relative electronegativities of the various atoms present. After passing through an energy filter, the secondary ions enter a mass analyser. Compositional analysis with 5-10 nm depth resolution can be obtained with very high sensitivity to low concentrations. SIMS can detect hydrogen, although quantification is difficult. The formation of polyatomic species as a result of sample ions bombardment can confuse the identification analysis (ie CH^+, C_2^+, C_2H^+,...).

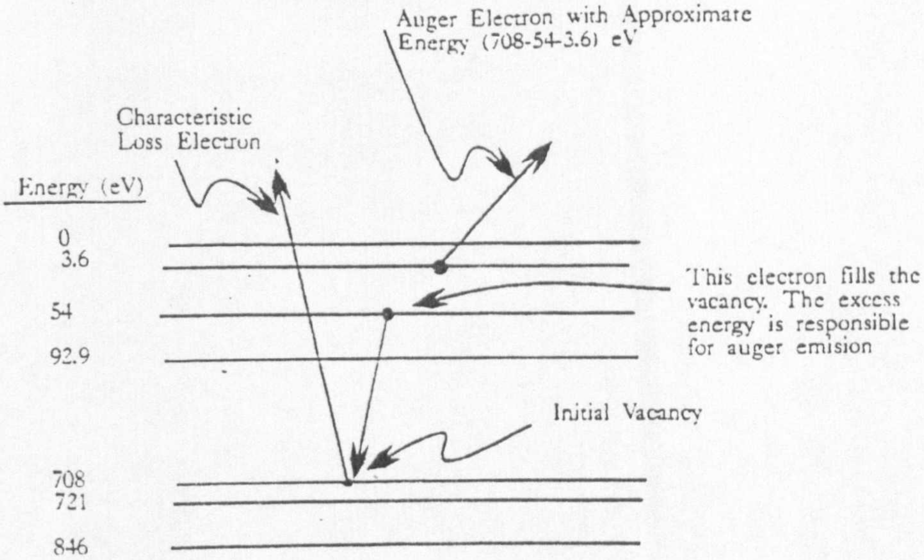

Fig. 5 Auger process in the Fe atom

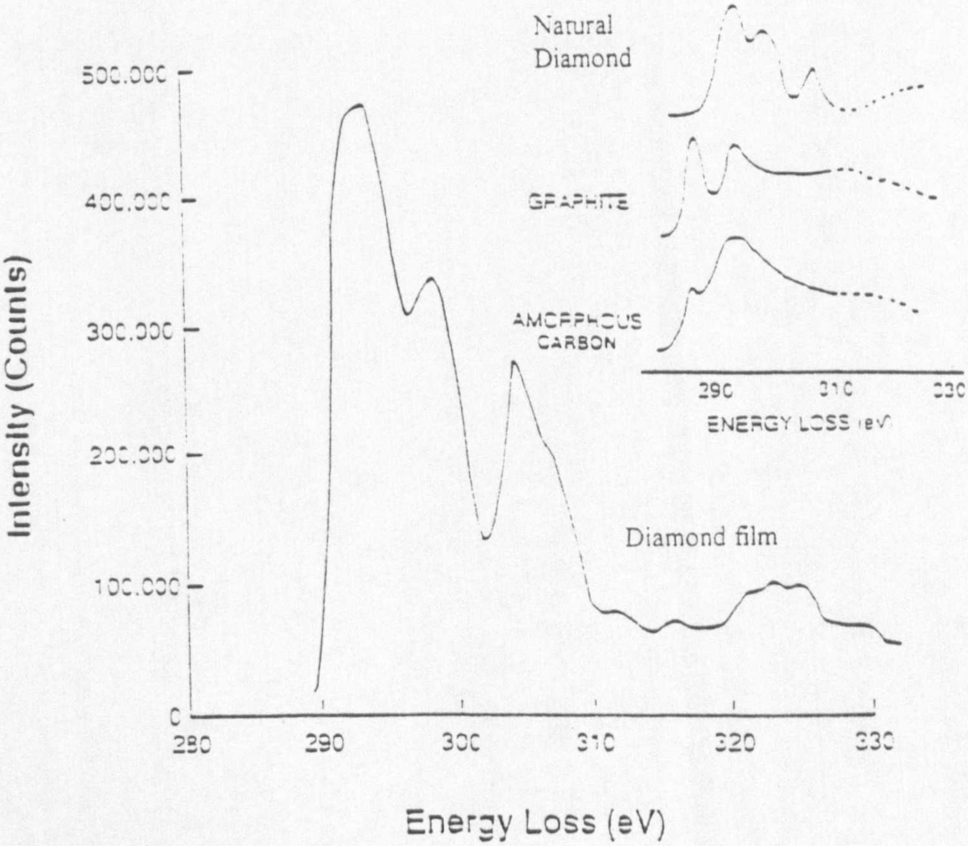

Fig. 6 Typical EELS spectra from different carbon phases [9]

(note the similarity between Diamond Film and Natural diamond-edge and shape)

Appendix References

1 P.Holiday PhD Thesis, Hull University 1993.

2 P. Drude. The theory of optics, p.361, Longmans, Green, New York (1901).

3 J. W.Hilton, W. A. Hilton, A.J.P. Volume 41 pp. 702-704 May 1973.

4 O. S. Heavens, Optical properties of thin solid films (Dover, 1965)

5 R. W. Wood, Physical Optics (Macmillan, New York, 1934), third ed. pp. 542 - 569.

6 D. Knight & W.White, J. Mater. Res. Vol.4(2), Mar/Apr 1989

7 M. L. Theye, L. Chahed, P. Roca i Cabarrocas, and K. Zellama, Phil. B63 (1991) 143.

8 J. F. Smith, D. C. Hinson Solid State Technology/November 1986. pp. 135-140.

9 J. T. Glass et al., "Diamond and Diamond Like Films", an intensive one day course, organised by COMST, Lausanne, Switzerland, 1990.